IDENTIFICATION OF MULTIPLE FAULT PARAMETERS IN ROTOR-BEARING-COUPLING SYSTEMS BASED ON FORCED RESPONSE MEASUREMENTS

A Thesis Submitted in

Partial Fulfilment of the Requirements

for the Degree of

DOCTOR OF PHILOSOPHY

By

Mohit Lal

Department of Mechanical Engineering

Indian Institute of Technology Guwahati

March 2013

CERTIFICATE

It is certified that the work contained in this thesis entitled ***IDENTIFICATION OF MULTIPLE FAULT PARAMETERS IN ROTOR-BEARING-COUPLING SYSTEMS BASED ON FORCED RESPONSE MEASUREMENTS*** by **Mohit Lal (Roll No. 08610305)** at Indian Institute of Technology Guwahati for the award of Doctor of Philosophy has been carried out under my supervision and the work has not been submitted elsewhere for a degree.

Dr. Rajiv Tiwari,
Professor,
Department of Mechanical Engineering,
Indian Institute of Technology Guwahati,
Guwahati-781039, INDIA

Dedicated to,

My Beloved Parents and My Wife

ACKNOWLEDGEMENTS

It is a great privilege for me to have an opportunity to acknowledge a feeling of great gratitude to my thesis supervisor, Professor Rajiv Tiwari for his guidance, encouragement and support throughout my research. Also, I really appreciate his patience and time that he spent with me to give advices and answer many questions that I had. I thank him for introducing me into such a challenging area of research.

I would like to thank Prof. Sashindra K. Kakoty, Prof. Santosha K. Dwivedy and Prof. Chitralekha Mahanta for being on my doctoral committee and reviewing my dissertation periodically.

I would like to thank Mr. D. J. Bordoloi for helping me to perform experiments and the staff of the Central Workshop of the institute for their help in fabrication of the experimental setup. I am thankful to Dr. Sachin K. Singh for helping me to understand the MATLAB at the initial stage of my research. I am also thankful to all laboratory mates and my friends at IITG, who made my campus life enjoyable and memorable.

I would like to express my deepest gratitude to my family members, for their patience and love which enabled me to overcome obstacles and complete my research. Finally, I am always thankful to GOD for his constant shower of blessing to me.

Mohit Lal

TABLE OF CONTENTS

LIST OF FIGURES…….. xi

LIST OF TABLES…… xix

NOMENCLATURE…… xxi

ABSTRACT…… xxv

1 Introduction and Literature Survey…… 1

1.1 Introduction…… 1

1.2 Background and Literature Survey…… 10

1.2.1 Background…… 10

1.2.2 Importance of the study…… 10

1.2.3 Literature survey on the rotor fault detection and diagnosis…… 11

1.2.4 Review on condensation schemes…… 35

1.3 Motivation of the Present Work and Objectives…… 37

1.4 Present Work…… 39

1.5 Organization of the Thesis…… 41

2 Identification of Multiple Fault Parameters in a Rigid-Rotor and Flexible Bearing-Coupling System…… 43

2.1 Introduction…… 43

2.2 System Modelling…… 44

2.2.1 Basic assumptions and the description of model …… 44

2.2.2 Equations of motion…… 46

2.2.3 Development of the identification algorithm…… 52

2.3 Procedure to Improve the Condition of Regression Matrix…… 57

2.3.1 Method I: Rotating the rotor in the same direction at different speeds….. 59

2.3.2 Method II: Rotating the rotor alternately in the CW or CCW direction..... 60

2.4 Numerical Experiments…….. 61

2.4.1 Method I: Rotating the rotor in the same direction at different speeds….. 66

2.4.2 Method II: Rotating the rotor alternately in the CW or CCW direction..... 71

2.4.3 Discussions on various numerical studies performed……..…….…….. 82

2.5 Summary…..…… 83

3 Multiple Fault Identification in a Flexible Rotor-Bearing-Coupling System 85

3.1 Introduction…… 85

3.2 System Modelling…….…….. 85

3.2.1 Basic assumptions and the description of model ……..……. 86

3.2.2 Modelling of the shaft……. 87

3.2.3 Modelling of the rigid disc…….. 88

3.2.4 Modelling of the bearing…… 88

3.2.5 Modelling of residual unbalance forces…….. 89

3.2.6 Modelling of coupling misalignments……..... 89

3.2.7 Equations of motion for the rotor substructure…….. 91

3.2.8 Equations of motion for bearings as a substructure…..……..…….. 91

3.2.9 System equations of motion in frequency domain…….. 92

3.3 Development of the Identification Algorithm……..…….. 94

3.4 Numerical Experiments……..…… 98

3.4.1 Method I: Rotating the rotor in the same direction at different speeds….. 102

3.4.2 Method II: Rotating the rotor alternately in the CW or CCW direction..... 107

3.4.3 Discussions on various numerical studies performed…..……...…… 119

3.5 Summary…… 121

4 Multiple Fault Identification in Flexible Rotor-Bearing-Coupling Systems with Incomplete Rundown or Run-up Data.....…….. 123

4.1 Introduction…… 123

4.2 System Modelling…….…….. 123

4.2.1 Basic assumptions and the description of model ……..……. 124

4.2.2 System equations of motion in frequency domain…….. 126

4.3 Development of the Identification Algorithm with the Dynamic Condensation… 126

4.4 Development of the Identification Algorithm with the High-frequency Condensation…….. 130

4.5 Numerical Experiments…….. 134

4.5.1 Method I: Rotating the rotor in the same direction at different speeds….. 141

4.5.2 Method II: Rotating the rotor alternately in the CW or CCW direction.… 143

4.5.3 Discussions on various numerical studies performed…….…… 151

4.6 Summary…… 152

5 Experimental Validation of the Identification Algorithm 155

5.1 Introduction…… 155

5.2 The Description of Rotor Model and Support Conditions……..…….. 155

5.3 Experimental Setup and Instrumentations…….. 161

5.3.1 Experimental setup……. 161

5.3.2 Proximity sensors and amplifier unit…….. 162

5.3.3 Constant DC power source unit…….. 164

5.3.4 Data acquisition system…….. 165

5.4 Test Procedure…… 166

5.5 Parameter Estimations without Misalignment…… 170

5.6 Validation of Estimated Parameters for without Misalignment……. 172

5.7 Parameter Estimation with Different Misalignment Conditions…… 178

5.8 Validation of Estimated Parameters with Misalignment Conditions……. 182

5.9 Summary…..…… 187

6 Conclusions and Scopes for Future Work…….. 189

6.1 Summary of the Present Work……... 189

6.2 General Conclusions from the Present Work…… 190

6.3 Major Conclusions from the Present Work…… 192

6.4 Applicability……...…… 192

6.5 Scopes for the Future Work……..……... 192

APPENDIX…….……... 195

Appendix A: Timoshenko Beam Model……. 195

A.1: Translational mass matrix……..……... 195

A.2: Rotational mass matrix……..……... 196

A.3: Stiffness matrix……..……... 197

A.4: Gyroscopic matrix……..……..…….. 197

A.5: Rigid disc model……..……..…… 198

Appendix B: Rayleigh Damping……. 199

Appendix C: Natural Frequencies for Simply Supported Rotor Systems……..…. 200

Appendix D: Conditioning of Ill-Conditioned Regression Matrix……..…. 201

Appendix E: Relationship Between Signals-to-Noise Ratio (SNR) in dB and Noise in Percentage……...…..…. 202

References…….…… 203

Publications from the Present Work…….…… 215

LIST OF FIGURES

Figure 1.1 A schematic diagram of the (a) angular (b) parallel (c) combined misalignments between two shafts 3

Figure 1.2 Mechanical coupling classifications 4

Figure 1.3 A sleeve or muff coupling 5

Figure 1.4 A flange coupling 5

Figure 1.5 A single point universal joint 6

Figure 1.6 An Oldham coupling 7

Figure 1.7 A gear coupling 7

Figure 1.8 A grid coupling 8

Figure 1.9 A beam coupling 8

Figure 1.10 A Three–pin coupling 9

Figure 1.11 An abstract representation of the modal testing and the model updating 30

Figure 2.1 A simple rotor–bearing–coupling system 46

Figure 2.2 (a) A schematic diagram of deflected rotor in *z*–*x* plane (b) A schematic diagram of the coupling model 46

Figure 2.3 Variation of the horizontal response at bearing location 1 with the spin speed 64

Figure 2.4 A flow chart of the identification algorithm 65

Figure 2.5 Comparison of errors of estimated parameters before and after column scaling for 1% measurement noise (for Case *A* under *Method I*) 66

Figure 2.6 Comparison of responses (a) without noise (b) with 1% noise (c) with 2% noise (d) with 5% noise (for *Case A* under *Method I*) 68

Figure 2.7 Comparison of errors of estimated parameters for different level of measurement noise (for *Case A* under *Method I*) 68

Figure 2.8 Comparison of responses generated from the assumed and estimated parameters (a) 1% noise (b) 5% noise (for *Case B* under *Method I*)..... 69

Figure 2.9 Comparison of errors of estimated parameters for different level of measurement noise (for *Case B* under *Method I*) 70

Figure 2.10 Comparison of responses (a) 1% noise (b) 5% noise (for *Case C* under *Method I*)71

Figure 2.11 Comparison of errors of estimated parameters for different level of measurement noise (for *Case C* under *Method I*) 71

Figure 2.12 Comparison of responses (a) 1% noise (b) 5% noise (for *Case A* under *Method II*) 73

Figure 2.13 Comparison of errors of estimated parameters for different level of measurement noise (for *Case A* under *Method II*) 73

Figure 2.14 Comparison of responses (a) 1% noise (b) 5% noise (for *Case B* under *Method II*) 74

Figure 2.15 Comparison of errors of estimated parameters for different level of measurement noise (for *Case B* under *Method II*) 74

Figure 2.16 Comparison of responses (a) 1% noise (b) 5% noise (for *Case C* under *Method II*) 75

Figure 2.17 Comparison of errors of estimated parameters for different level of measurement noise (for Case C under Method II 76

Figure 2.18 Misalignment forces and moments with spin speed for 5% noise (for *Case C* under *Method II*)..... 81

Figure 3.1 A flexible rotor–bearing–coupling system 86

Figure 3.2 A FE model of the rotor–bearing–coupling system 87

Figure 3.3 A schematic diagram of the coupling model in the *z*–*x* plane 87

Figure 3.4 The shaft misalignment at the coupling for (a) rigid shafts (b) flexible shafts 90

Figure 3.5 Variation of the horizontal response at bearing location 1 with the spin speed..... 99

Figure 3.6 Comparison of errors of estimated parameters before and after column scaling for 5% measurement noise (for *Case A* under *Method I*) 100

Figure 3.7 Comparison of errors of estimated parameters before and after column scaling for 5% measurement noise (for *Case B* under *Method I*) 101

Figure 3.8 Comparison of errors of estimated parameters before and after column scaling for 5% measurement noise (for *Case C* under *Method I*) 101

Figure 3.9 Comparison of errors of estimated parameters before and after column scaling for 5% measurement noise (for *Case A* under *Method II*) 101

Figure 3.10 Comparison of errors of estimated parameters before and after column scaling for 5% measurement noise (for *Case B* under *Method II*) 102

Figure 3.11 Comparison of errors of estimated parameters before and after column scaling for 5% measurement noise (for *Case C* under *Method II*) 102

Figure 3.12 Comparison of estimated ((a) stiffness (b) damping (c) unbalance) parameters for different levels of measurement noise (*Case A* under *Method I*).....103

Figure 3.13 Comparison of errors of estimated parameters for different level of measurement noise (for *Case A* under *Method I*) 104

Figure 3.14 Comparison of estimated ((a) stiffness (b) damping (c) unbalance) parameters for different levels of measurement noise (for *Case B* under *Method I*) 105

Figure 3.15 Comparison of errors of estimated parameters for different level of measurement noise (for *Case B* under *Method I*) 105

Figure 3.16 Comparison of estimated ((a) stiffness (b) damping (c) unbalance) parameters for different levels of measurement noise (for *Case C* under *Method I*) 106

Figure 3.17 Comparison of errors of estimated parameters for different level of measurement noise (for *Case C* under *Method I*).....107

Figure 3.18 Comparison of estimated ((a) stiffness (b) damping (c) unbalance) parameters for different levels of measurement noise (for *Case A* under *Method II*) 108

Figure 3.19 Comparison of errors of estimated parameters for different level of measurement noise (for *Case A* under *Method II* 109

Figure 3.20 Comparison of estimated ((a) stiffness (b) damping (c) unbalance) parameters for different levels of measurement noise (for *Case B* under *Method II*) 110

Figure 3.21 Comparison of errors of estimated parameters for different level of measurement noise (for *Case B* under *Method II*) 110

Figure 3.22 Comparison of estimated ((a) stiffness (b) damping (c) unbalance) parameters for different levels of measurement noise (for *Case C* under *Method II*) 111

Figure 3.23 Comparison of errors of estimated parameters for different level of measurement noise (for *Case C* under *Method II*) 112

Figure 3.24 Misalignment forces and moments with spin speed for 5% noise (for *Case C* under Method II) 119

Figure 4.1 A flexible multi−stage turbine−generator system 125

Figure 4.2 A FE model of the flexible multi−stage turbine−generator system ……..……..125

Figure 4.3 A schematic diagram of $(p-1)^{th}$ coupling 125

Figure 4.4 A finite element model of the rotor−bearing−coupling system 135

Figure 4.5 Variation of the horizontal response at the left of coupling location (i.e. node 6) with the spin speed 138

Figure 4.6 Comparison of errors of estimated parameters for different frequency bands under *Method I*, for 5% measurement noise 138

Figure 4.7 Comparison of errors of estimated parameters before and after column scaling for 1% measurement noise (for *Case A* under *Method I*) 139

Figure 4.8 Comparison of errors of estimated parameters before and after column scaling for 1% measurement noise (for *Case B* under *Method I*) 139

Figure 4.9 Comparison of errors of estimated parameters before and after column scaling for 1% measurement noise (for *Case* C_{fb3} under *Method I*) 140

Figure 4.10 Comparison of errors of estimated parameters before and after column scaling for 1% measurement noise (for *Case A* under *Method II*) 140

Figure 4.11 Comparison of errors of estimated parameters before and after column scaling for 1% measurement noise (for *Case B* under *Method II*) 140

Figure 4.12 Comparison of errors of estimated parameters before and after column scaling for 1% measurement noise (for *Case* C_{fb3} under *Method II*).....141

Figure 4.13 Comparison of errors of estimated parameters for different level of measurement noise (for *Case A* under *Method I*).....142

Figure 4.14 Comparison of errors of estimated parameters for different level of measurement noise (for *Case B* under *Method I*).....142

Figure 4.15 Comparison of errors of estimated parameters for different level of measurement noise (for *Case* C_{fb3} under *Method I*) 143

Figure 4.16 Comparison of errors of estimated parameters for different level of measurement noise (for *Case A* under *Method II*).....144

Figure 4.17 Comparison of errors of estimated parameters for different level of measurement noise (for *Case B* under *Method II*).....145

Figure 4.18 Comparison of errors of estimated parameters for different level of measurement noise (for *Case* C_{fb3} under *Method II*) 146

Figure 4.19 Comparison of estimated ((a) stiffness (b) damping (c) unbalance) parameters for different levels of measurement noise (*Case* C_{fb3} under *Method II*).....147

Figure 4.20 Comparison of errors of estimated parameters for *Case* C_{fb3}, under *Method I* and *Method II*, for 5% variation in E and ρ) 147

Figure 4.21 Misalignment forces and moments with spin speed for 5 % noise case (*Case* C_{fb3} under *Method II*) 148

Figure 5.1 An experimental setup of rotor–bearing–coupling system..... 157

Figure 5.2 Close view of (left) bearing housing (right) rolling bearing with soft padding..... 157

Figure 5.3 A close view of the coupling with a spiral cut..... 157

Figure 5.4 Types of misalignment between rigid shafts for (a) pure angular (b) pure parallel (c) combined angular and parallel 159

Figure 5.5(a) Misaligned rotor system (b) A close view of sheets used for the introduction of misalignment 159

Figure 5.6 A schematic of the rotor system with aluminium sheets used to create the misalignment (a) perfect aligned (b) pure angular (c) pure parallel (d) combined misalignment 160

Figure 5.7 An experimental setup developed with instrumentations..... 161

Figure 5.8 A schematic diagram of the experimental setup with instrumentations..... 162

Figure 5.9 (a) Proximity sensors and its mounting (b) A close view of proximity sensor and its mounting (without shaft)..... 163

Figure 5.10 A photovoltaic sensor and a reflecting strip 163

Figure 5.11 A proximity amplifier with four channels 163

Figure 5.12 A constant DC power source 164

Figure 5.13 A data acquisition system 164

Figure 5.14 A dial indicator for checking alignment of shafts at the coupling……..……..166

Figure 5.15 A sample time history data of the horizontal direction response at bearing location 1 at 17 Hz 167

Figure 5.16 The filtered and unfiltered signal for the sample time history of Figure 5.15..... 168

Figure 5.17 The time history of a response at bearing 1 at spin speed of 17 Hz with a phaser signal.....169

Figure 5.18 Experimentally estimated parameters (a) stiffness (b) damping (c) residual unbalance for three different sets of measured data.....171

Figure 5.19 A FFT plot from an impact test on rotor system 1 (near motor end) without couplings.....174

Figure 5.20 A FFT plot from an impact test on rotor system 2 (away from motor) without couplings.....174

Figure 5.21 A FFT plot from an impact test on Rotor systems 1 and 2 with only Coupling 2.174

Figure 5.22 A FFT plot from an impact test on Rotor systems 1 and 2 with both Couplings 1 and 2 175

Figure 5.23 First three modes of the rotor system.....176

Figure 5.24 A schematic diagram of experimental setup with forcing directions to excite different modes of vibration (a) first mode (b) second mode (c) third mode.....176

Figure 5.25 Comparison of natural frequencies (a) FE forced vibration solution with SSBC (critical speeds) (b) Impact test with 1st mode excitation (c) Impact test with 2nd mode excitation (d) Impact test with 3rd mode excitation (e) Updated FE model 177

Figure 5.26 Time history at bearing 1 for (a) *Case* A_1 (b) *Case* B_1 (c) *Case* C_1 at the spin speed of 17 Hz along with the phaser signal 179

Figure 5.27 Comparison of deviations of estimated parameters with aligned case and for pure angular misalignment conditions *Case* A_1 ($\Delta\alpha$=0.16°, $\Delta\delta$= 0mm) and *Case* A_2 ($\Delta\alpha$=0.32°, $\Delta\delta$= 0 mm).....180

Figure 5.28 Comparison of deviations of estimated parameters with aligned case and for pure parallel misalignment conditions *Case* B_1 ($\Delta\alpha$=0°, $\Delta\delta$= 0.5 mm) and *Case* B_2 ($\Delta\alpha$=0°, $\Delta\delta$=1.0 mm) 181

Figure 5.29 Comparison of deviations of estimated parameters with aligned case and for combined misalignment conditions *Case* C_1 ($\Delta\alpha$=0.16°, $\Delta\delta$= 0.5 mm) and *Case* C_2 ($\Delta\alpha$=0.32°, $\Delta\delta$= 1.0 mm) 182

Figure 5.30 A FFT plot from an impact test for *Case* A_1 (i.e. Δα=0.16°, Δδ= 0 mm) 183

Figure 5.31 A FFT plot from an impact test for *Case* B_1 (i.e. Δα=0°, Δδ= 0.5 mm) 183

Figure 5.32 A FFT plot from an impact test for *Case* C_1 (i.e. Δα=0.16°, Δδ= 0.5mm) 183

Figure 5.33 Comparison of natural frequencies (a) Impact test for *Case* A_1 (b) Impact test for *Case* B_1 (c) Impact test for *Case* C_1 (d) Updated FE model with misalignment condition (critical speeds)..... 185

LIST OF TABLES

Table 2.1 Unknown parameters with corresponding row locations in vector $\{X_2\}$ 56

Table 2.2 Rotor geometrical and physical properties 62

Table 2.3 Residual unbalances 62

Table 2.4 Assumed and identified bearing stiffness parameters for Case C of Method II 76

Table 2.5 Assumed and identified bearing damping parameters for *Case C* of *Method II* 77

Table 2.6 Assumed and identified coupling dynamic parameters for *Case C* of *Method II*..... 77

Table 2.7 Assumed and identified unbalance parameters for *Case C* of *Method II*..... 78

Table 2.8 Summary of estimated parameters having maximum % error and corresponding condition numbers for different cases 79

Table 2.9 Identified residual unbalances for different assumed residual unbalance for 5% measurement noise (for *Case C* under *Method II*) 80

Table 2.10 Identified residual unbalances for different disc masses for 5% measurement noise (for *Case C* under *Method II*)..... 81

Table 3.1 Shaft properties 98

Table 3.2 Disc and residual unbalance properties 99

Table 3.3 Assumed and identified bearing stiffness parameters for *Case C* of *Method II* 112

Table 3.4 Assumed and identified bearing damping parameters for *Case C* of *Method II* 113

Table 3.5 Assumed and identified coupling dynamic parameters for *Case C* of *Method II*.....113

Table 3.6 Assumed and identified unbalance parameters for *Case C* of *Method II*.....114

Table 3.7 Summary of estimated parameters having maximum % error and corresponding condition numbers for different cases 115

Table 3.8 Identified residual unbalances for different assumed residual unbalance (for *Case C* under *Method II*) 116

Table 3.9 Estimation performance for different set of assumed residual unbalances for 5% measurement noise (for *Case C* under *Method II*) 117

Table 3.10 Residual unbalance estimation for different set of disc masses for 5% measurement noise (for *Case C* under *Method II*) 118

Table 4.1 The disc and Residual unbalance properties 136

Table 4.2 Summary of the condition number for different cases……..149

Table 4.3 Summary of estimated parameters having maximum percentage error for different cases 150

Table 5.1 Rotor geometrical and physical properties..... 158

Table 5.2 Bearing specifications 158

Table 5.3 A sample stored response (in complex form with magnitude and phase information) at different operating speed 169

Table 5.4 Misalignment specifications..... 178

Table 5.5 Comparison of natural frequencies with and without misalignment conditions..... 184

Table 5.6 Summary of natural frequencies/critical speeds with and without misalignment conditions 186

NOMENCLATURE

A	Cross section area
$[A]$ and $\{B\}$	Regression matrix and vector, respectively
c_{ij}	Damping coefficients
$[C]$	Damping matrix
$[C^r]$	Regression matrix due to damping
e	Eccentricity
E	Young's modulus of elasticity
$\{F\}$	Force vector
$[G]$	Gyroscopic matrix
I	Diametral mass moment of inertia
k_{ij}	Linear stiffness coefficients
k_{φ}	Torsional stiffness coefficients
$[K]$	Stiffness matrix
$[K^r]$	Regression matrix due to stiffness
l	Length of each shaft
m	Mass
$[M]$	Mass matrix
T	Kinetic energy
$[u^r]$	Regression matrix due to unbalance
U	Unbalance
W	Virtual work
x, y	Linear displacements in (x-z) and (y-z) plane, respectively
$\{X\}$	Vector of unknown parameters

Greek symbols

α	Angular misalignment
δ	Parallel misalignment
ρ	Density
φ_y, φ_x	Angular displacements in (x-z) and (y-z) plane, respectively
ϕ	Phase
$\{\eta\}$	Displacement vector
ω	Spin speed
ζ	Damping ratio

Subscripts

b	Bearing
c	Coupling
d	Disc
G	Gyroscopic
nf	Natural frequency
res	Resonance
s	Shaft
x, y	Horizontal and vertical directions, respectively

Superscripts

B	Bearing
C	Coupling
D	Disc
i	Imaginary part
r	Real part
S	Shaft

u	Unbalance

Abbreviations

B	Bearing
$B_{1, \ldots, 4}$	Bearing locations
C	Coupling
CW	Clock wise
CCW	Counter clock wise
D	Disc
$D_{1, \ldots, 4}$	Disc locations
Damp	Damping
DOFs	Degrees of freedom
EOMs	Equations of motion
FE	Finite element
FEM	Finite element method
FFT	Fast Fourier Transformation
G	Centre of gravity
Mis	Misalignment
MFPs	Multiple fault parameters
S	Shaft
Stiff	Stiffness
Unb	Unbalance

ABSTRACT

This work focuses in two main facets of the rotor dynamics field, the analysis of rotor-bearing-coupling system (i.e., the direct problem) and the fault detection and diagnosis (i.e., the inverse problem). The linear analysis of rotor-bearing system is quite mature and now trend is towards the numerical simulation of complicated rotor systems. The fault detection and diagnostic is not straight forward since different faults may produce similar vibration signature. Frequent faults that appear in rotating machinery are the residual unbalances, shaft bow/bent, shaft misalignment, bearing faults, gear faults, rotor cracks, motor faults, etc.

Among identification (i.e., the fault detection and diagnosis) of various faults, the residual unbalance estimation in a rotor system is an ancient problem; however, the research on this field is still active and now the trend for the unbalance estimation is to reduce the number of test runs, number of measurements required, and the optimum placement of measurement sensors and balancing planes, especially for the large turbo-machineries where the downtime is very expensive and the accessibility of measurements is limited. After the residual unbalance, the second most common fault is the misalignment of shafts at bearings and couplings, and it causes reaction forces and moments at couplings as well as at bearings, and is often a major cause of machinery vibration and its failures. Especially in a rotor train, the misalignment at couplings and bearings is a well known problem and its identification is still a challenging area of the research.

First, an identification methodology has been developed for a turbine-generator system model with the rigid-rotor and flexible bearing-coupling assumptions, which quantitatively estimates multiple fault parameters (MFPs i.e., bearing and coupling dynamic parameters along with residual unbalances. An analytical approach i.e., the Lagrange's equation has been used to

obtain equations of motion (EOMs). The methodology uses the forced response information at different frequencies. Hence, in the numerical simulation, first the direct problem has been solved to generate the system responses and the white noise is added to system responses to mimic the actual measurement data. Also, the conditioning of regression matrix has been discussed and it is found that after the column scaling the condition number of the regression matrix improves appreciably. Significant improvement in the accuracy of estimated parameters is the important effect of column scaling.

The proposed methodology is then extended for the flexible rotor-bearing-coupling system. Here more realistic and more practical modelling approach i.e., the finite element method (FEM) was used to obtain system EOMs. Then identification algorithm has been developed to estimate bearing and coupling dynamic parameters along with residual unbalances. Numerical experiments are performed to check the effectiveness and the robustness of the identification algorithm. The effect on estimates of MFPs for various combinations of assumed unbalances and disc masses are discussed, and an excellent agreement on estimates for these parameters are observed.

The identification algorithm developed above for flexible rotor-bearing-coupling system has the main limitation in that it requires measurement of rotational displacements. To tackle the practical difficulty of limited measurements and the numerical difficulty of the conventional dynamic condensation in the development of identification algorithm, a novel condensation technique has been implemented especially to overcome measurement of rotational DOFs. Numerical examples are presented to show the effectiveness of the proposed identification. Along with the estimation of MFPs, bias error (5% variation in E (modulus of elasticity) and ρ (density)) in the model has also been analysed. And it has been found that most of the estimated

parameters except few cross-coupled bearing damping parameters show well agreement with the assumed values, with 5% variation in E and ρ.

Finally, the algorithm developed was tested with the real experimental setup developed at IIT Guwahati. First, forced responses (displacements) measured at bearing locations in two orthogonal directions were used in the identification algorithm to estimate bearing and coupling dynamic parameters along with residual unbalances experimentally. It was observed that with more number of measurements consistencies of estimated parameters were very good. After estimating the bearing and coupling dynamic parameters along with residual unbalances, the accuracy of the estimated parameters was checked by the updated FEM model and by correlating numerically obtained forward critical speeds with the standard impact test natural frequencies. Also, parameters estimation was performed for different level of misalignment conditions and it was observed that under the severe misalignment condition the splitting of natural frequency took place even in non-rotating conditions.

CHAPTER 1

Introduction and Literature Survey

1.1 Introduction

Rotating machineries are very common and widely used assets in the modern industrial world. Its application includes the machine tools, automobiles, aeroplanes, ships, submarines, power plants, household appliances and medical tools. The most commonly used rotating machines are turbines, generators, compressors, pumps, motors, engines, etc. A breakdown of the rotating machine may result in economic losses and even worse, damage to the human being. That is why the fault detection and diagnostics of the rotating machinery during operation is a very important and one of the most difficult engineering tasks on which the durability and safety of machine operation depends.

The turbo–generator system consists of the driver and driven shafts supported on flexible bearings and coupled through either the rigid or flexible couplings. Such dynamic systems need accurate and reliable prediction of the dynamic characteristic of its components and identification of associated impending faults (i.e., the condition monitoring). The vibration based condition monitoring techniques are becoming popular and could be classified in two broader ways (Isermann and Balle, 1997) as follows:

(a) *Signal based condition monitoring*: In signal based methods, vibration signature of the machine in faulty condition is compared with some reference vibration signature of the machine. The reference vibration signature is taken when there is no fault in the machine. The signal based condition monitoring can be further improved by spectral analysis (fast Fourier transformation (FFT), frequency response function (FRF), full–spectrum analysis, time–frequency analysis, etc.) to obtain more information and features.

(b) *Model based condition monitoring*: Model based methods (like parameters estimation, observer & parity equations and fault diagnosis methods) are based on the analytical or numerical models to simulate the behaviour of faulty machinery. The model based parameter estimation of critical components of rotating system has become an important focus amongst researchers and practitioners of the rotor dynamics since it helps in identification (i.e., the detection and the quantification) of probable faults of such machine components.

Among various kinds of fault in rotating machinery (e.g. residual unbalances, shaft cracks, the bend in a shaft, loose components, the bearing and gear faults, rotor–stator rubs, motor faults, etc.) the misalignment detection and diagnosis has not attracted that many researchers. The perfect alignment of rotor trains is critical in any rotating machinery because the misalignment generates unwanted forces and moments at the coupling as well as at bearings. The shaft misalignment is a condition in which the driver and driven shafts of a machine are not on the same centreline. There are two basic types of shaft misalignments (Piotrowski, 1986)

(i) *Angular misalignment:* In this the centre line of the driver and driven shafts intersect at the coupling location with some angle, however, no lateral offset is present in this case (Figure 1.1(a)). The amount of angular misalignment is represented as, $\Delta\alpha$.

(ii) *Parallel misalignment*: In this case the centre line of the driver and driven shafts are parallel and laterally offset from each other even at the coupling location (Figure 1.1 (b)). The amount of parallel misalignment is represented as, $\Delta\delta$.

In rotating machineries, a combination of angular and parallel misalignments is very common fault at the coupling (Figure 1.1(c)) as well as at the bearings (especially for long bearings). Such a misalignment of shafts leads to eventual failure of bearings or fatigue failure of shafts.

The vibration caused by the misalignment may also destroy the critical parts of the machine such as seals, gears, couplings, etc.

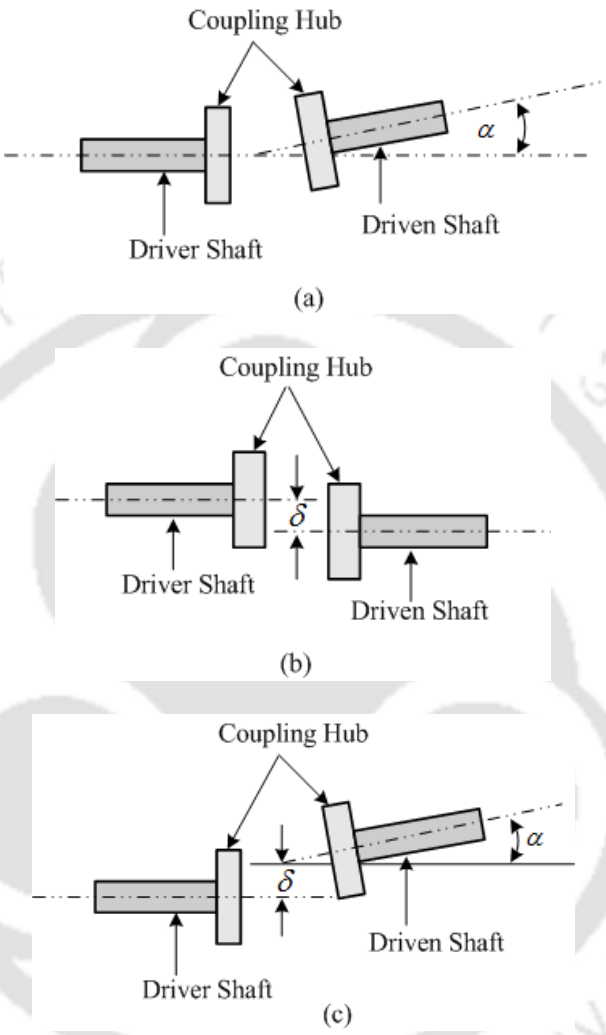

Figure 1.1 A schematic diagram of the (a) angular (b) parallel (c) combined misalignments between two shafts

The coupling is a device used to connect the driver and driven shafts together for transmitting power and to accommodate some amount of misalignment at their ends. Classification of mechanical couplings is presented in Figure 1.2 (Black and Adams, 1981; and Maleev and Hartman, 1999). In other kinds of coupling, the magnetic and hydraulic couplings are also in use.

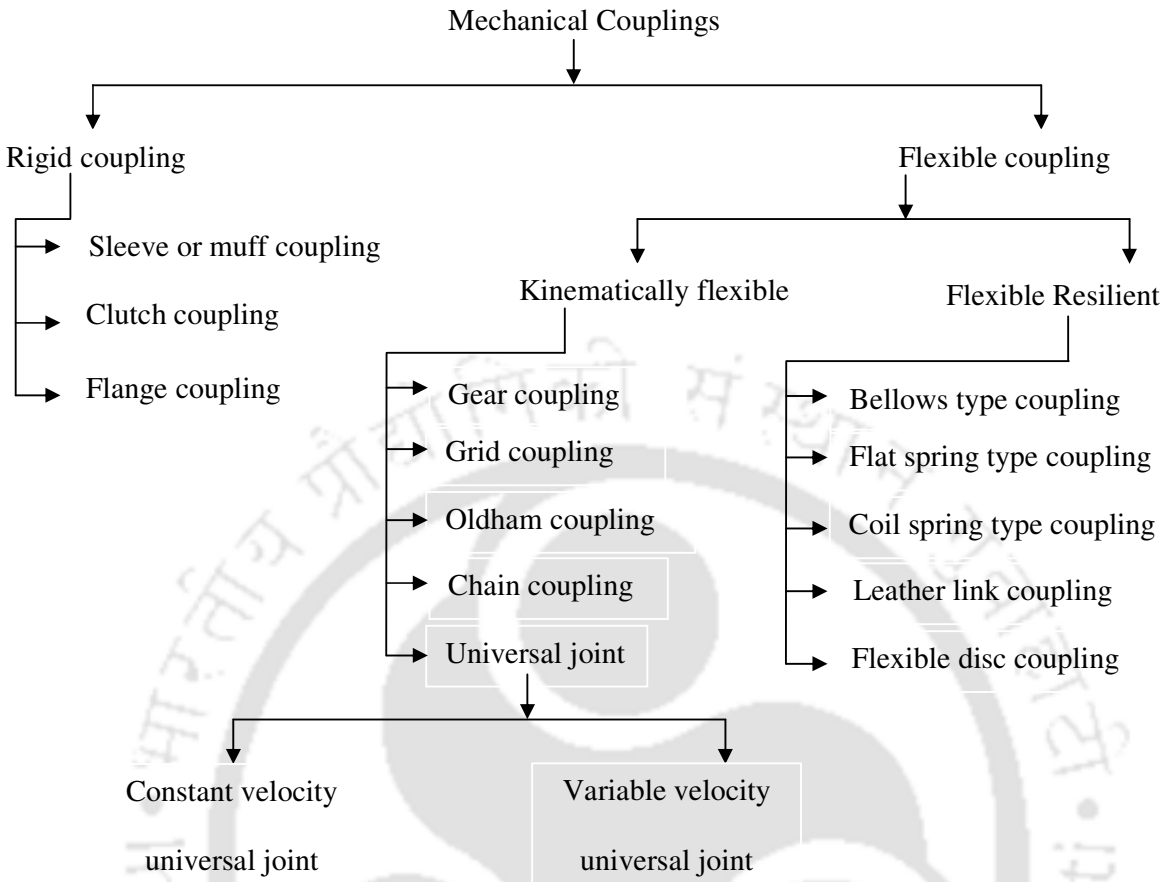

Figure 1.2 Mechanical coupling classifications

A brief overview of the basic type of couplings in use is described for completeness. Couplings can be classified in two broader ways

(i) *Rigid coupling*: A coupling used to rigidly connect two shafts, in which no misalignment is allowed, is called the rigid coupling. Hence, it is necessary for the shafts that are to be connected to be in good alignment, both laterally and angularity.

Rigid couplings can be further classified as follows (Piotrowski, 1986; and Wowk, 2000)

(a) Sleeve or muff coupling: It is simplest type of rigid coupling. It consists of a hollow cylinder or a sleeve called muff, whose inner diameter is same as that of the shaft. It is fitted over the shaft ends with the help of sunk keys. In this coupling the power is transmitted by means of key or sleeve (see Figure 1.3).

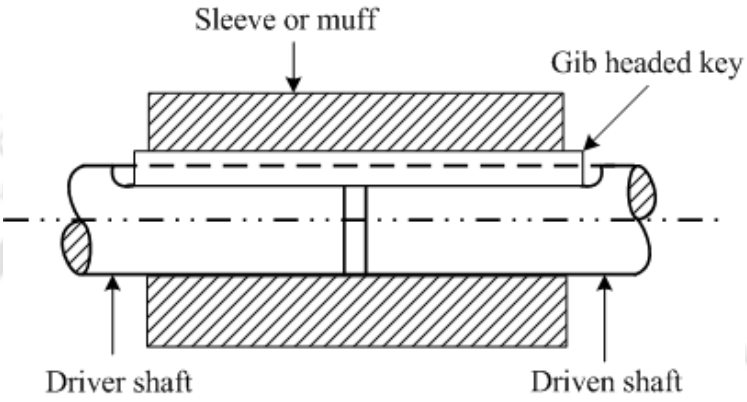

Figure 1.3 A sleeve or muff coupling

(b) Flange coupling: This type of rigid coupling consists of two flanges one keyed to the driver shaft and other to the driven shaft. The two flanges are connected together with the help of bolts (see Figure 1.4).

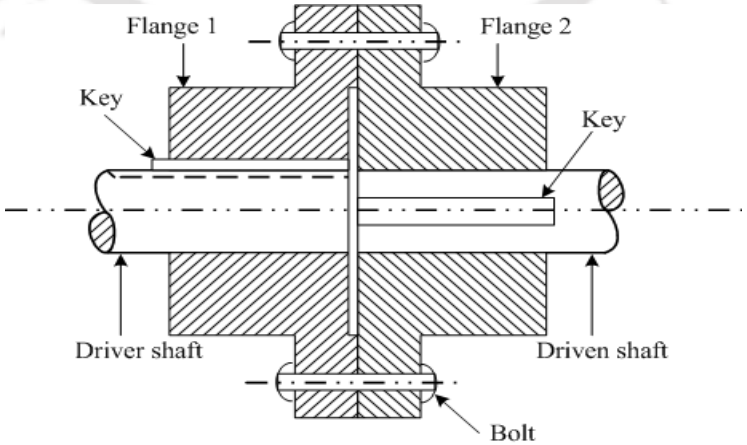

Figure 1.4 A flange coupling

(ii) *Flexible coupling*: A coupling used to connect two shafts having some misalignment is called the flexible coupling. Flexible couplings allow the fluctuation of torsional moment and angular speed.

Flexible couplings can be further classified as (Piotrowski, 1986; and Wowk, 2000)

(a) *Universal joint coupling*: The universal joint is one of the oldest of all flexible couplings (Figure 1.5). It is kinematically flexible. It is commonly known for its use on automobiles and trucks. The U–joints are mainly used to accommodate the large angular and small parallel misalignments. The output velocity fluctuates severely with the rotational angle and this limits its speed. A universal joint in its simplest form consists of two shaft yokes at right angles to each other and a four point cross which connects the yokes.

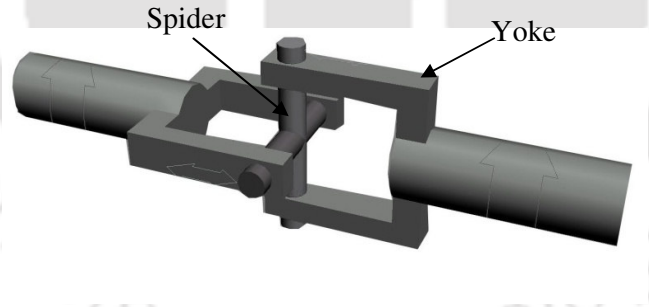

Figure 1.5 A single point universal joint

(b) *Oldham coupling*: The Oldham coupling (Figure 1.6) consists of two flanges which are connected perpendicular to the driver and driven shafts and an intermediate disc which rotates at the same speed as the driver and driven shafts. It is used to connect shafts that are not aligned and have parallel offset. It is also kinematically flexible.

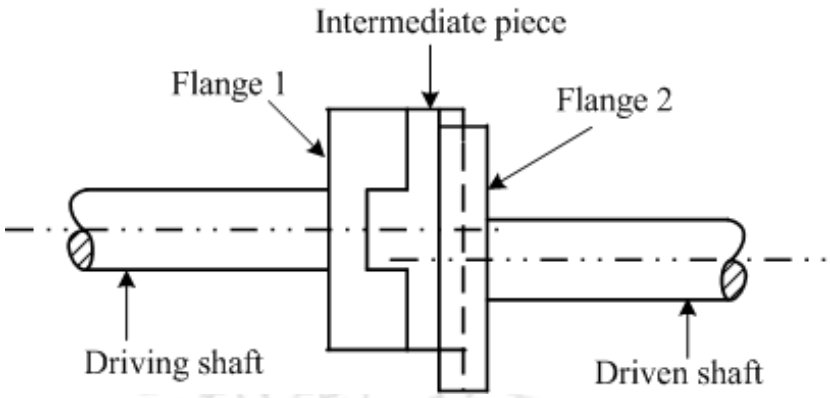

Figure 1.6 An Oldham coupling

(c) ***Gear coupling*****:** Gear couplings consist of two external gears on hubs that are keyed to the shaft and a one or two piece sleeve with internal gear teeth. The teeth may be straight or curved (crowned). For applications that require flexibility of more than a half degree, the curved teeth are better. These couplings obtain their flexibility from the backlash between two matting teeth. Gear couplings are used in the large equipment application (Figure 1.7).

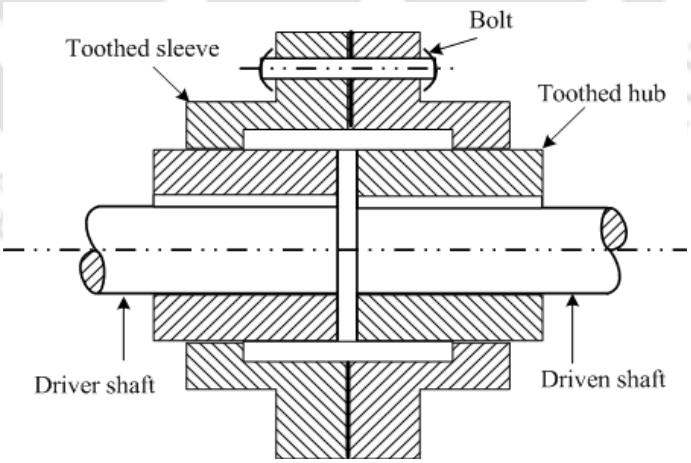

Figure 1.7 A gear coupling

(d) ***Grid coupling*****:** Grid couplings are very similar to gear couplings. It consists of two slotted flanges that are joined by a flexible steel band laced through the slot. These

couplings can dampen vibration and reduce shock loads by 10–30%. Grid couplings do not transmit much power as gear couplings but are less expansive. Grid couplings are used in the small equipment (Figure 1.8).

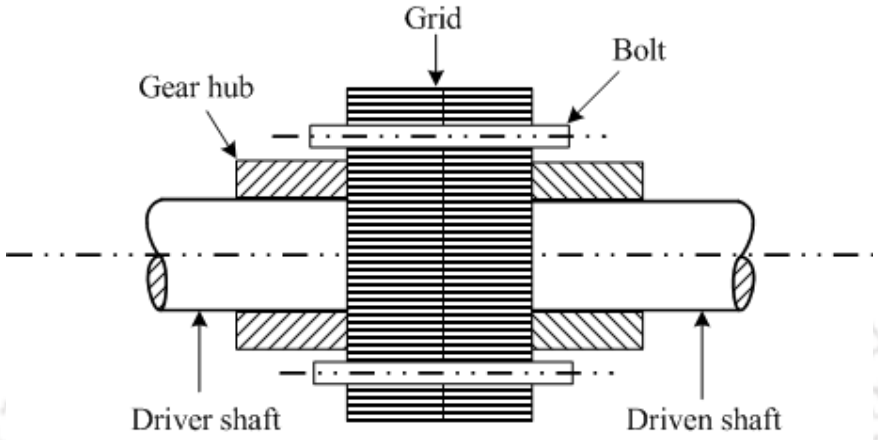

Figure 1.8 A grid coupling

(e) ***Beam coupling*****:** The beam coupling is made from a solid metal bar slotted with a continuous spiral cut. The beam is torsionally rigid with zero backlash. High speeds are possible up to 25,000 rpm with limited torque capability. Considerable axial movement is possible without affecting performance (Figure 1.9).

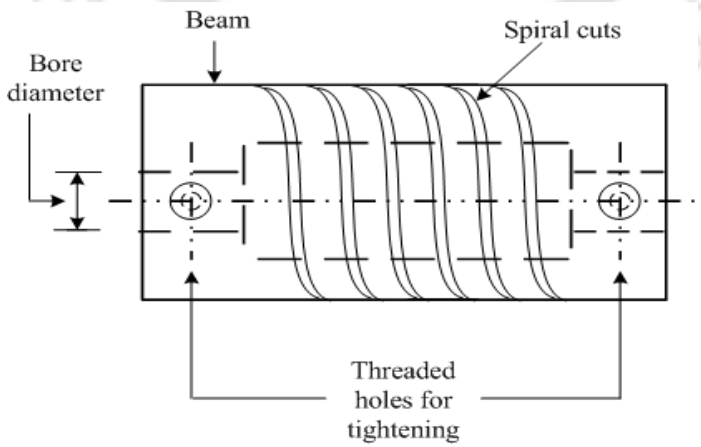

Figure 1.9 A beam coupling

(f) ***Three–Pin coupling***: The three–pin coupling consists of an upper interface plate with a triangular arrangement of shouldered or dowel pins. These pins are coupled to a plate with a triangular arrangement of oversized cutouts with flat or curved contact surfaces with which the pins make contact. The pins set against the contact surfaces by introducing an in plane preload force at the first pin using a bolt, compliant pin, or other mechanism (Hart *et al*., 2004).

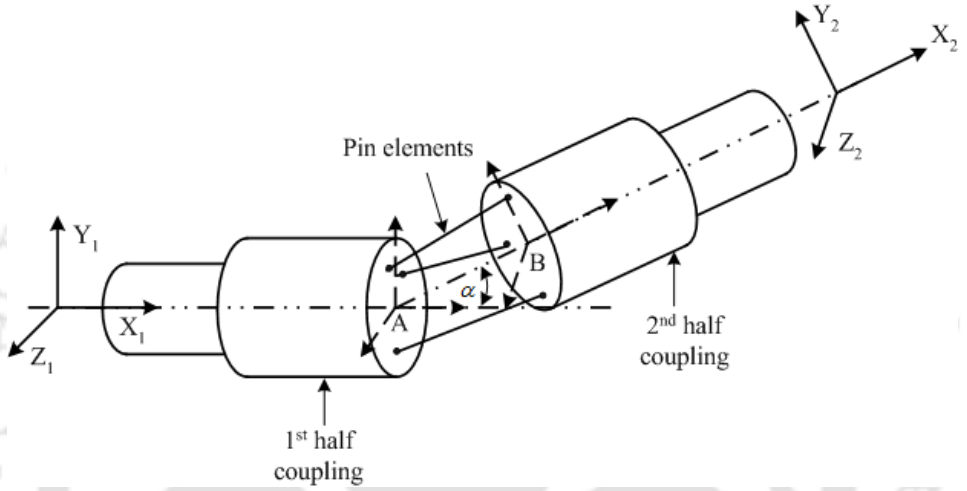

Figure 1.10 A Three–pin coupling

The misaligned rotor system received the early attention in later part of 1970's (Gibbons, 1976). Since then, this topic has become an important focus amongst the researchers and practitioners of the rotor dynamics. However, it has received considerable attention in last one decade (Li and Yu, 2001; Al–Hussain and Redmond, 2002; Prabhakar *et al*., 2002; Sinha *et al*., 2004a; Pennacchi and Vaina, 2005; Lees, 2007; Lees *et al*., 2009; Sarkar *et al*., 2010; Ganesan and Padmanabhan, 2011; Tadeo *et al*., 2011). The most of papers that have been discussed here modelled the fault as an equivalent force system which generally leads to erroneous results due to the non–unique solution. Thus the objective of the present study is to develop model based identification algorithm to estimate multiple machine–element faults including the estimation of misalignment forces and moments at couplings and bearings.

1.2 Background and Literature Survey

1.2.1 Background

As the present scenario is moving towards the super–critical, high–speed, light–weight and highly reliable drivelines; the rotating machineries are designed based on multi–objective functions involving the maximum strength and fatigue life, and the minimum weight and cost. The turbo–generator systems mounted on bearings and connected through couplings are basic machine elements of any rotating machinery. The proper functioning of these machinery greatly depends upon, the smooth and quiet running of the bearing and the amount of misalignment at the coupling location. In theory, the presence of misalignment in the rotating machine changes the dynamic characteristics of the machine and in reality it is very hard to observe the difference between dynamic characteristics of the healthy and misaligned rotors while they are in operation.

1.2.2 Importance of the Study

Although, the misalignment is a severe problem among various kinds of faults especially in turbine–generator systems which generate the misalignment forces and moments, it has not attracted that many researchers as it demands. Still its modelling has not reached up to the mature state. The unnecessary loads and unwanted vibrations generated due to the misalignment lead to a premature failure of the bearing, shaft or coupling. Although couplings are used to compensate the misalignment, still alignment of shafts is required for following reasons

- The coupling's useful life depends on the amount of misalignment.
- Shafts usually need to align much better than the coupling's capacity in order to run the rotor trains properlly.

- The initial alignment changes over time due to the bearing wear, foundation setting and thermal changes.

1.2.3 Literature Survey on the Rotor Fault Detection and Diagnosis

The literature survey on the estimation of multiple faults is presented in the present section. It is divided in following parts: (a) review articles (b) literature on estimation of residual unbalances (c) literature on estimation of bearing dynamic parameters (d) literature on estimation of misalignments, and finally (e) literature on estimation of multiple fault parameters (mainly bearing parameters, misalignment and residual unbalances). Subsequently, literature on condensation schemes has been reviewed. Condensation schemes have been extensively used in the present work.

(a) ***Review Articles on Faults in Rotating Machinery***

In this section review articles related to fault diagnosis techniques are summarised. Isermann (1997) reviewed works, which were published from later 1970's to later 1990's on different methods of the supervision, fault detection and fault diagnosis in rotating machineries. It begins with a consideration of knowledge based procedures that is based on analytical and heuristic information. Then different methods of fault detections are considered, which extracts information from measured signals and use signal models. These methods are based on the parameter estimation, state estimation and parity equations.

In the past few decades cracks in the rotor system has been well reviewed by Gasch, 1993; Dimarogonas, 1996; Sabnavis et al., 2004; Song and Chung, 2010. These works in the past has been carried out by considering the crack in the structure/shaft as the main fault in the system. A survey on the stability of a rotating shaft with a crack and its forced vibrations due to unbalance was provided by Gasch (1993). He established some possibilities for the early

crack detection using a Lavel (or Jeffcott) rotor (a single disc on an elastic shaft) with a simple crack model. Works, published from 1971 to 1994 on the dynamic response of rotors and other structures with the crack was reviewed by Dimarogonas (1996). There are three basic methods for dealing with the problem of crack modelling, such as the equivalent reduced section, the local flexibility from fracture mechanics theory and the cracked continuous bar. The methods for the crack identification in rotating shafts are the recognition of the vibration coupling due to cracks; the parametric vibration and the bilinear and non–linear effects.

Edwards et al. (1998) reviewed the fault diagnosis techniques developed for the condition monitoring of rotating machinery. The mass unbalance, bowed shafts and cracked shafts, these are the rotor faults received special attention in this paper. The modelling and diagnosis techniques of these faults have well reviewed in this paper. And concluded that model based fault diagnosis techniques were developed rapidly in order to meet the present demand of condition monitoring of the rotating machinery.

Doubling et al. (1998) provided an overview of methods to detect, locate and characterize faults in structural systems by examining changes in measured vibration responses. The scope of this paper was limited to methods that use changes in modal properties (i.e., modal frequencies, modal damping ratios and mode shapes) to infer changes in mechanical properties. They suggested the issues for further developments of the existing fault detection methods such as the ability to account for the effects of nonlinear structural responses, constraints on the number of measurement sensors and locations. It was also opined that the literature in general needs to be more focused on the specific applications and research should be focused more on testing of real machineries in the operating environment rather than laboratory tests of respective machineries. Sabnavis et al. (2004) reviewed literature published

since 1990 with some classical works on the crack detection and the estimation of severity of the crack in shafts. The review was based on three categories namely vibration based methods, modal testing and non traditional methods. They also discussed the types and causes of rotor cracks and fundamentals of crack propagation.

Lees et al. (2009) presented a review on developments in the model based identification of faults in rotating machineries. Unbalance, rotor bow, rotor misalignment, bearing dynamic parameters and rotor crack are the faults of which modelling has been discussed in this article. They concluded that although quantification of faults may require a number of tests to be performed but it was observed that model–based estimation played a significant role in the rapid resolution and quantification of faults. Heng et al. (2009) reviewed the diagnosis techniques available to monitor the health of rotating machineries. In this review article, they discussed the merits and demerits of present diagnosis techniques. They categorised the existing methods to predict rotating machinery failure as (a) the event data based prediction, (b) the condition data based prediction and (c) the prediction based on both the event and condition data.

Lei et al. (2013) reviewed the signal based diagnosis techniques available to monitor the faults in rotor systems. It dealt with the research and development of the empirical mode decomposition (EMD) technique in the fault diagnosis of rotating machineries. It surveyed the application of EMD in fault diagnosis based on the diagnosis objects such as the rotor, bearing, gear, etc.

The review works that are available up–to–date have been presented and cover the literature up to 2013. Researchers have found that vibration techniques have the scope to a flexible,

multidisciplinary and robust detection methodology for different faults in rotor and this would go a long way to increase the overall reliability and safety of rotating machinery, in general.

(b) ***Literature on Estimation of Residual Unbalances***

An unavoidable fault that generally present in the rotor system is residual unbalances. With the state–of–the–art in the residual unbalance estimation (Gnielka, 1983; Morton, 1985; Edwards et al., 1998; Zhou and Shi, 2001; Tiwari, 2005; Jardine et al., 2006; Lees et al., 2009), it is clear that the estimation of residual unbalances in rotor systems is an age–old problem among the identification of various other faults (for example shaft cracks, shaft misalignments, shaft bent/bow, gear–fault, bearing–fault, motor–fault, etc.). However, now the trend in the estimation of residual unbalances is to reduce the number of test runs (Edwards et al., 2000; Zhou and Shi, 2001; Pennacchi et al., 2006a; Lees e*t al.*, 2009, Sudhakar and Sekhar, 2011 and Zhang *et al.*, 2011), number of measurements required, and the optimum placement of measurement sensors and balancing planes, especially for the large turbo–machineries or rotor trains where the downtime is very expensive and accessibility is limited. In this section, literature containing estimation of residual unbalance in flexible rotors is summarised.

From the state of the art, methods of the balancing can be categorized into two groups; *the influence coefficient method*, which only requires the assumption of linearity of both the machine and measuring system, and *modal balancing* which in addition, requires accurate knowledge of the modal properties of the machine. The influence coefficient method requires less a priori knowledge of the system and techniques have been well developed to make optimum use of redundant information (Drechsler, 1980). The approach has a significant disadvantage of requiring a number of test runs onsite. Modal approaches require fewer test runs; Gnielka (1983) used a prior knowledge of mode shapes and modal masses, and

compared results to those from a numerical model of the machine. Morton (1985) proposed a method to balance a flexible shaft without the use of trial weights. In this paper, they also suggested a method to separate out the unbalance and bearing characteristics to find out bearing parameters by using known shaft responses. The work of Krodkiewski *et al.* (1994) has similar requirements and seeks to detect changes in unbalances from the rundown data. Both these approaches place reliance on the numerical model. Numerical models of rotating machinery have been used to great extent over a number of years (McCloskey, and Adams, 1992), and their accuracy and range of effectiveness have been steadily developing. Traditional techniques for balancing turbo generators require at least two run–downs, with and without the use of trial weights respectively, to enable the machine's state of unbalance to be accurately calculated (Parkinson, 1991). Lees and Friswell (1997) presented a method to evaluate state of unbalance of rotating machine utilising the measured pedestal vibration. Subsequently, Edwards *et al.* (2000) presented the experimental verification of the method (Lees and Friswell, 1997) to evaluate the state of unbalance of a rotating machine by using a single rundown data. The excitation due to both the unbalance and the shaft bend were considered in the analysis. The algorithm requires a single run–down response information to estimate the unbalance and foundation parameters. The authors reported that the vibration level was reduced by 92% after balancing the rotor system.

Shih and Lee (1997) proposed a method to estimate the unbalance distribution in a flexible rotor on rigid discs with constant eccentricity based on the transfer matrix method (TMM). The rotary inertia, gyroscopic effect and transverse shear effect was included in the flexible rotor modelling. The applicability and feasibility of the proposed method was checked by three different numerical examples and the estimation was found to be robust. The proposed method requires the state vector information at the free end only to estimate the unbalance. Zeng and Wang (1999) proposed a method called the *single–point discrete Fourier*

transformation to identify the unbalance and to achieve the field balancing on the basis of correlation theory. In their model they balanced a dual rotor system in which the inner rotor was enclosed wholly in the outer rotor. They used four planes for balancing: two for each rotor, to balance the rotor system completely.

Zhou and Shi (2001) presented a review on different techniques developed to perform the active balancing and the active vibration control for rotating machinery. This review mainly concerns with two major techniques of the active vibration control for rotating machinery (a) the direct active vibration control and (b) the active balancing techniques. They also summarised different techniques to model the rotor system.

A model based technique for the online identification of the unbalance in a rotor system was discussed by Jain and Kundra (2004), they modelled the fault as equivalent load. The model developed was validated through the numerical simulation as well as by experiment on a real rotor system. They concluded that the model based technique proposed was able to determine the position, extent and orientation of unbalance numerically and it compared well with the experimental findings.

Naucler and Soderstrom (2010) performed parameter estimation in which they estimated the unbalance in rotating machinery based on the influence coefficient method. In their regression model, unknown parameters entered as non–linear terms which were reformulated through a linear estimation procedure with a closed form solution. They have compared two procedures viz., the linear deterministic estimation and the non–linear regression. They also analysed these procedures with respect to their statistical accuracy for the unbalance estimation, and concluded that the non–linear estimation gave the better estimate.

Equivalent loads (i.e., the difference between equivalent loads estimated in the system due to faults and the load obtained from the theoretical model) minimization method is one of the model based technique to identify faults in the rotor system. However, the main disadvantage of this method is that it requires measurements at all DOFs (which has practical difficulty of measurement location and number of sensors) to minimize the error between equivalent load estimated and theoretical model value. This was addressed by Sudhakar and Sekhar (2011) in their identification procedure. They used the modal expansion technique instead of taking measurements at all DOFs. The FE modelling with 4–DOFs per node was considered to obtain the system frequency equation. They concluded that the unbalance (i.e., the location and severity) could be estimated with a fairly good accuracy.

The present literature survey covers the development in the estimation of unbalance and it could be concluded that literature are quite rich. And it could be observed that model based methods gained more importance in estimation of unbalance in rotor system due to their ability to identify both the location and the severity of other faults, also to be reviewed subsequently. In the subsequent section another important fault (bearing fault) associates with rotor system has been discussed.

(c) ***Literature on Estimation of Bearing Dynamic Parameters***

Rotating machineries supported on bearings play a vital role in determining the behaviour of the rotating system under dynamic loads. One of the most important factors governing the vibration characteristics of rotating machinery is the bearing and coupling dynamic parameters. The influence of bearing dynamic characteristics on the performance of the rotor–bearing was recognised for long time. One of the earliest attempts to model a journal bearing was reported by Stodola (1925), he represented the fluid film of bearing as a simple spring support, but his model was incapable of accounting for the observed finite amplitude of

oscillation of a shaft operating at a critical speed. Now rotors be modelled quite accurately, however, due to difficulty in obtaining actual test conditions and associated material parameters; the well developed theoretical analysis to obtain the bearing and seal dynamic parameters (Smith, 1969; Someya, 1976; Hamrock, 1994) fail to give satisfactory results (Goodwin 1991; Swanson and Kirk, 1997; Tiwari *et al*., 2004). Extensive literature are available on this topic and some important of them have been discussed below.

Morton (1975) developed an estimation procedure for the transient excitation by applying a step function forcing to the rotor. With the help of a calibrated link of known breaking load, the sudden removal of the load on the rotor in the form of a step–function (i.e., the broad band excitation in frequency domain) was used to excite the system. The Fourier transform was used to calculate the FRFs. He assumed the bearing dynamic parameters to be independent of the frequency of excitation. The analytical FRFs, which depend on the bearing dynamic coefficients, were fitted to the measured FRFs. He also included the influence of shaft deformation and shaft internal damping into the estimation of dynamic coefficients of bearings. Among the experimental methods, the impact excitation method proposed by Nordmann and Scholhorn (1980) to identify stiffness and damping coefficients of journal bearings is the most economical and convenient. The impulse force has an advantage that it contains many excitation frequencies simultaneously and a single impact force can excite several modes. In this work analytical frequency response functions, which depend on bearing dynamic coefficients were fitted to measured responses.

Tieu and Qiu (1994) developed a method to estimate the linearized coefficient of journal bearings by using unbalance responses based on the least–squares technique. The methodology developed was tested with a real experimentation on a test rig and they concluded that the experimentally calculated bearing dynamic parameters showed well

agreement with the theoretical result given by Lund and Thomsen (1978). Also concluded that the FFT combined with the re–sampling technique could greatly simplify the data process and minimises the noise influences. A technique to estimate non–linear stiffness parameters of rolling element bearings in the rotor–bearing system was developed by Tiwari and Vyas (1995) based on the random response analysis obtained from a rotor–bearing rig. The Fokker–Planck equation was used to model the rotor–bearing system. The advantage of the method is that it does not require an estimate of the excitation forces and works directly on the measured response signals of the system.

Hu *et al*. (2000) designed a rig where the rotor system was supported on four journal bearings. The vibration behaviour of a statically indeterminate rotor bearing system was predicted to be significantly depended on the lateral misalignment. Such misalignments affect the reaction forces at the bearing pad, the journal eccentricity, the static deflection line of the rotor, and the stiffness and damping coefficients of the journal bearing. Theoretical result showed that the changes in bearing reaction forces due to the misalignment not only altered the static deflection line but altered the journal steady state eccentricities in bearings, and thereby altering dynamic coefficients of the journal support.

Tiwari *et al*. (2002) developed an identification algorithm to quantitatively estimate the speed–dependent bearing dynamic parameters for a multi–degree–of–freedom (MDOF) system using unbalance responses. The conditioning of the regression matrix was also discussed by using the regularization and generalised singular value decomposition techniques. They reported that the information of clock–wise and counter clock–wise rotation direction measurement in the algorithm improves the condition of the regression matrix. Saavedra and Ramirez (2004a, b) proposed a coupling stiffness matrix and used it in the FEA of a misaligned rotor system. However, the derived stiffness coefficients vary with shaft

rotation even in the absence of misalignment, in addition the important torsional–DOFs were not considered and bending–axial coupling was also not evident.

From the above review, it could be concluded that literature on bearing dynamic parameters are in abundance. the advantage of estimating bearing dynamic parameters along with other fault parameters are in two folds, i.e. it reduces modelling error of bearings and an additional indicator of the impeding fault (e.g., the misalignment) in the system in the form of changes in bearing dynamic parameters to be reviewed in the subsequent section. The next section deals with the literature survey on the estimation of misalignment or coupling dynamic parameter.

(d) ***Literature on Estimation of Coupling Parameters or Misalignment***

A detailed literature review on the modelling and estimation of misalignment is presented in this section. Based on the literature survey conclusions would be derived for the potential research on the misalignment at couplings and bearings.

The misaligned rotor system received the first attention in later part of 1970's (Gibbons, 1976), he analysed the effect of forces and moments developed due to the misalignment. However, he did not discuss the vibration signature of the system. In this analysis he concluded that all the torsionally loaded misaligned couplings have restoring moments which tends to bow the machine shaft. The amount of bow, which can cause machine vibration, increases with the higher speed.

Nelson and McVaugh (1976) derived the generalized equations of motion (EOMs) in both the fixed and rotating frame of references for the complete rotor–bearing system by using the FEM. In the development of EOMs only the linear stiffness and the viscous damping is

considered, however, it is applicable for non–linear bearing parameters. The flexible coupling effect was included in the model to take the misalignment into account, to achieve the effect of misalignment a periodic force was considered at the coupling. Natural whirl speeds and modes were calculated in this analysis. They also concluded that the FE model can be utilized to model rotor–bearing systems for the purpose of determining critical speeds, stability bands, transient responses, unbalance responses, etc. Hori and Uematsu (1980) studied the influence of misalignment of the journal bearing on the stability of a multi–rotor system. The model used was composed of two different, as well as similar, rigidly coupled rotors mounted on four bearings. The transfer matrix method was used to simulate the problem and the quasi–catenary alignment (in this neither the shearing force nor the bending moment appears at the coupling) was used for the aligning. The frequency equation obtained from the transfer matrix method was solved by the Newton Raphson method, and the stability of the system was judged by the sign of the real part of its root. From numerical analyses, it was deduced that when two rotors were same, the best stability was obtained for the zero misalignment and in the case where they were different, the stability was obtained at a certain amount of the misalignment.

Dewell and Mitchell (1984) analyzed vibration frequencies for a misaligned metallic–disc flexible coupling. They performed the signal based analysis and reported that dominant frequencies were 2× and 4× of running speed components due to the angular misalignment. Lorenzen *et al.* (1989) investigated a comparison of critical speeds of a high–speed compressor train alternatively equipped with different types of couplings. In this, the unbalance response using different types of couplings was calculated, which led to the conclusion that the solid type couplings can make a system more stable compared to other types of couplings.

Krodkiewski and Ding (1993) developed a general approach for onsite identification of the misalignment of a turbo–generator system. In this analysis the estimation algorithm required dynamic forces acting on the bearing, which was calculated through a non–linear mathematical modelling done for the turbo–generator system. Jordan (1993) did the orbit analysis of the misaligned rotor and concluded that the misalignment initially affects 1× response resulting in an elliptical orbit, but in the case of severe misalignment the orbit plot may look like a figure eight due to the appearance of a 2× component in the response. These features are usually used for the detection of the rotor misalignment.

Xu and Marangoni (1994a) developed the theoretical model for a complete motor, flexible–coupling and rotor system subjected to the misalignment and the unbalance. Universal joint effect was included in this model to take the misalignment effect into account. The component–mode synthesis method, based on the theoretical model, was applied. They also derived generalized EOMs for a complete system by considering all the six–DOFs per node. In this study, each component is modelled independently by the FEM to get its modal character. Later, an experimental study on a rotor–kit to verify the theoretical model of the misalignment and the unbalance was performed by Xu and Marangoni (1994b). In this an experiment was performed by using a self–designed coupling and a commercial helical coupling, and validated the result with theoretically calculated data under the same misalignment and unbalance conditions. An inline shaft torque sensor is used to measure the dynamic torque signal. The alignment in both orthogonal directions was conducted to obtain the best alignment results. At the end they concluded that the change in the flexible coupling in a misaligned system may shift the natural frequency, may increase or decrease the vibration response but the frequency pattern in vibration spectrum remains the same.

Sekhar and Prabhu (1995) numerically evaluated the effect of coupling misalignment on vibration responses of the rotor. They considered four degrees–of–freedom (DOFs) per node to model the rotor system with a misalignment. Forces and moments due to the misalignment were determined. They reported that 2× vibration responses as the characteristic signature of the misaligned shaft. Lee and Lee (1999) derived the theoretical model for the rotor–coupling–bearing system with the misalignment. An axi–symmetry rubber coupling was used as the coupling element, which was more flexible than the shaft. The effect of misalignment on the dynamic characteristic such as the whirling orbit, frequency response and parameter sensitivity were investigated. The experimental and simulation results showed that the whirling orbit tended to collapse towards a straight line and the natural frequency associated with the misalignment direction increased linearly, as the angular misalignment increased due to the increase in effective moment stiffness of the bearing. On the other hand the parallel misalignment did not affect the whirling orbit and the natural frequency, also the whirling orbit and the natural frequency did not changed when a very flexible coupling was used.

Li and Yu (2001) modelled the non–linear coupled lateral and torsional vibrations of a rotor bearing system with a misaligned gear coupling. In this based on engagement conditions of gear couplings, constraint equations were developed, which described an inherent relationship between the lateral and torsional DOFs. The FE model was used to simulate the problem. The theoretical analysis showed that the forces and moments acting on gear couplings due to the initial misalignment were from inertia forces of the sleeve and the internal damping between the meshing teeth. The numerical analysis revealed that the even integer multiples of the rotating speed of the lateral vibration and odd integer multiples of the torsional vibration

occurred in the misaligned system and integer multiples of vibrations were apparent around the gear coupling.

Al–Hussain and Redmond (2002) analysed, two rotors system connected by a rigid–coupling with a pure parallel misalignment, first theoretically and then numerically. For the numerical analysis a combination of the Newmark and Newton–Raphson methods were used to determine dimensionless frequency and transient responses of the misalignment magnitude. They concluded that at the steady state condition 1× rotational speed was present in the translation and angular directions, which indicated that the parallel misalignment was a source of the lateral and torsional excitations. Al–Hussain (2003) analyzed the stability of two rigid rotors connected by a flexible coupling with an angular misalignment. The rotor system was mounted on hydrodynamic bearings that contained the direct and cross–coupled stiffness and damping coefficients, which were function of hydrodynamic characteristic and calculated from the solution of Reynolds equation. Energy expressions were derived and the stability criteria were obtained by using the Liapunov's direct method. At the end they concluded that the stability region increases as the angular misalignment and the coupling stiffness term increases.

DeSmidt *et al*. (2004) developed a non–dimensional model that included both the shaft bending and torsion flexibility along with the kinematics of misalignment between the universal joints (U–joints). They also explored the effect of internal damping, external damping, misalignment, and load torque on the stability of a rotor system connected with a U–joint. It was also discovered that the misalignment and the load torque had stabilizing and destabilizing effect for a certain value of the external damping, the misalignment and the load torque. Muszynska (2005) pointed out that any constant radial force (or a constant moment

about a radial axis) on a rotor could be a cause of the misalignment and could shift the normal operating point of the rotor within the bearings, which in consequence may trigger the nonlinearity. This nonlinearity in the system is the reason for the presence of second and other higher order harmonics.

Pennacchi and Vania (2005) used a complete mathematical model of a gas turbine–generator unit of a small power plant to estimate the angular misalignment in a flexible coupling. They calculated the response of the system due to moments applied at the coupling and compared this with a least–squares fit method based on responses a machine at a series of frequencies. Attiahili *et al*. (2005) presented two approaches adopted for the study of the angular misalignment that allowed the characterization and the identification of the defect from the vibration response. The defect is essentially characterized, in frequency domain by the presence of two dominant peaks, the first corresponds to the running frequency and the second to two times the running frequency.

Lees (2007) analysed rigidly coupled rotors mounted on linear bearings. In this model, two shaft systems connected by a series of bolts that on the first shaft were distributed around the perimeter at a radius and on the second shaft displaced by an amount, which was the amount of parallel misalignment. He also derived the EOM for the system and showed that the torsional and bending motions are coupled because of the misalignment.

Cho and Jeong (2008) proposed a method for the use of genetic algorithm based feature selection and signal filtering to construct a reliable calibration model of the shaft misalignment. Alignment measurements were made using a laser alignment system. The study showed that for the shaft misalignment it produced better performance than traditional multivariate statistical approaches such as the principle component regression and the partial

least–squares. Determination of the timing of maintenance could be stated as the multivariate problem. The main goal of this calibration model was to predict the misalignment from the experimental or historical data. Zhao *et al*. (2008) investigated the influence of meshing force on the misaligned–rotor splined–coupling system and numerically simulated by the Newmark–β numerical integral method. The dynamic EOM for the complete system was derived by the FEM. This investigation showed, as the amount of the spline thickness and the parallel misalignment increased the meshing force increased non–linearly.

Bouaziz *et al*. (2009) presented the dynamic behaviour of a misaligned rotor system, here the rotor was mounted on two hydrodynamic journal bearings and had two–DOF. The rotor system was discretized by means of FEM and then solved numerically by the Newmark method. The bearing characteristics were obtained from the Reynolds equation by using the Gauss–Seidal method. EOMs were obtained by applying the Lagrange's equation. At the end they concluded that the amplitude of vibration decreases with the increase in the value of relative eccentricity. Hariharan and Srinivasan (2009) performed experimental studies on the vibration signature of the misaligned rotor system. They used self–designed 3–pin flexible coupling in a rotor system. They compared the experimental result with the ANSYS result and reported agreement between these two results.

Patel and Darpe (2009a and 2009b) investigated the influence of types of misalignment on the rotor vibration. The coupled rotor system was modelled using Timoshenko beam elements with all six–DOF. The force vector was found using the misalignment coupling stiffness matrix derived from the experimental data and the applied misalignment between two rotors. Along with the lateral vibration, the axial and torsional vibrations were also examined and it was found that the misalignment couples the vibration in the bending, longitudinal and torsional modes. Tasi and Huang (2009) derived the transfer matrix for a rotor coupler system

with the parallel misalignment. The model was composed of flexible shafts, unbalanced disks, elastic supports and a shaft coupler. The shaft used was Rayleigh's type (i.e. including the rotary inertia as well) and the coupler was modelled as a linear spring combined with the bending spring between two shafts. The investigation showed that the shaft coupler altered the rotors critical speeds and the misalignment caused an external preload and dominates the response at the most of rotor speeds.

A rotor bearing system under misalignment condition was studied by Huer and Zhaojian (2010). In this study they compared two kinds of vibration characteristics i.e., the zero torque excitation and the linear torque excitation. The FFT and wavelet transform was used to analyse the experimental data and concluded that certain torque excitation could control the oil–whirl to a certain extent. On the other hand, the linear torque excitation increases the amount of misalignment. Changlin and Yiqun (2010) analyzed the nonlinear characteristic of the rotor–bearing model due to the misalignment force. In this study they used the gear coupling to connect two rotor shafts. Equations of motion were obtained by using the numerical value integral method. In this analysis they concluded that misalignment couples the periodic, quasi–periodic and chaos motions.

Sarkar *et al.* (2010) proposed a two–step nonlinear FE analysis for the misaligned multi–disk rotor mounted on short oil–film bearings. In their analysis the stiffness terms are considered as the displacement dependent and misalignments are modelled using Lagrange multipliers. Ganesan and Padmanabhan (2011) analysed the dynamic characteristic of a flexible coupling with the parallel misalignment by modelling stiffness parameters as a time–varying with the help of finite element method (FEM). They also considered a stiffening effect due to

centrifugal forces in the modelling of the coupling by the FEM and that lead to speed–dependent dynamic properties of the coupling.

Tadeo *et al*. (2011) investigated the dynamic characteristic of the flexible coupling. In this analysis they compared four different coupling models to see which model best predict the dynamic behaviour of the coupling. Finally, came to the conclusion that a second model by Nelson and Crandall (1992) that included the rotational stiffness and damping with the inertia effect best predicted the dynamic behaviour of the coupling.

Pennacchi *et* al. (2012) studied the non linear characteristic of the misaligned rotor mounted on journal bearings. The main aim of the present paper was to study the super harmonic components i.e., the nonlinear behaviour, in the rotor vibration spectrum as a consequence of the rigid coupling misalignment. They reported that during a complete shaft revolution, a periodical change of the bearings load occurs on hyper–static shaft lines due to the coupling misalignment. Didier *et* al. (2012) proposed a methodology to understand the effect of uncertainties on the nonlinear dynamic response of the rotating machinery due to multiple faults, i.e. the unbalance, asymmetric shaft, rotor bow and misalignment. They proposed the harmonic balance method with a polynomial chaos expansion to handle uncertainties in this kind of nonlinear problem.

The aim of the present section was to summarize diagnostic methods and coupling models developed to take the misalignment effect into account. Coupling imparts dynamic parameters to rotor systems and often they are speed–dependent and even time–varying. From this survey, it could be concluded that the misalignment is a severe problem in rotor system but still its quantitative estimation and modelling has not attracted as many researchers as it

actually requires. In the subsequent section detailed survey on estimation of multiple faults has been presented with the misalignment as one of the major fault in the rotor system.

(e) ***Literature on Estimation of Multiple Faults***

In the present scenario, the trend is towards the characterization of model parameters of multiple machine–element faults from experimental measurements. In the field of model–based identification of multiple faults, very few authors have attempted different fault conditions together or the same fault at multiple places in rotor systems. Identification procedures of multiple faults have the complexity many fold as compared to the single fault because the number of unknown fault parameters increases drastically.

An abstract representation of the multiple fault condition and its identification procedure is illustrated in Figure 1.11. Figure 1.11(a) illustrates the standard model testing (Ewins, 1984), in which we seek system modal parameters from the force and response information during the identification; however, we do not seek individual machine–element parameters. Figure 1.11(b) and Figure 1.11(c) represent model updating (Friswell and Mottershead, 1995) of a single machine–element and multiple machine–elements, respectively. The shaft modelling could be done quite accurately with available modelling methods, e.g. by the FEM with Timoshenko beam theory. Thus, in the model–updating one only seeks identification of parameters of machine–elements that are difficult to model accurately. The model updating identification procedures work even with the partial information of the force and the response, which is not the case with the modal testing. In Figure 1.11, the grey colour within the system (i.e., the rectangular box) represents unknown information and various shapes (i.e., square, circle and triangle with grey colour filled) represent different critical machine–elements of which identification of parameters has to be performed. A detailed

review on the modelling, analysis and the estimation of MFPs has now been presented in the present section.

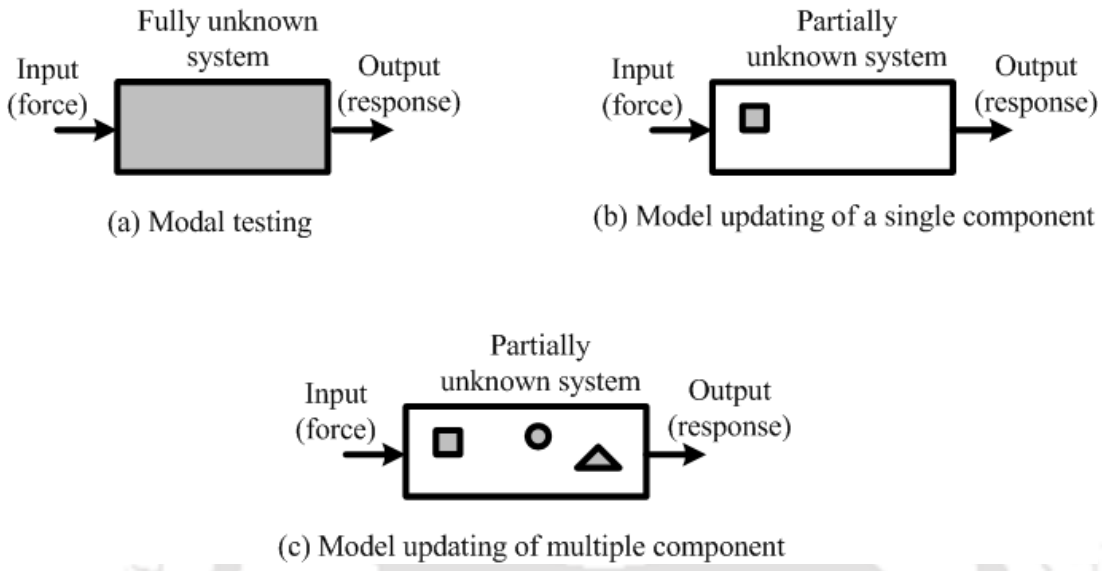

Figure 1.11 An abstract representation of the modal testing and the model updating

Sekhar and Rao (1996) analysed a rotor–bearing–coupling system with two major faults i.e., the misalignment and the crack, together. The shaft–to–shaft misalignment at the coupling location and the flexible coupling model was considered in this analysis. They studied 1× and 2× component of vibration responses to distinguish the crack from the coupling misalignment and concluded that the rate of increase in 2× is greater in the case of misalignment as compared to that caused by the crack. Sinha *et al*. (2002) proposed a methodology to estimate the unbalance and foundation dynamic parameters of the flexible rotating machinery by dividing the whole frequency range into different frequency bands. The advantage of using different frequency band is that it has the information of different modes separately which gives reliable estimation.

Prabhakar *et al*. (2002) analysed the crack versus the coupling misalignment on rotor system responses in transient conditions. They came with the conclusion that the coupling misalignment had symptoms very similar to cracks in the shaft but the continuous wavelet transform (CWT) is more sensitive to a small amount of misalignment as compared to a small crack depth. The misalignment effect has been modelled here by considering the harmonics of forces and moments generated at the coupling due to the misalignment. Bachschmid *et al*. (2002) presented a model–based identification method for multiple faults (i.e., the unbalance, rotor bow, rigid coupling misalignment, transverse crack, journal ovalization, etc.) by a least–squares fitting approach in frequency domain, by means of the minimization of a multi–dimensional residual between vibrations in some measuring planes on the machine and calculated vibrations due to the acting faults. The method requires the definition of models of elements that compose the system; i.e., the rotor, bearings and the foundation, as well as the models of the faults, which could be represented by harmonic components of the equivalent force or moment systems. The identification procedure was validated with experimental responses obtained from a test–rig.

Bachschmid and Pennacchi (2003) presented a model based identification technique to estimate the residual unbalance, thermal bow, fatigue crack, and the radial and angular misalignments. The aim of the article was to show that the developed method was able to locate the actual fault, to evaluate its severity and to discriminate among faults that had similar symptoms. An experimental validation of the proposed methodology was performed on both on real machinery and on a laboratory test rig. Residual unbalance was evaluated experimentally to check the accuracy of the developed method.

The method developed based on the measurement of a single run–down data to estimate the state of unbalance and foundation parameters was used by Sinha *et al*. (2004a) to develop a methodology to estimate the rotor unbalance and the misalignment together with foundation parameters. The steady load in bearings has a great influence on the bearing dynamic characteristic, so to investigate the influence and to evaluate the steady load in oil–film bearings Sinha *et al*. (2004b) performed a non–linear optimization of the curve–fit between the measured and model behaviour. The theory developed was supported by two distinct examples one was a simple test rig (consist of a shaft mounted over two fluid–film bearings at ends and connected to motor shaft through a flexible coupling) another was the Aston rig (consist of two shafts connected together with a rigid coupling mounted over four oil lubricated journal bearings). However, they used theoretical models for bearings that were expected to give large modelling errors.

Tiwari (2005) proposed algorithms for the simultaneous estimation of residual unbalances and bearing dynamic parameters in a rotor–bearing system. In this analysis three different methods proposed to improve the condition of regression matrices and concluded that the measurement involved by the auxiliary unbalance unit to get responses corresponding to forces, alternatively in the clock–wise and counter clock–wise directions, gave the best estimates of bearing dynamic parameters along with unbalances. Pennacchi *et al*. (2006a and 2006b) developed a model–based fault–identification technique for large rotating machinery. The effect of faults was modelled by means of equivalent force systems and an identification technique based on the least–squares was proposed. Faults considered here were the rotor bow, rigid coupling misalignment and rotor crack.

Jayaswal *et al*. (2008) presented a review article on developments in the machine fault signature analysis especially to the vibration signature analysis. They reported that different machine faults e.g. gear faults, rolling contact bearing faults, flexible coupling faults and electrical machine faults that could be detected from vibration signature analysis. However, authors mainly concentrate on the rolling element bearing fault signature analysis. Ping and Guang (2009) proposed a method for the multi–fault diagnosis of rotor systems using the blind source separation (BSS) technique for separating vibrational features produced by several faults that exist in the rotor system. Main faults dealt were impact rubs, cracks and oil whirl.

Tiwari and Chakravarthy (2009) experimentally estimated the residual unbalance and bearing dynamic parameters simultaneously in a rotor–bearing system. To check the suitability of identified parameters these were substituted in a FE numerical model of the test rig to generate the simulated response and showed that simulated responses were in well agreement with experimental responses in terms of mimicking the predominant resonance. Jalan and Mohanty (2009) developed a model based technique for the fault diagnosis of a rotor–bearing–coupling system under the misalignment and the unbalance at a steady state condition with the help of the residual generation technique. At the end they concluded that the frequency response of the healthy rotor system shows 1× running speed component only, whereas the rotor system with the parallel and angular misalignments with the unbalance shows 1× and 2× running speed components. Where 1× component is corresponding to the unbalance and 2× is corresponding to the misalignment.

Guo and Li (2009) presented a two stage method to determine the location and extent of multiple structural damages by using the information fusion technique and the genetic

algorithm. From numerical examples on a cantilever beam, it was found that the evidence theory are better than those frequency multiple damage location method. Singh and Tiwari (2010) developed a two–stage i.e., multi–crack detection and localization algorithm which identifies the number of cracks, their locations on a cracked shaft, their sizes, and the orientation angle of the cracks. The Timoshenko beam theory was applied to model the non–rotating shaft and FEM was used to obtain the system frequency equation. The methodology uses transverse forced vibrations of a non–rotating cracked shaft in two orthogonal planes at different frequencies. The genetic algorithm (GA) was used to fit the experimental measurement with the theoretical model by suitably defining the objective function. The proposed methodology identifies the presence of crack also estimates the location and size of the crack.

Kim and Lee (2010) analyzed beam like structures with a fatigue crack. They proposed a damage detection algorithm, which did not require comparative measurement of an intact structure. The method needed several measurements at different level of excitation forces of the cracked structure. The algorithm was verified with experiments as well as FE modeling.

Yang (2011) presented a method for the structural damage identification based on the flexibility disassembly. The basic idea of the method was to decompose a structural flexibility matrix into a matrix representation of the connectivity between DOFs and a diagonal matrix containing the magnitude information. The scheme could compute the stiffness perturbation parameter without any higher order sensitivity analysis or iteration. Shravankumar and Tiwari (2012) studied a Laval rotor with a disc unbalance in the presence of a transverse surface crack. They developed a model based identification algorithm to identify the unbalance, damping and crack parameters in the rotor system. The crack was modelled by using the

switching crack excitation function. The estimation of the switching crack function was also performed with different level of measurement noise.

Based on the literature survey discussed above it could be concluded that identification of multiple faults in rotor systems is indeed a challenging problem due to the increase in the number of unknown parameters and associated complexity in the modelling. The most of papers reviewed are using the signal based identification, i.e. the qualitative estimation. The disadvantage of signal based identification is that it can detect any fault but one cannot be sure that identified symptom is for a particular fault, because different faults may have similar symptoms. Even some researchers have attempted model based identification, i.e. the quantitative estimation of faults but the modelling of the coupling and its identification procedure has still not reached up to the mature state. Most of the work in coupling has been performed in isolation without considering bearings. As such coupling misalignment affects both the coupling as well as bearings since these are interrelated and coupled. The identification of dynamic parameters of couplings and bearings must be done simultaneously to capture actual conditions during the misalignment. This is the main motivation of the present work. Another problem which generally occurs in the large turbo−machinery is the practical difficulty of measurement location and number of sensors, so the numerical model requires some reduction schemes, which have been surveyed in subsequent section and it has been extensively carried out in the present research work.

1.2.4 Review on Condensation Schemes

When a rotor train is considered for its dynamic characteristics, it becomes more complex due to large DOFs. This leads to extensive computing time and corresponding costs. To overcome this, various techniques have been used to reduce the size of the full−model involved in the formulation.

The static (Guyan, 1965) and dynamic (Paz, 1984) condensations are the conventional and efficient techniques of the model reduction and are firstly applied to large FE models for the faster computation of the natural frequencies and mode shapes. In recent years, it has also been used in test–analysis of models correlation (Hou and Chen, 1995), and the vibration control and dynamic response analysis (Mills and Ing, 1996). Kane and Torby (1991) extended the modal reduction method to handle the non–symmetric rotor dynamic problems by eliminating unimportant modes and DOFs from the analytical model.

An iterative procedure for the dynamic condensation was proposed by Singh and Suarez (1992), while calculating eigen properties of the structure. An iterative improved reduction system (IRS) method that converges to the same transformation as the system equivalent reduction expansion process (SEREP) was given by Friswell *et al*. (1994). Friswell and Mottershead (1995) discussed various reduction schemes in order to eliminate DOFs to avoid the limitation of sensors and practical difficulty of measuring angular DOFs. Kim and Choi (2000) presented an analytical method, for the selection of DOFs in the condensation of eigen problems. The method was based on the energy associated with the DOFs in eigen modes of structural systems. The energy of the selected DOFs was used to predict the solution accuracy in each mode.

Dharmaraju *et al*. (2004) used the dynamic reduction method in their identification algorithm to reduce the number of response measurements. The identification algorithm had major limitation in that it requires measurement of rotational DOFs, since the conventional reduction method fails to eliminate them at the crack element nodes. This limitation was overcome by Tiwari and Dharmaraju (2006) in which they developed a novel hybrid

reduction scheme to eliminate the rotational DOFs without affecting the crack parameters at crack element nodes.

This brief survey on condensation schemes suggest that still depending on the requirement in numerical analysis and experimental model updating new condensation schemes are being developed.

Overall most of literature, as discussed above, has focused on modelling of couplings and its rotor dynamic analysis including the qualitative signature analysis for a possible identification of the misalignment. However, a very few have dealt with development of method for the quantitative experimental estimation of misalignment parameters, especially the model based, so as to have more insight into the misalignment effect and its identification procedure. Also the simultaneous effect of the misalignment in couplings and bearings in a rotor–bearing–coupling is a vital challenge that requires more careful explorations.

1.3 Motivation of the Present Work and Objectives

From the introduction and the literature survey discussed above it could be concluded that most of the rotating machinery, such as the power station turbo–generators, consists of a driver machine and a driven machine, which are coupled through either the rigid or flexible couplings. Combinations of the angular and parallel misalignments of the driver and driven shafts are the most common at couplings. The identification of bearing dynamic parameters in isolation and treating the shaft as rigid has been extensively addressed (Tiwari *et al*, 2004), however, for the flexible rotor–bearing system still its estimation requires more investigations (Tiwari and Chakravarthy, 2006). In a rotor train, misalignments at couplings and at bearings are a common problem and its identification is still a challenging area of research because it is difficult to theoretically model the misalignment at the coupling and bearings simultaneously;

and hardly any work has been reported showing its effect through experiments. Moreover, till now most of work has been carried out on the rigid rotor model to analyse misalignment but in the flexible rotor the amount of misalignment changes with different modes of excitation that has been addressed in the present work. Analyzing the combined effect of misalignment on each bearing and coupling is the real challenge in a turbo–generator rotor model. Effects on dynamic parameters of couplings and bearings due to misalignment conditions in a rotor–bearing–coupling system could be an excellent severity indicator of fault conditions due to misalignments.

Scopes

(1) Comparative study of rotor system could be performed by using different types of coupling models.

(2) Dynamic analysis of rotor train under combined misalignment condition i.e., misalignment at bearings as well as at couplings.

(3) Study of vibration signatures generated due to multiple faults associated with rotor system.

(4) Development of flexible, multidisciplinary and robust detection methodology to quantitatively identify multiple rotor faults together.

(5) Coupling model could be improved by adding more dynamic parameters of the coupling i.e., cross–coupled dynamic parameters (linear and angular cross coupling).

(6) Coupling model could be enhanced with the inclusion of speed–dependent and time–dependent dynamic parameters.

The main objectives of the present investigation are as follows:

- Development of a more realistic coupling model would be attempted, which could incorporate misalignment conditions in the rigid as well as flexible rotors.

- Development of an identification algorithm of MFPs (i.e., bearing and coupling dynamic parameters along with residual unbalances) and numerical testing would be performed for
    - (i) a rigid–rotor and flexible bearing–coupling system
    - (ii) a flexible rotor–bearing–coupling system
    - (iii) a flexible rotor–bearing–coupling system with the incomplete rundown data
- Experimental validation of the identification algorithm with different misalignment conditions on a test rig with the incomplete rundown data would be attempted.

These have been described briefly in the following sections.

1.4 Present Work

First, an identification algorithm has been developed for a model of the turbine–generator system with the rigid–rotor and flexible bearing–coupling assumptions to quantitatively estimate the bearing and coupling dynamic parameters along with residual unbalances; and the estimation of misalignment forces and moments. The Lagrange's equation has been used to obtain EOMs. Numerical examples have been presented to illustrate the working of the identification algorithm. The proposed algorithm relies on forced (unbalance) response measurements of the system at several frequencies (i.e., rotor speeds). Hence, in the numerical simulation, first the direct problem has been solved to generate the system responses and white noise is added to system responses to mimic the actual measurement data. The conditioning of regression matrix has also been discussed for the improvement in estimates of parameters.

The previous identification algorithm estimates MFPs in a rigid–rotor and flexible bearing–coupling system by using the analytical approach. Since this model is not realistic and approach is not practical, so a more realistic and more practical method has been used next to model the system and to develop an identification algorithm. So in this work, a more realistic model i.e. flexible rotor–bearing–coupling system has been considered and a more practical approach i.e. the FEM has been used to model the system. An identification algorithm has been developed to incorporate flexible bearings and couplings with flexible shaft trains to estimates the bearing and coupling dynamic parameters along with residual unbalances at chosen balancing planes. Numerical experiments have been performed to check the effectiveness and the robustness of the identification algorithm.

The identification algorithm developed in previous work has the main limitation in that it requires measurement of rotational displacements. To tackle the practical difficulty of limited measurements and the numerical difficulty of the conventional dynamic condensation in the development of identification algorithm, a novel condensation technique has been implemented especially to overcome the measurement of rotational DOFs. Numerical examples are also presented to show the effectiveness of the proposed method. Along with the estimation of MFPs, bias error (5% variation in E (modulus of elasticity) and ρ (density)) in the model has also been analysed.

Finally, the algorithm developed was tested with the real experimental setup developed in the Vibration and Acoustic laboratory at IIT Guwahati. The experimental setup consists of two shafts connected together with a flexible coupling and each shaft is mounted over two deep–grove ball bearings at ends is considered for the experiment. Eddy current sensors have been used to get the forced response measurements at bearing locations in two orthogonal directions. These forced vibrations were fed to identification algorithm to estimate the bearing

and coupling dynamic parameters along with residual unbalances. The accuracy of the estimated bearing and coupling dynamic parameters is checked by matching forward critical speeds (up to third modes) from the updated FEM model (by putting the bearing and coupling dynamic parameters obtained experimentally) that with the experimental impact test natural frequencies. Since effect of gyroscopic effect was negligible these frequencies match very well for the present case.

1.5 Organisation of the Thesis

The introduction and literature review are presented in **Chapter 1**. An identification algorithm for the rigid–rotor and flexible bearing–coupling system to estimate the bearing and coupling dynamic parameters along with residual unbalances has been presented in **Chapter 2**. The identification algorithm developed has been improved for multi supported flexible rotor–bearing–coupling systems in **Chapter 3**. To tackle the practical difficulty of limited measurements and the numerical difficulty of the conventional dynamic condensation in the development of identification algorithm, a novel condensation technique has been implemented in **Chapter 4**. Experimentation has been performed to check the applicability and robustness of the developed algorithm in **Chapter 5**. Conclusions and scopes for future work have been presented in **Chapter 6.**

CHAPTER 2

Identification of Multiple Fault Parameters in a Rigid–Rotor and Flexible–Bearing–Coupling System

2.1 Introduction

An identification algorithm has been developed in the present chapter to estimate multiple fault parameters in a turbo–generator system rotor model based on the forced response information. A simple discrete model of the system has been developed with the assumption of the rigid–rotor, flexible–bearings and the flexible–coupling. This model is capable of describing the vibration resulting from coupling misalignments and rotor unbalances. A simple flexible–joint is used to model the coupling between the two adjacent shafts to take the misalignment effect into account, which accounts for coupling forces and moments due to the restoring and dissipative effects. EOMs of the system are derived by using the Lagrange's equation. An identification algorithm based on the least–squares fit technique in frequency domain has been developed for the simultaneous estimation of bearing and coupling dynamic parameters along with residual unbalances. These could be used for estimating the misalignment forces and moments at the coupling and bearings from forced responses of the system. Numerical experiments have been performed to illustrate the effectiveness of the developed identification algorithm. The algorithm is tested against the measurement noise. The main difference between the state of the art in literature and the present work could be listed as (a) A new coupling model is proposed in which apart from translational coefficients the rotational coefficients have also been introduced (b) the combined effect of misalignment on the dynamic parameters of the coupling and bearings have been attempted (iii) Effect of flexible modes on the estimates of coupling and bearings due to misalignment have been investigates.

2.2 System Modelling

In the present section assumptions involved in modelling the system under consideration have been stated. Details of the misaligned rotor bearing model have also been presented. An identification algorithm is developed to estimate the bearing and coupling dynamic parameters along with residual unbalances.

2.2.1 Basic Assumptions and the Description of Model

A simple rotor model is considered as shown in Figure 2.1. It is composed of two rigid rotors and each of them are supported on two flexible bearings, and connected by a flexible coupling. The gyroscopic effect is neglected in the present study for brevity. The schematic diagram of the rotor model in a deflected position in one of the plane, i.e. the vertical plane (i.e., z–x plane) is shown in Figure 2.2(a). Here B_1 to B_4 are bearing locations, D_1 to D_4 are disc locations, G_1 and G_2 are shaft centres of gravity, and (x, φ_y) are the transverse linear and angular displacements of the shaft (refer the Nomenclature for details). Both rotor shafts (i.e., 1 and 2) are considered as rigid with the mass m_i^S (i = 1, 2) and the diametral mass moment of inertia, $I_{d_i}^S$. In each shaft two heavy rigid discs are mounted. Each disc has the mass, m_i^D (i = 1, 2, 3, 4), the diametral mass moment of inertia, $I_{d_i}^D$, and the residual unbalance, U_i. Each bearing is modelled by standard eight linearized damping, $c_{ij}^{B_n}$, and stiffness, $k_{ij}^{B_n}$, coefficients (all bearings have distinct the direct as well as cross–coupled terms, i.e. $i, j = x, y$ and n = 1, 2, 3, 4 for four bearings). Since the main aim of the present study is to analyze the effect of misalignment on the rotor system and under the general misalignment condition (i.e., the parallel and the angular) the shaft centre line and bearing centre line will not be parallel which otherwise happens in aligned conditions. Hence, due to the misalignment the tilting of shaft takes place which leads to the tilting of a plane carrying rolling elements in rolling bearings (or

a non–uniform axial gap develops between the shaft and bearing bore in the case of hydrodynamic bearings). So bearing forces is expected to be coupled (even in the case of rolling bearings) in two orthogonal directions at bearing locations, and to capture these effects cross–coupled terms has also been considered in the present study. For the bearing model now the eight linear stiffness and damping coefficients is very common. Coupling terms anyway has been considered small as compared to direct ones in numerical simulations. However, in the present work coefficients have been considered independent of speed to aim at a simple estimation process. Since the flexible coupling can take up transverse forces and moments, it is modelled as the linearized direct stiffness (k_{xx}^{C} and k_{yy}^{C}) and damping (c_{xx}^{C} and c_{yy}^{C}), the cross–coupled stiffness (k_{xy}^{C} and k_{yx}^{C}) and damping (c_{xy}^{C} and c_{yx}^{C}) coefficients, and the direct bending rotational stiffness, ($k_{\varphi_x}^{C}$ and $k_{\varphi_y}^{C}$). A schematic diagram of the coupling with generalised coordinates in the vertical plane (z–x) is shown in Figure 2.2(b). Superscripts *B*, *C*, *D*, and *S* in above symbols represent bearing, coupling, disc and shaft, respectively. The torsional and longitudinal vibration effects and its coupling with transverse vibrations are not considered in the present analysis. The purpose of the formulation is to evolve the methodology by keeping mathematical model simple so that detailed expressions could be presented for clarity. A more general formulation could have led to matrices, which would have difficult to present in the thesis because of its size. However, in subsequent chapters it has been generalized with the FEM, in which compact form of formulation is more popular and comprehensive.

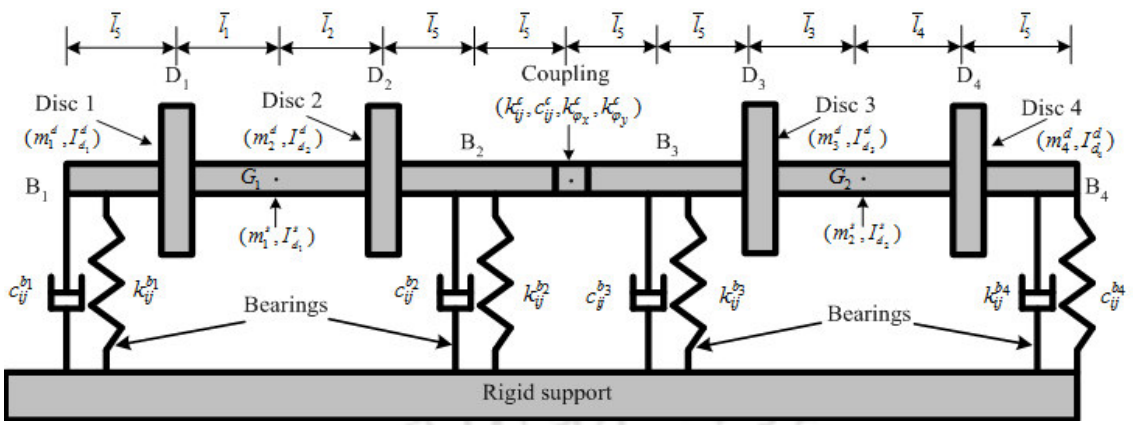

Figure 2.1 A simple rotor–bearing–coupling system

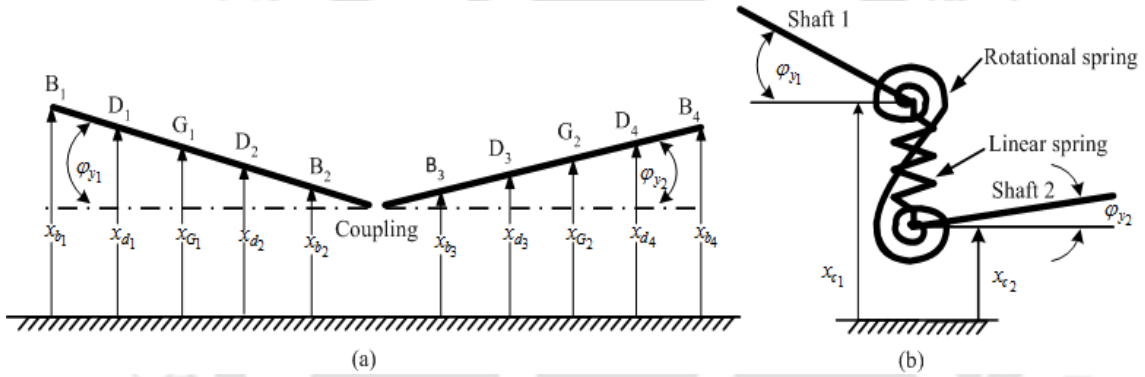

Figure 2.2 (a) A schematic diagram of deflected rotor in z–x plane (b) A schematic diagram of the coupling model

2.2.2 Equations of Motion

Here to derive EOMs, both planes motion of the rotor is considered since it is coupled through the flexible coupling. Hence, to describe the motion of the rotor–bearing–coupling system in each plane four generalised coordinates are required. Linear displacements of shafts at bearing locations are chosen as generalised coordinates. Thus, a total of eight generalised coordinates are required to describe the motion of the present system. Relations of the linear and angular displacements at various locations of rigid rotors in (x–z) and (y–z) planes (refer Figure 2.2(a)) are given by following expressions

$$x_{d_1} = 0.25(3x_{b_1} + x_{b_2}), \quad x_{d_2} = 0.25(x_{b_1} + 3x_{b_2}), \quad x_{d_3} = 0.25(3x_{b_3} + x_{b_4}), \quad x_{d_4} = 0.25(x_{b_3} + 3x_{b_4})$$

$$y_{d_1} = 0.25(3y_{b_1} + y_{b_2}), \; y_{d_2} = 0.25(y_{b_1} + 3y_{b_2}), \quad y_{d_3} = 0.25(3y_{b_3} + y_{b_4}), \quad y_{d_4} = 0.25(y_{b_3} + 3y_{b_4})$$

$$x_{G_1} = 0.5(x_{b_1} + x_{b_2}), \quad x_{G_2} = 0.5(x_{b_3} + x_{b_4}), \quad y_{G_1} = 0.5(y_{b_1} + y_{b_2}), \quad y_{G_2} = 0.5(y_{b_3} + y_{b_4})$$

$$\varphi_{y_1} = \frac{1}{l_1}(x_{b_1} - x_{b_2}), \quad \varphi_{y_2} = \frac{1}{l_2}(x_{b_4} - x_{b_3}), \quad \varphi_{x_1} = \frac{1}{l_1}(y_{b_1} - y_{b_2}), \quad \varphi_{x_2} = \frac{1}{l_2}(y_{b_4} - y_{b_3})$$

$$x_{c_1} = (-0.25x_{b_1} + 1.25x_{b_2}), \quad x_{c_2} = (1.25x_{b_3} - 0.25x_{b_4}), \quad y_{c_1} = (-0.25y_{b_1} + 1.25y_{b_2}),$$

$$y_{c_2} = (1.25y_{b_3} - 0.25y_{b_4}) \tag{2.1}$$

where $1.25l$ is the full length of each shaft, and $0.25l$ is the overhang length in each shaft towards the coupling (subscripts 1 and 2 is used to represent the left and right sides of the shaft, respectively). Subscripts *b*, *c*, *d*, and *G* in above symbols represent the bearing, coupling, disc and centre of shaft, respectively. The kinetic energy, *T*, is given as

$$\begin{aligned} T = & \tfrac{1}{2} m_1^D \dot{x}_{d_1}^2 + \tfrac{1}{2} m_2^D \dot{x}_{d_2}^2 + \tfrac{1}{2} m_1^S \dot{x}_{G_1}^2 + \tfrac{1}{2} I_1 \dot{\varphi}_{y_1}^2 + \tfrac{1}{2} m_3^D \dot{x}_{d_3}^2 + \tfrac{1}{2} m_4^D \dot{x}_{d_4}^2 + \tfrac{1}{2} m_2^S \dot{x}_{G_2}^2 + \tfrac{1}{2} I_2 \dot{\varphi}_{y_2}^2 \\ & + \tfrac{1}{2} m_1^D \dot{y}_{d_1}^2 + \tfrac{1}{2} m_2^D \dot{y}_{d_2}^2 + \tfrac{1}{2} m_1^S \dot{y}_{G_1}^2 + \tfrac{1}{2} I_1 \dot{\varphi}_{x_1}^2 + \tfrac{1}{2} m_3^D \dot{y}_{d_3}^2 + \tfrac{1}{2} m_4^D \dot{y}_{d_4}^2 + \tfrac{1}{2} m_2^S \dot{y}_{G_2}^2 + \tfrac{1}{2} I_2 \dot{\varphi}_{x_2}^2 \end{aligned} \tag{2.2}$$

with

$$I_1 = (I_{d_1}^D + m_1^D \bar{l}_1^2) + (I_{d_2}^D + m_2^D \bar{l}_2^2) + I_{d_1}^S; \qquad I_2 = (I_{d_3}^D + m_3^D \bar{l}_3^2) + (I_{d_4}^D + m_4^D \bar{l}_4^2) + I_{d_2}^S$$

where m_i^D and $\overline{l_i}$ (i =1, 2, 3, 4) are mass of disc and the distance between a disc and the shaft centre, respectively. The virtual work due to forces (for the bearing and coupling stiffness and damping forces, and unbalance forces) are given as

$$\delta W = \delta W_{stiff} + \delta W_{damp} + \delta W_{unb} \tag{2.3}$$

$$\begin{aligned}\delta W_{stiff} = &-k_{xx}^{B_1} x_{b_1} \delta x_{b_1} - k_{xy}^{B_1} y_{b_1} \delta x_{b_1} - k_{yx}^{B_1} x_{b_1} \delta y_{b_1} - k_{yy}^{B_1} y_{b_1} \delta y_{b_1} - k_{xx}^{B_2} x_{b_2} \delta x_{b_2} - k_{xy}^{B_2} y_{b_2} \delta x_{b_2} - k_{yx}^{B_2} x_{b_2} \delta y_{b_2} - k_{yy}^{B_2} y_{b_2} \delta y_{b_2} \\ &- k_{xx}^{B_3} x_{b_3} \delta x_{b_3} - k_{xy}^{B_3} y_{b_3} \delta x_{b_3} - k_{yx}^{B_3} x_{b_3} \delta y_{b_3} - k_{yy}^{B_3} y_{b_3} \delta y_{b_3} - k_{xx}^{B_4} x_{b_4} \delta x_{b_4} - k_{xy}^{B_4} y_{b_4} \delta x_{b_4} - k_{yx}^{B_4} x_{b_4} \delta y_{b_4} - k_{yy}^{B_4} y_{b_4} \delta y_{b_4} \\ &- k_{xx}^{C} (x_{c_1} - x_{c_2}) \delta (x_{c_1} - x_{c_2}) - k_{xy}^{C} (y_{c_1} - y_{c_2}) \delta (x_{c_1} - x_{c_2}) - k_{yx}^{C} (x_{c_1} - x_{c_2}) \delta (y_{c_1} - y_{c_2}) \\ &- k_{yy}^{C} (y_{c_1} - y_{c_2}) \delta (y_{c_1} - y_{c_2}) - k_{\varphi_x}^{C} (\varphi_{x_1} - \varphi_{x_2}) \delta (\varphi_{x_1} - \varphi_{x_2}) - k_{\varphi_y}^{C} (\varphi_{y_1} - \varphi_{y_2}) \delta (\varphi_{y_1} - \varphi_{y_2})\end{aligned} \tag{2.4}$$

$$\begin{aligned}\delta W_{damp} = &-c_{xx}^{B_1} \dot{x}_{b_1} \delta x_{b_1} - c_{xy}^{B_1} \dot{y}_{b_1} \delta x_{b_1} - c_{yx}^{B_1} \dot{x}_{b_1} \delta y_{b_1} - c_{yy}^{B_1} \dot{y}_{b_1} \delta y_{b_1} - c_{xx}^{B_2} \dot{x}_{b_2} \delta x_{b_2} - c_{xy}^{B_2} \dot{y}_{b_2} \delta x_{b_2} - c_{yx}^{B_2} \dot{x}_{b_2} \delta y_{b_2} - c_{yy}^{B_2} \dot{y}_{b_2} \delta y_{b_2} \\ &- c_{xx}^{B_3} \dot{x}_{b_3} \delta x_{b_3} - c_{xy}^{B_3} \dot{y}_{b_3} \delta x_{b_3} - c_{yx}^{B_3} \dot{x}_{b_3} \delta y_{b_3} - c_{yy}^{B_3} \dot{y}_{b_3} \delta y_{b_3} - c_{xx}^{B_4} \dot{x}_{b_4} \delta x_{b_4} - c_{xy}^{B_4} \dot{y}_{b_4} \delta x_{b_4} - c_{yx}^{B_4} \dot{x}_{b_4} \delta y_{b_4} - c_{yy}^{B_4} \dot{y}_{b_4} \delta y_{b_4} \\ &- c_{xx}^{C} (\dot{x}_{c_1} - \dot{x}_{c_2}) \delta (x_{c_1} - x_{c_2}) - c_{xy}^{C} (\dot{y}_{c_1} - \dot{y}_{c_2}) \delta (x_{c_1} - x_{c_2}) - c_{yx}^{C} (\dot{x}_{c_1} - \dot{x}_{c_2}) \delta (y_{c_1} - y_{c_2}) - c_{yy}^{C} (\dot{y}_{c_1} - \dot{y}_{c_2}) \delta (y_{c_1} - y_{c_2})\end{aligned} \tag{2.5}$$

and

$$\begin{aligned}\delta W_{unb} = &F_1^{u_x}(t) \delta (x_{c_1} + l_1 \varphi_{y_1}) + F_2^{u_x}(t) \delta (x_{c_1} + 0.5 l_1 \varphi_{y_1}) + F_3^{u_x}(t) \delta (x_{c_2} + 0.5 l_2 \varphi_{y_2}) + F_4^{u_x}(t) \delta (x_{c_2} + l_1 \varphi_{y_2}) \\ &+ F_1^{u_y}(t) \delta (y_{c_1} + l_1 \varphi_{x_1}) + F_2^{u_y}(t) \delta (y_{c_1} + 0.5 l_1 \varphi_{x_1}) + F_3^{u_y}(t) \delta (y_{c_2} + 0.5 l_2 \varphi_{x_2}) + F_4^{u_y}(t) \delta (y_{c_2} + l_1 \varphi_{x_2})\end{aligned} \tag{2.6}$$

where $F_i^{u_x}(t)$ and $F_i^{u_y}(t)$ are unbalance forces in the (x–z) and (y–z) planes respectively, and are related as $F_i^{u_y} = \pm \mathrm{j} F_i^{u_x}$ (the sign depends upon direction of rotation of the rotor with respect to the axis system). Residual unbalances are given as $u_i = U_i e^{\mathrm{j}(\omega t + \phi_i)}$ with $i = 1,2,3,4$, where

$U_i = m_i^u e_i$ is the magnitude of unbalance, ω is the spin speed of the rotor, ϕ is the phase angle, and δ is the variational operator, m^u is the unbalance mass, and e is the disc eccentricity. The virtual work expression δW could be arranged, noting Eqn. (2.3), in such a way that we obtain the form in terms of generalised coordinates, as

$$\delta W = F_1 \delta x_{b_1} + F_2 \delta x_{b_2} + F_3 \delta x_{b_3} + F_4 \delta x_{b_4} + F_5 \delta y_{b_1} + F_6 \delta y_{b_2} + F_7 \delta y_{b_3} + F_8 \delta y_{b_4} \tag{2.7}$$

where F_1 to F_8 contain forces due to residual unbalances, and the damping and stiffness coefficients of bearings and the coupling. On the application of the Lagrange's equation on Eqns. (2.2) and (2.7), EOMs for the rotor–bearing–coupling system could be written as

$$[M]\{\ddot{\eta}\} + [C]\{\dot{\eta}\} + [K]\{\eta\} = \{f(t)\} \tag{2.8}$$

where the displacement and force vectors are given as

$$\{\eta(t)\} = \left\{ x_{b_1}(t) \;\; x_{b_2}(t) \;\; x_{b_3}(t) \;\; x_{b_4}(t) \;\; y_{b_1}(t) \;\; y_{b_2}(t) \;\; y_{b_3}(t) \;\; y_{b_4}(t) \right\}^T$$

$$\{f(t)\} = \omega^2 \begin{Bmatrix} U_{x_1} e^{j\phi_1} + U_{x_2} e^{j\phi_2} \\ U_{x_1} e^{j\phi_1} + 0.5 U_{x_2} e^{j\phi_2} \\ U_{x_3} e^{j\phi_3} + U_{x_4} e^{j\phi_4} \\ 0.5 U_{x_3} e^{j\phi_3} + U_{x_4} e^{j\phi_4} \\ U_{y_1} e^{j\phi_1} + U_{y_2} e^{j\phi_2} \\ U_{y_1} e^{j\phi_1} + 0.5 U_{y_2} e^{j\phi_2} \\ U_{y_3} e^{j\phi_3} + U_{y_4} e^{j\phi_4} \\ 0.5 U_{y_3} e^{j\phi_3} + U_{y_4} e^{j\phi_4} \end{Bmatrix} e^{j\omega t} = \omega^2 \begin{Bmatrix} U_{x_1} e^{j\phi_1} + U_{x_2} e^{j\phi_2} \\ U_{x_1} e^{j\phi_1} + 0.5 U_{x_2} e^{j\phi_2} \\ U_{x_3} e^{j\phi_3} + U_{x_4} e^{j\phi_4} \\ 0.5 U_{x_3} e^{j\phi_3} + U_{x_4} e^{j\phi_4} \\ -\mathrm{j}\,(U_{x_1} e^{j\phi_1} + U_{x_2} e^{j\phi_2}) \\ -\mathrm{j}\,(U_{x_1} e^{j\phi_1} + 0.5 U_{x_2} e^{j\phi_2}) \\ -\mathrm{j}\,(U_{x_3} e^{j\phi_3} + U_{x_4} e^{j\phi_4}) \\ -\mathrm{j}\,(0.5 U_{x_3} e^{j\phi_3} + U_{x_4} e^{j\phi_4}) \end{Bmatrix} e^{j\omega t} \tag{2.9}$$

where ω is the spin speed, and $\phi_i (i = 1, 2, 3, 4)$ are the angular position of unbalance masses from some reference point on the shaft. Elements of matrices $[M]$, $[K]$ and $[C]$ are given as

$$M_{11}=M_{55}=\frac{1}{16}\left(9m_1^D+m_2^D+4m_1^S+\frac{16}{l_1^2}I_1\right), \quad M_{44}=M_{88}=\frac{1}{16}\left(m_3^D+9m_4^D+4m_2^S+\frac{16}{l_2^2}I_2\right),$$

$$M_{22}=M_{66}=\frac{1}{16}\left(m_1^D+9m_2^D+4m_1^S+\frac{16}{l_1^2}I_1\right), \quad M_{12}=M_{21}=M_{56}=M_{65}=\frac{1}{16}\left(3m_1^D+3m_2^D+4m_1^S-\frac{16}{l_1^2}I_1\right),$$

$$M_{33}=M_{77}=\frac{1}{16}\left(9m_3^D+m_4^D+4m_2^S+\frac{16}{l_2^2}I_1\right), \quad M_{34}=M_{43}=M_{78}=M_{87}=\frac{1}{16}\left(3m_3^D+3m_4^D+4m_2^S-\frac{16}{l_2^2}I_2\right)$$

In Eqn. (2.8), the forcing has the form of $\{f(t)\}=\{\bar{f}\}e^{j\omega t}$. Hence, by taking the solution of Eqn. (2.8) in the form of $\{\eta(t)\}=\{\bar{\eta}\}e^{j\omega t}$, where vectors $\{\bar{f}\}$ and $\{\bar{\eta}\}$ contain the magnitude and phase information of forces and displacements, respectively; and in general they are complex. On substituting these expressions into Eqn. (2.8), we get

$$\left([K]+j\omega[C]-\omega^2[M]\right)\{\bar{\eta}\}=\{\bar{f}\} \tag{2.10}$$

For the known unbalance information and rotor–bearing–coupling dynamic parameters, Eqn. (2.10) could be used to obtain the displacement amplitude and phase components at various spin speed of the rotor. In subsequent section, the same equation would be used to develop an identification algorithm for estimation of parameters of multiple faults (i.e., the bearing and coupling dynamic parameters along with residual unbalances). In the above expression, the force vector $\{f(t)\}$ contains the parameter due to unbalance only.

$$[K]=\begin{bmatrix}
k_{xx}^{B_1}+\frac{1}{16}k_{xx}^{C}+\frac{1}{l_1^2}k_{\varphi_x}^{C} & -\frac{5}{16}k_{xx}^{C}-\frac{1}{l_1^2}k_{\varphi_x}^{C} & \frac{5}{16}k_{xx}^{C}+\frac{1}{l_2^2}k_{\varphi_x}^{C} & -\frac{1}{16}k_{xx}^{C}-\frac{1}{l_2^2}k_{\varphi_x}^{C} & k_{xy}^{B_1}+\frac{1}{16}k_{xy}^{C} & -\frac{5}{16}k_{xy}^{C} & \frac{5}{16}k_{xy}^{C} & -\frac{1}{16}k_{xy}^{C} \\
-\frac{5}{16}k_{xx}^{C}-\frac{1}{l_1^2}k_{\varphi_x}^{C} & k_{xx}^{B_2}+\frac{25}{16}k_{xx}^{C}+\frac{1}{l_1^2}k_{\varphi_x}^{C} & -\frac{25}{16}k_{xx}^{C}-\frac{1}{l_1 l_2}k_{\varphi_x}^{C} & \frac{5}{16}k_{xx}^{C}+\frac{1}{l_1 l_2}k_{\varphi_x}^{C} & -\frac{5}{16}k_{xy}^{C} & k_{xy}^{C_2}+\frac{25}{16}k_{xy}^{C} & -\frac{25}{16}k_{xy}^{C} & \frac{5}{16}k_{xy}^{C} \\
\frac{5}{16}k_{xx}^{C}+\frac{1}{l_1 l_2}k_{\varphi_x}^{C} & -\frac{25}{16}k_{xx}^{C}-\frac{1}{l_1 l_2}k_{\varphi_x}^{C} & k_{xx}^{B_3}+\frac{25}{16}k_{xx}^{C}+\frac{1}{l_2^2}k_{\varphi_x}^{C} & -\frac{5}{16}k_{xx}^{C}-\frac{1}{l_2^2}k_{\varphi_x}^{C} & \frac{5}{16}k_{xy}^{C} & -\frac{25}{16}k_{xy}^{C} & k_{xy}^{B_3}+\frac{25}{16}k_{xy}^{C} & -\frac{5}{16}k_{xy}^{C} \\
-\frac{1}{16}k_{xx}^{C}-\frac{1}{l_1 l_2}k_{\varphi_x}^{C} & \frac{5}{16}k_{xx}^{C}+\frac{1}{l_1 l_2}k_{\varphi_x}^{C} & -\frac{5}{16}k_{xx}^{C}-\frac{1}{l_2^2}k_{\varphi_x}^{C} & k_{xx}^{B_4}+\frac{5}{16}k_{xx}^{C}+\frac{1}{l_2^2}k_{\varphi_x}^{C} & -\frac{1}{16}k_{xy}^{C} & \frac{5}{16}k_{xy}^{C} & -\frac{5}{16}k_{xy}^{C} & k_{xy}^{B_4}+\frac{1}{16}k_{xy}^{C} \\
k_{yx}^{B_1}+\frac{1}{16}k_{yx}^{C} & -\frac{5}{16}k_{yx}^{C} & \frac{5}{16}k_{yx}^{C} & -\frac{1}{16}k_{yx}^{C} & k_{yy}^{B_1}+\frac{1}{16}k_{yy}^{C}+\frac{1}{l_1^2}k_{\varphi_y}^{C} & -\frac{5}{16}k_{yy}^{C}-\frac{1}{l_1^2}k_{\varphi_y}^{C} & \frac{5}{16}k_{yy}^{C}+\frac{1}{l_1 l_2}k_{\varphi_y}^{C} & -\frac{5}{16}k_{yy}^{C}-\frac{1}{l_1 l_2}k_{\varphi_y}^{C} \\
-\frac{5}{16}k_{yx}^{C} & k_{yx}^{B_2}+\frac{25}{16}k_{yx}^{C} & -\frac{25}{16}k_{yx}^{C} & \frac{5}{16}k_{yx}^{C} & -\frac{5}{16}k_{yy}^{C}-\frac{1}{l_1^2}k_{\varphi_y}^{C} & k_{yy}^{B_2}+\frac{25}{16}k_{yy}^{C}+\frac{1}{l_1^2}k_{\varphi_y}^{C} & -\frac{25}{16}k_{yy}^{C}-\frac{1}{l_1 l_2}k_{\varphi_y}^{C} & \frac{5}{16}k_{yy}^{C}+\frac{1}{l_1 l_2}k_{\varphi_y}^{C} \\
\frac{5}{16}k_{yx}^{C} & -\frac{25}{16}k_{yx}^{C} & k_{yx}^{B_3}+\frac{25}{16}k_{yx}^{C} & -\frac{5}{16}k_{yx}^{C} & \frac{5}{16}k_{yy}^{C}+\frac{1}{l_1 l_2}k_{\varphi_y}^{C} & -\frac{25}{16}k_{yy}^{C}-\frac{1}{l_1 l_2}k_{\varphi_y}^{C} & k_{yy}^{B_3}+\frac{25}{16}k_{yy}^{C}+\frac{1}{l_2^2}k_{\varphi_y}^{C} & -\frac{5}{16}k_{yy}^{C}-\frac{1}{l_2^2}k_{\varphi_y}^{C} \\
-\frac{1}{16}k_{yx}^{C} & \frac{5}{16}k_{yx}^{C} & -\frac{5}{16}k_{yx}^{C} & k_{yx}^{B_4}+\frac{1}{16}k_{yx}^{C} & -\frac{1}{16}k_{yy}^{C}-\frac{1}{l_1 l_2}k_{\varphi_y}^{C} & \frac{5}{16}k_{yy}^{C}+\frac{1}{l_1 l_2}k_{\varphi_y}^{C} & -\frac{5}{16}k_{yy}^{C}-\frac{1}{l_2^2}k_{\varphi_y}^{C} & k_{yy}^{B_4}+\frac{5}{16}k_{yy}^{C}+\frac{1}{l_2^2}k_{\varphi_y}^{C}
\end{bmatrix}$$

$$[C]=\begin{bmatrix}
c_{xx}^{B_1}+0.062c_{xx}^{C} & -0.312c_{xx}^{C} & 0.312c_{xx}^{C} & -0.062c_{xx}^{C} & c_{xy}^{B_1}+0.062c_{xy}^{C} & -0.312c_{xy}^{C} & 0.312c_{xy}^{C} & -0.062c_{xy}^{c} \\
-0.312c_{xx}^{C} & c_{xx}^{B_2}+1.562c_{xx}^{C} & -1.562c_{xx}^{C} & 0.312c_{xx}^{C} & -0.312c_{xy}^{C} & c_{xy}^{B_2}+1.562c_{xy}^{C} & -1.562c_{xy}^{C} & 0.312c_{xy}^{C} \\
0.312c_{xx}^{C} & -1.562c_{xx}^{C} & c_{xx}^{B_3}+1.562c_{xx}^{C} & -0.312c_{xx}^{C} & 0.312c_{xy}^{C} & -1.562c_{xy}^{C} & c_{xy}^{B_3}+1.562c_{xy}^{C} & -0.312c_{xy}^{C} \\
-0.062c_{xx}^{C} & 0.312c_{xx}^{C} & -0.312c_{xx}^{C} & c_{xx}^{B_4}+0.312c_{xx}^{C} & -0.062c_{xy}^{C} & 0.312c_{xy}^{C} & -0.312c_{xy}^{C} & c_{xy}^{B_4}+0.062c_{xy}^{C} \\
c_{yx}^{B_1}+0.062c_{yx}^{C} & -0.312c_{yx}^{C} & 0.312c_{yx}^{C} & -0.062c_{yx}^{C} & c_{yy}^{B_1}+0.062c_{yy}^{C} & -0.312c_{yy}^{C} & 0.312c_{yy}^{C} & -0.312c_{yy}^{C} \\
-0.312c_{yx}^{C} & c_{yx}^{B_2}+1.562c_{yx}^{C} & -1.562c_{yx}^{C} & 0.312c_{yx}^{C} & -0.312c_{yy}^{C} & c_{yy}^{B_2}+1.562c_{yy}^{C} & -1.562c_{yy}^{C} & 0.312c_{yy}^{C} \\
0.312c_{yx}^{C} & -1.562c_{yx}^{C} & c_{yx}^{B_3}+1.562c_{yx}^{C} & -0.312c_{yx}^{C} & 0.312c_{yy}^{C} & -1.562c_{yy}^{C} & c_{yy}^{B_3}+1.562c_{yy}^{C} & -0.312c_{yy}^{C} \\
-0.062c_{yx}^{C} & 0.312c_{yx}^{C} & -0.312c_{yx}^{C} & c_{yx}^{B_4}+0.062c_{yx}^{C} & -0.062c_{yy}^{C} & 0.312c_{yy}^{C} & -0.312c_{yy}^{C} & c_{yy}^{B_4}+0.312c_{yy}^{C}
\end{bmatrix}$$

The effect of misalignment forces and moments has been considered in the form of restoring and damping forces, and these are included in the stiffness and damping matrices. One can calculate the amount of misalignment force and moment by knowing the coupling stiffness and damping coefficients $(k_{ij}^C, k_{\varphi_x}^C, c_{ij}^C, c_{\varphi_x}^C)$, and displacement values at bearing location $(x_{b_1}, x_{b_2}, x_{b_3}, x_{b_4})$, noting Eqn. (2.1), as

$$F^{mis} = \begin{Bmatrix} F_x^{mis} \\ F_y^{mis} \\ M_{xz}^{mis} \\ M_{yz}^{mis} \end{Bmatrix} \tag{2.11}$$

with

$$F_x^{mis} = k_{xx}^C(x_{c_1} - x_{c_2}) + k_{xy}^C(y_{c_1} - y_{c_2}) + c_{xx}^C(\dot{x}_{c_1} - \dot{x}_{c_2}) + c_{xy}^C(\dot{y}_{c_1} - \dot{y}_{c_2}); \qquad M_{xz}^{mis} = k_{\varphi_x\varphi_x}(\varphi_{y_1} - \varphi_{y_2});$$

$$F_y^{mis} = k_{yx}^C(x_{c_1} - x_{c_2}) + k_{yy}^C(y_{c_1} - y_{c_2}) + c_{yx}^C(\dot{x}_{c_1} - \dot{x}_{c_2}) + c_{yy}^C(\dot{y}_{c_1} - \dot{y}_{c_2}); \qquad M_{yz}^{mis} = k_{\varphi_y\varphi_y}(\varphi_{x_1} - \varphi_{x_2}) \tag{2.12}$$

where F_x^{mis} and F_y^{mis} are misalignment forces in x and y direction respectively, and M_{xz}^{mis} and M_{yz}^{mis} are moments due to misalignment in the x–z and y–z planes, respectively. Advantage of the modelling of coupling of the above form ensures the system as a linear, which is of course valid for small amount of misalignment (Jordan, 1993).

2.2.3 Development of the Identification Algorithm

Eqn. (2.10), can be rearranged such that all the unknown quantities (i.e. the bearing and coupling dynamic parameters; and residual unbalances) are in a vector, $\{X_1\}$, in the left–hand

side and all the known quantities (i.e. the rotor model parameters and measurable responses) are in the left–hand side matrix, $[A_1(\omega)]$, and in the right–hand side vector, $\{B_1(\omega)\}$, in the following regression equation form

$$\left[A_1(\omega)\right]_{8\times 50}\left\{X_1\right\}_{50\times 1}=\left\{B_1(\omega)\right\}_{8\times 1} \tag{2.13}$$

with

$$\left[A_1\right]_{8\times 50}=\left[\left[k^r\right]_{8\times 22}\ \left[c^r\right]_{8\times 20}\ \left[u^r\right]_{8\times 8}\right]_{8\times 50}$$

where $[k^r]$, $[c^r]$ and $[u^r]$ are contributions to the final regression matrices from the stiffness and damping coefficients of bearings and the coupling, and residual unbalances, respectively. In Eqn. (2.13), the subscript represents the size of the matrix or the vector. Elements of matrix $[A_1]$ and vector $\{B_1\}$ are in the complex form could be given as:

Elements of regression matrix in complex form due to stiffness $[k^r]$ *are:*

$k_{11}^r = x_{b_1}$, $k_{12}^r = y_{b_1}$, $k_{1,17}^r = k_{5,19}^r = 0.062(x_{b_1} - 5x_{b_2} + 5x_{b_3} - x_{b_4})$,

$k_{1,18}^r = k_{5,20}^r = 0.062(y_{b_1} - yx_{b_2} + yx_{b_3} - y_{b_4})$,

$k_{25}^r = x_{b_2}$, $k_{26}^r = y_{b_2}$, $k_{2,17}^r = k_{6,19}^r = 0.062(-5x_{b_1} + 25x_{b_2} - 25x_{b_3} + 5x_{b_4})$,

$k_{2,18}^r = k_{6,20}^r = 0.062(-5y_{b_1} + 25y_{b_2} - 25y_{b_3} + 5y_{b_4})$,

$k_{39}^r = x_{b_3}$, $k_{3,10}^r = y_{b_3}$, $k_{3,17}^r = k_{7,19}^r = 0.062(5x_{b_1} - 25x_{b_2} + 25x_{b_3} - 5x_{b_4})$,

$k_{3,18}^r = k_{7,20}^r = 0.062(5y_{b_1} - 25y_{b_2} + 25y_{b_3} - 5y_{b_4})$,

$k_{4,13}^r = x_{b_4}$, $k_{4,14}^r = y_{b_4}$, $k_{4,17}^r = k_{8,19}^r = 0.062(-x_{b_1} + 5x_{b_2} - 5x_{b_3} + x_{b_4})$,

$k_{4,18}^r = k_{8,20}^r = 0.062(-y_{b_1} + 5y_{b_2} - 5y_{b_3} + y_{b_4})$,

$k_{53}^r = x_{b_1}$, $k_{54}^r = y_{b_1}$, $k_{67}^r = x_{b_2}$, $k_{68}^r = y_{b_2}$, $k_{7,11}^r = x_{b_3}$, $k_{7,12}^r = y_{b_3}$, $k_{8,15}^r = x_{b_4}$, $k_{8,16}^r = y_{b_4}$,

$$k^r_{1,21}=\left(\frac{x_{b_1}-x_{b_2}}{l_1^2}\right)+\left(\frac{x_{b_3}-x_{b_4}}{l_2^2}\right), k^r_{2,21}=\left(\frac{x_{b_2}-x_{b_1}}{l_1^2}\right)+\left(\frac{x_{b_4}-x_{b_3}}{l_1l_2}\right), \quad k^r_{3,21}=\left(\frac{x_{b_1}-x_{b_2}}{l_1l_2}\right)+\left(\frac{x_{b_3}-x_{b_4}}{l_2^2}\right),$$

$$k^r_{4,21}=\left(\frac{x_{b_2}-x_{b_1}}{l_1l_2}\right)+\left(\frac{x_{b_4}-x_{b_3}}{l_2^2}\right), k^r_{5,22}=\left(\frac{y_{b_1}-y_{b_2}}{l_1^2}\right)+\left(\frac{y_{b_3}-y_{b_4}}{l_2^2}\right), \; k^r_{6,22}=\left(\frac{y_{b_2}-y_{b_1}}{l_1^2}\right)+\left(\frac{y_{b_4}-y_{b_3}}{l_1l_2}\right),$$

$$k^r_{7,22}=\left(\frac{y_{b_1}-y_{b_2}}{l_1l_2}\right)+\left(\frac{y_{b_3}-y_{b_4}}{l_2^2}\right), \quad k^r_{8,22}=\left(\frac{y_{b_2}-y_{b_1}}{l_1l_2}\right)+\left(\frac{y_{b_4}-y_{b_3}}{l_2^2}\right)$$

Elements of regression matrix in complex form due to damping $[c^r]$ *are:*

$$c^r_{11}=-\mathrm{j}\omega x_{b_1}, \qquad c^r_{12}=-\mathrm{j}\omega y_{b_1}, \qquad c^r_{1,17}=c^r_{5,19}=-0.062\,\mathrm{j}\,\omega(x_{b_1}-5x_{b_2}+5x_{b_3}-x_{b_4}),$$

$$c^r_{1,18}=c^r_{5,20}=-0.062\,\mathrm{j}\,\omega(y_{b_1}-yx_{b_2}+yx_{b_3}-y_{b_4}),$$

$$c^r_{25}=-\mathrm{j}\omega x_{b_2}, \qquad c^r_{26}=-\mathrm{j}\omega y_{b_2}, \qquad c^r_{2,17}=c^r_{6,19}=-0.062\,\mathrm{j}\,\omega(-5x_{b_1}+25x_{b_2}-25x_{b_3}+5x_{b_4})a,$$

$$c^r_{2,18}=c^r_{6,20}=-0.062\,\mathrm{j}\,\omega(-5y_{b_1}+25y_{b_2}-25y_{b_3}+5y_{b_4}),$$

$$c^r_{39}=-\mathrm{j}\omega x_{b_3}, \qquad c^r_{3,10}=-\mathrm{j}\omega y_{b_3}, \qquad c^r_{3,17}=c^r_{7,19}=-0.062\,\mathrm{j}\,\omega(5x_{b_1}-25x_{b_2}+25x_{b_3}-5x_{b_4}),$$

$$c^r_{3,18}=c^r_{7,20}=-0.062\,\mathrm{j}\,\omega(5y_{b_1}-25y_{b_2}+25y_{b_3}-5y_{b_4}),$$

$$c^r_{4,13}=-\mathrm{j}\omega x_{b_4}, \qquad c^r_{4,14}=-\mathrm{j}\omega y_{b_4}, \qquad c^r_{4,17}=c^r_{8,19}=-0.062\,\mathrm{j}\,\omega(-x_{b_1}+5x_{b_2}-5x_{b_3}+x_{b_4}),$$

$$c^r_{4,18}=c^r_{8,20}=-0.062\,\mathrm{j}\,\omega(-y_{b_1}+5y_{b_2}-5y_{b_3}+y_{b_4}),$$

$$c^r_{53}=-\mathrm{j}\omega x_{b_1},\; c^r_{54}=-\mathrm{j}\omega y_{b_1}, \quad c^r_{67}=-\mathrm{j}\omega x_{b_2}, \; c^r_{68}=-\mathrm{j}\omega y_{b_2}, \quad c^r_{7,11}=-\mathrm{j}\omega x_{b_3}, \; c^r_{7,12}=-\mathrm{j}\omega y_{b_3},$$

$$c^r_{8,15}=-\mathrm{j}\omega x_{b_4}, \quad c^r_{8,16}=-\mathrm{j}\omega y_{b_4}$$

Elements of the regression matrix in complex form due to residual unbalance $[u^r]$ *are*

$$u^r_{11}=0.75\omega^2e^{j\omega\phi_1}, \qquad u^r_{12}=0.25\omega^2e^{j\omega\phi_2}, \qquad u^r_{21}=0.25\omega^2e^{j\omega\phi_1}, \qquad u^r_{22}=0.75\omega^2e^{j\omega\phi_2},$$

$$u^r_{33}=0.75\omega^2e^{j\omega\phi_3}, \qquad u^r_{34}=0.25\omega^2e^{j\omega\phi_4}, \qquad u^r_{43}=0.25\omega^2e^{j\omega\phi_3}, \qquad u^r_{44}=0.75\omega^2e^{j\omega\phi_4},$$

$$u^r_{51}=-\mathrm{j}u^r_{11}, \qquad u^r_{52}=-\mathrm{j}u^r_{12}, \qquad u^r_{61}=-\mathrm{j}u^r_{21}, \qquad u^r_{62}=-\mathrm{j}u^r_{22},$$

$$u^r_{73} = -\mathrm{j}u^r_{33}, \qquad u^r_{74} = -\mathrm{j}u^r_{34}, \qquad u^r_{83} = -\mathrm{j}u^r_{43}, \qquad u^r_{84} = -\mathrm{j}u^r_{44}$$

Rest of the terms of the regression matrix are zero.

Elements of vector [B^r] in complex form are

$$b^r_{11} = \frac{1}{16}\omega^2\left\{\left(9m_1 + m_2 + 4m^s_1 + \frac{16}{l_1^2}I_{d_1}\right)x_{b_1} + \left(3m_1 + 3m_2 + 4m^s_1 - \frac{16}{l_1^2}I_{d_1}\right)x_{b_2}\right\},$$

$$b^r_{21} = \frac{1}{16}\omega^2\left\{\left(3m_1 + 3m_2 + 4m^s_1 - \frac{16}{l_1^2}I_{d_1}\right)x_{b_1} + \left(m_1 + 9m_2 + 4m^s_1 + \frac{16}{l_1^2}I_{d_1}\right)x_{b_2}\right\},$$

$$b^r_{31} = \frac{1}{16}\omega^2\left\{\left(9m_3 + m_4 + 4m^s_2 + \frac{16}{l_2^2}I_{d_2}\right)x_{b_3} + \left(3m_3 + 3m_4 + 4m^s_2 - \frac{16}{l_2^2}I_{d_2}\right)x_{b_4}\right\},$$

$$b^r_{41} = \frac{1}{16}\omega^2\left\{\left(3m_3 + 3m_4 + 4m^s_2 - \frac{16}{l_2^2}I_{d_2}\right)x_{b_3} + \left(m_3 + 9m_4 + 4m^s_2 + \frac{16}{l_2^2}I_{d_2}\right)x_{b_4}\right\},$$

$$b^r_{51} = \frac{1}{16}\omega^2\left\{\left(9m_1 + m_2 + 4m^s_1 + \frac{16}{l_1^2}I_{d_1}\right)y_{b_1} + \left(3m_1 + 3m_2 + 4m^s_1 - \frac{16}{l_1^2}I_{d_1}\right)y_{b_2}\right\},$$

$$b^r_{61} = \frac{1}{16}\omega^2\left\{\left(3m_1 + 3m_2 + 4m^s_1 - \frac{16}{l_1^2}I_{d_1}\right)y_{b_1} + \left(m_1 + 9m_2 + 4m^s_1 + \frac{16}{l_1^2}I_{d_1}\right)y_{b_2}\right\},$$

$$b^r_{71} = \frac{1}{16}\omega^2\left\{\left(9m_3 + m_4 + 4m^s_2 + \frac{16}{l_2^2}I_{d_2}\right)y_{b_3} + \left(3m_3 + 3m_4 + 4m^s_2 - \frac{16}{l_2^2}I_{d_2}\right)y_{b_4}\right\},$$

$$b^r_{81} = \frac{1}{16}\omega^2\left\{\left(3m_3 + 3m_4 + 4m^s_2 - \frac{16}{l_2^2}I_{d_2}\right)y_{b_3} + \left(m_3 + 9m_4 + 4m^s_2 + \frac{16}{l_2^2}I_{d_2}\right)y_{b_4}\right\}$$

Eqn. (2.13) is the estimation equation in which all unknown parameters (i.e., the bearing and coupling dynamic parameters; and residual unbalances) are stacked in a column vector$\{X_1\}$. Eqn. (2.13), is in the complex form that can be separated out in the real and imaginary parts, and the required estimation equation becomes as

$$\left[A_2(\omega)\right]_{16\times 50}\left\{X_2\right\}_{50\times 1}=\left\{B_2(\omega)\right\}_{16\times 1} \tag{2.14}$$

with

$$\{X_2\}=\{k_{xx}^{B_1},k_{xy}^{B_1},k_{yx}^{B_1},k_{yy}^{B_1},k_{xx}^{B_2},k_{xy}^{B_2},k_{yx}^{B_2},k_{yy}^{B_2},k_{xx}^{B_3},k_{xy}^{B_3},k_{yx}^{B_3},k_{yy}^{B_3},k_{xx}^{B_4},k_{xy}^{B_4},k_{yx}^{B_4},k_{yy}^{B_4},k_{xx}^{C},k_{xy}^{C},k_{yx}^{C},k_{yy}^{C},k_{\varphi_x}^{C},k_{\varphi_y}^{C},c_{xx}^{B_1},c_{xy}^{B_1},$$

$$c_{yx}^{B_1},c_{yy}^{B_1},c_{xx}^{B_2},c_{xy}^{B_2},c_{yx}^{B_2},c_{yy}^{B_2},c_{xx}^{B_3},c_{xy}^{B_3},c_{yx}^{B_3},c_{yy}^{B_3},c_{xx}^{B_4},c_{xy}^{B_4},c_{yx}^{B_4},c_{yy}^{B_4},c_{xx}^{C},c_{xy}^{C},c_{yx}^{C},c_{yy}^{C},U_{x_1}^{r},U_{x_1}^{i},U_{x_2}^{r},U_{x_2}^{i},U_{x_3}^{r},U_{x_3}^{i},U_{x_4}^{r},U_{x_4}^{i}\}^{T}$$

and

$$\left[A_2\right]_{16\times 50}=\left[\left[k^{r}\right]_{16\times 22}\ \left[c^{r}\right]_{16\times 20}\ \left[u^{r}\right]_{16\times 8}\right]_{8\times 50}$$

All the unknown parameters stacked in vector $\{X_2\}$ are summarised in Table 2.1 with corresponding row locations for the easy interpretation of results presented in subsequent sections.

Table 2.1 Unknown parameters with corresponding row locations in vector $\{X_2\}$

Row no	**1**	**2**	**3**	**4**	**5**	**6**	**7**	**8**	**9**	**10**	**11**	**12**	**13**
Parameters	$k_{xx}^{B_1}$	$k_{xy}^{B_1}$	$k_{yx}^{B_1}$	$k_{yy}^{B_1}$	$k_{xx}^{B_2}$	$k_{xy}^{B_2}$	$k_{yx}^{B_2}$	$k_{yy}^{B_2}$	$k_{xx}^{B_3}$	$k_{xy}^{B_3}$	$k_{yx}^{B_3}$	$k_{yy}^{B_3}$	$k_{xx}^{B_4}$
Row no	**14**	**15**	**16**	**17**	**18**	**19**	**20**	**21**	**22**	**23**	**24**	**25**	**26**
Parameters	$k_{xy}^{B_4}$	$k_{yx}^{B_4}$	$k_{yy}^{B_4}$	k_{xx}^{C}	k_{xy}^{C}	k_{yx}^{C}	k_{yy}^{C}	$k_{\varphi_x}^{C}$	$k_{\varphi_y}^{C}$	$c_{xx}^{B_1}$	$c_{xy}^{B_1}$	$c_{yx}^{B_1}$	$c_{yy}^{B_1}$
Row no	**27**	**28**	**29**	**30**	**31**	**32**	**33**	**34**	**35**	**36**	**37**	**38**	**39**
Parameters	$c_{xx}^{B_2}$	$c_{xy}^{B_2}$	$c_{yx}^{B_2}$	$c_{yy}^{B_2}$	$c_{xx}^{B_3}$	$c_{xy}^{B_3}$	$c_{yx}^{B_3}$	$c_{yy}^{B_3}$	$c_{xx}^{B_4}$	$c_{xy}^{B_4}$	$c_{yx}^{B_4}$	$c_{yy}^{B_4}$	c_{xx}^{C}
Row no	**40**	**41**	**42**	**43**	**44**	**45**	**46**	**47**	**48**	**49**	**50**		
Parameters	c_{xy}^{C}	c_{yx}^{C}	c_{yy}^{C}	$u_{x_1}^{r}$	$u_{x_1}^{i}$	$u_{x_2}^{r}$	$u_{x_2}^{i}$	$u_{x_3}^{r}$	$u_{x_3}^{i}$	$u_{x_4}^{r}$	$u_{x_4}^{i}$		

Eqn. (2.14), can be used to obtain these unknown parameters with the knowledge of measurable responses corresponding to different spin speeds and rotor parameters. From Eqn. (2.14), it can be seen that the number of unknowns (i.e., fifty) are far more than the number of equations (i.e., sixteen). This is the case of underdetermined system of linear simultaneous equations. The entire unknown can only be obtained with the help of sets of independent force–response measurements such that the number of equations are increased at least equal or more than the unknowns. The minimum number of independent measurements to be taken is four so that number of independent equations becomes 64. However, the condition of the regression matrix to be inverted has an important role in obtaining the better estimate of parameters. The advantage of the above regression equation is that it contains linear DOFs at bearing locations, which all are practically measurable. In the subsequent section, different cases are presented to make the system as determinate, and methods to handle the condition of regression matrix are also discussed. These cases would be illustrated through numerically simulated forces and responses.

2.3 Procedures to Improve the Condition of Regression Matrix

From the previous section discussions, it is clear that the present system of equations is an underdetermined system of linear simultaneous equations. And to make it over–determinate independent sets of measurements are required often it becomes the ill–condition if sets of measurements are not independent. Hence, to overcome this problem, the present section proposes various possibilities of getting independent sets of measurements of the force–response data required for the identification algorithm. Since the unbalance force changes with the square of speed hence the responses also changes non–linearly. Moreover, the bearings and coupling dynamic parameters have been chosen as speed–independent so single rundown data is sufficient to get estimates. The method is already in use such as by

Edwards et al. (2000). They estimated the speed–independent foundation parameters along with residual unbalances using a single run–down data. Measurements are analysed under three different cases, i. e.

Case A: By rotating the rotor near critical speeds (i.e., near and outside the half–power points)

Case B: By rotating the rotor far away from critical speeds

Case C: By rotating the rotor at several numbers of speeds.

Furthermore, following two measurement methods are adopted for the present case

(*I*) Rotate the rotor in the same sense of direction at different sets of speeds,

(*II*) Rotate the rotor in the clock–wise (CW) and then counter clock–wise (CCW) directions, alternatively, at same or different sets of speeds. This could also be done by an independent (auxiliary) excitation unit (such as external exciters or magnetic actuators or active magnetic bearings).

For each of the above cases the condition number of the regression matrix has also been discussed. Half–power points are two frequencies at either side of resonance often referred as side bands corresponding to $X = 0.707X_{res}$, where X_{res} is resonant amplitude and X is amplitude at sideband frequencies. To avoid the measurement error near critical speeds due to transients often measurements outside the half–power frequency band is advisable. Moreover, within half–power (H–P) points the non–linear effect may come due to large displacements and the present model may not be valid. However, near and outside H–P points the signal–to–noise ratio is expected to be high so it is advantageous for the parameter estimation. The condition number of a matrix (with respect to inversion of the matrix) measures the sensitivity of the solution of a system of linear equations to errors in the data. It gives an

indication of the accuracy of the results from the matrix inversion during solution of linear simultaneous equations. A value of the condition number near one indicates a well–conditioned matrix. The 2–norm condition number, which is used in the present case, is defined as the ratio of the largest singular value of the regression matrix to the smallest (Kreyszig, 2006).

2.3.1 Method I: Rotating the Rotor in the Same Direction at Different Speeds

Take measurements by rotating the rotor in the same direction only (for all the three cases A–C as discussed in the previous section). For *Method I*, measurements at a minimum of four speeds are required to make the system over–determinate. For which the number of equations are increased to sixty–four to estimate the fifty parameters. Noting Eqn. (2.14), the form of regression equation would be

$$\left[A_I(\omega)\right]_{64\times 50}\left\{X_I\right\}_{50\times 1}=\left\{B_I(\omega)\right\}_{64\times 1} \tag{2.15}$$

with

$$[A_I(\omega)]=\begin{bmatrix} A_2(\omega_1)\\ A_2(\omega_2)\\ A_2(\omega_3)\\ A_2(\omega_4)\end{bmatrix},\qquad \{B_I(\omega)\}=\begin{Bmatrix} B_2(\omega_1)\\ B_2(\omega_2)\\ B_2(\omega_3)\\ B_2(\omega_4)\end{Bmatrix}$$

where $[A_I(\omega)]$ and $\{B_I(\omega)\}$ have the same form as in Eqn. (2.14), only with different spin speeds. Eqn. (2.15), is a standard form of regression equation, and it can be used to obtain the bearing and coupling dynamic parameters along with residual unbalances with the help of least–squares fit as follows

$$\left\{X_I\right\}_{50\times 1}=\left(\left[A_I(\omega)\right]^T_{50\times 64}\left[A_I(\omega)\right]_{64\times 50}\right)^{-1}_{50\times 50}\left[A_I(\omega)\right]^T_{50\times 64}\left\{B_I(\omega)\right\}_{64\times 1} \tag{2.16}$$

It should be noted that solution of Eqn. (2.16), requires inversion of the square matrix $([A_I(\omega)]^T[A_I(\omega)])_{50\times50}$. The condition of the matrix can be judged by obtaining the condition number of the square matrix.

2.3.2 Method II: Rotating the Rotor Alternately in the CW or CCW Direction

Take measurements by rotating the rotor first in the CW direction and then in the CCW direction (for all the three cases A–C as discussed in beginning of Section 2.3). Here also measurements at a minimum of four speeds are required to make the system over–determinate. Out of these, first two speeds are corresponding to the CW direction and other two are same speeds (it may be different also) but in the CCW direction. Now numbers of equations are increased to sixty–four to estimate fifty parameters. Noting Eqn. (2.14), the form of regression equation would be

$$[A_{II}(\omega)]_{64\times50}\{X_{II}\}_{50\times1}=\{B_{II}(\omega)\}_{64\times1} \tag{2.17}$$

with

$$[A_{II}(\omega)]=\begin{bmatrix} A_2(\omega_1) \\ A_2(\omega_2) \\ A_2(-\omega_1) \\ A_2(-\omega_2) \end{bmatrix}, \qquad \{B_{II}(\omega)\}=\begin{Bmatrix} B_2(\omega_1) \\ B_2(\omega_2) \\ B_2(-\omega_1) \\ B_2(-\omega_2) \end{Bmatrix}$$

where $[A_{II}(\omega)]$ and $\{B_{II}(\omega)\}$ have the same form as in Eqn. (2.14), only with the different spin speeds and the sense of directions. Eqn. (2.17), is a standard form of regression equation and it can be used to obtain the bearing and coupling dynamic parameters along with residual unbalances with the help of least–squares fit as follows

$$\{X_{II}\}_{50\times1} = \left([A_{II}(\omega)]^T_{50\times64}[A_{II}(\omega)]_{64\times50}\right)^{-1}_{50\times50}[A_{II}(\omega)]^T_{50\times64}\{B_{II}(\omega)\}_{64\times1} \tag{2.18}$$

Hear also the solution of Eqn. (2.18), require inversion of the square matrix $([A_{II}(\omega)]^T[A_{II}(\omega)])_{50\times50}$. It has been found often that the matrices $([A_I(\omega)]^T[A_I(\omega)])$ and $([A_{II}(\omega)]^T[A_{II}(\omega)])$ are highly ill–conditioned since the matrix is nearly singular, i.e. $\left|[A_I(\omega)]^T[A_I(\omega)]\right| \approx 0$ and $\left|[A_{II}(\omega)]^T[A_{II}(\omega)]\right| \approx 0$. This poses difficulty in identifying the required parameters uniquely. However, due to the way measurements have been taken in both sense of rotations (i.e. CW and CCW) the possibility of ill–condition reduces due to availability of the modal information related to forward and backward whirls, which are otherwise unavailable in measurements. And in fact it is expected to improve estimates when more and more modal information of the system is available in measurements. Mathematically, such measurements would be more independent to improve the condition of the regression matrix. To further improve the condition number of the matrix, the last eight columns of the matrix $[A_I]$ and $[A_{II}]$ are scaled by inverse of the average of spin speed range considered.

2.4 Numerical Experiments

For illustration of the present identification algorithm, a rotor model as shown in Figure 2.1, is considered. Rotor dimensions and residual unbalances are given in Table 2.2 & Table 2.3, respectively. For numerical simulation of responses, the bearing and coupling dynamic parameters and residual unbalances are assumed. The second column of Table 2.4–Table 2.7 contains all the bearing and coupling dynamic parameters, and residual unbalances assumed for the numerical simulation of forced responses. First by considering the free vibration of the system for the assumed values of system parameters the natural frequencies of the present

rotor model are obtained. These are ω_{nf1}= 161 rad/s, ω_{nf2}= 209 rad/s, ω_{nf3}=290 rad/s, ω_{nf4}= 353 rad/s, ω_{nf5}=359 rad/s, ω_{nf6} = 652 rad/s, ω_{nf7}=1170 rad/s, and ω_{nf8}= 1558 rad/s. A typical variation of the forced response with the spin speed is shown in Figure 2.3. It could be seen that at all above natural frequencies, the resonance condition (i.e., forward critical speeds) prevails both in the amplitude and the phase. These are same due to gyroscopic effects are ignored in the present study.

Table 2.2 Rotor geometrical and physical properties

S.N.	Shaft no	Length (m)	Diameter (m)	Density (kg/m^3)	Mass (kg)	Diametral mass moment of inertia (kg–m^2)
1	Shaft 1	1.25	0.01	7800	0.765	0.0996
2	Shaft 2	1.25	0.01	7800	0.765	0.0996

Table 2.3 Residual unbalances

S.N.	Location	Diameter (m)	Mass (kg)	Diametral mass moment of inertia (kg–m^2)	Residual unbalances	
					Magnitude (kg–m)	Angular position (deg.)
1	Disc 1	0.15	5	2.48×10^{-5}	9.5×10^{-3}	36
2	Disc 2	0.13	3	1.40×10^{-5}	6.0×10^{-3}	108
3	Disc 3	0.12	2	1.01×10^{-5}	7.9×10^{-3}	240
4	Disc 4	0.14	6	1.88×10^{-5}	11.2×10^{-3}	300

For the estimation of the bearing and coupling dynamic parameters along with residual unbalances, the present technique requires forced vibration response measurements, which have been generated through a numerical simulation using Eqn. (2.10). A flowchart of the numerical simulation of the identification procedure is given in Figure 2.4. To improve the accuracy of estimates column scaling of regression matrices $[A_I]$ and $[A_{II}]$ have been done. For example, the effect of column scaling can be seen from Figure 2.5, which shows the comparison of error in the estimation of parameters for *Case A* under *Method I* for 1% measurement noise. To mimic the actual experimental response signal the white noise has been added to the numerically simulated response signal using MATLAB.

Procedure to Add the Noise in the Simulated Signal

- First random numbers have been generated in MATLAB using 'rand' command and stored in a vector $\{R\}_{n\times1}$.
- The size of the vector $\{R\}_{n\times1}$ must be equal to the size of the response vector $\{X\}_{n\times1}$.
- Find out maxima of vector $\{R\}$ i.e. $R_{\max}$.
- The elements of vector$\{R\}$ are divided by $R_{\max}$ to make its range from 0 to 1 and then subtracted by 0.5 to make its range −0.5 to 0.5, i.e.

$$\{R_{\pm0.5}\}_{n\times1} = \{R\}_{n\times1}/\{R_{\max}\}_{1\times1} - 0.5 \tag{2.19}$$

- Now the noisy response could be obtain as

$$\{X\}_{\text{noisy}} = \{X\}_{n\times1} + (\{X\}_{n\times1}\times\{R_{\pm0.5}\}_{n\times1}) \times N_P/100 \tag{2.20}$$

$N_P/100$ is the percentage of noise. $N_P = (0, 1, 2, \ldots, N)$, N is the real number

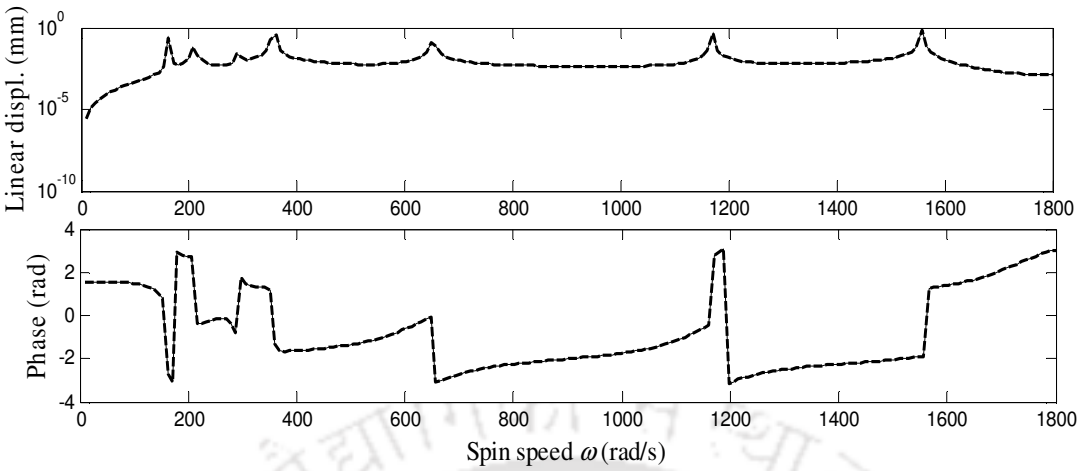

Figure 2.3 Variation of the horizontal response at bearing location 1 with the spin speed

In Figure 2.5, the number in the abscissa represents an estimated parameter corresponding to the row number in the vector $\{X\}$ of Eqn. (2.14) and these parameters are also summarised with corresponding row locations in Table 2.1. It could also be seen from Figure 2.5 that the percentage improvement in the accuracy of the estimated parameters is around 20% after column scaling. From Table 2.8, it can be seen that the condition number of regression matrix is improved by the order 10^{12}. It should be noted that the order of improvement in the condition number is least for the illustrated case i.e., *Case A* under *Method I.* (refer Table 2.8). It is so because near and outside H–P points the signal–to–noise ratio is expected to be high and because of this co–linearity of the elements in the matrix is least. The following sub–section comprises of comparing responses from assumed parameters and that from estimated parameters for different cases discussed in Section 2.3.

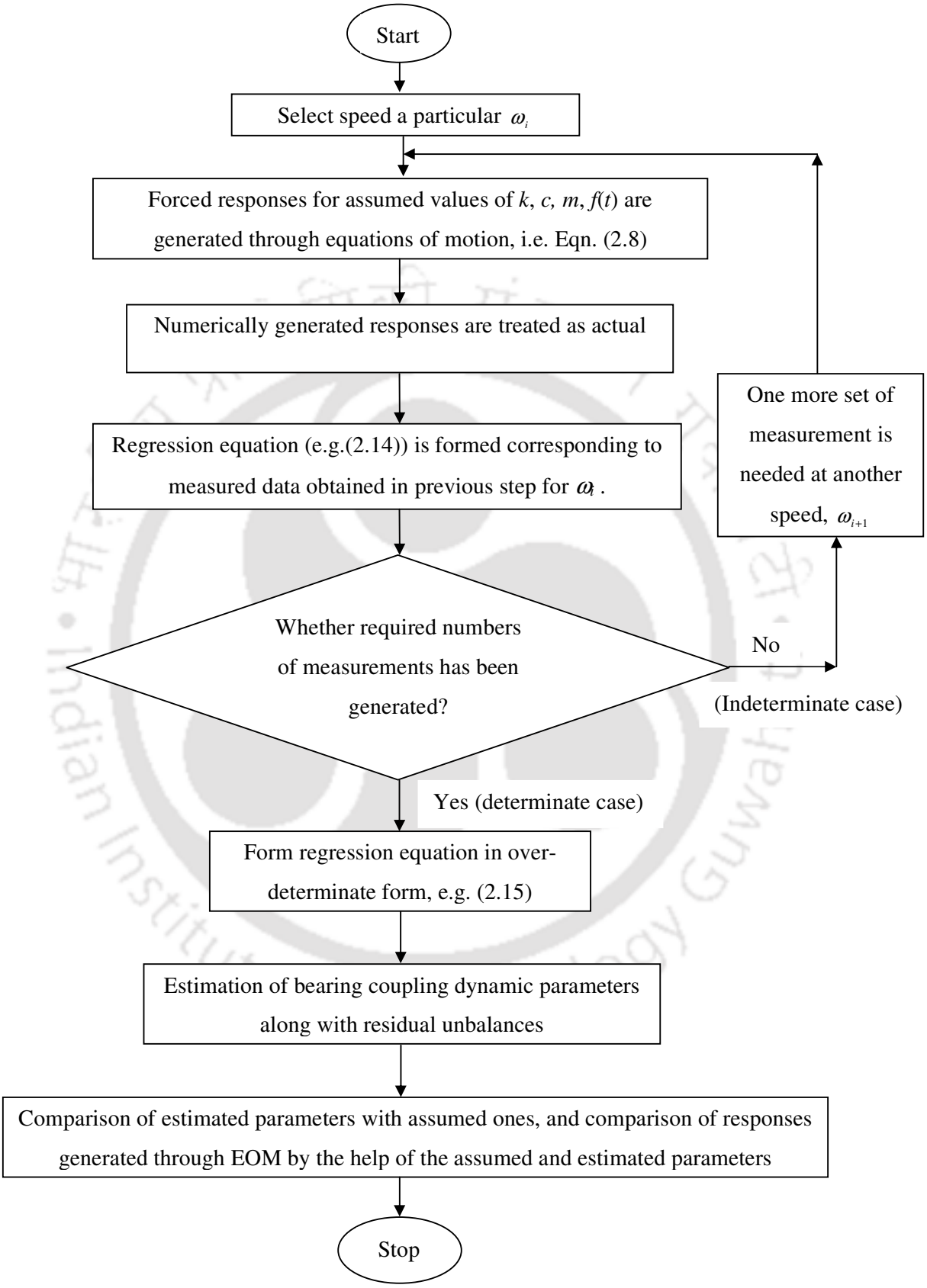

Figure 2.4 A flow chart of the identification algorithm

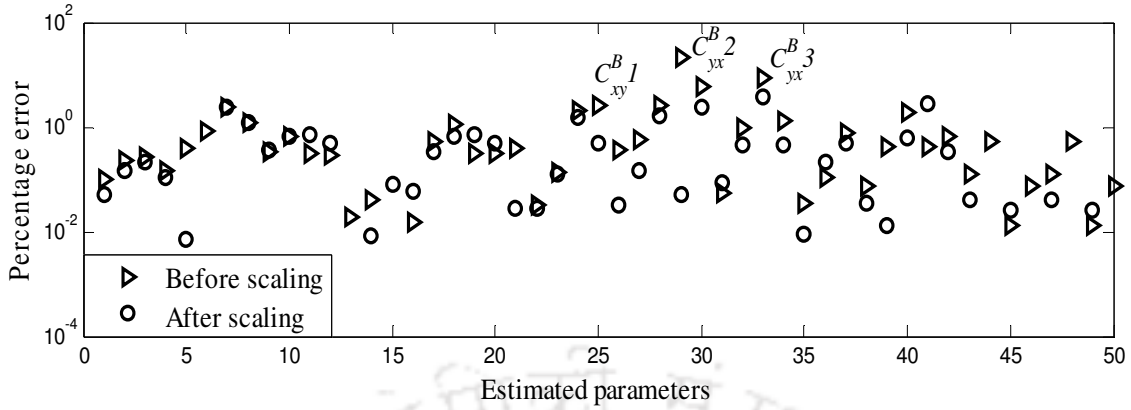

Figure 2.5 Comparison of errors of estimated parameters before and after column scaling for 1% measurement noise (for Case *A* under *Method I*)

2.4.1 Method I: Rotating the Rotor in the Same Direction at Different Speeds

***Case A*:** Parameters are estimated from responses at selected set of spin speed near, however, outside of half−power points. Displacements are calculated at four speeds, i.e. ω_1= 150 rad/s, ω_2= 170 rad/s, ω_3=200 rad/s, and ω_4= 220 rad/s. From Figure 2.6, it can be seen that responses generated from initially assumed parameters and that of estimated parameters are nearly equal for without noise case, and quite close for 1% noise condition. However, as we increase the noise percentage in a range from 2% to 5%, the estimated parameters deviate appreciably then the assumed parameters. It can also be seen in Figure 2.7 that the error in estimation of some of parameters is around 5% and 30% for 1% and 5% noise conditions, respectively. From Table 2.8, it can be seen that after column scaling, the condition number of regression matrix is improved by the order of 10^{12}.

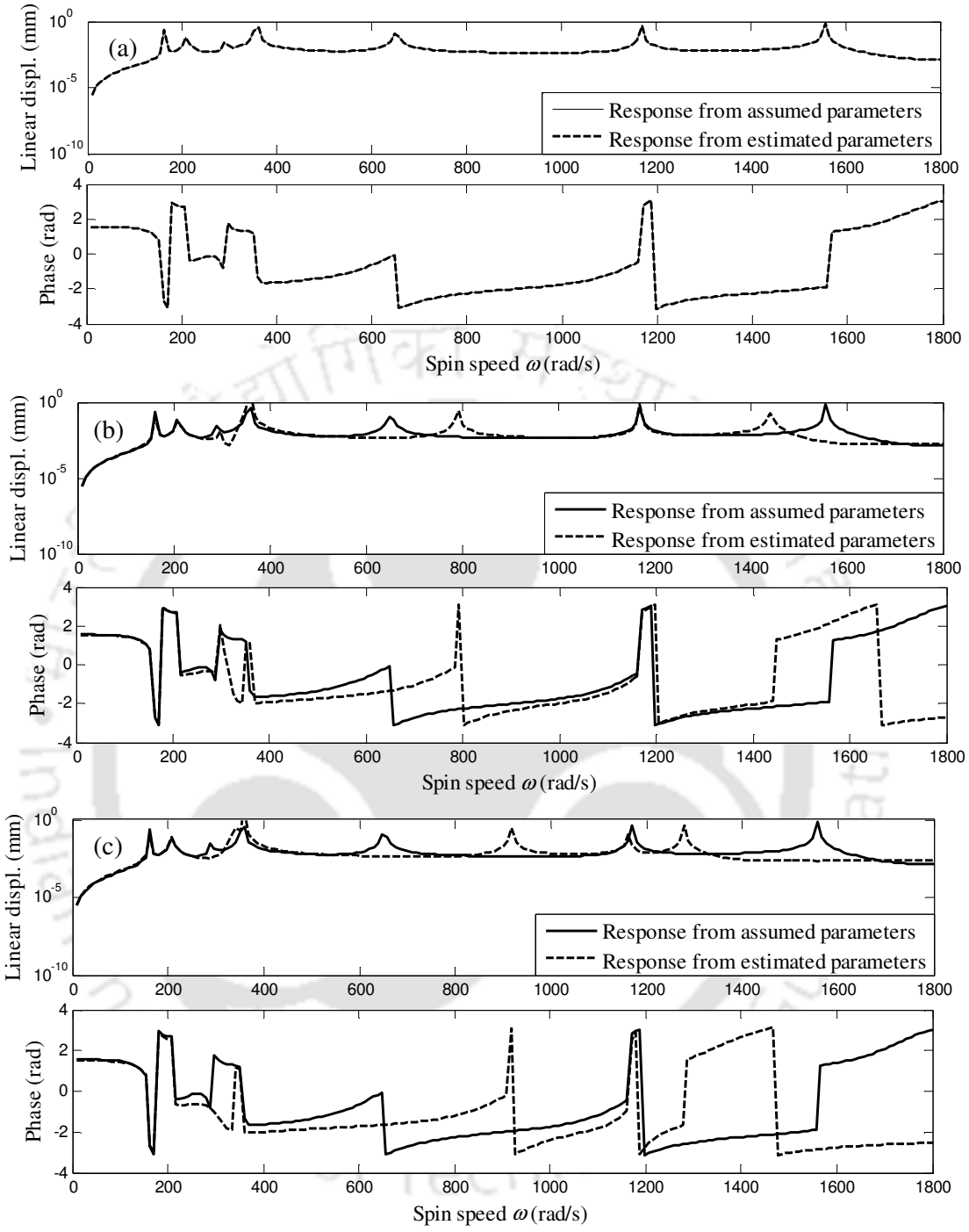

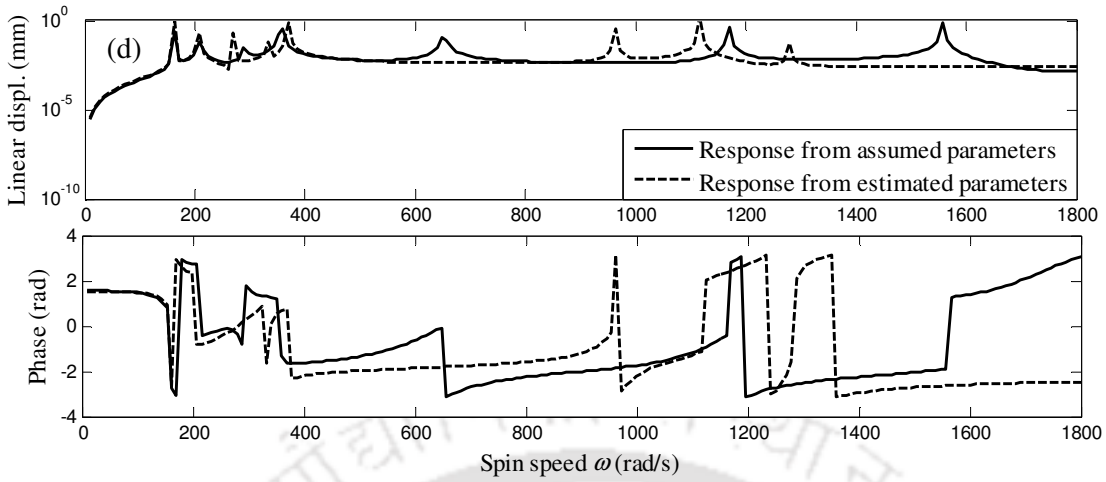

Figure 2.6 Comparison of responses (a) without noise (b) with 1% noise (c) with 2% noise (d) with 5% noise (for *Case A* under *Method I*)

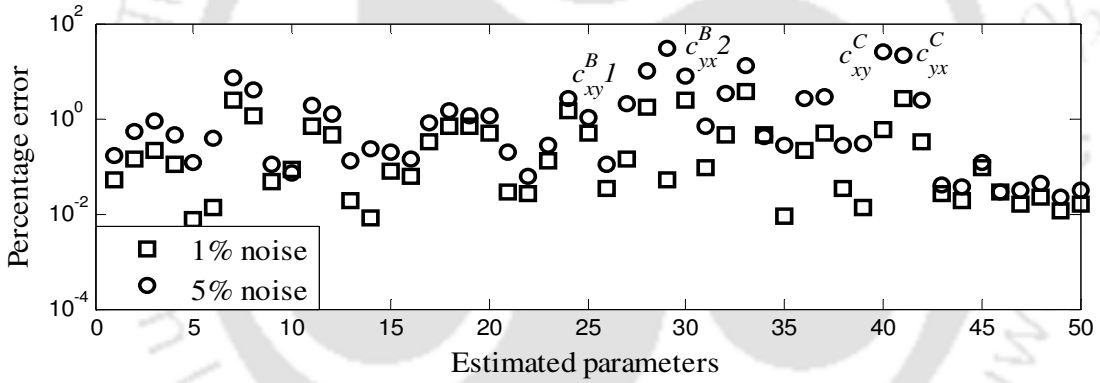

Figure 2.7 Comparison of errors of estimated parameters for different level of measurement noise (for *Case A* under *Method I*)

***Case B*:** Parameters are identified from forced responses at selected set of spin speeds away from half–power points. Displacements are calculated at four speeds, i.e. ω_1=100 rad/s, ω_2=185 rad/s, ω_3=240 rad/s, and ω_4= 330 rad/s. From Figure 2.8, it can be analysed that responses generated from initially assumed parameters and responses generated from estimated parameters are nearly same for 1% noise. From Figure 2.9, it can be seen that the maximum error is around 2% for this case. But as we increase the noise up to 5%, estimated

parameters deviate from assumed parameters by 5%. For the present case mostly damping parameters show deviations. After column scaling the condition number is improved of the order of 10^{13} (refer Table 2.8).

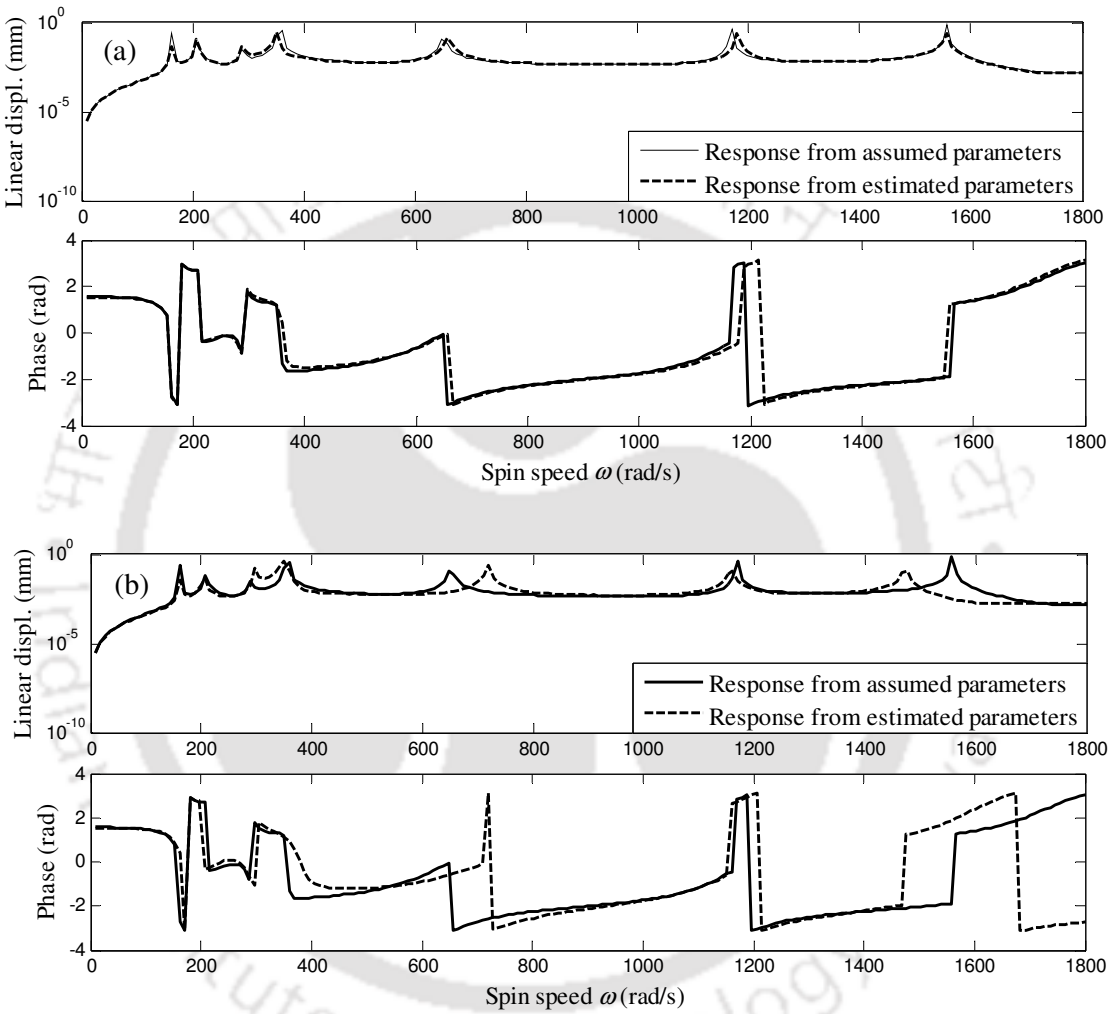

Figure 2.8 Comparison of responses generated from the assumed and estimated parameters (a) 1% noise (b) 5% noise (for *Case B* under *Method I*)

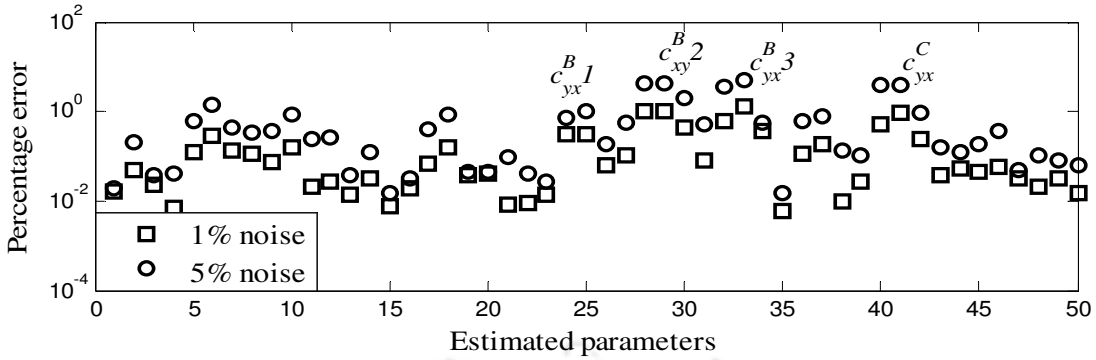

Figure 2.9 Comparison of errors of estimated parameters for different level of measurement noise (for *Case B* under *Method I*)

***Case C*:** Parameters are identified from forced responses by increasing the number of measurement speeds up to 200 in numbers. Displacements are calculated at speeds, i.e. for CW: ω = (0–2000) rad/s with step size of 10 rad/s. From Figure 2.10, it can be analysed that responses generated from assumed parameters and responses generated from estimated parameters are quite close for 1% noise. It can also be seen from Figure 2.11 that the maximum error in estimated parameters is around 0.2% for this case. As we increase the noise up to 5%, estimated parameters deviate negligibly from assumed parameters and the maximum error is around 0.9%. From Table 2.8, it can be seen that the condition number of regression matrix is improved after column scaling by the order of 10^{15}.

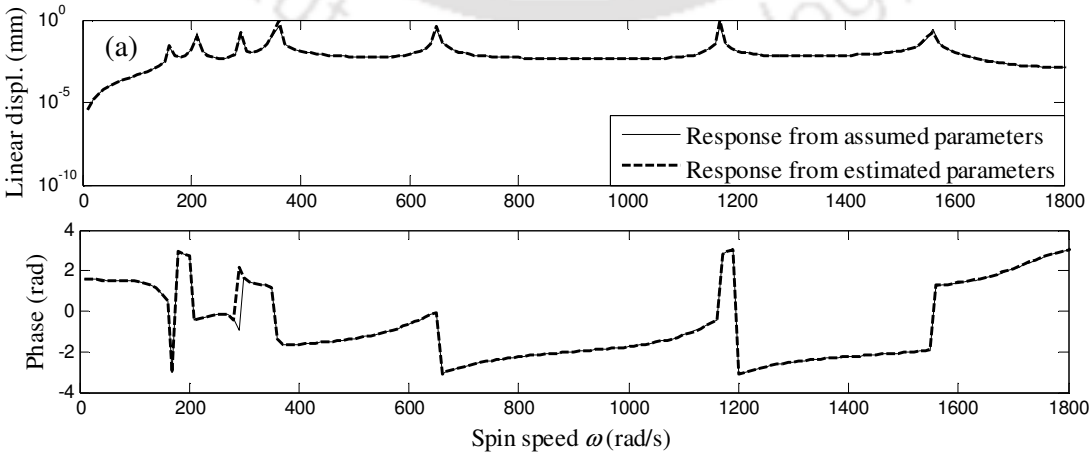

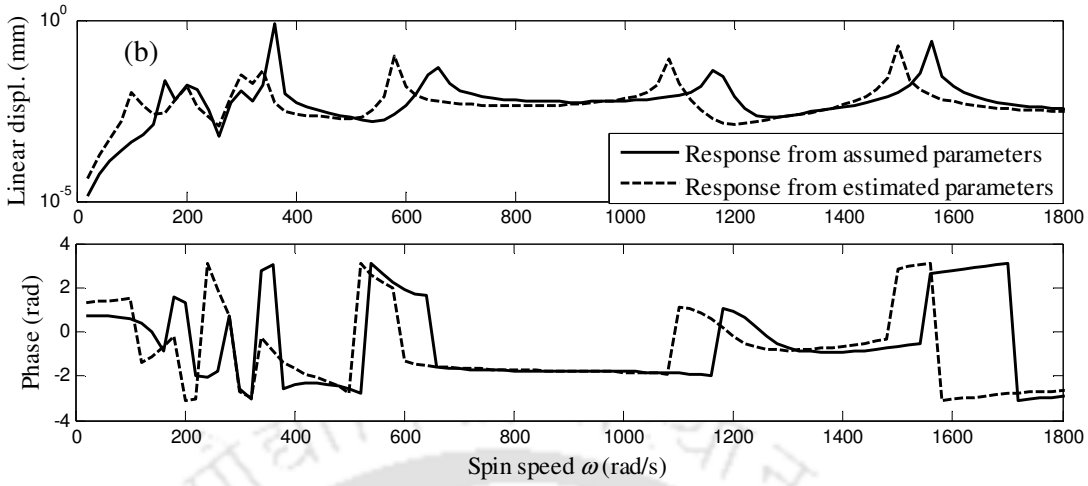

Figure 2.10 Comparison of responses (a) 1% noise (b) 5% noise (for *Case C* under *Method I*)

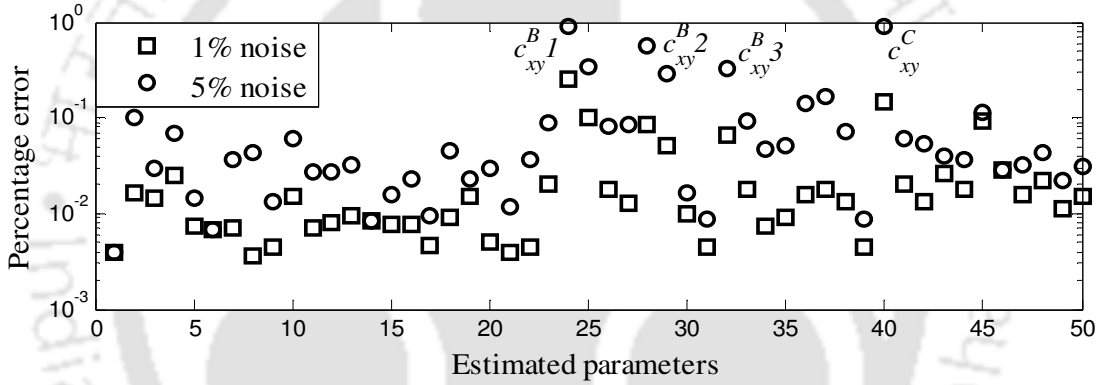

Figure 2.11 Comparison of errors of estimated parameters for different level of measurement noise (for *Case C* under *Method I*)

2.4.2 Method II: Rotating the Rotor Alternately in the CW or CCW Direction

From the above section, it is evident that the proposed estimation *Method I* is effective to estimate the bearing and coupling dynamic parameters along with residual unbalances only up to 1% noise condition for different cases discussed above. However, the estimation is very poor as we increase the noise percentage level. So *Method II* has been proposed on taking measurements by rotating rotor CW and CWW alternatively to improve the effectiveness of the estimation and to sort out the problem arises in *Method I*. It should be noted that such

excitation can also be generated by an independent excitation unit without rotating rotor in CW or CCW, alternately (Tiwari, 2005).

***Case A*:** Parameters are identified by operating the rotor system at selected speed (near, however, outside half–power points). Displacement values are calculated at four speeds, i.e. for CW: ω_1=150 rad/s and ω_2=170 rad/s, and for CCW: ω_1= 150 rad/s and ω_2= 170 rad/s. From Figure 2.12, it can be analysed that responses generated from initially assumed parameters and that of estimated parameters deviate appreciably at 1% noise, and as we increase the noise up to 5% deviation increases drastically. It can also be seen in Figure 2.13 that the error in the estimation of some of parameters are around 7% and 11% for 1% and 5% noise conditions, respectively. By column scaling the condition number is improved by the order 10^{13} (refer Table 2.8). As compared to *Case A* under *Method I* in the aforementioned case the percentage error in estimation is reduced appreciably from 30% to 10% (refer Table 2.8).

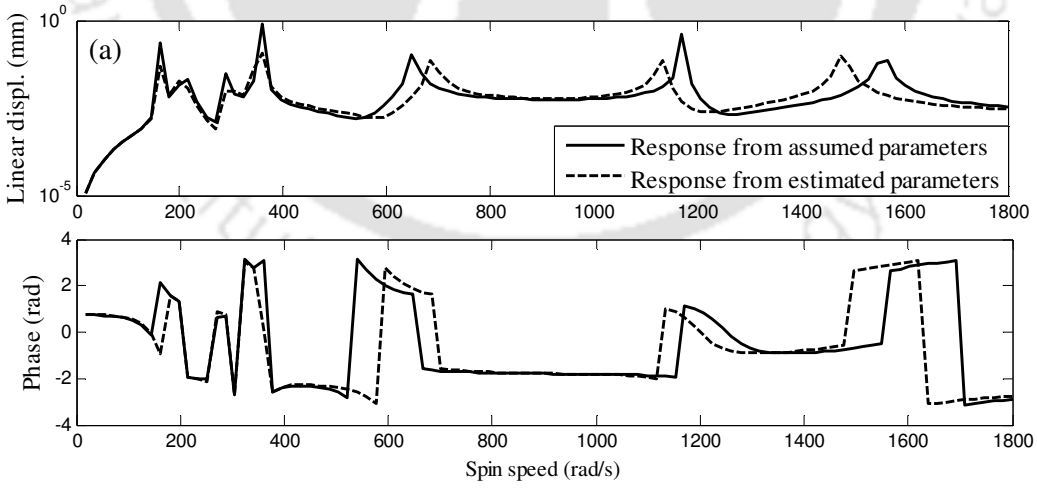

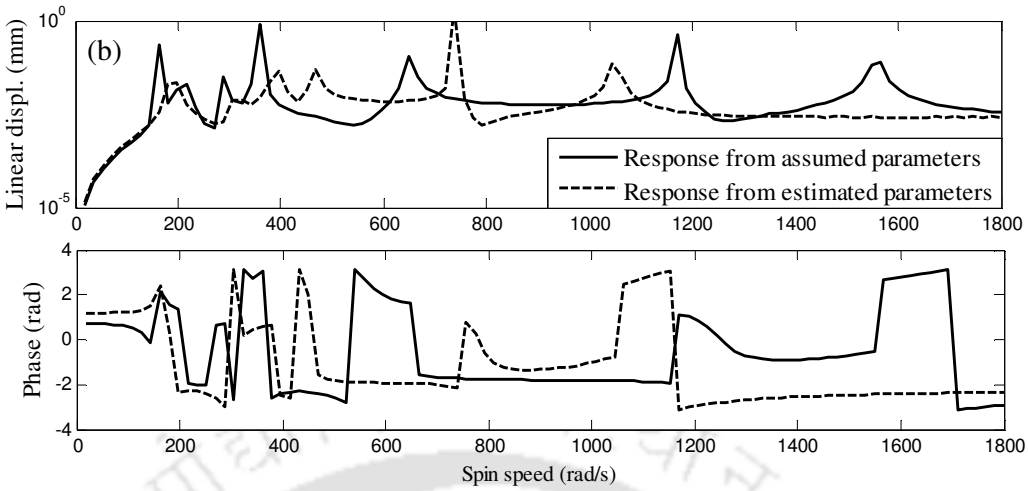

Figure 2.12 Comparison of responses (a) 1% noise (b) 5% noise (for *Case A* under *Method II*)

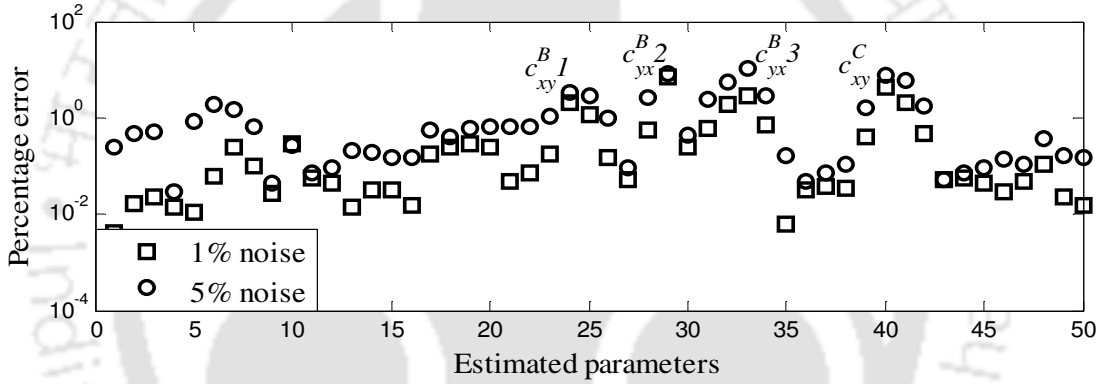

Figure 2.13 Comparison of errors of estimated parameters for different level of measurement noise (for *Case A* under *Method II*)

***Case B*:** Parameters are identified from forced responses at randomly selected set of spin speeds that are away from half–power points. Displacements are calculated at four speeds, i.e. for CW: ω_1=100 rad/s and ω_2=240 rad/s, and for CCW: ω_1= 100 rad/s and ω_2= 240 rad/s. From Figure 2.14, it can be analysed that responses generated from assumed parameters and responses generated from estimated parameters are nearly same for 1% noise. From Figure 2.15, it can be seen that the error is below 0.5%. But as we increase the noise up to 5%, estimated parameters deviate from assumed parameters by 2.5%. From Table 2.8, it can be seen that the condition number is improved by the order 10^{13} for the aforementioned case. In

this case as compared to *Case B* under *Method I*, the percentage error in estimation is reduced from 5% to 2.4% (refer Table 2.8).

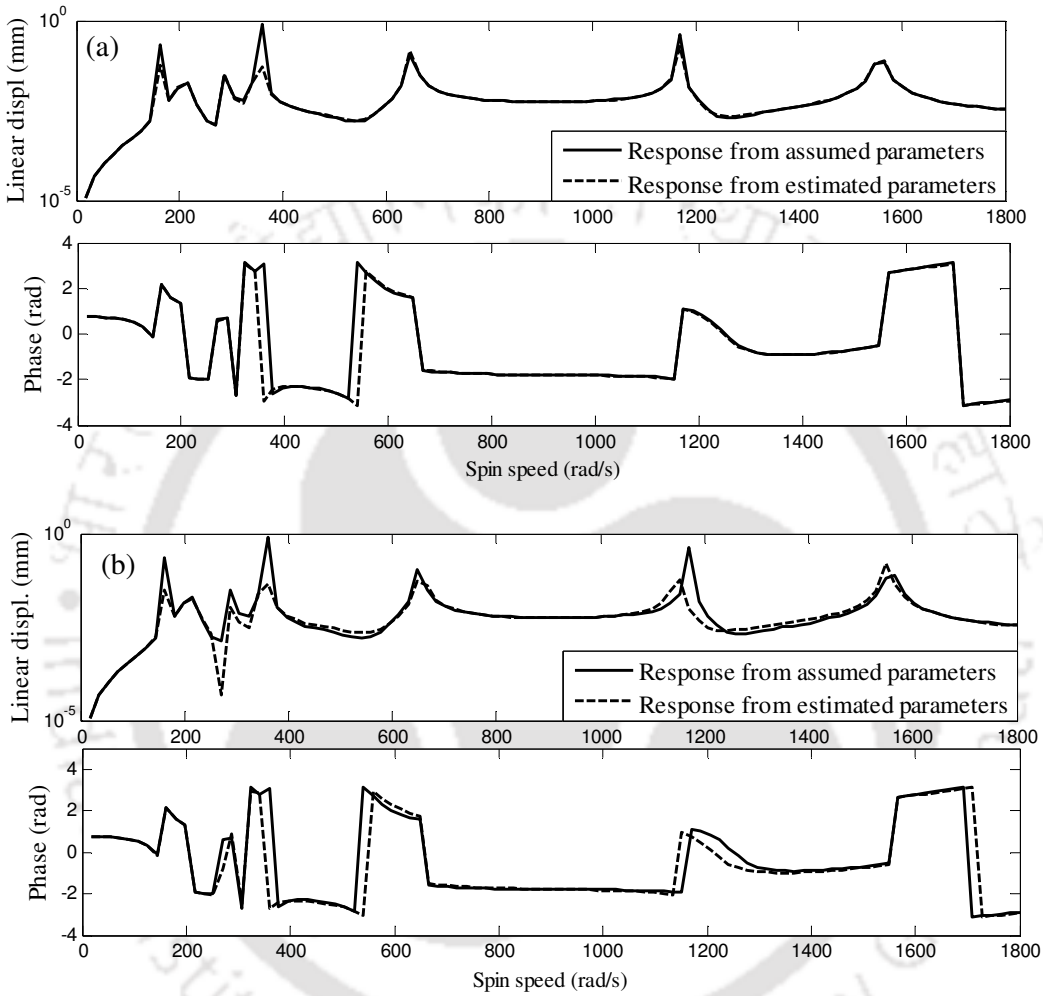

Figure 2.14 Comparison of responses (a) 1% noise (b) 5% noise (for *Case B* under *Method II*)

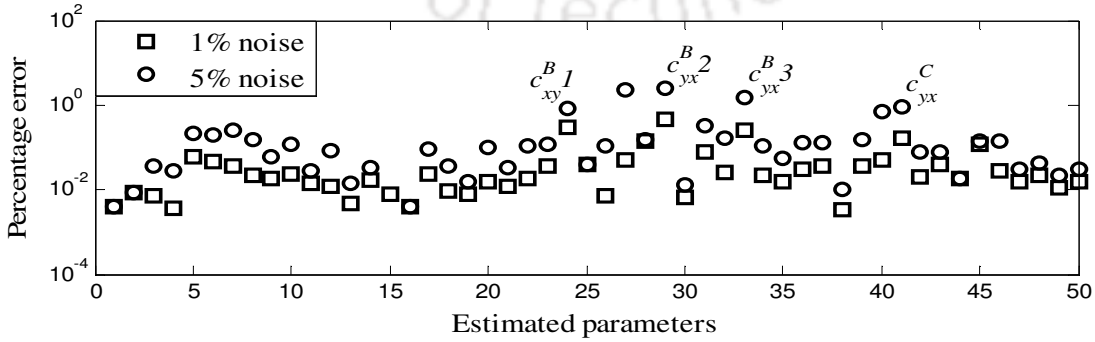

Figure 2.15 Comparison of errors of estimated parameters for different level of measurement noise (for *Case B* under *Method II*)

***Case C*:** Parameters are identified from forced responses by increasing the number of measurement speeds up to 200 in numbers. Displacements are calculated at speeds, i.e. for CW: ω = (0–2000) rad/s with step size of 20 rad/s, i.e. 100 numbers of different speeds; for CCW: ω = (0–2000) rad/s with step size of 20 rad/s, i.e.100 numbers of different speeds. From Figure 2.16 one can come to the conclusion that responses generated from assumed parameters and that of the estimated parameters deviate negligibly small even for 5% noise. It can be observed in Figure 2.17 that the maximum error for estimation is around 0.08% for 5% noise case, it can also be seen that the bearing and coupling dynamic parameters and residual unbalances are estimated accurately up to 5% noise condition from Table 2.8. The condition number is improved by the order 10^{16} for this case (refer Table 2.8). In the aforementioned case as compared to *Case C* under *Method I*, the percentage error in estimation is reduced from 0.9% to 0.07% (refer Table 2.8).

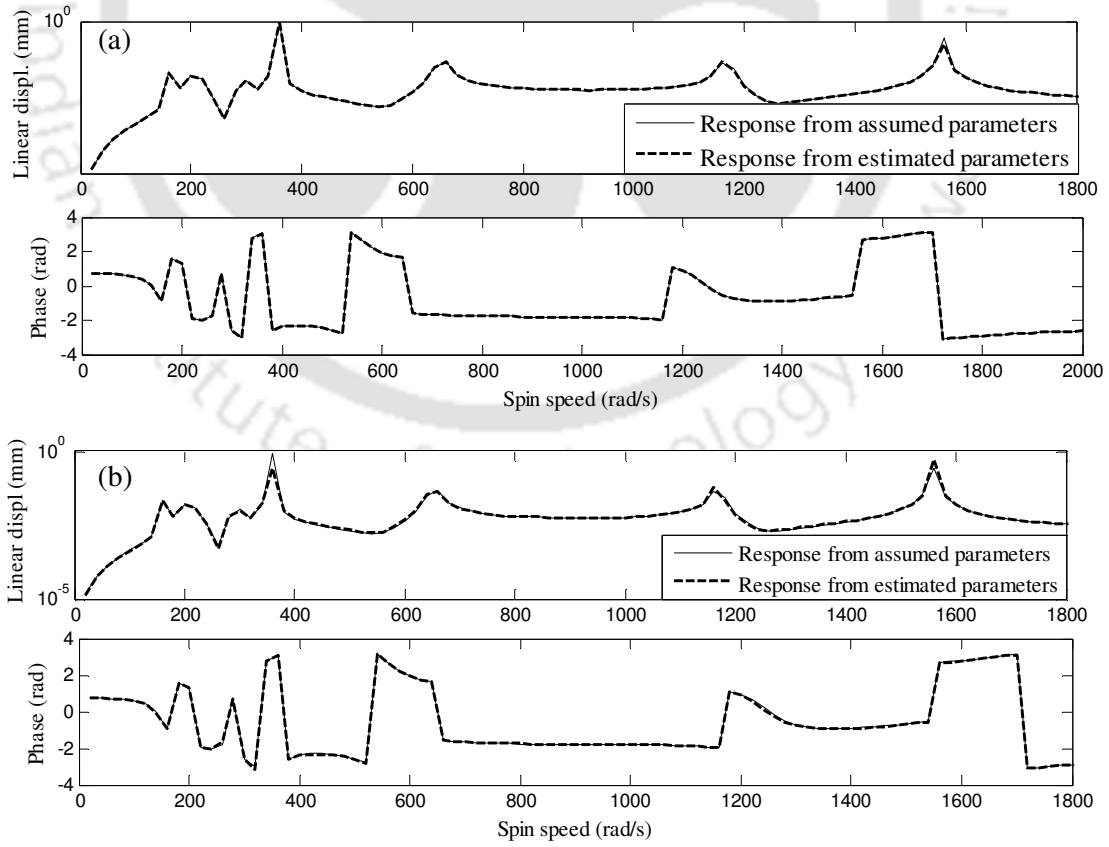

Figure 2.16 Comparison of responses (a) 1% noise (b) 5% noise (for *Case C* under *Method II*)

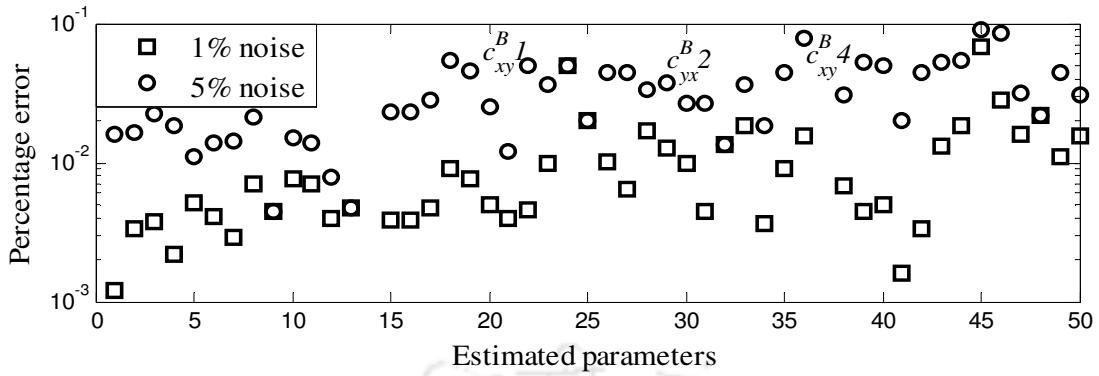

Figure 2.17 Comparison of errors of estimated parameters for different level of measurement noise (for Case C under Method II

Table 2.4 Assumed and identified bearing stiffness parameters for Case C of Method II

Parameters	Assumed values	Estimated values			
		Without noise	With 1% noise	With 2%noise	With 5%noise
$k^{b_1}_{xx}$ (N/m)	2.5000×10^5	2.5246×10^5	2.5289×10^5	2.5377×10^5	2.5888×10^5
$k^{b_1}_{xy}$ (N/m)	1.2000×10^5	1.2120×10^5	1.2121×10^5	1.2130×10^5	1.2199×10^5
$k^{b_1}_{yx}$ (N/m)	1.3500×10^5	1.3635×10^5	1.3632×10^5	1.3639×10^5	1.3711×10^5
$k^{b_1}_{yy}$ (N/m)	2.7500×10^5	2.7770×10^5	2.7874×10^5	2.8023×10^5	2.8708×10^5
$k^{b_2}_{xx}$ (N/m)	2.7500×10^5	2.7762×10^5	2.7813×10^5	2.7853×10^5	2.7907×10^5
$k^{b_2}_{xy}$ (N/m)	1.4600×10^5	1.4740×10^5	1.4732×10^5	1.4729×10^5	1.4740×10^5
$k^{b_2}_{yx}$ (N/m)	1.3900×10^5	1.4034×10^5	1.4069×10^5	1.4105×10^5	1.4211×10^5
$k^{b_2}_{yy}$ (N/m)	2.8200×10^5	2.8468×10^5	2.8391×10^5	2.8313×10^5	2.8077×10^5
$k^{b_3}_{xx}$ (N/m)	2.2700×10^5	2.2919×10^5	2.2914×10^5	2.2927×10^5	2.3053×10^5
$k^{b_3}_{xy}$ (N/m)	1.3100×10^5	1.3226×10^5	1.3245×10^5	1.3265×10^5	1.3337×10^5
$k^{b_3}_{yx}$ (N/m)	1.4400×10^5	1.4538×10^5	1.4526×10^5	1.4519×10^5	1.4521×10^5
$k^{b_3}_{yy}$ (N/m)	2.5300×10^5	2.5544×10^5	2.5519×10^5	2.5508×10^5	2.5546×10^5
$k^{b_4}_{xx}$ (N/m)	2.1400×10^5	2.1610×10^5	2.1579×10^5	2.1589×10^5	2.1835×10^5
$k^{b_4}_{xy}$ (N/m)	1.2100×10^5	1.2222×10^5	1.2259×10^5	1.2307×10^5	1.2502×10^5
$k^{b_4}_{yx}$ (N/m)	1.2900×10^5	1.3031×10^5	1.3050×10^5	1.3080×10^5	1.3226×10^5
$k^{b_4}_{yy}$ (N/m)	2.5600×10^5	2.5851×10^5	2.5876×10^5	2.5939×10^5	2.6331×10^5

Table 2.5 Assumed and identified bearing damping parameters for *Case C* of *Method II*

Parameters used for simulation	Assumed values	Estimated values			
		Without noise	With 1% noise	With 2%noise	With 5%noise
$c_{xx}^{b_1}$ (Ns/m)	300.00	302.95	302.22	301.78	302.00
$c_{xy}^{b_1}$ (Ns/m)	20.00	20.19	20.21	20.25	20.52
$c_{yx}^{b_1}$ (Ns/m)	50.00	50.50	50.57	50.63	50.78
$c_{yy}^{b_1}$ (Ns/m)	399.00	402.92	401.50	400.38	398.64
$c_{xx}^{b_2}$ (Ns/m)	315.00	317.98	319.41	321.25	328.94
$c_{xy}^{b_2}$ (Ns/m)	59.00	59.55	59.18	58.99	59.48
$c_{yx}^{b_2}$ (Ns/m)	79.00	79.76	80.09	80.47	81.85
$c_{yy}^{b_2}$ (Ns/m)	300.00	302.84	303.25	304.09	308.93
$c_{xx}^{b_3}$ (Ns/m)	225.00	227.19	226.94	226.55	224.59
$c_{xy}^{b_3}$ (Ns/m)	75.00	75.73	75.81	75.73	74.60
$c_{yx}^{b_3}$ (Ns/m)	55.00	55.53	55.37	55.10	53.71
$c_{yy}^{b_3}$ (Ns/m)	275.00	277.67	278.27	278.75	279.46
$c_{xx}^{b_4}$ (Ns/m)	335.00	338.41	337.39	336.38	333.37
$c_{xy}^{b_4}$ (Ns/m)	64.00	64.57	64.82	65.03	65.47
$c_{yx}^{b_4}$ (Ns/m)	55.00	55.48	55.12	54.75	53.50
$c_{yy}^{b_4}$ (Ns/m)	295.00	298.06	299.18	300.46	305.18

Table 2.6 Assumed and identified coupling dynamic parameters for *Case C* of *Method II*

Parameters used for simulation	Assumed values	Estimated values			
		Without noise	With 1% noise	With 2% noise	With 5% noise
k_{xx}^{c} (N/m)	2.1200×10^{5}	2.1241×10^{5}	2.1262×10^{5}	2.1216×10^{5}	2.0727×10^{5}
k_{xy}^{c} (N/m)	1.1100×10^{5}	1.1122×10^{5}	1.1075×10^{5}	1.0988×10^{5}	1.0516×10^{5}
k_{yx}^{c} (N/m)	1.3100×10^{5}	1.3127×10^{5}	1.3108×10^{5}	1.3039×10^{5}	1.2567×10^{5}
k_{yy}^{c} (N/m)	1.9900×10^{5}	1.9940×10^{5}	1.9928×10^{5}	1.9853×10^{5}	1.9287×10^{5}
$k_{\varphi_x}^{c}$ (Nm/rad)	2.5000×10^{5}	2.5013×10^{5}	2.4976×10^{5}	2.4857×10^{5}	2.4072×10^{5}
$k_{\varphi_y}^{c}$ (Nm/rad)	2.2000×10^{5}	2.2013×10^{5}	2.1942×10^{5}	2.1796×10^{5}	2.0967×10^{5}
c_{xx}^{c} (Ns/m)	225.00	225.42	224.70	223.06	213.26
c_{xy}^{c} (Ns/m)	20.00	20.08	19.96	20.01	20.56
c_{yx}^{c} (Ns/m)	50.00	50.05	50.08	50.09	50.13
c_{yy}^{c} (Ns/m)	295.00	295.56	295.25	293.71	282.45

Table 2.7 Assumed and identified unbalance parameters for *Case C* of *Method II*

Parameters used for simulation	Assumed values	Estimated values			
		Without noise	With 1% noise	With 2%noise	With 5%noise
$u_{real}^{res_1}$ (kg-m)	0.0076	0.0077	0.0077	0.0078	0.0080
$u_{img}^{res_1}$ (kg-m)	0.0055	0.0056	0.0056	0.0057	0.0058
$u_{real}^{res_2}$ (kg-m)	0.0044	0.0049	0.0049	0.0049	0.0048
$u_{img}^{res_2}$ (kg-m)	0.0035	0.0035	0.0035	0.0036	0.0038
$u_{real}^{res_3}$ (kg-m)	0.0063	0.0064	0.0064	0.0065	0.0065
$u_{img}^{res_3}$ (kg-m)	0.0046	0.0046	0.0047	0.0047	0.0047
$u_{real}^{res_4}$ (kg-m)	0.0090	0.0091	0.0091	0.0092	0.0094
$u_{img}^{res_4}$ (kg-m)	0.0065	0.0066	0.0066	0.0066	0.0067

After estimating coupling dynamic parameters and responses at coupling location it can be used to estimate the misalignment forces and moments by Eqn. (2.12). For the best estimated case of the bearing and coupling dynamic parameters (i.e. *Case C* under *Method II*), the variation of misalignment forces and moments are plotted with respect to the spin speed in Figure 2.18. It is to be noted that the misalignment forces and moments are dependent on the spin speed and because of it the misalignment forces and moments are very high at or near critical speeds of the system. Table 2.9 and Table 2.10, show identified residual unbalances (magnitude and phase) of the system for different assumed residual unbalances and disc masses, respectively, for 5% measurement noise for Case C under Method II. From Table 2.9, it can also be observed that with the change in magnitude and phase angle of assumed residual unbalances, the variation in estimates of residual unbalances is very less. In Table 2.10, different sets of disc masses has been considered for estimating residual unbalances and it shows good agreement between assumed and estimated residual unbalances for different sets of disc masses.

Table 2.8 Summary of estimated parameters having maximum % error and corresponding condition numbers for different cases

Methods	Cases	Estimated parameters having maximum % error			Condition number before column scaling			Condition number after column scaling			Order of improvement in condition number for 5% noise
		For 1% noise	For 2% noise	For 5% noise	For 1% noise	For 2% noise	For 5% noise	For 1% noise	For 2% noise	For 5% noise	
Method *I*	Case A	$c_{yx}^{b_3}$=3.69	c_{yx}^{c}=10.90	$c_{yx}^{b_2}$=30.01	2.49×10^{18}	2.41×10^{19}	9.26×10^{18}	2.57×10^{6}	3.86×10^{6}	5.69×10^{6}	1.62×10^{12}
	Case B	$c_{yx}^{b_3}$=1.25	$c_{yx}^{b_3}$=2.40	$c_{yx}^{b_3}$=5.05	1.92×10^{18}	2.37×10^{19}	3.71×10^{19}	1.71×10^{6}	2.22×10^{6}	2.42×10^{6}	1.53×10^{13}
	Case C	$c_{xy}^{b_1}$=0.25	$c_{xy}^{b_1}$=0.45	$c_{xy}^{b_1}$=0.90	1.40×10^{18}	1.78×10^{18}	2.41×10^{19}	2.95×10^{3}	2.98×10^{3}	3.55×10^{3}	6.78×10^{15}
Method *II*	Case A	$c_{xy}^{b_2}$=6.98	$c_{yx}^{b_2}$=10.94	$c_{yx}^{b_3}$=10.63	2.34×10^{19}	2.69×10^{19}	5.97×10^{19}	2.84×10^{6}	2.89×10^{6}	4.15×10^{6}	1.43×10^{13}
	Case B	$c_{yx}^{b_2}$=0.47	$c_{yx}^{b_2}$=0.95	$c_{yx}^{b_2}$=2.41	7.32×10^{18}	1.38×10^{19}	4.17×10^{19}	2.75×10^{6}	2.84×10^{6}	2.80×10^{6}	1.48×10^{13}
	Case C	$c_{xy}^{b_4}$=0.01	$c_{xy}^{b_4}$=0.03	$c_{xy}^{b_4}$=0.07	7.23×10^{18}	9.57×10^{18}	1.57×10^{19}	6.87×10^{3}	7.01×10^{3}	1.18×10^{3}	1.33×10^{16}

Table 2.9 Identified residual unbalances for different assumed residual unbalance for 5% measurement noise (for *Case C* under *Method II*)

S.N.	Residual unbalance in plane 1 (kg–m@deg)		Residual unbalance in plane 2 (kg–m@deg)		Residual unbalance in plane 3 (kg–m@deg)		Residual unbalance in plane 4 (kg–m@deg)	
	Assumed	Estimated	Assumed	Estimated	Assumed	Estimated	Assumed	Estimated
1	9.6×10^{-3} @36.0	9.9×10^{-3} @36.8	6.0×10^{-3} @108.0	6.1×10^{-3} @108.4	7.5×10^{-3} @240.0	7.7×10^{-3} @240.9	11.1×10^{-3} @300.0	11.5×10^{-3} @300.2
2	10.5×10^{-3} @46.0	10.8×10^{-3} @47.0	6.5×10^{-3} @112.0	6.7×10^{-3} @112.8	8.3×10^{-3} @220.0	8.6×10^{-3} @220.8	13.1×10^{-3} @315.0	13.5×10^{-3} @315.6
3	11.8×10^{-3} @66.0	12.1×10^{-3} @66.8	7.5×10^{-3} @130.0	7.7×10^{-3} @130.9	9.6×10^{-3} @200.0	9.9×10^{-3} @201.2	15.0×10^{-3} @330.0	15.4×10^{-3} @330.7
4	13.2×10^{-3} @70.0	13.5×10^{-3} @71.2	9.5×10^{-3} @145.0	9.8×10^{-3} @146.4	11.5×10^{-3} @190.0	11.9×10^{-3} @191.2	9.0×10^{-3} @280.0	9.3×10^{-3} @280.9

Table 2.10 Identified residual unbalances for different disc masses for 5% measurement noise (for *Case C* under *Method II*)

Set no.	Assumed disc mass (kg)	Estimated residual unbalance (kg–m@deg)			
		Plane 1	Plane 2	Plane 3	Plane 4
		9.6×10^{-3} @36.0	6.0×10^{-3} @108.0	7.5×10^{-3} @240.0	11.1×10^{-3} @300.0
Set–1	m_1^d=5.0, m_2^d=3 .0 m_3^d=2.0, m_4^d=6.0	9.9×10^{-3} @36.8	6.1×10^{-3} @108.4	7.7×10^{-3} @240.9	11.5×10^{-3} @300.8
Set–2	m_1^d=3.0, m_2^d=1.5, m_3^d=1.0, m_4^d=2.0	9.8×10^{-3} @36.4	6.1×10^{-3} @108.4	7.6×10^{-3} @240.4	11.3×10^{-3} @300.5
Set–3	m_1^d=1.5, m_2^d=2.0, m_3^d=0.5, m_4^d=1.0	9.8×10^{-3} @36.4	6.0×10^{-3} @108.2	7.6×10^{-3} @240.4	11.2×10^{-3} @300.4

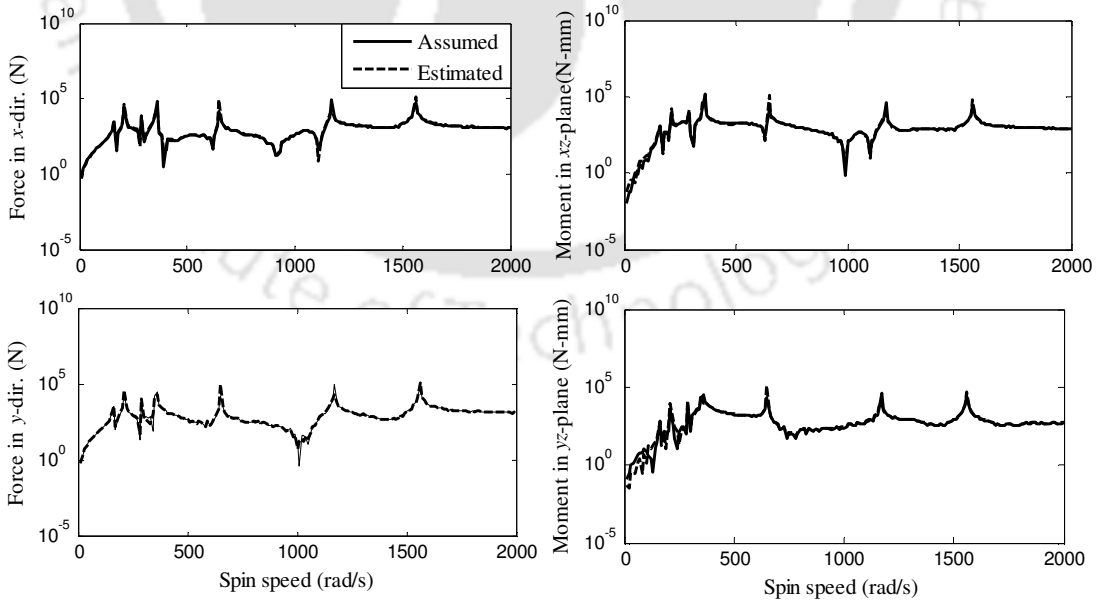

Figure 2.18 Misalignment forces and moments with spin speed for 5% noise (for *Case C* under *Method II*)

2.4.3 Discussions on Various Numerical Studies Performed

To check the suitability of estimation procedures, initially assumed parameters and estimated parameters are compared as well as responses generated by these parameters are compared. These studies have been performed for various noise levels also. Following observations could be made from discussions of Sections 2.4.1 and 2.4.2.

- It is observed that for no noise condition, responses from assumed parameters and that from estimated parameters are same for both the methods (i.e., (*I*) Rotate the rotor in same direction at different speeds; (*II*) Rotate the rotor at different speeds in the CW and CCW directions, alternatively) and under all three *Cases* A–C (i.e., (A) by rotating the near critical speeds (B) by rotating the rotor away from critical speeds and (C) by rotating the rotor at *n* number of speeds).

- *Case A* is the worst case for both methods (i.e., *I* & *II*) in which deviation of responses starts at 1% noise condition and the maximum error observed in this case is around 5% and 7% for *Methods I* and *II*, respectively.

- For *Case C* under *Method I*, the maximum error occurred is around 1%. The order of improvement in the condition number is the maximum for this case under *Method I*.

- The *Case C* under *Method II* is the best case for estimation of parameters; the maximum error observed in this case is around 0.08%. Among all the three cases discussed above for both methods (i.e., *I* & *II*) the order of improvement in the condition number is maximum in this case (i.e., 10^{16}).

The algorithm is also tested under three different noise levels as shown in Table 2.4–Table 2.7, to get the robustness properties of the algorithm on theoretically simulated data. So from the above comparison it can be concluded that the *Case C* under *Method II* is the best method

for estimating the parameters. Even for different level of assumed unbalances and rotor masses the estimates are found to be excellent for the aforementioned case. It should be noted that although the percentage error in the estimation of some of the cross–coupled (mostly bearing damping) parameters is more but the absolute deviation of these parameters are less or comparable as compared to direct parameters. From Table 2.5 and Table 2.6, it could be seen that the absolute magnitude (assumed values) of the direct bearing damping parameters are (4 to 12) times more than these cross–coupled bearing damping parameters.

2.5 Summary

An identification algorithm is proposed to quantitatively identify the multiple fault parameters by the use of rundown or run–up data. The algorithm has been developed for the estimation of bearing and coupling dynamic parameters along with residual unbalances. The present identification method relies on the measurement of rotor forced responses at bearing locations. Then the algorithm has been tested against different level of the measurement noise. The advantage of the present method in respect to existing methods is that it does not assume equivalent forces and moments of faults, which often suffers from erroneous estimation of fault parameters due to severe ill–conditioning of regression equations. The effect of change in assumed unbalance parameters and disc masses on estimates of residual unbalance is discussed and it is observed that the estimates show good agreement with change in these parameters. In the present methodology of model based identification the accuracy of estimates depends upon model for a particular fault (for example the present procedure could be extended for the speed–dependent bearing and coupling dynamic parameters. Moreover, the challenge would be use more versatile and practical numerical modelling method such as the FEM for the multi–fault parameter identification, where concept of the misalignment would be different than in rigid rotor cases. As such results are expected to be near to the

assumed values to check the method and the present method gives that in numerical simulation. Existing methods for finding coupling and bearing parameters rely on 3–D FEM modeling of coupling and Reynolds equations for bearings, which are quite complicated and gives unpractical results when actual test conditions are unknown.

CHAPTER 3

Multiple Fault Identification in a Flexible Rotor–Bearing–Coupling System

3.1 Introduction

A simple rigid rotor and flexible bearing–coupling model used in previous chapter has been improved with the assumption of the flexible rotor–bearings–coupling system. This chapter concerns with the development of an identification algorithm by using the finite element (FE) formulation to estimate parameters of multiple faults in a turbo–generator system rotor model based on forced responses. The Timoshenko beam theory with the gyroscopic effect is considered in the system FE modelling. To account for the coupling forces and moments due to the restoring and dissipative effects, a simple coupling model has been considered between two adjacent shafts that also takes the misalignment effect into account. To test the proposed algorithm, responses of MDOF flexible rotor–bearing–coupling systems in frequency domain are numerically simulated due to unbalance forces. These responses are used in the proposed identification algorithms based on least–squares techniques to identify the bearing and coupling dynamic parameters along with residual unbalances. The proposed algorithm has the flexibility to incorporate any number of bearings and couplings as well as balancing planes. Numerical experiments have been performed to illustrate the effectiveness of the developed algorithm. The algorithm is tested against the measurement noise.

3.2 System Modelling

In the present section assumptions involved in modelling the system under consideration have been stated. Details of the misaligned rotor bearing model have also been presented. An identification algorithm developed in previous chapter to estimate the bearing and coupling

dynamic parameters along with residual unbalances for rigid rotor and flexible bearing–coupling system has been improved for flexible rotor–bearing–coupling system.

3.2.1 Basic Assumptions and the Description of Model

A flexible rotor model, as shown in Figure 3.1, is considered in the present chapter. It is composed of two flexible shafts and each of them are supported on two flexible anisotropic bearings, and connected together with a flexible coupling. The FE model of the rotor system is shown in Figure 3.2. In the present chapter both the rotor shafts (i.e., 1 and 2) are considered as flexible and the Timoshenko beam theory with the FEM has been applied to obtain mass, stiffness and damping (i.e., Rayleigh's damping) matrices of the shaft. A schematic diagram of the coupling with nodal coordinates in the vertical (z–x) plane is shown in Figure 3.3. The torsional and longitudinal vibrations effects and its coupling with transverse vibrations have not been considered in the present analysis. No internal damping has been considered in the present study.

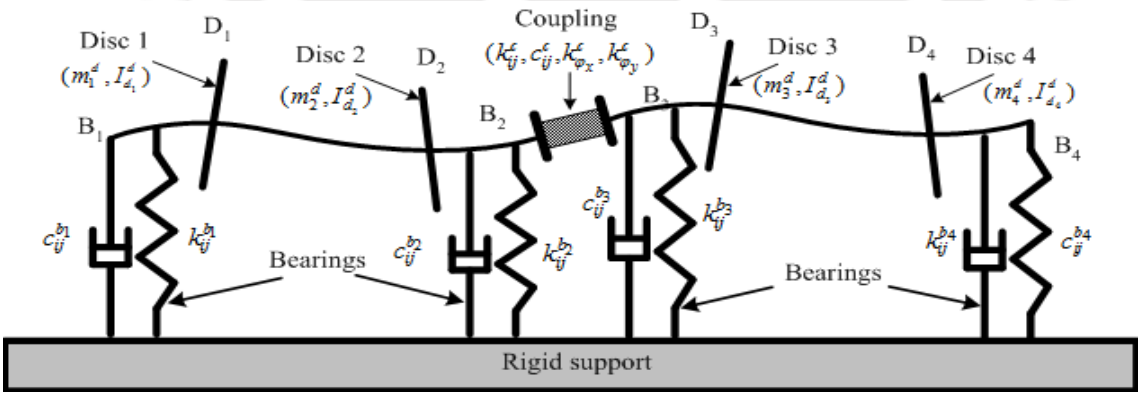

Figure 3.1 A flexible rotor–bearing–coupling system

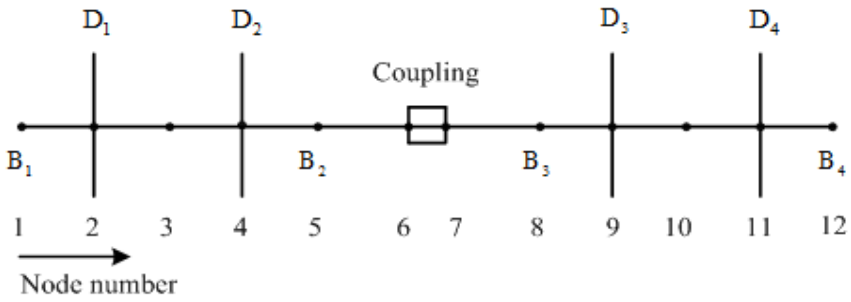

Figure 3.2 A FE model of the rotor–bearing–coupling system

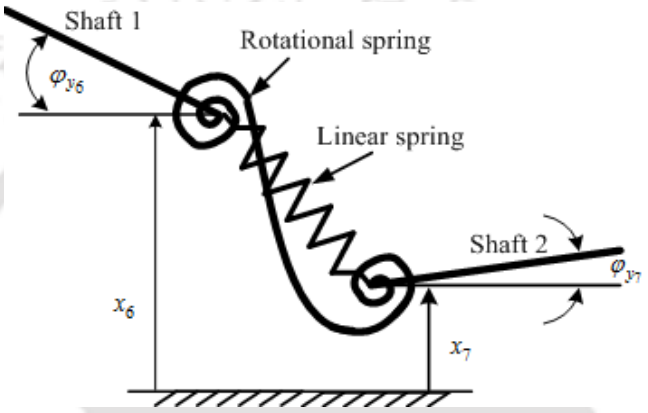

Figure 3.3 A schematic diagram of the coupling model in the *z*–*x* plane

3.2.2 Modelling of the Shaft

The shaft is divided into finite number of elements and could be represented as shown in Figure 3.2. The approximate number of elements is determined depending on the order of vibration modes expected to be captured, the geometry of the shaft, disc locations, etc. The EOM for the shaft element can be given as

$$[M]^S\{\ddot{\eta}(t)\}^S+\left([C]^S-\omega[G]^S\right)\{\dot{\eta}(t)\}^S+[K]^S\{\eta(t)\}^S=\{f(t)\}^S \tag{3.1}$$

Where $\{\eta\}^s$ and $\{f\}^s$ are called the elemental nodal displacement and force vectors, respectively; and matrices $[M]^s,[G]^s,[C]^s$ and $[K]^s$ are the elemental mass, gyroscopic, damping and stiffness matrices, respectively, for the shaft; and are given as

$$[M]^S = [M_t]_0 + \phi[M_t]_1 + \phi^2[M_t]_2 + [M_r]_0 + \phi[M_r]_1 + \phi^2[M_r]_2 \tag{3.2}$$

$$[G]^S = [G]_0 + \phi[G]_1 + \phi^2[G]_2 \tag{3.3}$$

$$[K]^S = [K]_0 + \phi[K]_1 \tag{3.4}$$

$$[C]^S = a_0[M]^S + a_1[K]^S \tag{3.5}$$

Details of the elemental mass, gyroscopic and stiffness matrices are given in Appendix A. In Eqn. (3.5), a_0 and a_1 are Rayleigh's damping coefficients, and the details are given in Appendix B.

3.2.3 Modelling of the Rigid Disc

Discs are assumed to be rigid and are modelled using the mass and mass moment of inertia terms at respective nodes. The EOM for the rigid disc can be given as

$$[M]^D \{\ddot{\eta}(t)\}^D - \omega[G]^D \{\dot{\eta}(t)\}^D = \{f(t)\}^D \tag{3.6}$$

where vectors $\{\eta\}^D$ and $\{f\}^D$ are the disc nodal displacement and force vectors, respectively; and matrices $[M]^D$ and $[G]^D$ are the disc mass and gyroscopic matrices, respectively. Details of these matrices are given in Appendix A.

3.2.4 Modelling of the Bearing

Each bearing is modelled by the standard eight linearized damping, $c_{ij}^{B_n}$, and stiffness, $k_{ij}^{B_n}$, coefficients (all bearings have distinct the direct as well as cross–coupled coefficients). Bearing forces at each bearing is assumed of the following form

$$\begin{bmatrix} c_{xx}^{B} & c_{xy}^{B} \\ c_{yx}^{B} & c_{yy}^{B} \end{bmatrix} \{\dot{\eta}(t)\}^{B} + \begin{bmatrix} k_{xx}^{B} & k_{xy}^{B} \\ k_{yx}^{B} & k_{yy}^{B} \end{bmatrix} \{\eta(t)\}^{B} = \{f(t)\}^{B} \tag{3.7}$$

where vectors $\{\eta\}^{B}$ and $\{f\}^{B}$ are the bearing nodal displacement and force vectors, respectively.

3.2.5 Modelling of Residual Unbalance Forces

Here the residual unbalance force vector is defined as

$$\{f_{unb}(t)\} = \{F_{unb}\} e^{j\omega t} \tag{3.8}$$

where $\{F_{unb}\}$ is the residual unbalance force vector (elements of which are complex quantities and contains the amplitude and phase information).

3.2.6 Modelling of Coupling Misalignments

The effect of misalignment forces and moments of the coupling has been considered in the form of restoring and damping forces, and these are included in stiffness and damping matrices. Figure 3.4 shows the rigid versus flexible rotor coupling misalignment. In case of rigid rotor (Figure 3.4(a)) amount of misalignment does not change with different modes whereas in flexible rotor (Figure 3.4(b)) amount of misalignment depends upon the different modes and would reflect in terms of stiffness and damping forces during motion which would change with speed. The EOM of the coupling could be written as

$$[C]^{C} \{\dot{\eta}(t)\}^{C} + [K]^{C} \{\eta(t)\}^{C} = \{0\} \tag{3.9}$$

where

$$[K]^C = \begin{bmatrix} k_{xx}^C & k_{xy}^C & 0 & 0 & -k_{xx}^C & -k_{xy}^C & 0 & 0 \\ k_{yx}^C & k_{yy}^C & 0 & 0 & -k_{yx}^C & -k_{yy}^C & 0 & 0 \\ 0 & 0 & k_{\varphi_y\varphi_y}^C & 0 & 0 & 0 & -k_{\varphi_y\varphi_y}^C & 0 \\ 0 & 0 & 0 & k_{\varphi_x\varphi_x}^C & 0 & 0 & 0 & -k_{\varphi_x\varphi_x}^C \\ -k_{xx}^C & -k_{xy}^C & 0 & 0 & k_{xx}^C & k_{xy}^C & 0 & 0 \\ -k_{yx}^C & -k_{yy}^C & 0 & 0 & k_{yx}^C & k_{yy}^C & 0 & 0 \\ 0 & 0 & -k_{\varphi_y\varphi_y}^C & 0 & 0 & 0 & k_{\varphi_y\varphi_y}^C & 0 \\ 0 & 0 & 0 & -k_{\varphi_x\varphi_x}^C & 0 & 0 & 0 & k_{\varphi_x\varphi_x}^C \end{bmatrix}$$

$$[C]^C = \begin{bmatrix} c_{xx}^C & c_{xy}^C & 0 & 0 & -c_{xx}^C & -c_{xy}^C & 0 & 0 \\ c_{yx}^C & c_{yy}^C & 0 & 0 & -c_{yx}^C & -c_{yy}^C & 0 & 0 \\ 0 & 0 & 0 & 0 & 0 & 0 & 0 & 0 \\ 0 & 0 & 0 & 0 & 0 & 0 & 0 & 0 \\ -c_{xx}^C & -c_{xy}^C & 0 & 0 & c_{xx}^C & c_{xy}^C & 0 & 0 \\ -c_{yx}^C & -c_{yy}^C & 0 & 0 & c_{yx}^C & c_{yy}^C & 0 & 0 \\ 0 & 0 & 0 & 0 & 0 & 0 & 0 & 0 \\ 0 & 0 & 0 & 0 & 0 & 0 & 0 & 0 \end{bmatrix}$$

and

$$\{\eta(t)\}^C = \{x_6 \quad y_6 \quad \varphi_{y_6} \quad \varphi_{x_6} \quad x_7 \quad y_7 \quad \varphi_{y_7} \quad \varphi_{x_7}\}^T$$

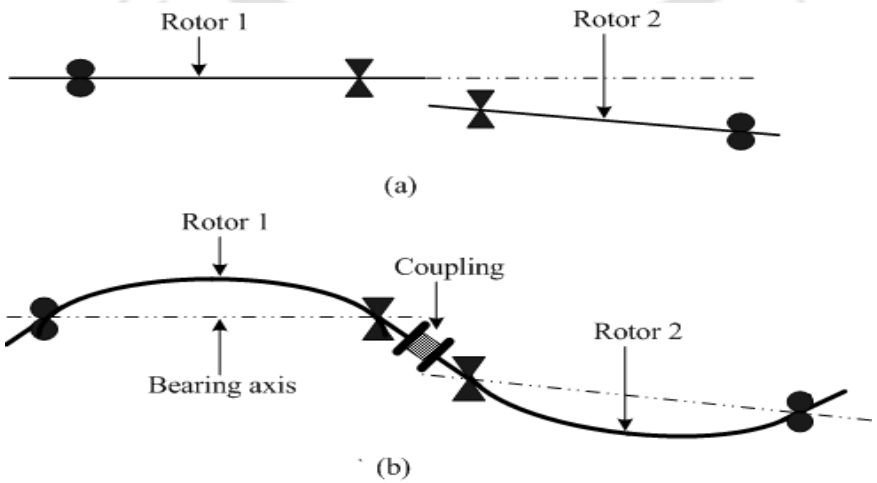

Figure 3.4 The shaft misalignment at the coupling for (a) rigid shafts (b) flexible shafts

The mass and the mass moment of inertia of the coupling can be considered easily in the present method. However, we planned for a small flexible coupling in the test rig so it is ignored in the simulation and for brevity only the linear direct and cross–coupled damping coefficients of the coupling have been considered in the present case. One can calculate the amount of misalignment force and moment by knowing the coupling stiffness and damping coefficients $\left(k_{ij}^{C}, k_{\varphi_x\varphi_x}^{C}, c_{ij}^{C} \ldots\right)$ and displacement values $(x_6, y_6, \varphi_{x_6}, \varphi_{y_6})$ and $(x_7, y_7, \varphi_{x_7}, \varphi_{y_7})$ at the coupling locations, by referring to Eqn. (2.12).

3.2.7 Equations of Motion for the Rotor Substructure

The rotor substructure includes rigid discs and flexible shafts. The EOM of the rotor substructure could be obtained by assembling the contribution of each elemental EOMs (i.e. Eqns. (3.1) and (3.6)) and expressed as,

$$[M]\{\ddot{\eta}(t)\}^R + \omega([C] - \omega[G])\{\dot{\eta}(t)\}^R + [K]\{\eta(t)\}^R = \{f(t)\}^R \tag{3.10}$$

where

$$[M] = [M]^S + [M]^D, \quad [G] = [G]^S + [G]^D, \quad [C] = [C]^s, \quad [K] = [K]^s \tag{3.11}$$

Where superscripts *D*, *R* and *S* represent the disk, rotor and shaft, respectively; $\{\eta\}^R$ and $\{f\}^R$ are the rotor displacement and force vectors, respectively. Matrices [*M*], [*C*], [*G*] and [*K*] are the mass, damping, gyroscopic and stiffness matrices of the rotor substructure, respectively.

3.2.8 Equations of Motion for Bearings as a Substructure

The EOM of bearings as a substructure could be obtained by assembling the EOM of individual bearings (i.e. Eqn. (3.7)), as follows

$$[C]^B \{\dot{\eta}(t)\}^B + [K]^B \{\eta(t)\}^B = \{0\} \tag{3.12}$$

Where vector $\{\eta(t)\}^B$ contains the rotor DOFs at bearing locations, called connection DOFs; and matrices $[C]^B$ and $[K]^B$ are the assembled damping and stiffness matrices, respectively, for the bearing substructure.

3.2.9 System Equations of Motion in Frequency Domain

The EOM of the coupling, rotor and bearing as substructures are given by Eqns. (3.9), (3.10) and (3.12), respectively. The forcing can be expressed by Eqn. (3.8). Now by taking the solution of Eqns. (3.9), (3.10) and (3.12) in the following form

$$\{\eta(t)\} = \{\bar{\eta}\} e^{j\omega t} \tag{3.13}$$

Where $\{\bar{\eta}\}$ contains the amplitude and phase information of displacements. On substituting Eqns. (3.8) and (3.13) in Eqns. (3.9), (3.10) and (3.12) it gives, governing equations in frequency domain for the coupling, rotor and bearing substructures, respectively, as

$$[Z_C]_{8\times8}\{\eta_C\}_{8\times1} = \{F_C\}_{8\times1} \tag{3.14}$$

$$[Z_R]_{48\times48}\{\eta_R\}_{48\times1} = \{F_R\}_{48\times1} \tag{3.15}$$

and

$$[Z_B]_{8\times8}\{\eta_B\}_{8\times1} = \{F_B\}_{8\times1} \tag{3.16}$$

Where the number attached with matrices and vectors represent respective size. The individual dynamic matrix, *Z*, of each of these substructures are given as

$$[Z_C]_{8\times8} = \left([K_C] + j\omega[C_C]\right) \tag{3.17}$$

$$[Z_R]_{48\times48} = \left([K_R] + j\omega\left([C_R] - \omega[G_R]\right) - \omega^2[M_R]\right) \tag{3.18}$$

and

$$[Z_B]_{8\times8} = \left([K_B] + \mathrm{j}\omega[C_B]\right) \tag{3.19}$$

DOFs of the rotor–bearing system (i.e. Eqns. (3.17)–(3.19)) is composed of the internal and connection DOFs. All DOFs of the rotor at bearing locations are called connection DOFs, $\eta_{R,B}$; and DOFs of the rotor other than at bearing locations are called as the internal DOFs, $\eta_{R,I}$. The EOM of above mentioned substructures (i.e. Eqns. (3.17)–(3.19)) can be partitioned into the internal and connection DOFs as

$$\left[Z_{C,CC}\right]_{8\times8}\left\{\eta_{R,C}\right\}_{8\times1} = \left\{F_{C,C}\right\}_{8\times1} \tag{3.20}$$

$$\begin{bmatrix} \left[Z_{R,II}\right]_{32\times32} & \left[Z_{R,IB}\right]_{32\times8} & \left[Z_{R,IC}\right]_{32\times8} \\ \left[Z_{R,BI}\right]_{8\times32} & \left[Z_{R,BB}\right]_{8\times8} & \left[Z_{R,BC}\right]_{8\times8} \\ \left[Z_{R,CI}\right]_{8\times32} & \left[Z_{R,CB}\right]_{8\times8} & \left[Z_{R,CC}\right]_{8\times8} \end{bmatrix} \begin{Bmatrix} \left\{\eta_{R,I}\right\}_{32\times1} \\ \left\{\eta_{R,B}\right\}_{8\times1} \\ \left\{\eta_{R,C}\right\}_{8\times1} \end{Bmatrix} = \begin{Bmatrix} \left\{F_{R,I}\right\}_{32\times1} \\ -\left\{F_{R,B}\right\}_{8\times1} \\ -\left\{F_{R,C}\right\}_{8\times1} \end{Bmatrix} \tag{3.21}$$

and

$$\left[Z_{B,BB}\right]_{8\times8}\left\{\eta_{R,B}\right\}_{8\times1} = \left\{F_{B,B}\right\}_{8\times1} \tag{3.22}$$

Combining Eqns. (3.20)–(3.22) leads to a general EOM for the complete rotor–bearing–coupling system, and it can be written as

$$\begin{bmatrix} \left[Z_{R,II}\right]_{32\times32} & \left[Z_{R,IB}\right]_{32\times8} & \left[Z_{R,IC}\right]_{32\times8} \\ \left[Z_{R,BI}\right]_{8\times32} & \left[Z_{R,BB}+Z_{B,BB}\right]_{8\times8} & \left[Z_{R,BC}\right]_{8\times8} \\ \left[Z_{R,CI}\right]_{8\times32} & \left[Z_{R,CB}\right]_{8\times8} & \left[Z_{R,CC}+Z_{C,CC}\right]_{8\times8} \end{bmatrix} \begin{Bmatrix} \left\{\eta_{R,I}\right\}_{32\times1} \\ \left\{\eta_{R,B}\right\}_{8\times1} \\ \left\{\eta_{R,C}\right\}_{8\times1} \end{Bmatrix} = \begin{Bmatrix} \left\{F_{R,I}\right\}_{32\times1} \\ \left\{0\right\}_{8\times1} \\ \left\{0\right\}_{8\times1} \end{Bmatrix} \tag{3.23}$$

Here we have considered a rigid foundation, so the bearing can be defined by using the DOFs of the rotor only, so the bearing model does not contain any internal DOFs. Eqn. (3.23), would be used in subsequent section for the simultaneous estimation of the residual unbalances, and the bearing and coupling dynamic parameters. In the section of numerical experiments the same equation would be used to get simulated responses for testing the proposed multi–fault identification algorithm.

3.3 Development of the Identification Algorithm

Eqn. (3.23) describes governing equations of a general MDOF flexible rotor–bearing–coupling system and are considered for developing an identification algorithm to estimate the bearing and coupling dynamic parameters along with residual unbalances. Eqn. (3.23), could be expressed as

$$\left[Z_{R,II}\right]\left\{\eta_{R,I}\right\}+\left[Z_{R,IB}\right]\left\{\eta_{R,B}\right\}+\left[Z_{R,IC}\right]\left\{\eta_{R,C}\right\}=\left\{F_{R,I}\right\} \tag{3.24}$$

$$\left[Z_{R,BI}\right]\left\{\eta_{R,I}\right\}+\left[Z_{R,BB}+Z_{B,BB}\right]\left\{\eta_{R,B}\right\}+\left[Z_{R,BC}\right]\left\{\eta_{R,C}\right\}=0 \tag{3.25}$$

and

$$\left[Z_{R,CI}\right]\left\{\eta_{R,I}\right\}+\left[Z_{R,CB}\right]\left\{\eta_{R,B}\right\}+\left[Z_{R,CC}+Z_{C,CC}\right]\left\{\eta_{R,C}\right\}=0 \tag{3.26}$$

Eqn. (3.24) can be written as

$$\left\{\eta_{R,I}\right\}=\left[Z_{R,II}\right]^{-1}\left(\left\{F_{R,I}\right\}-\left[Z_{R,IB}\right]\left\{\eta_{R,B}\right\}-\left[Z_{R,IC}\right]\left\{\eta_{R,C}\right\}\right) \tag{3.27}$$

In Eqn. (3.27), vectors $\left\{\eta_{R,B}\right\}$ and $\left\{\eta_{R,c}\right\}$ are measurable quantities in most of the practical cases. The vector $\left\{F_{R,I}\right\}$ contains the effect of residual unbalances only, the effect of

misalignment is considered as dissipating and restoring forces/moments, respectively, in the stiffness and damping matrices of the system. On substituting Eqn. (3.27) in Eqns. (3.25) and (3.26), eliminates the internal DOFs vector $\{\eta_{R,I}\}$, which is immeasurable or inaccessible in most of the practical cases, we get

$$\left[Z_{R,BI}\right]\left[Z_{R,II}^{-1}\right]\left(\{F_{R,I}\}-\left[Z_{R,IB}\right]\{\eta_{R,B}\}-\left[Z_{R,IC}\right]\{\eta_{R,C}\}\right)+\left[Z_{R,BB}+Z_{B,BB}\right]\{\eta_{R,B}\}+\left[Z_{R,BC}\right]\{\eta_{R,C}\}=0 \quad (3.28)$$

and

$$\left[Z_{R,CI}\right]\left[Z_{R,II}^{-1}\right]\left(\{F_{R,I}\}-\left[Z_{R,IB}\right]\{\eta_{R,B}\}-\left[Z_{R,IC}\right]\{\eta_{R,C}\}\right)+\left[Z_{R,CB}\right]\{\eta_{R,B}\}+\left[Z_{R,CC}+Z_{C,CC}\right]\{\eta_{R,C}\}=0 \quad (3.29)$$

Eqns. (3.28) and (3.29) could be rearranged so that all the unknown terms (i.e., the bearing and coupling dynamic parameters along with residual unbalances) are on the left–hand side, and all the known terms are on the right–hand side of the expression, so that it can be written as

$$\left[Z_{B,BB}\right]\{\eta_{R,B}\}+\left[Z_{R,BI}\right]\left[Z_{R,II}^{-1}\right]\{F_{R,I}\}=\{P_{n1}\} \quad (3.30)$$

and

$$\left[Z_{C,CC}\right]\{\eta_{R,C}\}+\left[Z_{R,CI}\right]\left[Z_{R,II}^{-1}\right]\{F_{R,I}\}=\{P_{n2}\} \quad (3.31)$$

with

$$\{P_{n1}\}=\left(\left[Z_{R,BI}\right]\left[Z_{R,II}^{-1}\right]\left[Z_{R,IB}\right]-\left[Z_{R,BB}\right]\right)\{\eta_{R,B}\}+\left(\left[Z_{R,BI}\right]\left[Z_{R,II}^{-1}\right]\left[Z_{R,IC}\right]-\left[Z_{R,BC}\right]\right)\{\eta_{R,C}\} \quad (3.32)$$

and

$$\{P_{n2}\}=\left(\left[Z_{R,CI}\right]\left[Z_{R,II}^{-1}\right]\left[Z_{R,IB}\right]-\left[Z_{R,CB}\right]\right)\{\eta_{R,B}\}+\left(\left[Z_{R,CI}\right]\left[Z_{R,II}^{-1}\right]\left[Z_{R,IC}\right]-\left[Z_{R,CC}\right]\right)\{\eta_{R,C}\} \quad (3.33)$$

On writing Eqns. (3.30) and (3.31) in the matrix form leads to

$$\begin{bmatrix} [Z_{B,BB}] & 0 \\ 0 & [Z_{C,CC}] \end{bmatrix}_{16\times16} \begin{Bmatrix} \{\eta_{R,B}\} \\ \{\eta_{R,C}\} \end{Bmatrix}_{16\times1} + \begin{bmatrix} [Z_{B,BI}][Z_{R,II}^{-1}] \\ [Z_{B,CI}][Z_{R,II}^{-1}] \end{bmatrix}_{16\times32} \{F_{R,I}\}_{32\times1} = \begin{Bmatrix} \{P_{n1}\} \\ \{P_{n2}\} \end{Bmatrix}_{16\times1} \tag{3.34}$$

and

$$\{F_{R,I}\} = \omega^2 [T]_{32\times8} \{U\}_{8\times1} \tag{3.35}$$

with

$$T_{31} = 1, \quad T_{32} = \mathrm{j}, \quad T_{41} = -\mathrm{j}, \quad T_{42} = 1, \quad T_{11,3} = 1, \quad T_{11,4} = \mathrm{j}, \quad T_{12,3} = -\mathrm{j}, \quad T_{12,4} = 1,$$

$$T_{19,5} = 1, \quad T_{19,6} = \mathrm{j}, \quad T_{20,5} = -\mathrm{j}, \quad T_{20,6} = 1, \quad T_{27,7} = 1, \quad T_{27,8} = \mathrm{j}, \quad T_{28,7} = -\mathrm{j}, \quad T_{28,8} = 1$$

Rest of the elements of matrix [*T*] are zero.

$$\{U\}_{8\times1} = \begin{Bmatrix} u_{x_1}^r & u_{x_1}^i & u_{x_2}^r & u_{x_2}^i & u_{x_3}^r & u_{x_3}^i & u_{x_4}^r & u_{x_4}^i \end{Bmatrix}^T \tag{3.36}$$

Superscripts *r* and *i* represent the real and imaginary parts, respectively; and [*T*] is the transformation matrix. The first term in Eqn. (3.34), is then regrouped into a vector $\{\beta\}_{42\times1}$, containing all the unknown bearing and coupling dynamic parameters and a corresponding matrix $[W_n]_{16\times42}$, containing the related response terms at a single spin speed, ω. Noting Eqns. (3.34)–(3.36), it takes the following form

$$[W_n]_{16\times42} \{\beta\}_{42\times1} + [R_n]_{16\times8} \{U\}_{8\times1} = \{P_n\}_{16\times1} \tag{3.37}$$

with

$$\{\beta\}_{42\times1} = \{k_{xx}^{b_1}, k_{xy}^{b_1}, k_{yx}^{b_1}, k_{yy}^{b_1}, k_{xx}^{b_2}, k_{xy}^{b_2}, k_{yx}^{b_2}, k_{yy}^{b_2}, k_{xx}^{b_3}, k_{xy}^{b_3}, k_{yx}^{b_3}, k_{yy}^{b_3}, k_{xx}^{b_4}, k_{xy}^{b_4}, k_{yx}^{b_4}, k_{yy}^{b_4}, k_{xx}^{c}, k_{xy}^{c}, k_{yx}^{c}, k_{yy}^{c}, k_{\varphi_x}^{c}, k_{\varphi_y}^{c},$$
$$c_{xx}^{b_1}, c_{xy}^{b_1}, c_{yx}^{b_1}, c_{yy}^{b_1}, c_{xx}^{b_2}, c_{xy}^{b_2}, c_{yx}^{b_2}, c_{yy}^{b_2}, c_{xx}^{b_3}, c_{xy}^{b_3}, c_{yx}^{b_3}, c_{yy}^{b_3}, c_{xx}^{b_4}, c_{xy}^{b_4}, c_{yx}^{b_4}, c_{yy}^{b_4}, c_{xx}^{c}, c_{xy}^{c}, c_{yx}^{c}, c_{yy}^{c}\}^T$$

Parameters contained in the vector, $\{\beta\}$, depends upon the form of dynamic matrices specified for the bearing and the coupling. In the present case, the bearing and the coupling are modelled as having stiffness and damping with direct and cross−coupled terms as described in Sections 3.2.4 and 3.2.6. In Eqn. (3.37), $[W_n]$, $[R_n]$ and $\{P_n\}$ are in the complex form, now after separating out the real and imaginary parts, Eqn. (3.37), becomes

$$\begin{bmatrix}[W_n^r]\\ [W_n^i]\end{bmatrix}_{32\times 42}\{\beta\}_{42\times 1}+\begin{bmatrix}[R_n^r]\\ [R_n^i]\end{bmatrix}_{32\times 8}\{U\}_{8\times 1}=\begin{Bmatrix}\{P_n^r\}\\ \{P_n^i\}\end{Bmatrix}_{32\times 1} \tag{3.38}$$

Eqn. (3.38), could be written as

$$[W]_{32\times 42}\{\beta\}_{42\times 1}+[R]_{32\times 8}\{U\}_{8\times 1}=\{P\}_{32\times 1} \tag{3.39}$$

Rearranging Eqn. (3.39), leads to

$$\left[[W]_{32\times 42}\ [R]_{32\times 8}\right]\begin{Bmatrix}\{\beta\}_{42\times 1}\\ \{U\}_{8\times 1}\end{Bmatrix}=\{P\}_{32\times 1} \tag{3.40}$$

$$[A(\omega)]_{32\times 50}\{X\}_{50\times 1}=\{B(\omega)\}_{32\times 1} \tag{3.41}$$

with

$$[A]=\left[[K^r]_{32\times 22}[C^r]_{32\times 20}[U^r]_{32\times 8}\right]$$

$$\{X\}=\{k_{xx}^{B_1},k_{xy}^{B_1},k_{yx}^{B_1},k_{yy}^{B_1},k_{xx}^{B_2},k_{xy}^{B_2},k_{yx}^{B_2},k_{yy}^{B_2},k_{xx}^{B_3},k_{xy}^{B_3},k_{yx}^{B_3},k_{yy}^{B_3},k_{xx}^{B_4},k_{xy}^{B_4},k_{yx}^{B_4},k_{yy}^{B_4},k_{xx}^{C},k_{xy}^{C},k_{yx}^{C},k_{yy}^{C},k_{\varphi_x}^{C},k_{\varphi_y}^{C},c_{xx}^{B_1},c_{xy}^{B_1},$$
$$c_{yx}^{B_1},c_{yy}^{B_1},c_{xx}^{B_2},c_{xy}^{B_2},c_{yx}^{B_2},c_{yy}^{B_2},c_{xx}^{B_3},c_{xy}^{B_3},c_{yx}^{B_3},c_{yy}^{B_3},c_{xx}^{B_4},c_{xy}^{B_4},c_{yx}^{B_4},c_{yy}^{B_4},c_{xx}^{C},c_{xy}^{C},c_{yx}^{C},c_{yy}^{C},u_{x_1}^{r},u_{x_1}^{i},u_{x_2}^{r},u_{x_2}^{i},u_{x_3}^{r},u_{x_3}^{i},u_{x_4}^{r},u_{x_4}^{i}\}^T$$

Where $[K^r]$ and $[C^r]$ are the contribution to the final regression matrix from the stiffness and damping coefficients of the bearing and the coupling, and $[U^r]$ is the contribution from residual unbalances. Eqn. (3.41) is the estimation equation, in which all unknown parameters

(i.e. the bearing and coupling dynamic parameters along with residual unbalances) are stacked in a column vector, $\{X\}$. From Eqn. (3.41), it could be seen that the number of unknowns (i.e., fifty) are far more than the number of equations (i.e., thirty two). This is the case of underdetermined system of linear simultaneous equations. The entire unknown can only be obtained with the help of sets of independent force–response measurements such that the number of equations is increased at least equal or more than the unknowns. For the present case, the minimum number of independent measurements required is two which could be obtain in the same way as discussed in Chapter 2, Section 2.3.

3.4 Numerical Experiments

For illustration of the present identification algorithm, a rotor model, as shown in Figure 3.1, is considered. Rotor properties and residual unbalances are given in Table 3.1 and Table 3.2, respectively. In Table 3.3–Table 3.6, second column contains all the bearing and coupling dynamic parameters and residual unbalances; that is assumed for the numerical simulation of forced responses. A typical variation of the forced response with the spin speed is shown in Figure 3.5. The forward critical speed of the system are ω_{cr1}= 105.2 rad/s, ω_{cr2}= 114.4 rad/s, ω_{cr3}=126.4 rad/s, ω_{cr4}= 130.5 rad/s, ω_{cr5}=193.4 rad/s, ω_{cr6} = 212.8 rad/s, ω_{cr7}=256.1 rad/s, and ω_{cr8}= 263.5 rad/s. It could be seen that at all above critical speeds the resonance condition manifest both in the amplitude and the phase.

Table 3.1 Shaft properties

S.N.	Shaft no.	Length (m)	Diameter (m)	Density (kg/m^3)	Mass (kg)	Diametral mass moment of inertia (kg–m^2)
1	Shaft 1	1.25	0.02	7800	3.06	0.398
2	Shaft 2	1.25	0.02	7800	3.06	0.398

Table 3.2 Disc and residual unbalance properties

S.N.	Location	Diameter (m)	Mass (kg)	Diametral mass moment of inertia (kg–m^2)	Residual unbalances	
					Magnitude (kg)	Angular position (deg.)
1	Disc 1	0.15	2	5.63×10^{-3}	9.5×10^{-3}	36
2	Disc 2	0.13	1.5	3.16×10^{-3}	6.0×10^{-3}	108
3	Disc 3	0.12	2.5	4.50×10^{-3}	7.9×10^{-3}	240
4	Disc 4	0.14	1.6	3.92×10^{-3}	11.2×10^{-3}	300

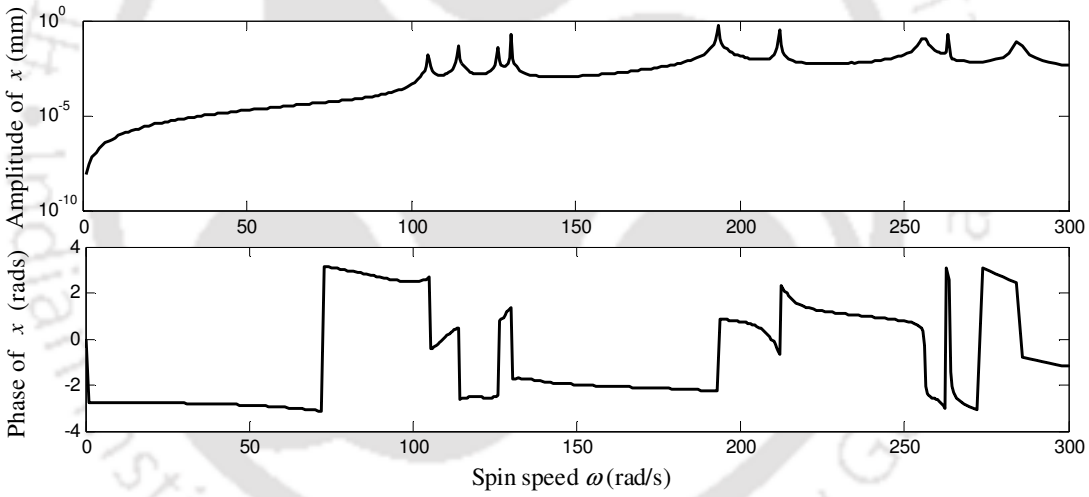

Figure 3.5 Variation of the horizontal response at bearing location 1 with the spin speed

For the estimation of bearing and coupling dynamic parameters along with residual unbalances the present technique requires forced vibration response measurements, which have been generated through a numerical simulation using Eqn. (3.23). To mimic the actual experimental response white noise has been added to the simulated response. To improve the accuracy of estimates scaling of columns of the regression matrix $[A_I]$ and $[A_{II}]$ have been performed. The effect of column scaling could be seen from Figure 3.6–Figure 3.11, which

shows the comparison of error (ratio of the difference between estimated and assumed values to the assumed value of parameters) in the estimation of parameters before and after column scaling for 5 percent measurement noise for all the three cases (i.e. *Case A*, *B* and *C*) under both the methods (i.e. *Method I* & *II*) discussed in Chapter 2, Section 2.3, respectively. The number in the abscissa represents estimated parameter corresponding to the row number in the vector $\{X\}$ of Eqn. (3.41) and these parameters are summarised with corresponding row locations in Chapter 2, Table 2.1. Another important effect of column scaling is the improvement in the condition number of the regression matrix. The improvement in condition number and percent improvement in accuracy (i.e. the ratio of difference between estimated values before and after column scaling to the estimated values before column scaling) in estimates after column scaling are found and are summarised in Table 3.7 and Table 3.8, respectively. The following sub–section comprises of comparing estimated parameters with assumed values of the coupling, bearings and unbalances.

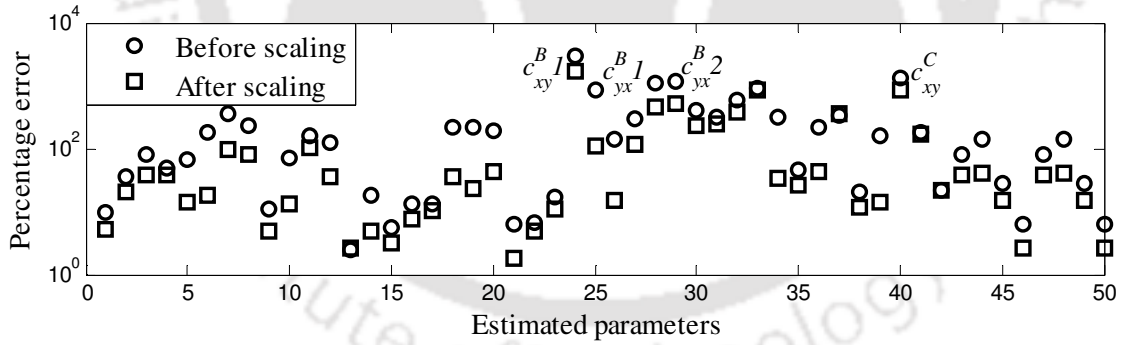

Figure 3.6 Comparison of errors of estimated parameters before and after column scaling for 5% measurement noise (for *Case A* under *Method I*)

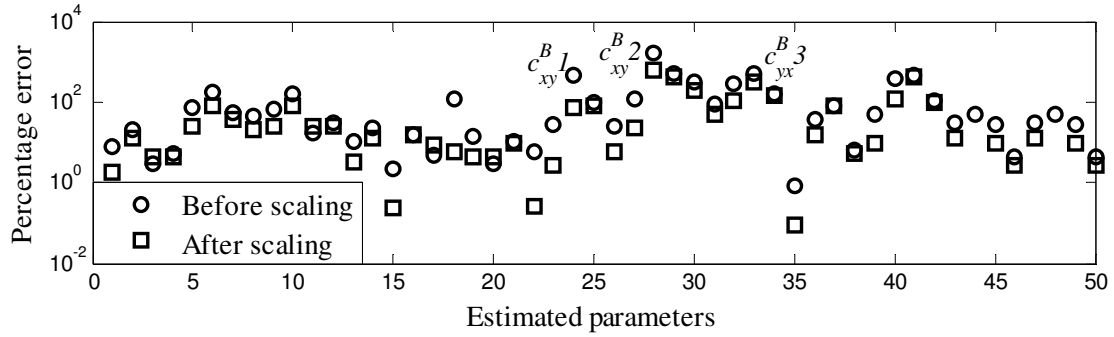

Figure 3.7 Comparison of errors of estimated parameters before and after column scaling for 5% measurement noise (for *Case B* under *Method I*)

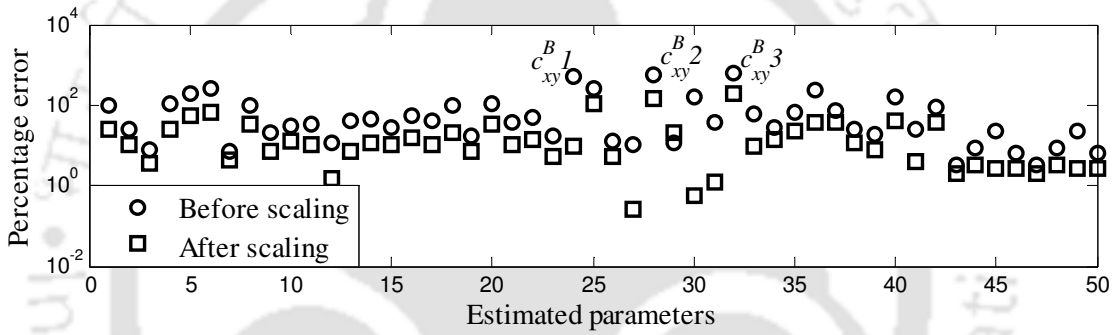

Figure 3.8 Comparison of errors of estimated parameters before and after column scaling for 5% measurement noise (for *Case C* under *Method I*)

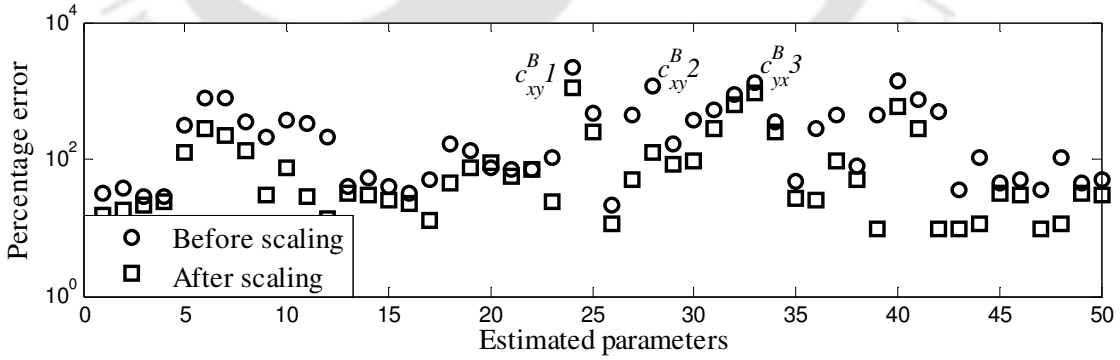

Figure 3.9 Comparison of errors of estimated parameters before and after column scaling for 5% measurement noise (for *Case A* under *Method II*)

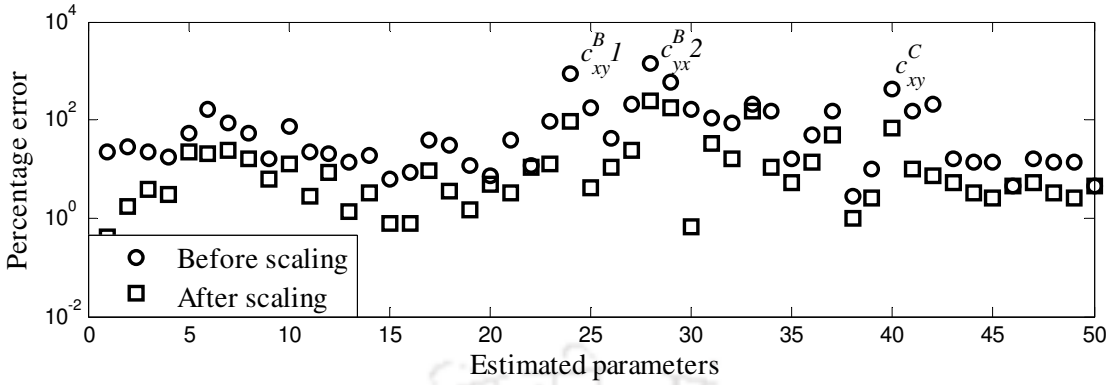

Figure 3.10 Comparison of errors of estimated parameters before and after column scaling for 5% measurement noise (for *Case B* under *Method II*)

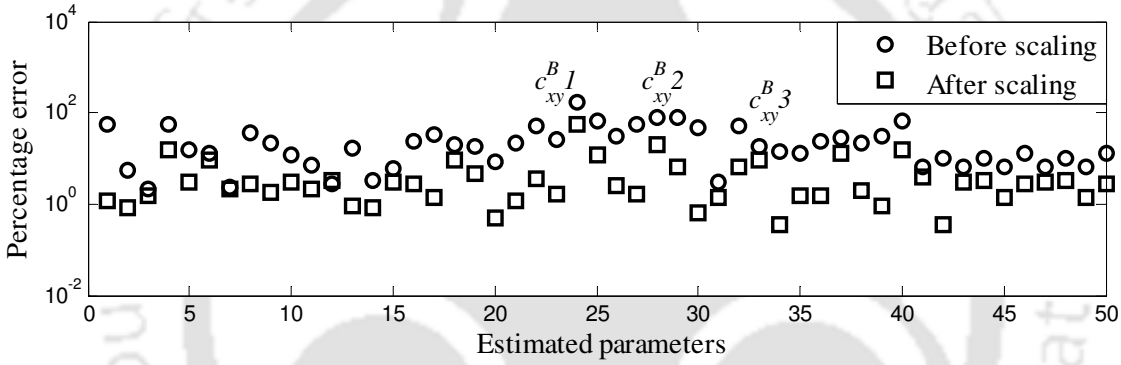

Figure 3.11 Comparison of errors of estimated parameters before and after column scaling for 5% measurement noise (for *Case C* under *Method II*)

3.4.1 Method I: Rotating the Rotor in the Same Direction at Different Speeds

***Case A*:** Diverse machine–element parameters are estimated from responses at selected set of spin speeds near, however, outside the half–power points. Displacements are calculated at two speeds, i.e. ω_1= 100 rad/s and ω_2= 110 rad/s. From Figure 3.12, it could be seen that the most of the stiffness and damping parameters deviate, whereas, the most of unbalance parameters show well agreement at 1% noise case. This variation in estimates increases as the noise percentage increases (considered up to 5%), and some of the stiffness and damping parameters are estimated with different signs (i.e., the negative) which shows the

ill–conditioning of the system equations. From Table 3.7, it can be seen that by the column scaling, the condition number of the regression matrix is improved by the order 10^{18}. From Figure 3.13 and Table 3.8, it is comprehensible that the percentage improvement in the estimation of some of the parameters are 38% and 45% after column scaling for 1% and 5% noise case, respectively.

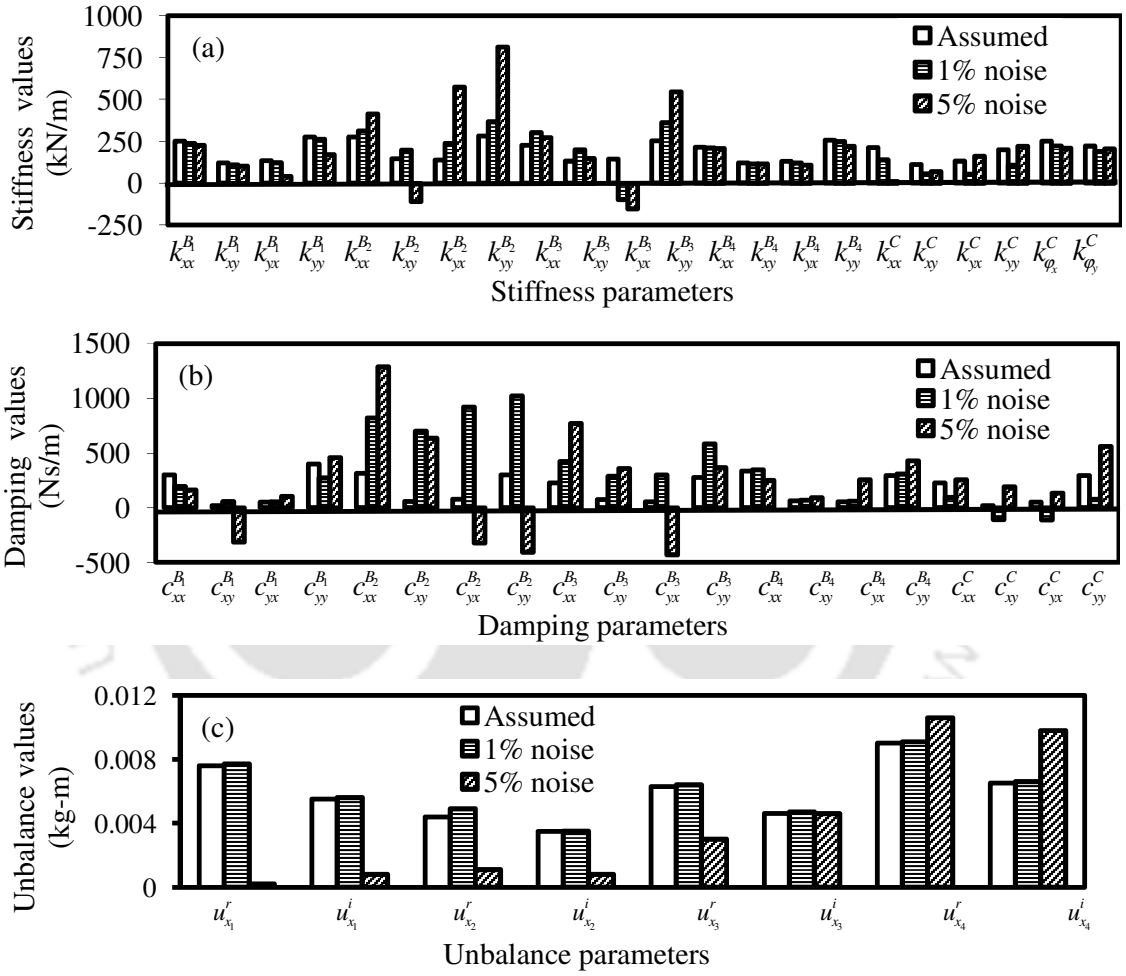

Figure 3.12 Comparison of estimated ((a) stiffness (b) damping (c) unbalance) parameters for different levels of measurement noise (*Case A* under *Method I*)

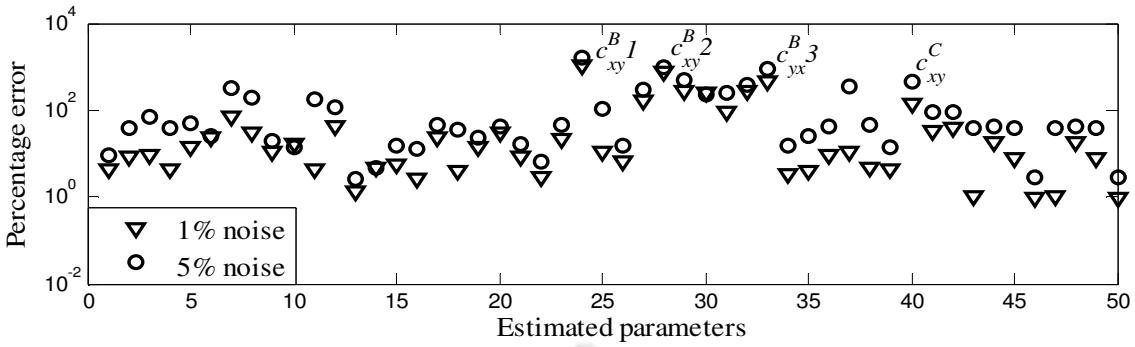

Figure 3.13 Comparison of errors of estimated parameters for different level of measurement noise (for *Case A* under *Method I*)

***Case B*:** Diverse machine–element parameters are identified at selected set of spin speeds away from half–power points. Displacements are calculated at two speeds, i.e. ω_1=60 rad/s and ω_2=160 rad/s. From Figure 3.14, it could be analysed that most of the stiffness and unbalance parameters represent good agreement with assumed values at 1% measurement noise case, whereas, some of the damping (mostly bearing damping) parameters show considerable variation even at 1% noise case and increases as noise percentage increases (i.e., up to 5%). Some of the damping parameters are estimated negative (mostly cross–coupled terms) for 5% noise case. From Table 3.7, it could also be seen that after column scaling the condition number of the regression matrix is improved by the order 10^{19}. From Figure 3.15 and Table 3.8, it could be seen that the percent increase in accuracy of estimates are around 85% and 65% for 1% and 5% noise cases, respectively.

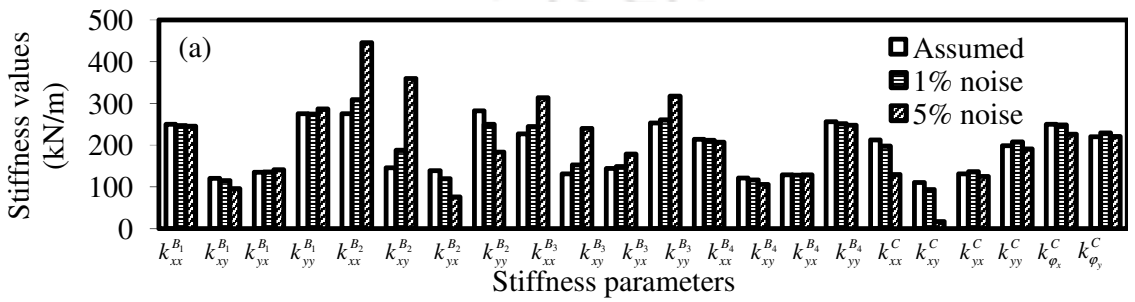

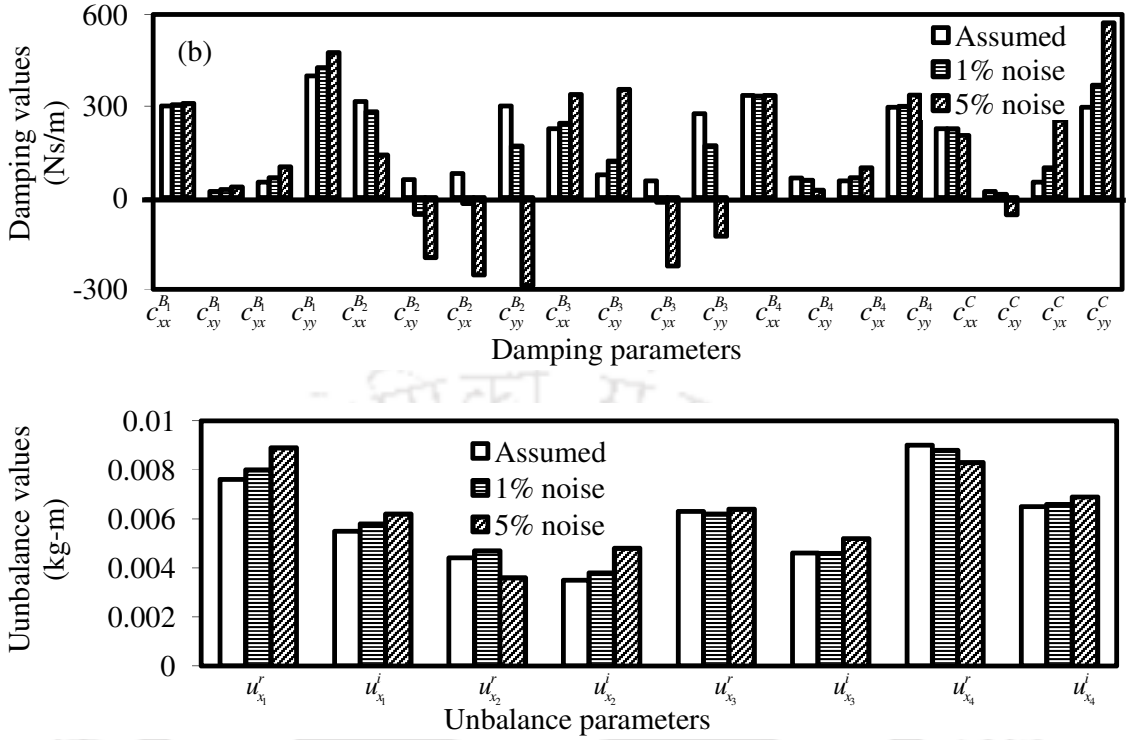

Figure 3.14 Comparison of estimated ((a) stiffness (b) damping (c) unbalance) parameters for different levels of measurement noise (for *Case B* under *Method I*)

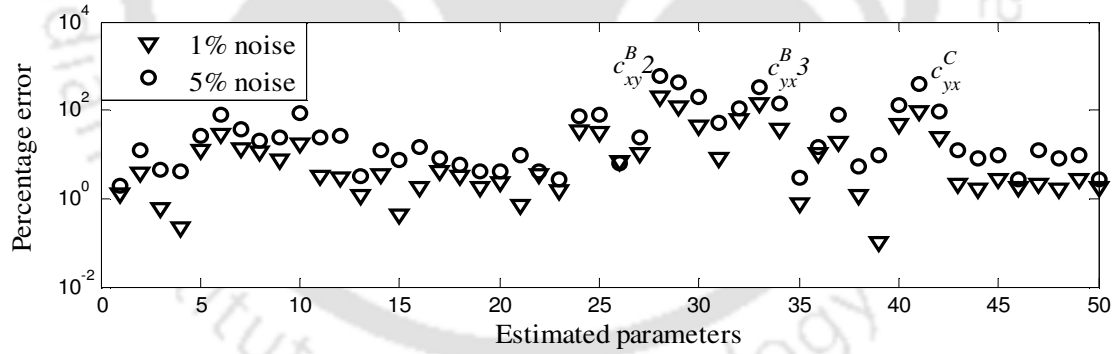

Figure 3.15 Comparison of errors of estimated parameters for different level of measurement noise (for *Case B* under *Method I*)

Case C: Diverse machine–element parameters are identified by increasing the number of measurement speeds up to 300 rad/s. Displacements are calculated at speeds, i.e. for CW: ω = (0–300) rad/s with a step size of 1 rad/s. From Figure 3.16, it could be analysed that most of the stiffness, damping and unbalance parameters of machine elements represent good

agreement with assumed values up to 5% noise case, except few stiffness and damping parameters. From Table 3.7, it could be concluded that after column scaling the condition number of the regression matrix is improved by the order of 10^{22}. From Figure 3.17 and Table 3.8, it could also be analysed that there is appreciable reduction in percentage error after column scaling of some of the parameters is by 95% and 71% for 1% and 5% measurement noise, respectively.

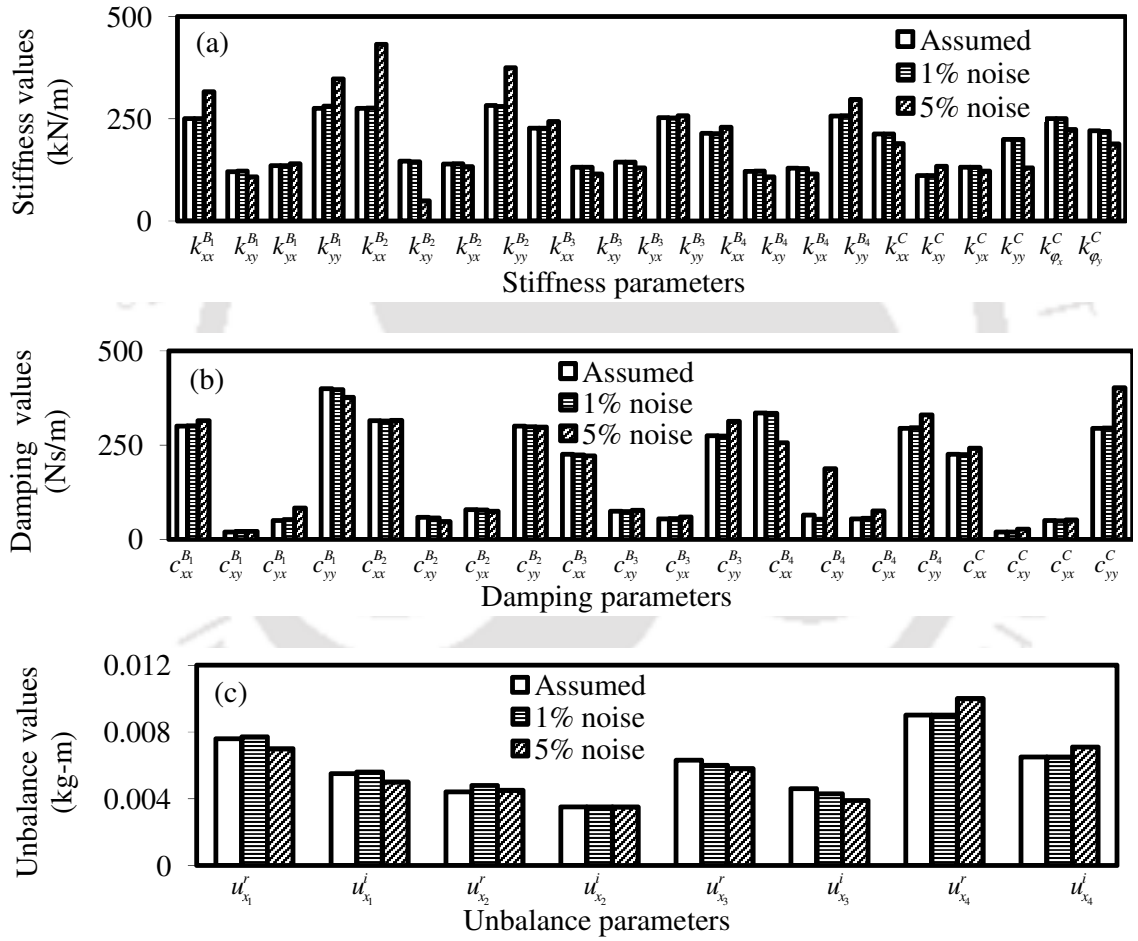

Figure 3.16 Comparison of estimated ((a) stiffness (b) damping (c) unbalance) parameters for different levels of measurement noise (for *Case C* under *Method I*)

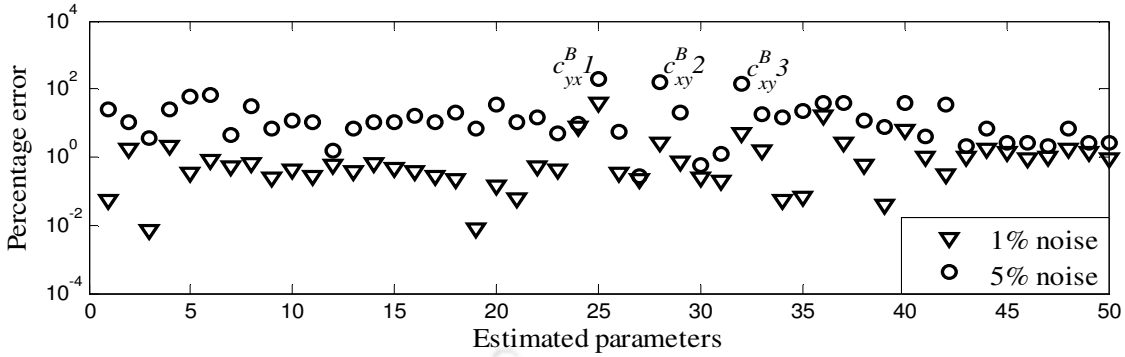

Figure 3.17 Comparison of errors of estimated parameters for different level of measurement noise (for *Case C* under *Method I*)

3.4.2 Method II: Rotating the Rotor Alternately in the CW or CCW Direction

From the previous section, it is evident that the proposed estimation *Method I*, is effective to estimate the bearing and coupling dynamic parameters and residual unbalances only up to 1% noise condition for different cases discussed. However, the estimation is very poor as we increase the noise percentage level. So *Method II* is proposed to take measurements by rotating the rotor alternately in the CW and CWW directions, to improve the effectiveness of the estimation and to sort out the problem arises in *Method I*. It should be noted that such excitation can be generated by using independent unbalance excitation unit (e.g. a free–wheel mounted on shaft and drive independently by separate drives) (Tiwari, 2005) or auxiliary active devices could be used such as active magnetic bearings (Sawicki *et al*., 2011).

***Case A*:** Machine–element parameters are identified by operating the rotor system at selected set of speeds (near, however, outside half–power points). Displacement values are calculated at two speeds, i.e. for CW: ω_1=110 rad/s and for CCW: ω_1= 110 rad/s. From Figure 3.18 and Figure 3.19, it could be seen that the most of the stiffness and damping parameters deviate, whereas, some of the unbalance parameters deviate negligibly small at 1% noise case. This variation in estimate increases as the noise percentage increases (up to 5% shown) and some of the stiffness and damping parameters are estimated negative mostly cross–coupled bearing

parameters. From Table 3.7, it could also be seen that by the column scaling, the condition number of the regression matrix is improved by the order 10^{18}. From Figure 3.19 and Table 3.8, it could be seen that the percentage error is reduced appreciably around 40% and 50% for 1% and 5% noise cases, respectively.

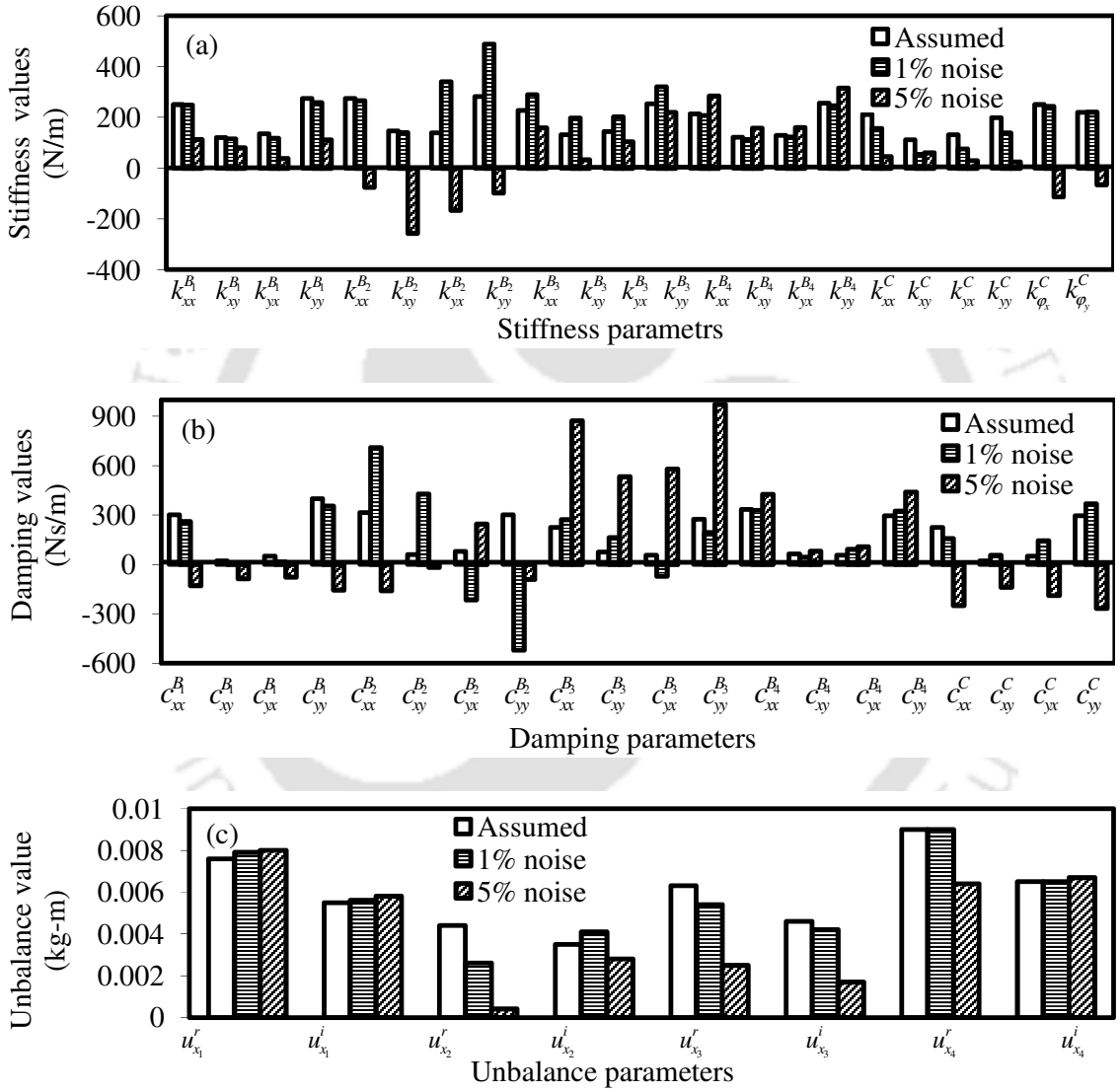

Figure 3.18 Comparison of estimated ((a) stiffness (b) damping (c) unbalance) parameters for different levels of measurement noise (for *Case A* under *Method II*)

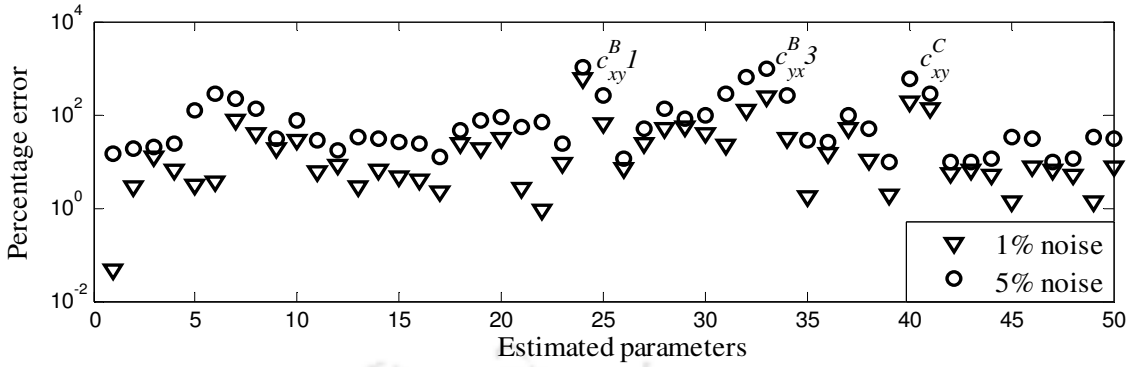

Figure 3.19 Comparison of errors of estimated parameters for different level of measurement noise (for *Case A* under *Method II*

***Case B*:** Machine–element parameters are identified at selected set of spin speeds away from half–power points. Displacements are calculated at two speeds i.e. for CW: ω_1=160 rad/s and for CCW: ω_1= 160 rad/s. From Figure 3.20, it can be seen that most of the stiffness and damping parameters show good agreement with assumed values for 1% noise case. However, unbalance parameters have good agreement even up to 5 % noise case. Some of the damping and few stiffness parameters show variation at 5% noise case. From Table 3.7, it could also be analysed that after the column scaling, the condition number is improved by the order 10^{18}. From Figure 3.21 and Table 3.8, it could be seen that percentage improvement in accuracy on estimates is around 94% and 82% for 1% and 5% noise cases, respectively, for the aforementioned case.

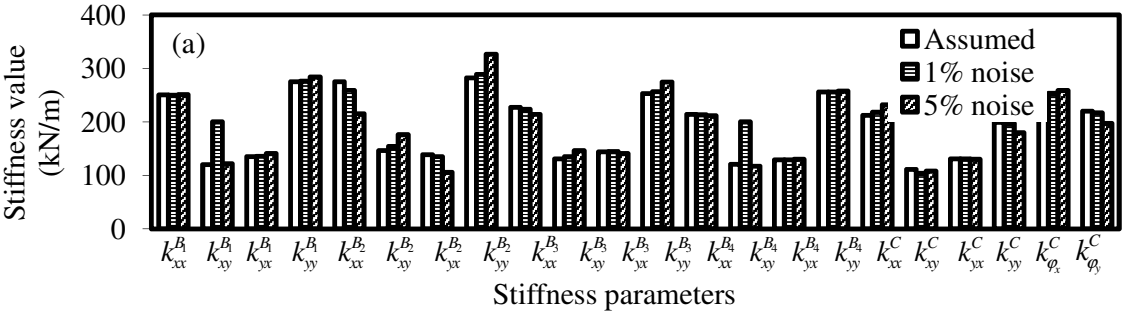

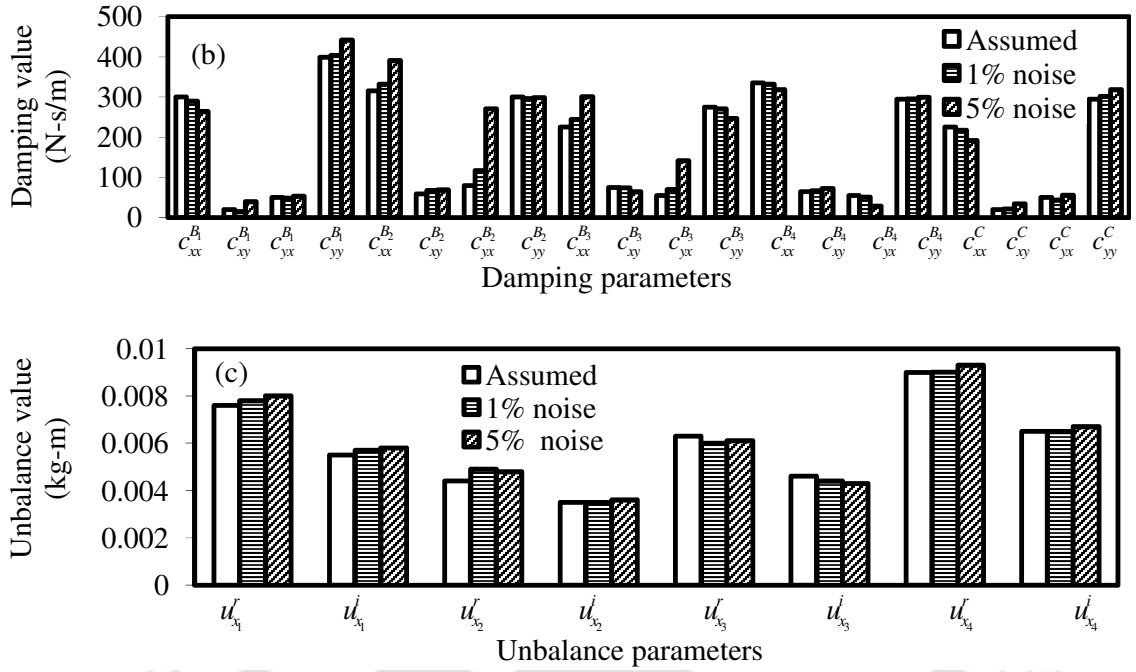

Figure 3.20 Comparison of estimated ((a) stiffness (b) damping (c) unbalance) parameters for different levels of measurement noise (for *Case B* under *Method II*)

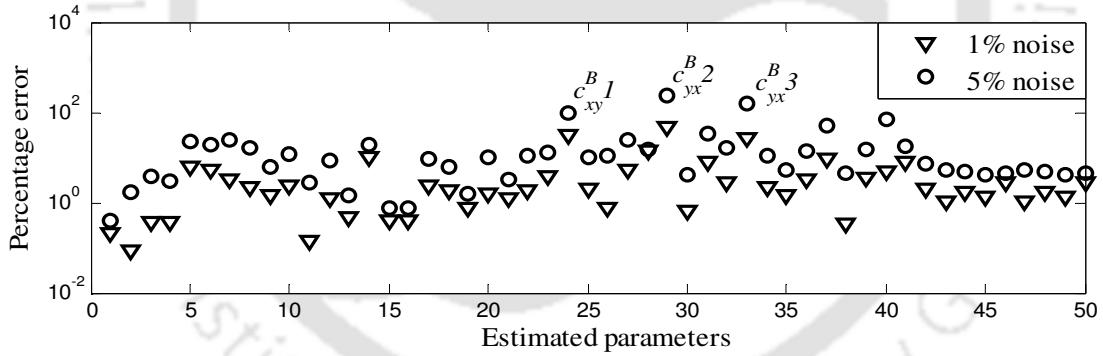

Figure 3.21 Comparison of errors of estimated parameters for different level of measurement noise (for *Case B* under *Method II*)

***Case C*:** Machine–element parameters are identified by increasing the number of measurement speeds up to 300 rad/s. Displacements are calculated at various speeds, i.e. for CW and CCW: ω = (0–300) rad/s with step size of 2 rad/s, (i.e. 150 numbers of different speeds). From Figure 3.22, it could be analysed that most of the stiffness, damping and unbalance parameters of machine elements represent well agreement with assumed ones at

1% noise case, and deviates negligibly small at 5% noise case except few cross–coupled damping parameters. After column scaling, the condition number is improved by the order 10^{23}. It could be seen that percentage improvement in accuracy on estimates of parameters are 84% and 67% for 1% and 5% noise cases, respectively, for the aforementioned case (refer Figure 3.23 and Table 3.8).

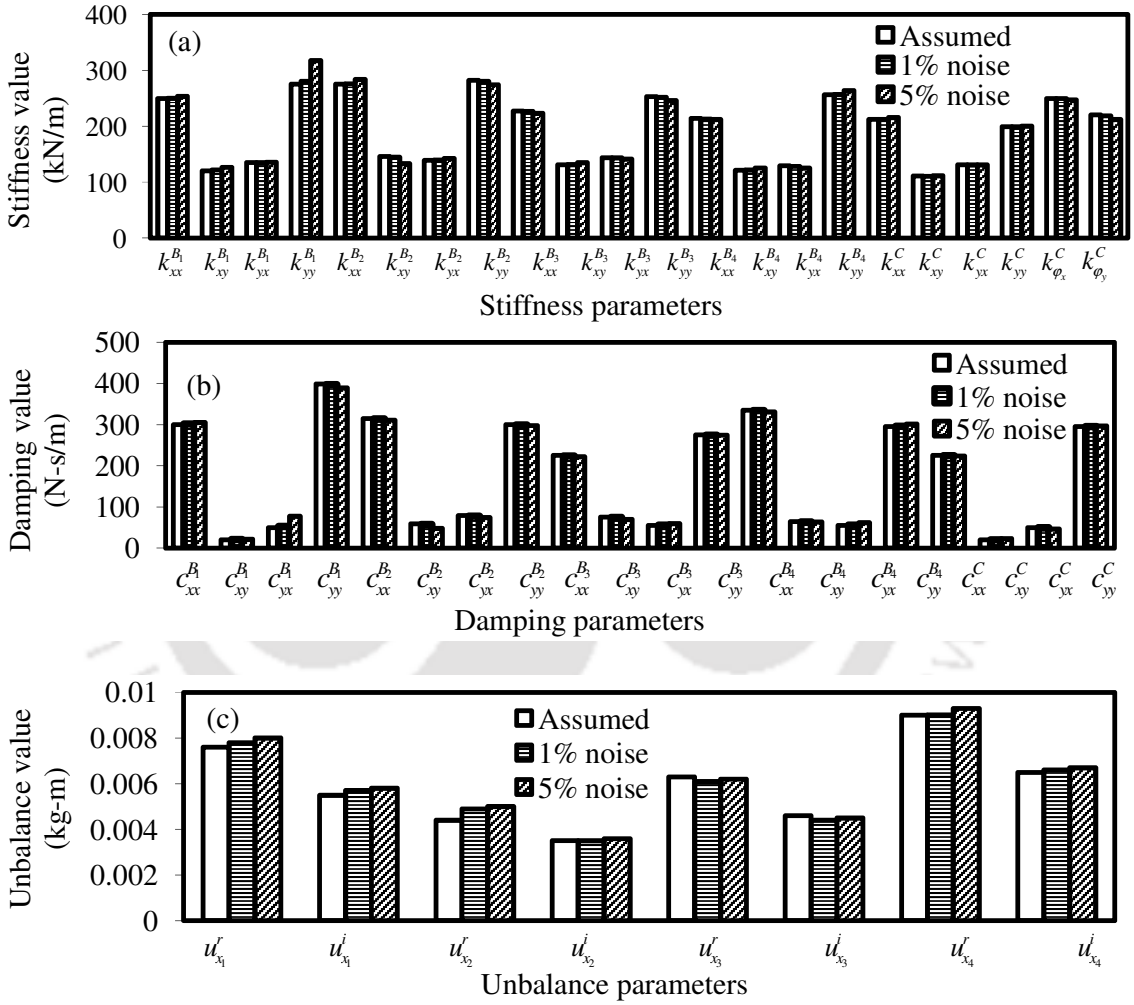

Figure 3.22 Comparison of estimated ((a) stiffness (b) damping (c) unbalance) parameters for different levels of measurement noise (for *Case C* under *Method II*)

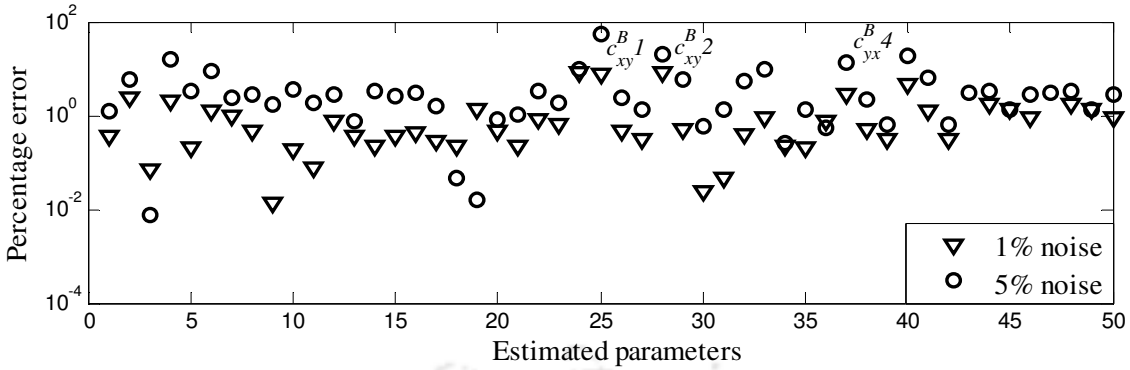

Figure 3.23 Comparison of errors of estimated parameters for different level of measurement noise (for *Case C* under *Method II*)

Table 3.3 Assumed and identified bearing stiffness parameters for *Case C* of *Method II*

Parameters	Assumed values	Estimated values			
		Without noise	With 1% noise	With 2%noise	With 5%noise
$k_{xx}^{B_1}$ (N/m)	2.5000×10^5	2.5021×10^5	2.4986×10^5	2.5017×10^5	2.5362×10^5
$k_{xy}^{B_1}$ (N/m)	1.2000×10^5	1.2017×10^5	1.2212×10^5	1.2385×10^5	1.2677×10^5
$k_{yx}^{B_1}$ (N/m)	1.3500×10^5	1.3511×10^5	1.3501×10^5	1.3510×10^5	1.3585×10^5
$k_{yy}^{B_1}$ (N/m)	2.7500×10^5	2.7508×10^5	2.8055×10^5	2.8766×10^5	3.1751×10^5
$k_{xx}^{B_2}$ (N/m)	2.7500×10^5	2.7518×10^5	2.7594×10^5	2.7731×10^5	2.8387×10^5
$k_{xy}^{B_2}$ (N/m)	1.4600×10^5	1.4480×10^5	1.4477×10^5	1.4285×10^5	1.3325×10^5
$k_{yx}^{B_2}$ (N/m)	1.3900×10^5	1.3885×10^5	1.3973×10^5	1.4046×10^5	1.4268×10^5
$k_{yy}^{B_2}$ (N/m)	2.8200×10^5	2.8116×10^5	2.8020×10^5	2.7854×10^5	2.7433×10^5
$k_{xx}^{B_3}$ (N/m)	2.2700×10^5	2.2691×10^5	2.2643×10^5	2.2575×10^5	2.2315×10^5
$k_{xy}^{B_3}$ (N/m)	1.3100×10^5	1.3093×10^5	1.3155×10^5	1.3234×10^5	1.3505×10^5
$k_{yx}^{B_3}$ (N/m)	1.4400×10^5	1.4344×10^5	1.4361×10^5	1.4315×10^5	1.4139×10^5
$k_{yy}^{B_3}$ (N/m)	2.5300×10^5	2.5233×10^5	2.5159×10^5	2.5017×10^5	2.4588×10^5
$k_{xx}^{B_4}$ (N/m)	2.1400×10^5	2.1373×10^5	2.1318×10^5	2.1260×10^5	2.1210×10^5
$k_{xy}^{B_4}$ (N/m)	1.2100×10^5	1.2097×10^5	1.2178×10^5	1.2263×10^5	1.2558×10^5
$k_{yx}^{B_4}$ (N/m)	1.2900×10^5	1.2901×10^5	1.2840×10^5	2.7834×10^5	1.2513×10^5
$k_{yy}^{B_4}$ (N/m)	2.5600×10^5	2.55599×10^5	2.5701×10^5	2.5824×10^5	2.6398×10^5

Table 3.4 Assumed and identified bearing damping parameters for *Case C* of *Method II*

Parameters used for simulation	Assumed values	Estimated values			
		Without noise	With 1% noise	With 2%noise	With 5%noise
$c_{xx}^{B_1}$ (N-s/m)	300.00	301.26	301.33	302.56	305.60
$c_{xy}^{B_1}$ (N-s/m)	20.00	20.46	21.52	22.45	21.98
$c_{yx}^{B_1}$ (N-s/m)	50.00	50.33	53.40	57.93	77.72
$c_{yy}^{B_1}$ (N-s/m)	399.00	398.26	397.66	395.99	389.12
$c_{xx}^{B_2}$ (N-s/m)	315.00	304.13	314.28	313.50	310.82
$c_{xy}^{B_2}$ (N-s/m)	59.00	59.53	57.43	55.48	47.83
$c_{yx}^{B_2}$ (N-s/m)	79.00	79.93	78.41	77.70	74.83
$c_{yy}^{B_2}$ (N-s/m)	300.00	306.60	299.28	298.76	298.24
$c_{xx}^{B_3}$ (N-s/m)	225.00	223.93	224.57	224.07	222.12
$c_{xy}^{B_3}$ (N-s/m)	75.00	75.73	74.27	73.43	70.29
$c_{yx}^{B_3}$ (N-s/m)	55.00	56.66	55.88	56.84	60.15
$c_{yy}^{B_3}$ (N-s/m)	275.00	278.06	274.85	274.85	274.59
$c_{xx}^{B_4}$ (N-s/m)	335.00	335.26	334.77	334.41	330.89
$c_{xy}^{B_4}$ (N-s/m)	64.00	65.53	63.80	63.67	63.67
$c_{yx}^{B_4}$ (N-s/m)	55.00	54.00	56.47	57.92	62.14
$c_{yy}^{B_4}$ (N-s/m)	295.00	294.66	296.76	298.30	301.74

Table 3.5 Assumed and identified coupling dynamic parameters for *Case C* of *Method II*

Parameters used for simulation	Assumed values	Estimated values			
		Without noise	With 1% noise	With 2%noise	With 5%noise
k_{xx}^{C} (N/m)	2.1200×10^5	2.1590×10^5	2.1256×10^5	2.1324×10^5	2.1587×10^5
k_{xy}^{C} (N/m)	1.1100×10^5	1.1046×10^5	1.1075×10^5	1.1070×10^5	1.1172×10^5
k_{yx}^{C} (N/m)	1.3100×10^5	1.3146×10^5	1.3099×10^5	1.3100×10^5	1.3105×10^5
k_{yy}^{C} (N/m)	1.9900×10^5	2.0370×10^5	1.9929×10^5	1.9957×10^5	2.0038×10^5
$k_{\varphi_x}^{C}$ (N-m/rad)	2.5000×10^5	2.5004×10^5	2.4984×10^5	2.4950×10^5	2.4747×10^5
$k_{\varphi_y}^{C}$ (N-m/rad)	2.2000×10^5	2.2002×10^5	2.1883×10^5	2.1746×10^5	2.1223×10^5
c_{xx}^{C} (N-s/m)	225.00	219.53	224.91	224.75	223.88
c_{xy}^{C} (N-s/m)	20.00	20.40	20.30	20.76	23.01
c_{yx}^{C} (N-s/m)	50.00	50.06	49.48	48.91	46.97
c_{yy}^{C} (N-s/m)	295.00	295.40	295.93	296.52	296.40

Table 3.6 Assumed and identified unbalance parameters for *Case C* of *Method II*

Parameters used for simulation	Assumed values	Estimated values			
		Without noise	With 1% noise	With 2%noise	With 5%noise
$u_{x_1}^r$ (kg-m)	0.0076	0.0077	0.0078	0.0078	0.0080
$u_{x_1}^i$ (kg-m)	0.0055	0.0056	0.0057	0.0057	0.0058
$u_{x_2}^r$ (kg-m)	0.0044	0.0049	0.0049	0.0049	0.0050
$u_{x_2}^i$ (kg-m)	0.0035	0.0035	0.0035	0.0036	0.0036
$u_{x_3}^r$ (kg-m)	0.0063	0.0064	0.0061	0.0061	0.0062
$u_{x_3}^i$ (kg-m)	0.0046	0.0046	0.0044	0.0045	0.0045
$u_{x_4}^r$ (kg-m)	0.0090	0.0091	0.0090	0.0091	0.0093
$u_{x_4}^i$ (kg-m)	0.0065	0.0066	0.0066	0.0066	0.0067

After estimating coupling dynamic parameters and responses at coupling location these could be used to estimate the misalignment forces and moments by referring Chapter 2, Eqn. (2.12). For the best estimation case (i.e., *Case C* under *Method II*) the variation of misalignment forces and moments are plotted with respect to the spin speed. From Figure 3.24, it is to be noted that the misalignment forces and moments are dependent on the spin speed and because of it the misalignment forces and moments are very high at or near critical speeds of the system. To check the performance of algorithm for different set of assumed residual unbalances, Table 3.9 shows identified residual unbalances (magnitude and phase) for *Case C* under *Method II* for 5 percent measurement noise. To check the performance of algorithm for different set of disc masses, Table 3.10 shows identified residual unbalances (magnitude and phase) for *Case C* under *Method II* for 5 percent measurement noise. In both cases well agreement between the assumed and estimated residual unbalances are observed.

Table 3.7 Summary of estimated parameters having maximum % error and corresponding condition numbers for different cases

Methods	Cases	Condition number before column scaling		Condition number after column scaling		Order of improvement in condition number	
		For 1% noise	For 5% noise	For 1% noise	For 5% noise	For 1% noise	For 5% noise
Method *I*	Case A	6.26×10^{28}	8.08×10^{28}	2.49×10^{10}	5.26×10^{10}	2.51×10^{18}	3.21×10^{18}
	Case B	5.48×10^{28}	7.37×10^{29}	2.17×10^{10}	4.44×10^{10}	2.52×10^{18}	1.65×10^{19}
	Case C	3.69×10^{28}	3.40×10^{29}	1.40×10^{6}	3.49×10^{6}	2.63×10^{22}	9.74×10^{22}
Method *II*	Case A	3.41×10^{28}	7.69×10^{28}	2.69×10^{10}	4.57×10^{10}	1.26×10^{18}	1.68×10^{18}
	Case B	2.29×10^{28}	3.57×10^{29}	1.62×10^{10}	4.49×10^{10}	1.41×10^{18}	7.95×10^{18}
	Case C	1.78×10^{28}	2.38×10^{29}	1.01×10^{6}	1.84×10^{6}	1.76×10^{22}	1.29×10^{23}

Table 3.8 Identified residual unbalances for different assumed residual unbalance (for *Case C* under *Method II*)

Methods	Cases	Estimated parameters having max. % error before column scaling		Estimated parameters having max. % error after column scaling		% improvement in accuracy or % reduction in error on estimates after column scaling	
		For 1% noise	For 5% noise	For 1% noise	For 5% noise	For 1% noise	For 5% noise
Method *I*	Case A	$c_{xy}^{B_1}$ (1660.98)	$c_{xy}^{B_1}$ (2996.23)	$c_{xy}^{B_1}$ (1030.41)	$c_{xy}^{B_1}$ (1663.00)	37.95	44.50
	Case B	$c_{xy}^{B_2}$ (1359.05)	$c_{xy}^{B_2}$ (1695.69)	$c_{xy}^{B_2}$ (191.79)	$c_{xy}^{B_2}$ (600.05)	85.94	64.60
	Case C	$c_{yx}^{B_1}$ (291.72)	$c_{xy}^{B_2}$ (659.81)	$c_{yx}^{B_1}$ (15.93)	$c_{xy}^{B_2}$ (193.25)	94.84	70.71
Method *II*	Case A	$c_{xy}^{B_1}$ (1055.92)	$c_{xy}^{B_1}$ (2175.59)	$c_{xy}^{B_1}$ (626.23)	$c_{xy}^{B_1}$ (1085.52)	40.66	50.11
	Case B	$c_{yx}^{B_2}$ (796.59)	$c_{yx}^{B_2}$ (1398.79)	$c_{yx}^{B_2}$ (46.83)	$c_{yx}^{B_2}$ (241.72)	94.22	82.76
	Case C	$c_{xy}^{B_1}$ (39.83)	$c_{xy}^{B_1}$ (168.21)	$c_{xy}^{B_1}$ (6.59)	$c_{xy}^{B_1}$ (54.92)	84.61	67.85

Table 3.9 Estimation performance for different set of assumed residual unbalances for 5% measurement noise (for *Case C* under *Method II*)

S.N.	Residual unbalance in plane 1 (kg–m@deg)		Residual unbalance in plane 2 (kg–m@deg)		Residual unbalance in plane 3 (kg–m@deg)		Residual unbalance in plane 4 (kg–m@deg)	
	Assumed	Estimated	Assumed	Estimated	Assumed	Estimated	Assumed	Estimated
1	9.4×10^{-3} @36	9.8×10^{-3} @37.9	5.6×10^{-3} @108	6.2×10^{-3} @107.2	7.8×10^{-3} @240	7.6×10^{-3} @240.9	11.1×10^{-3} @300	11.4×10^{-3} @301.2
2	10.1×10^{-3} @46	11.8×10^{-3} @47.3	6.5×10^{-3} @112	7.7×10^{-3} @113.8	8.3×10^{-3} @220	8.8×10^{-3} @221.8	13.1×10^{-3} @315	14.5×10^{-3} @313.7
3	11.2×10^{-3} @66	12.1×10^{-3} @67.9	7.7×10^{-3} @130	8.9×10^{-3} @132.3	9.6×10^{-3} @200	10.3×10^{-3} @200.2	14.0×10^{-3} @330	15.4×10^{-3} @332.7
4	12.5×10^{-3} @70	13.3×10^{-3} @72.2	8.9×10^{-3} @145	9.5×10^{-3} @145.9	11.5×10^{-3} @190	12.9×10^{-3} @192.2	9.0×10^{-3} @280	10.3×10^{-3} @281.9

Table 3.10 Residual unbalance estimation for different set of disc masses for 5% measurement noise (for *Case C* under *Method II*)

S.N.	Assumed disc mass (kg)	Estimated residual unbalance (kg–m@deg)			
		Plane 1	Plane 2	Plane 3	Plane 4
		9.4×10^{-3} @36.0	5.6×10^{-3} @108.0	7.8×10^{-3} @240.0	11.1×10^{-3} @300.0
Set–1	m_1^d=2.0, m_2^d=1. 5, m_3^d=2.5, m_4^d=1.6	9.8×10^{-3} @37.9	6.2×10^{-3} @107.2	7.6×10^{-3} @240.9	11.4×10^{-3} @301.2
Set–2	m_1^d=1.3, m_2^d=0.5, m_3^d=1.0, m_4^d=2.0	9.0×10^{-3} @36.7	5.9×10^{-3} @107.4	7.2×10^{-3} @239.4	12.3×10^{-3} @302.3
Set–3	m_1^d=2.5, m_2^d=2.0, m_3^d=0.5, m_4^d=2.0	10.2×10^{-3} @38.4	6.6×10^{-3} @109.4	6.6×10^{-3} @238.5	12.9×10^{-3} @302.7

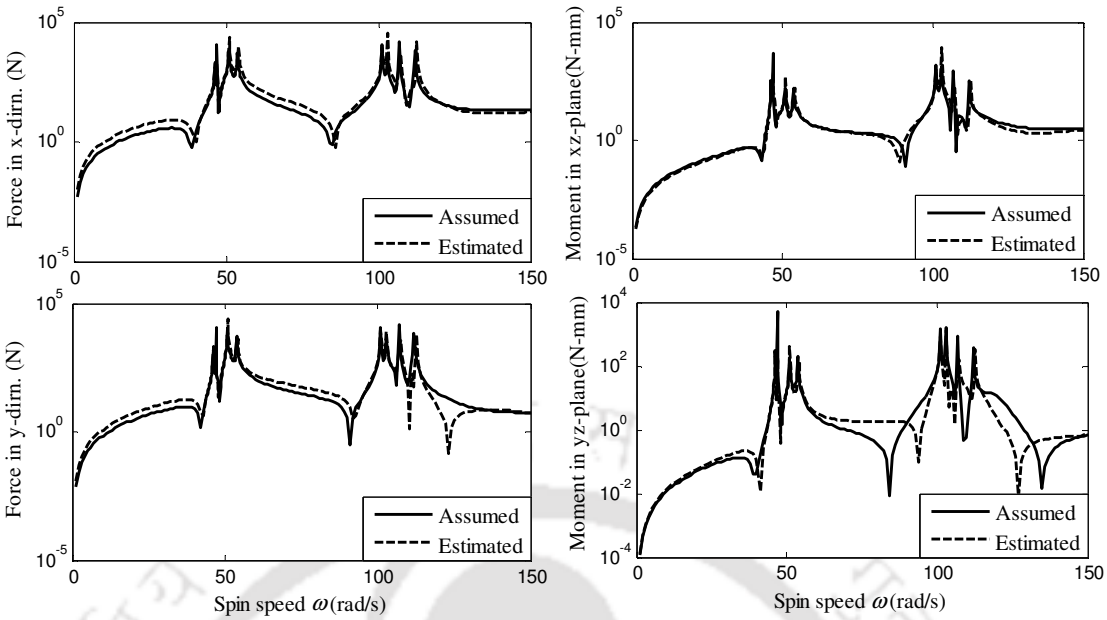

Figure 3.24 Misalignment forces and moments with spin speed for 5% noise (for *Case C* under Method II)

3.4.3 Discussion on Various Numerical Studies Performed

From Figure 3.5, it could be seen that at all critical speeds, resonance condition prevails both in the amplitude and the phase. Thereafter, the assumed and estimated parameters are compared in Sections 3.4.1 and 3.4.2, for different cases discussed in Chapter 2 Section 2.3. These studies have been performed for various measurement noise levels also. Following observations could be made from discussions of Sections 3.4.1 and 3.4.2.

- It is observed that for the no noise condition, estimated parameters show very well agreement with assumed parameters for both the methods (i.e. *Method I* & *II*) and under all three cases (i.e. *Cases A, B* & *C*).

- *Case A* is the worst case of estimation for both methods (i.e., *Method I* & *II*) in which deviation starts even at 1% noise condition and increases as the noise percentage increases.

- Under *Method I*, *Case C* is the best estimation case in which the maximum error occurred is around 15% at 1% noise. The order of improvement in condition number is the maximum for this case under *Method I*.

- *Case C* under *Method II* is the overall best case for estimation of parameters; the maximum error observed in this case is around 6% at 1% noise. Among all the three cases discussed above for both methods (i.e., *Method I* & *II*) the order of improvement in condition is maximum for this case i.e., 10^{23}.

- From Table 3.7, it can be analysed that only the cross–coupled damping parameters show the maximum deviation in estimates for most of the cases discussed above. It is be noted that the assumed values of these cross–coupled damping parameters are very less compared to direct damping parameters (direct damping parameters are 5–10 times more than the cross–coupled damping parameters). So, even the percentage error is more for these cross–coupled terms but the absolute magnitude deviations of these estimates are appreciably less or comparable to other parameters.

- From Sections 3.4.1, 3.4.2 and Table 3.7, it is apparent that the cross–coupled damping parameters $c_{xy}^{B_1}$, $c_{yx}^{B_1}$, $c_{xy}^{B_2}$ and $c_{yx}^{B_2}$ are more sensitive and shows maximum percentage error in most of the cases.

The algorithm is also tested under different levels of measurement noise as shown in Table 3.3–Table 3.6, to get the robustness properties of the algorithm on theoretically simulated data. So from the above comparison it can be concluded that the C*ase C* under *Method II* is the best method for estimating the parameters. However, due to the way measurements have been taken in both sense of rotations (i.e. CW and CCW) the possibility of ill–condition

reduces due to availability of the modal information related to forward and backward whirls, which are otherwise unavailable in measurements. And in fact it is expected to improve estimates when more and more modal information of the system is available in measurements.

3.5 Summary

An identification algorithm developed in Chapter 2, for the simultaneous estimation of the bearing and coupling dynamic parameters along with residual unbalances is improved in the present chapter for multi–DOF flexible rotor–bearing–coupling system. A relatively new concept is introduced in regards to misalignment as the amount of misalignment changes with different modes for flexible rotor coupling misalignment. The identification algorithm also has the flexibility to incorporate any number of bearings, couplings and balancing planes. Residual unbalances are obtained at predefined balancing planes. The identification algorithm is illustrated by simulated numerical examples. The effect on estimates of residual unbalance with the change in assumed unbalance and disc masses is discussed and excellent agreements on estimates with change in these parameters are observed. In the present technique of model based identification the accuracy of estimates depends upon the model for a specific fault (for example the present technique could be extended for the speed–dependent bearing and coupling parameters, etc.). In rotating machines, accessibility is very limited and measurement points are rather inadequate so application of suitable reduction procedure would be a real assessment and that has been handled in the subsequent chapter.

CHAPTER 4

Multiple Fault Identification in Flexible Rotor–Bearing–Coupling Systems with Incomplete Rundown or Run-up Data

4.1 Introduction

The practical difficulty of measurement of rotational DOFs arise in Chapter 3, has been handled in the present Chapter. To tackle the practical difficulty of limited measurements or responses that are difficult to measure (i.e., rotational DOFs) and the numerical difficulty of the conventional dynamic condensation in the development of identification algorithm to estimate the bearing and coupling dynamic parameters along with residual unbalances has been handled in the present chapter. In practice at very few locations the measurements of responses can be performed. Moreover, the rotational DOF measurement at coupling is very difficult or practically impossible, which is otherwise required for estimation of coupling parameters because of rotational stiffness coefficients. In the present work, this has been relaxed by high–frequency condensation and hence the incomplete data word is used. Measured data are there for several speeds so the rundown or run–up data word has been used. A novel condensation technique has been implemented especially to overcome measurement of rotational DOFs. Numerical examples are also presented to show the effectiveness of the proposed method. The measurement noise has been added in numerically simulated responses that are used in the present algorithm to identify the parameters and the algorithm is found to be robust. Modelling errors of few physical parameters have also been considered and the estimates are found to be excellent.

4.2 System Modelling

In the present section assumptions involved in modelling the system under consideration have been stated. Details of the misaligned rotor bearing model have also been presented.

4.2.1 Basic Assumptions and the Description of Model

In Chapter 3 Section 3.2, FE formulation for a MDOF system has been performed and the EOM has been obtained for the system. The practical difficulty of number of measurements arise in Chapter 3 has been taken care in the present Chapter. The rotor model, as shown in Figure 4.1, composed of several flexible shafts and each of them are supported on flexible anisotropic bearings, and connected together by a flexible coupling is considered in the present chapter. A typical FE model of the rotor system is shown in Figure 4.2. Here B_1 to B_{2p} are bearing locations, D_1 to D_m are disc locations. Each shaft is having m numbers of rigid discs and that could act as balancing planes depending on number of flexible modes to be balanced. Each disc has the mass, m_i^D (i = 1 to m), the diametral mass moment of inertia, $I_{d_i}^D$, and the residual unbalance, U_i. No external exciter is used in the present study. Independent excitation unit has been suggested for CW/CCW rotation of trial unbalances in case reversal of rotor speed is not feasible. All the forces considered are modelled as a centrifugal force. A schematic diagram of the $(p-1)^{th}$ coupling with nodal coordinates is shown in Figure 4.3. Symbols (x, y) and (φ_y, φ_x) are the transverse linear and angular displacements of the shaft, respectively, in the two orthogonal directions. Superscripts: B, C, and D in above symbols represent the bearing, the coupling, and the disc, respectively. The Timoshenko beam theory with gyroscopic effect has been used. The torsional and longitudinal vibrations effects and its coupling with transverse vibrations are not considered in the present analysis. Internal damping has been ignored in the present study.

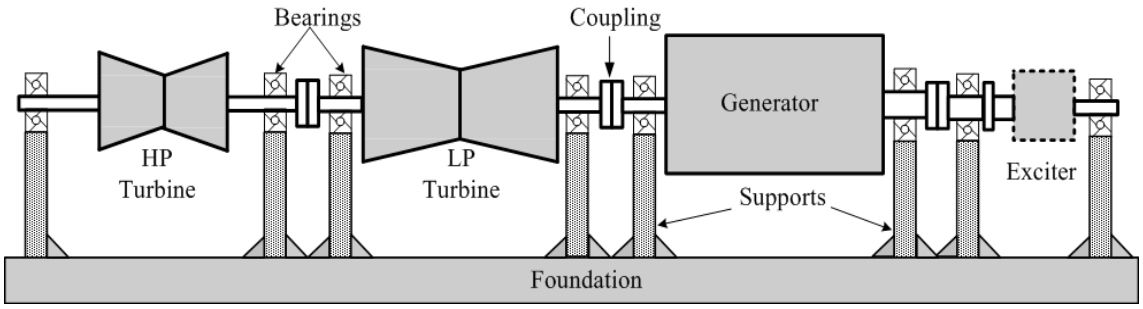

Figure 4.1 A flexible multi–stage turbine–generator rotor system

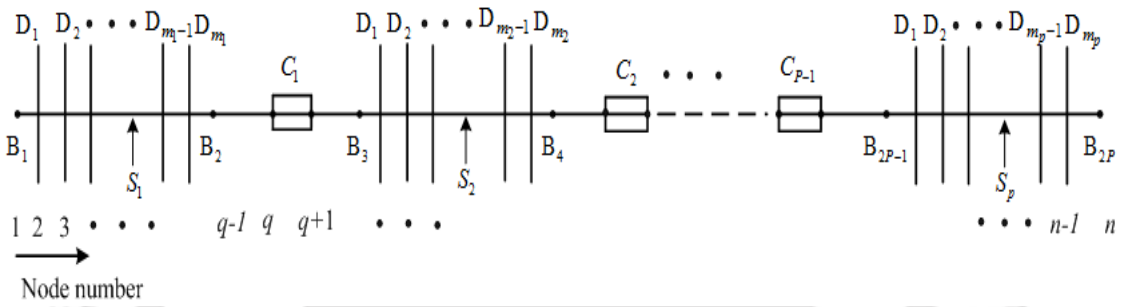

Figure 4.2 A FE model of the flexible multi–stage turbine–generator rotor system

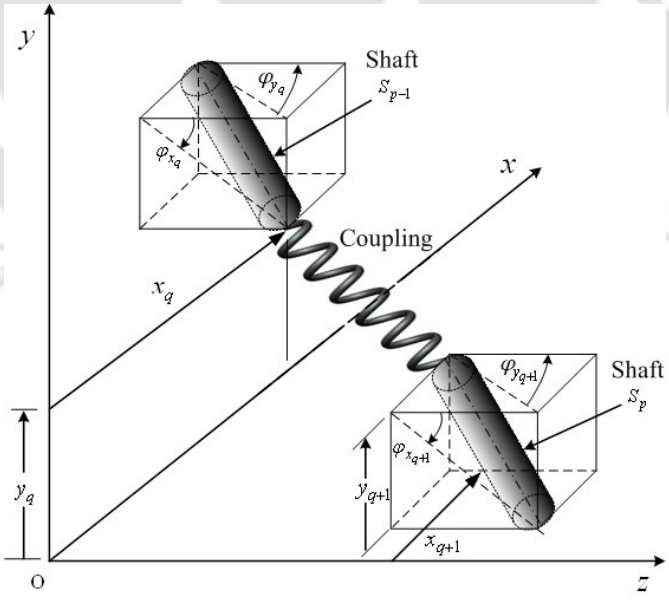

Figure 4.3 A schematic diagram of $(p-1)^{th}$ coupling

4.2.2 System Equations of Motion in Frequency Domain

Referring to Chapter 3 Section 3.2, the EOM in frequency domain for the complete MDOF flexible rotor–bearing–coupling system could be obtained as

$$\begin{bmatrix} [Z_{R,II}] & [Z_{R,IB}] & [Z_{R,IC}] \\ [Z_{R,BI}] & [Z_{R,BB}+Z_{B,BB}] & [Z_{R,BC}] \\ [Z_{R,CI}] & [Z_{R,CB}] & [Z_{R,CC}+Z_{C,CC}] \end{bmatrix} \begin{Bmatrix} \{\eta_{R,I}\} \\ \{\eta_{R,B}\} \\ \{\eta_{R,C}\} \end{Bmatrix} = \begin{Bmatrix} \{F_{R,I}\} \\ \{0\} \\ \{0\} \end{Bmatrix} \tag{4.42}$$

Eqn. (4.42), would be used in subsequent section for the simultaneous estimation of the bearing and coupling dynamic parameters along with residual unbalances. In the section of numerical experiments the same equation would be used to get simulated responses for testing the proposed identification algorithms.

4.3 Development of the Identification Algorithm with the Dynamic Condensation

In general Eq. (4.42), can be written as

$$\left(-\omega^2 [M]_{4n\times 4n} + \mathrm{j}\omega\left([C]_{4n\times 4n} - \omega[G]_{4n\times 4n}\right) + [K]_{4n\times 4n}\right)\{\eta\}_{4n\times 1} = \{F\}_{4n\times 1} \tag{4.43}$$

where subscript n represents number of nodes and the number attached with matrices and vectors represent the respective sizes. Since in rotating machinery accessibility is limited and it is difficult to measure all rotational DOFs accurately, the dynamic condensation scheme has been applied at various DOFs (i.e., the translational as well as the rotational) except at bearing and coupling locations. From Eqn. (4.43), the mass, damping, gyroscopic and stiffness matrices, and the force and displacement vectors, can be divided into sub–matrices and vectors as (refer Friswell and Mottershead (1995))

$$\left(-\omega^2\begin{bmatrix}[M^d_{mm}] & [M^d_{ms}]\\ [M^d_{sm}] & [M^d_{ss}]\end{bmatrix}+\mathrm{j}\omega\left(\begin{bmatrix}[C^d_{mm}] & [C^d_{ms}]\\ [C^d_{sm}] & [C^d_{ss}]\end{bmatrix}-\omega\begin{bmatrix}[G^d_{mm}] & [G^d_{ms}]\\ [G^d_{sm}] & [G^d_{ss}]\end{bmatrix}\right)+\begin{bmatrix}[K^d_{mm}] & [K^d_{ms}]\\ [K^d_{sm}] & [K^d_{ss}]\end{bmatrix}\right)\begin{Bmatrix}\{\eta^d_m\}_{m^d\times 1}\\ \{\eta^d_s\}_{s^d\times 1}\end{Bmatrix} = \begin{Bmatrix}\{F^d_m\}_{m^d\times 1}\\ \{F^d_s\}_{s^d\times 1}\end{Bmatrix} \tag{4.44}$$

where subscripts m and s represent the master and slave DOFs, respectively. Subscripts m^d and s^d represent the size of master and slave DOFs, respectively. Superscript d stands for the dynamic condensation. For the present case transverse translational DOFs corresponding to bearing locations and all DOFs (i.e., both transverse translational and rotational DOFs) corresponding to coupling location has been considered as master DOFs that have to be retained in EOMs. Whereas rotational DOFs corresponding to bearing locations and all DOFs at other nodes (refer Figure 4.2) except coupling location has been considered as slave DOFs that has to be eliminated from EOMs. Eqn. (4.44), could be expressed in two equations as

$$-\omega^2\left(\left[M^d_{mm}\right]\{\eta^d_m\}+\left[M^d_{ms}\right]\{\eta^d_s\}\right)+\mathrm{j}\omega\left(\left[C^d_{mm}\right]-\omega\left[G^d_{mm}\right]\right)\{\eta^d_m\}+\mathrm{j}\omega\left(\left[C^d_{ms}\right]-\omega\left[G^d_{ms}\right]\right)\{\eta^d_s\} + \left[K^d_{mm}\right]\{\eta^d_m\}+\left[K^d_{ms}\right]\{\eta^d_s\}=\{F^d_m\} \tag{4.45}$$

and

$$-\omega^2\left(\left[M^d_{sm}\right]\{\eta^d_m\}+\left[M^d_{ss}\right]\{\eta^d_s\}\right)+\mathrm{j}\omega\left(\left[C^d_{sm}\right]-\omega\left[G^d_{sm}\right]\right)\{\eta^d_m\}+\mathrm{j}\omega\left(\left[C^d_{ss}\right]-\omega\left[G^d_{ss}\right]\right)\{\eta^d_s\} + \left[K^d_{sm}\right]\{\eta^d_m\}+\left[K^d_{ss}\right]\{\eta^d_s\}=\{F^d_s\} \tag{4.46}$$

By following the assumptions involved in the dynamic condensation for the undamped and non−gyroscopic system (Friswell and Mottershead, 1995), the transformation matrix for the present case could be obtained from Eqn. (4.46), and it could be written as

$$-\omega^2\left(\left[M_{sm}^{d}\right]\left\{\eta_m^d\right\}_{m^d\times 1}+\left[M_{ss}^{d}\right]\left\{\eta_s^d\right\}_{s^d\times 1}\right)+\left[K_{sm}^{d}\right]\left\{\eta_m^d\right\}_{m^d\times 1}+\left[K_{ss}^{d}\right]\left\{\eta_s^d\right\}_{s^d\times 1}=\{0\} \tag{4.47}$$

$$\left\{\eta_s^d\right\}_{s^d\times 1}=-\left(\left[K_{ss}^{d}\right]-\omega^2\left[M_{ss}^{d}\right]\right)^{-1}\left(\left[K_{sm}^{d}\right]-\omega^2\left[M_{sm}^{d}\right]\right)\left\{\eta_m^d\right\}_{m^d\times 1} \tag{4.48}$$

With an identity matrix, the state vector $\left\{\eta_m^d\right\}_{m^d\times 1}$ can be written as

$$\left\{\eta_m^d\right\}_{m^d\times 1}=[I]_{m^d\times m^d}\left\{\eta_m^d\right\}_{m^d\times 1} \tag{4.49}$$

Eqns. (4.48) and (4.49) could be combined as

$$\begin{Bmatrix}\{\eta_m^d\}_{m^d\times 1}\\ \{\eta_s^d\}_{s^d\times 1}\end{Bmatrix}=\left[T^d\right]_{4n\times m^d}\left\{\eta_m^d\right\}_{m^d\times 1} \tag{4.50}$$

with

$$\left[T^d\right]_{4n\times m^d}=\begin{bmatrix}[I]_{m^d\times m^d}\\ \hline -\left(\left[K_{ss}^{d}\right]-\omega^2\left[M_{ss}^{d}\right]\right)^{-1}\left(\left[K_{sm}^{d}\right]-\omega^2\left[M_{sm}^{d}\right]\right)\end{bmatrix} \tag{4.51}$$

where $[T^d]$ is the transformation matrix for the dynamic condensation. On substituting Eqn. (4.50), into frequency domain Eqn. (4.44), the resulting equation becomes

$$\left(-\omega^2\left[M^d\right]_{m^d\times m^d}+\mathrm{j}\omega\left(\left[C^d\right]_{m^d\times m^d}-\omega\left[G^d\right]_{m^d\times m^d}\right)+\left[K^d\right]_{m^d\times m^d}\right)\left\{\eta_m^d\right\}_{m^d\times 1}=\left\{F_m^d\right\}_{m^d\times 1} \tag{4.52}$$

with

$$\left[M^d\right]_{m^d\times m^d}=\left[T^d\right]_{m^d\times 4n}^{T}\left[M\right]_{4n\times 4n}\left[T^d\right]_{4n\times m^d},\quad \left[K^d\right]_{m^d\times m^d}=\left[T^d\right]_{m^d\times 4n}^{T}\left[K\right]_{4n\times 4n}\left[T^d\right]_{4n\times m^d},$$

$$\left[C^d\right]_{m^d\times m^d}=\left[T^d\right]^T_{m^d\times 4n}\left[C\right]_{4n\times 4n}\left[T^d\right]_{4n\times m^d},\quad \left[G^d\right]_{m^d\times m^d}=\left[T^d\right]^T_{m^d\times 4n}\left[G\right]_{4n\times 4n}\left[T^d\right]_{4n\times m^d},$$

$$\left\{F^d_m\right\}_{m^d\times 1}=\left[T^d\right]^T_{m^d\times 4n}\left\{F\right\}_{4n\times 1}$$

and

$$\left\{\eta^d_m\right\}_{m^d\times 1}=\left\{x^b_1, y^b_1, x^d_1, y^d_1,\cdots, x^d_m, y^d_m, x^b_{q-1}, y^b_{q-1}, x^c_q, y^c_q, \varphi^c_{y_q}, \varphi^c_{x_q}, x^c_{q+1}, y^c_{q+1}, \varphi^c_{y_{q+1}}, \varphi^c_{x_{q+1}},\cdots, x^b_n, y^b_n\right\}^T \quad (4.53)$$

where (x, y) and (φ_y, φ_x) are the linear and angular displacements in two orthogonal planes at different nodes (refer Figure 4.2, the subscript represents node numbers and the superscript represents respective bearing, disc and coupling locations). From Eqn. (4.53), it is clear that some immeasurable DOFs at coupling and disc locations appear in master DOFs. However, the conventional dynamic condensation scheme could not be performed to eliminate these DOFs since these DOFs contains the unknown coupling dynamic and residual unbalance parameters as coefficients that needs to be estimated. While applying the conventional dynamic condensation scheme these unknown parameters are also getting eliminated. These aspects are covered in (Tiwari and Dharmaraju, 2006) in detail. A brief explanation is provided here for the completeness. In the inverse problem (parameter estimation), condensation schemes are used in practice to reduce the analytical model DOFs to the same as the number of measured responses corresponding to master DOFs. In fact in condensation schemes the eliminated DOFs (i.e., the slave DOFs) are estimated from the analytical model. In condensation schemes the transformation matrix parameters must be known (they consists of mass and stiffness parameters corresponding to slave DOFs), and that is why slave DOFs are chosen such that these are not critical locations (e.g., bearings, disc, coupling, crack, etc.). If we choose coupling DOFs as slave DOFs their parameters will appear in transformation matrix and since these are unknown the transformation could not be performed. On the other hand if we retain them as master DOF then we require measurement of corresponding DOFs

(i.e., transverse translational and rotational DOFs at coupling). However, since these are difficult to measure in practice (especially the rotational DOFs), and hence these DOFs are to be eliminated by some condensation scheme. While applying conventional condensation scheme (static or dynamic condensation schemes) since these DOFs at coupling are multiplied by its stiffness and damping terms so along with the DOFs these parameters will also be eliminated from transformed equations. In fact as stated above such transformation with conventional condensation schemes would not be possible since these parameters are in fact unknown. However, with the high–frequency condensation scheme this problem can be eliminated since its transformation matrix wholly depends upon the mass matrix, which is usually known in practice. So in the subsequent section a novel condensation approach has been presented to tackle this problem and to eliminate rotational DOFs at discs and coupling locations without eliminating unknown parameters at these locations.

4.4 Development of Identification Algorithm with the High–frequency Condensation

In order to apply the high frequency condensation (Dharmaraju *et al.*, 2005), while developing the identification algorithm, Eqn. (4.52), needs to be subdivided into the masters and slaves DOFs as

$$\left(-\omega^2\begin{bmatrix}[M^h_{mm}] & [M^h_{ms}]\\ [M^h_{sm}] & [M^h_{ss}]\end{bmatrix}+\mathrm{j}\omega\left(\begin{bmatrix}[C^h_{mm}] & [C^h_{ms}]\\ [C^h_{sm}] & [C^h_{ss}]\end{bmatrix}-\omega\begin{bmatrix}[G^h_{mm}] & [G^h_{ms}]\\ [G^h_{sm}] & [G^h_{ss}]\end{bmatrix}\right)+\begin{bmatrix}[K^h_{mm}] & [K^h_{ms}]\\ [K^h_{sm}] & [K^h_{ss}]\end{bmatrix}\right)\begin{Bmatrix}\{\eta^h_m\}_{m^h\times 1}\\ \{\eta^h_s\}_{s^h\times 1}\end{Bmatrix} = \begin{Bmatrix}\{F^h_m\}_{m^h\times 1}\\ \{F^h_s\}_{s^h\times 1}\end{Bmatrix} \tag{4.54}$$

where subscripts (i.e. m^h and s^h) attached with vectors represent the size of masters and slave DOFs respectively, and superscript h represents the high frequency condensation. In the proposed reduction scheme stiffness terms (including damping and gyroscopic couple matrices in line with dynamic condensation) are assumed to be negligible as compared to the

inertia terms since at high frequencies the inertia term dominates especially in heavy rotors. Now by following the procedure, from Eqn. (4.45)–(4.51), Eqn. (4.54) can be written as

$$\left(-\omega^2\left[M^h\right]+\mathrm{j}\omega\left(\left[C^h\right]-\omega\left[G^h\right]\right)+\left[K^h\right]\right)\left\{\eta_m^h\right\}=\left\{F_m^h\right\} \tag{4.55}$$

where

$$\left[M^h\right]_{m^h\times m^h}=\left[T^h\right]^T_{m^h\times m^d}\left[M^d\right]_{m^d\times m^d}\left[T^h\right]_{m^d\times m^h},\qquad \left[K^h\right]_{m^h\times m^h}=\left[T^h\right]^T_{m^h\times m^d}\left[K^d\right]_{m^d\times m^d}\left[T^h\right]_{m^d\times m^h},$$

$$\left[C^h\right]_{m^h\times m^h}=\left[T^h\right]^T_{m^h\times m^d}\left[C^d\right]_{m^d\times m^d}\left[T^h\right]_{m^d\times m^h},\qquad \left[G^h\right]_{m^h\times m^h}=\left[T^h\right]^T_{m^h\times m^d}\left[G^d\right]_{m^d\times m^d}\left[T^h\right]_{m^d\times m^h},$$

$$\left\{F_m^h\right\}_{m^h\times 1}=\left[T^h\right]^T_{m^h\times m^d}\left\{F^d\right\}_{m^d\times 1}\qquad \text{and}$$

$$\left\{\eta_m^h\right\}_{m^h\times 1}=\left\{x_1^b,\ y_1^b,\ x_2^b,\ y_2^b,\ \cdots,\ x_{2p-1}^b,\ y_{2p-1}^b,\ x_{2p}^b,\ y_{2p}^b\right\}^T \tag{4.56}$$

with

$$\left[T^h\right]_{m^d\times m^h}=\begin{bmatrix}[I]_{m^h\times m^h}\\ \cdots\cdots\cdots\cdots\\ -\left[M_{ss}^h\right]^{-1}\left[M_{sm}^h\right]\end{bmatrix} \tag{4.57}$$

where $[T^h]$ is the transformation matrix for the high frequency condensation. From Eqn. (4.56), it is clear that masters DOFs having only bearing linear displacements which are practically measurable quantity. It could also be observed that the limitation of conventional dynamic reduction scheme has now been overcome by the high frequency reduction scheme. Eqn. (4.55) could be rearranged so that all the unknown terms (i.e., the bearing and coupling dynamic parameters; and residual unbalances) are on the left–hand side, and all known terms are on the right–hand side of the expression, so that it can be written as

$$\left(\mathrm{j}\omega\left(\left[C^h\right]_{m^h\times m^h}\right)+\left[K^h\right]_{m^h\times m^h}\right)\left\{\eta_m^h\right\}_{m^h\times 1}-\left\{F^h\right\}_{m^h\times 1}=\omega^2\left(\left[M^h\right]_{m^h\times m^h}+\mathrm{j}\left[G^h\right]_{m^h\times m^h}\right)\left\{\eta_m^h\right\}_{m^h\times 1} \quad (4.58)$$

with

$$\left\{F_m^h\right\}_{m^h\times 1}=\omega^2\left[T\right]_{m^h\times 2m}\left\{U\right\}_{2m\times 1} \quad (4.59)$$

and

$$T_{i,i}=1,\quad T_{i,i+1}=\mathrm{j},\quad T_{i+1,i}=-\mathrm{j},\quad T_{i+1,i+1}=1 \qquad \text{(for subscript } i\text{= 1, 3, 5, …, } (m^h-1)\text{)}$$

The rest of elements of matrix [T] are zero

$$\left\{U\right\}_{2m\times 1}=\left\{U_{x_1}^r \quad U_{x_1}^i \quad U_{x_2}^r \quad U_{x_2}^i \quad \cdots \quad U_{x_m}^r \quad U_{x_m}^i\right\}^T \quad (4.60)$$

where the subscript m is the total number of discs considered in the complete rotor–bearing–coupling system with $m = m_1 + m_2 + ... + m_p$, for p number of shafts. In Eqn. (4.58), the first term is regrouped into a vector $\{\beta\}_{(p_b n_b+p_c n_c)\times 1}$, containing all the unknown bearing and coupling dynamic parameters and a corresponding matrix $[W_n]_{m^h\times(p_b n_b+p_c n_c)}$, containing the related response terms at a single spin speed, ω. Therein n_b and n_c are number of bearings and couplings, respectively; and p_b and p_c are number of parameters considered for each bearing and coupling. Eqn. (4.58)–(4.60) take the following form

$$\left[W_n\right]_{m^h\times(p_b n_b+p_c n_c)}\left\{\beta\right\}_{(p_b n_b+p_c n_c)\times 1}+\left[R_n\right]_{m^h\times 2m}\left\{U\right\}_{2m\times 1}=\left\{P_n\right\}_{m^h\times 1} \quad (4.61)$$

with

$$\left\{P_n\right\}_{m^h\times 1}=\omega^2\left(\left[M^h\right]_{m^h\times m^h}+\mathrm{j}\left[G^h\right]_{m^h\times m^h}\right)\left\{\eta_m^h\right\}_{m^h\times 1} \quad (4.62)$$

In Eqn.(4.61), $[W_n]$, $[R_n]$ and $\{P_n\}$ are in the complex form, now after separating out the real and imaginary parts, Eqn. (4.61) becomes

$$\begin{bmatrix}[W_n^r]\\ [W_n^i]\end{bmatrix}_{2m^h\times(p_bn_b+p_cn_c)}\{\beta\}_{(p_bn_b+p_cn_c)\times1}+\begin{bmatrix}[R_n^r]\\ [R_n^i]\end{bmatrix}_{2m^h\times2m}\{U\}_{2m\times1}=\begin{Bmatrix}\{P_n^r\}\\ \{P_n^i\}\end{Bmatrix}_{2m^h\times1} \tag{4.63}$$

The above equation could be written as

$$[W]_{2m^h\times(p_bn_b+p_cn_c)}\{\beta\}_{(p_bn_b+p_cn_c)\times1}+[R]_{2m^h\times2m}\{U\}_{2m^h\times1}=\{P\}_{2m^h\times1} \tag{4.64}$$

On rearranging the above equation leads to

$$\left[[W]\ [R]\right]\begin{Bmatrix}\{\beta\}\\ \{U\}\end{Bmatrix}=\{P\} \tag{4.65}$$

The above equation can be generalised for different spin speed ω_k where k =1, 2, … s. All such equations for the speed–dependent bearing and coupling dynamic parameters could be grouped and written as

$$\left[[W(\omega_k)]\ [R(\omega_k)]\right]\begin{Bmatrix}\{\beta(\omega_k)\}\\ \{U\}\end{Bmatrix}=\{P(\omega_k)\} \tag{4.66}$$

The above equation can be written as

$$[A(\omega_k)]^h_{(2m^h)s\times(p_bn_b+p_cn_c+2m)}\{X(\omega_k)\}^h_{(p_bn_b+p_cn_c+2m)s\times1}=\{B(\omega_k)\}^h_{(2m^h)s\times1} \tag{4.67}$$

with

$$[A(\omega)_k]^h_{(2m^h)s\times(p_bn_b+p_cn_c+2m)} = \begin{bmatrix} W(\omega_1) & 0 & \dots & 0 & R(\omega_1) \\ 0 & W(\omega_2) & \dots & 0 & R(\omega_2) \\ 0 & 0 & \ddots & \vdots & \vdots \\ 0 & 0 & \dots & W(\omega_s) & R(\omega_m) \end{bmatrix} \tag{4.68}$$

$$\{X(\omega_k)\}^h_{(p_bn_b+p_cn_c+2m)s\times 1} = \{\{\beta(\omega_1)\}\ \{\beta(\omega_2)\}\ \cdots\ \{\beta(\omega_s)\}\ \{U\}\}^T \tag{4.69}$$

$$\{B(\omega)_k\}^h_{(2mh)s\times 1} = \{\{P(\omega_1)\}\ \{P(\omega_2)\}\ \cdots\ \cdots\ \{P(\omega_s)\}\}^T \tag{4.70}$$

Eqn. (4.67), is the required form of estimation equation in which all the unknown parameters (i.e. the speed dependent bearing and coupling dynamic parameters, and residual unbalances) are stacked in a column vector, $\{X(\omega_k)\}^h$. The final regression matrix $[A(\omega_k)]^h$ has the contribution from the stiffness and damping coefficients of bearings and couplings in $[W(\omega_k)]$, whereas in $[R(\omega_k)]$ the contribution from residual unbalances for different spin speeds.

4.5 Numerical Experiments

A simplified FE model of a rotor system, as shown in Figure 4.4, is considered for the numerical illustration of the present identification algorithm. Parameters used for the present numerical simulation are: Number of shafts considered p = 2, number of discs per shaft m_1 = m_2= 2, number of bearings n_b= 4, number of masters DOFs for high frequency condensation m^h= $2n_b$ = 8, number of couplings n_c= 1, number of parameters in each bearing p_b= 8, number of parameters in each coupling p_c = 10 and number of spin speeds s = 1. That means in the present case numerical illustration deals with only the speed–independent bearing and coupling dynamic parameters for brevity.

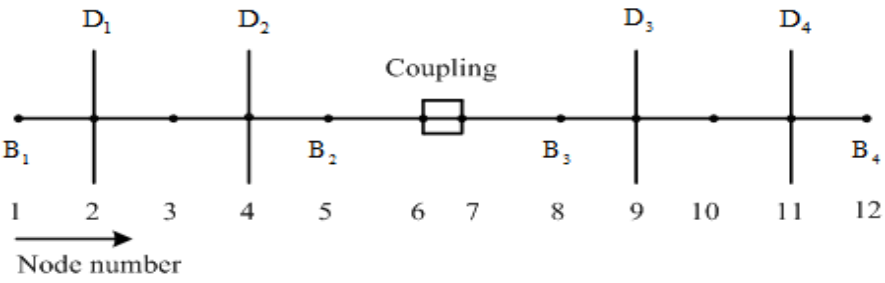

Figure 4.4 A finite element model of the rotor–bearing–coupling system

Putting these parameters in Eqn. (4.67), gives the size of individual regression matrix for the present case as

$$\left[A(\omega)\right]^{h}_{16\times 50}\left\{X\right\}^{h}_{50\times 1}=\left\{B(\omega)\right\}^{h}_{16\times 1} \tag{4.71}$$

with

$$\left\{X\right\}^{h}_{50\times 1}=\{k^{B_1}_{xx},k^{B_1}_{xy},k^{B_1}_{yx},k^{B_1}_{yy},k^{B_2}_{xx},k^{B_2}_{xy},k^{B_2}_{yx},k^{B_2}_{yy},k^{B_3}_{xx},k^{B_3}_{xy},k^{B_3}_{yx},k^{B_3}_{yy},k^{B_4}_{xx},k^{B_4}_{xy},k^{B_4}_{yx},k^{B_4}_{yy},k^{C}_{xx},k^{C}_{xy},k^{C}_{yx},k^{C}_{yy},k^{C}_{\varphi_x},k^{C}_{\varphi_y},c^{B_1}_{xx},c^{B_1}_{xy},$$
$$c^{B_1}_{yx},c^{B_1}_{yy},c^{B_2}_{xx},c^{B_2}_{xy},c^{B_2}_{yx},c^{B_2}_{yy},c^{B_3}_{xx},c^{B_3}_{xy},c^{B_3}_{yx},c^{B_3}_{yy},c^{B_4}_{xx},c^{B_4}_{xy},c^{B_4}_{yx},c^{B_4}_{yy},c^{C}_{xx},c^{C}_{xy},c^{C}_{yx},c^{C}_{yy},U^{r}_{x_1},U^{i}_{x_1},U^{r}_{x_2},U^{i}_{x_2},U^{r}_{x_3},U^{i}_{x_3},U^{r}_{x_4},U^{i}_{x_4}\}^{T}$$

From above equation, it could be seen that this is the case of underdetermined system of linear simultaneous equations in which number of unknowns (i.e., $(p_b n_b + p_c n_c + 2m)s = 50$) are more than the number of equations (i.e. $(2m^h)s = 16$). To obtain entire unknown, sets of independent force–response measurements are required such that the number of equations increased at least equal to or more than the unknowns. Whereas for speed–dependent bearing and coupling dynamic parameters more number of independent measurements could be obtained by (i) taking different trial unbalance mass combinations (both magnitude and phase) and (ii) by using independent unbalance excitation unit (e.g. a free–wheel mounted on the shaft and rotate it independently by a separate drive) could be used (Tiwari, 2005). These would make the system of estimation equation over–determined. For the present case, the minimum

number of independent measurements required is four. However, the condition of the regression matrix to be inverted has an important role in obtaining the better estimate of parameters. The advantage of the above regression equation is that it contains all the practically measurable linear DOFs at bearing locations. The present algorithm requires forced vibration responses for the estimation of the bearing and coupling dynamic parameters and residual unbalances; which have been generated through a numerical simulation using Eqn.(4.42). The bearing and coupling dynamic parameters and residual unbalances are assumed for obtaining simulated responses. Both shafts are of the same diameter, length, density and modulus of elasticity as 0.02 m, 1.25 m, 7800 kg/m^3 and 2.1×10^9 N/m^2, respectively. Disc and RU properties are given in Table 4.1. A typical variation of the forced response with the spin speed is shown in Figure 4.5. The forward critical speed of the system are ω_{cr1}= 105.2 rad/s, ω_{cr2}= 114.4 rad/s, ω_{cr3}=126.4 rad/s, ω_{cr4}= 130.5 rad/s, ω_{cr5}=193.4 rad/s, ω_{cr6} = 212.8 rad/s, ω_{cr7}=256.1 rad/s, and ω_{cr8}= 263.5 rad/s. It could be seen that at all above critical speeds the resonance condition prevails both in the amplitude and the phase.

Table 4.1 The disc and Residual unbalance properties

S.N.	Location	Diameter (m)	Mass (kg)	Diametral mass moment of inertia (kg–m^2)	Residual unbalances	
					Magnitude (kg)	Angular position (deg.)
1	Disc 1	0.15	2	5.63×10^{-3}	9.5×10^{-3}	36
2	Disc 2	0.13	1.5	3.16×10^{-3}	6.0×10^{-3}	108
3	Disc 3	0.12	2.5	4.50×10^{-3}	7.9×10^{-3}	240
4	Disc 4	0.14	1.6	3.92×10^{-3}	11.2×10^{-3}	300

Now various possibilities of getting independent sets of measurements of the force–response data have been discussed to make the present system as the over–determined system of linear

simultaneous equations. Hence, for solving the above problem and to have an idea of effects of the modal information on estimates of parameters, different frequency ranges have been considered. Measurements are analysed under three different cases, i.e.

Case A: By rotating the rotor near critical speeds (i.e., near half−power points)

Case B: By rotating the rotor away from critical speeds

Case C: It comprises of three sub−cases (i) *Case* C_{fb1}: frequency band of 150−175 rad/s, (ii) *Case* C_{fb2}: frequency band of 275−300 rad/s, and (iii) *Case* C_{fb3}: combination of frequency bands 150−175 rad/s, and 275−300 rad/s, with a step size of 0.5 rad/s for all three sub categories.

Different frequency bands considered here has been decided based on the possibility of obtaining information of different modes in responses.

Furthermore, following two measurement methods are adopted for the present case

(*I*) Rotate the rotor in the same direction only at different sets of speeds.

(*II*) Rotate the rotor in the CW and then CCW directions, alternatively, at same or different sets of speeds. This could also be done by an independent unbalance excitation unit.

Figure 4.6 shows the effect of different frequency bands (discussed under *Case C*, *Method I*) on estimated parameters and it could be concluded that ***Case*** $\boldsymbol{C_{fb3}}$, is the most effective case to identify the parameters. So ***Case*** $\boldsymbol{C_{fb3}}$ has been used for the analysis and comparison in the subsequent subsection. The column scaling of the regression matrix [*A*] corresponding to the damping and residual unbalance parameters has been done to improve the accuracy of estimates.

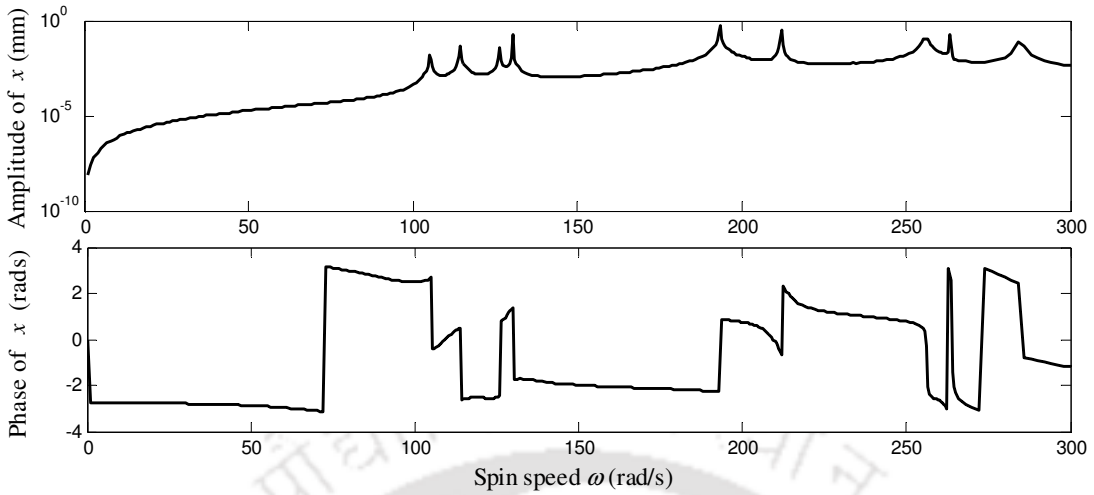

Figure 4.5 Variation of the horizontal response at the left of coupling location (i.e. node 6) with the spin speed

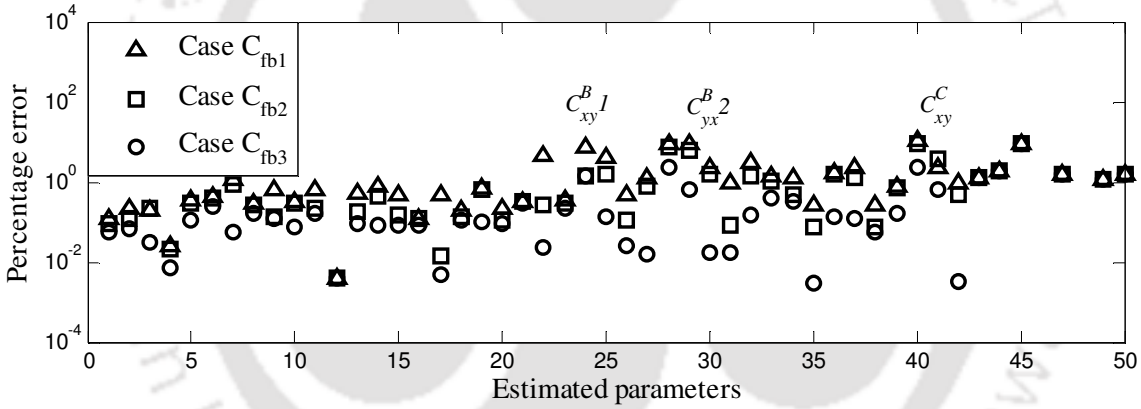

Figure 4.6 Comparison of errors of estimated parameters for different frequency bands under *Method I*, for 5% measurement noise

The scaling factor used is $(1/\omega_a)$, where ω_a is average of spin speeds. The effect of column scaling could be seen from Figure 4.7–Figure 4.12, which shows the comparison of error (ratio of the difference between estimated and assumed values to the assumed value of parameters) in the estimation of parameters before and after column scaling for 1 percent measurement noise for all the three cases (i.e. *Case A*, *B* and C_{fb3}) under both methods (i.e. *Method I* & *II*), respectively. The number in the abscissa represents the estimated parameter corresponding to the row number in the vector $\{X\}$ of Eqn. (4.71) and these parameters are

summarised with corresponding row locations in Table 2.1. The important effect of the column scaling is the improvement in the condition number of the regression matrix and are summarised in Table 4.2. The comparison of errors in the estimation of these parameters for different level of measurement noise and for different cases as discussed previously has been provided in Table 4.3 and discussed in the following sub−section.

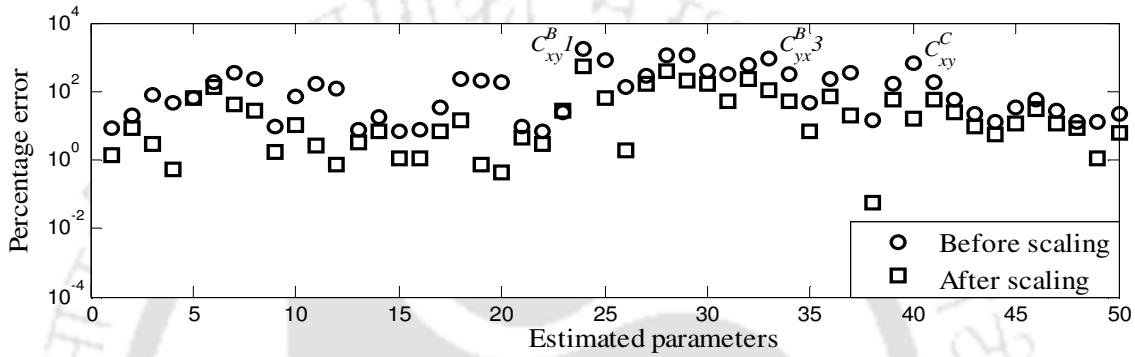

Figure 4.7 Comparison of errors of estimated parameters before and after column scaling for 1% measurement noise (for *Case A* under *Method I*)

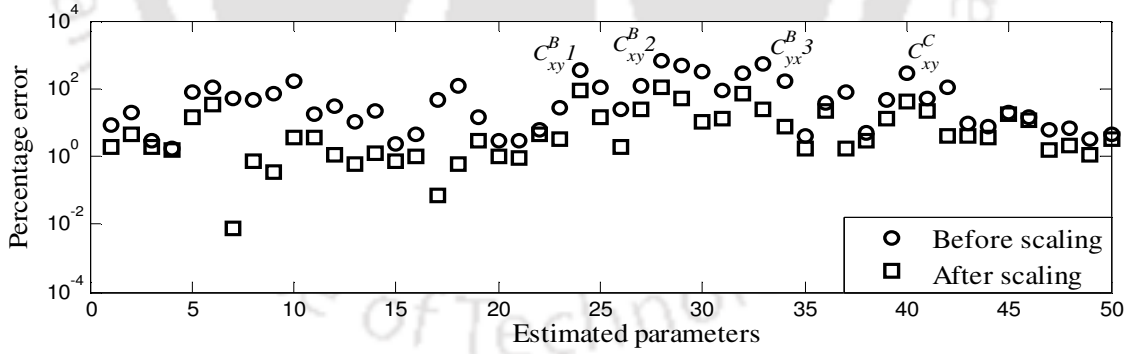

Figure 4.8 Comparison of errors of estimated parameters before and after column scaling for 1% measurement noise (for *Case B* under *Method I*)

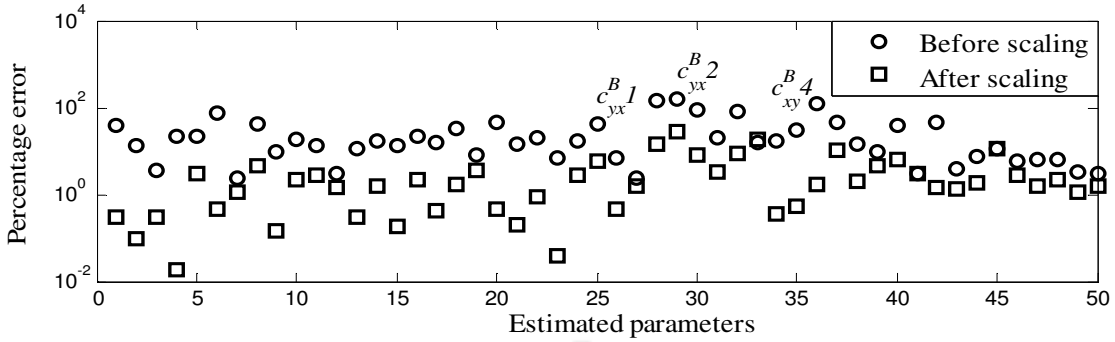

Figure 4.9 Comparison of errors of estimated parameters before and after column scaling for 1% measurement noise (for *Case* C_{fb3} under *Method I*)

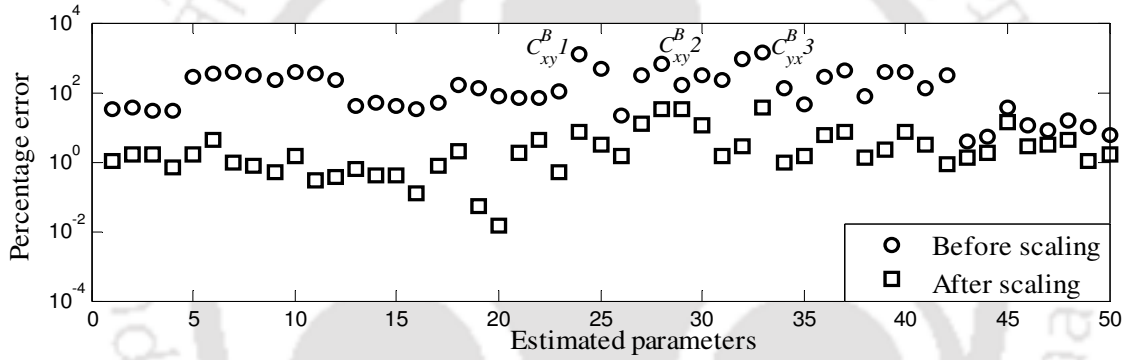

Figure 4.10 Comparison of errors of estimated parameters before and after column scaling for 1% measurement noise (for *Case A* under *Method II*)

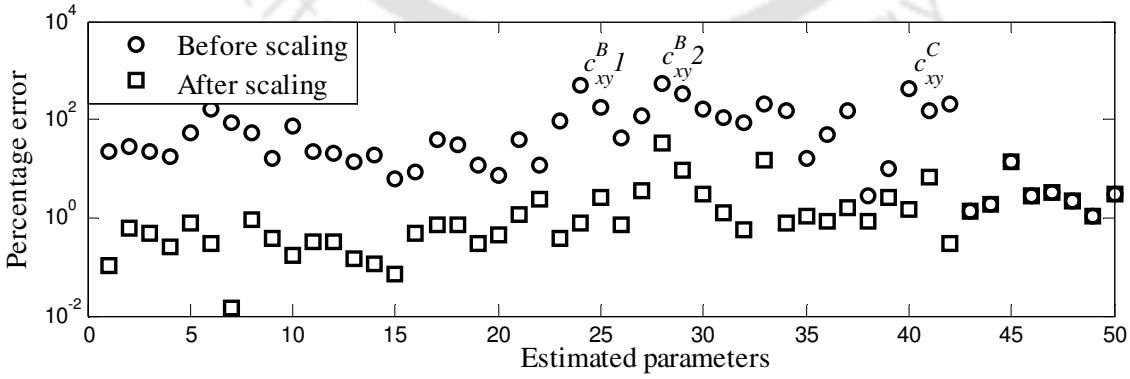

Figure 4.11 Comparison of errors of estimated parameters before and after column scaling for 1% measurement noise (for *Case B* under *Method II*)

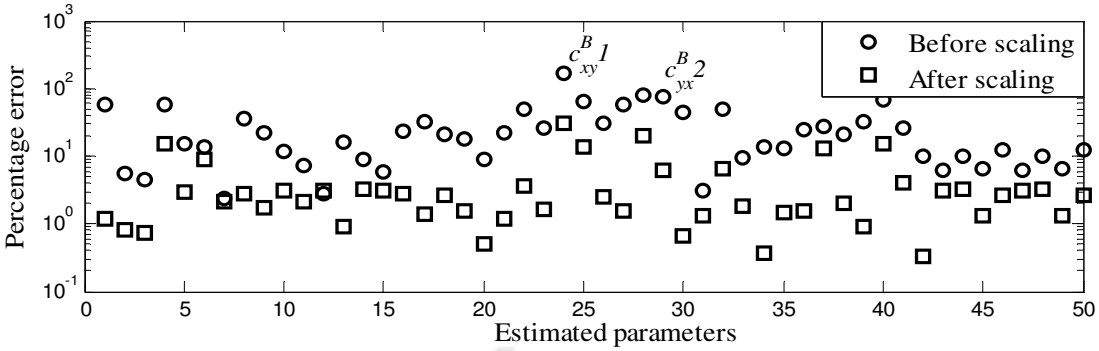

Figure 4.12 Comparison of errors of estimated parameters before and after column scaling for 1% measurement noise (for *Case* C_{fb3} under *Method II*)

4.5.1 Method I: Rotating the Rotor in the Same Direction at Different Speeds

***Case A*:** Parameters are estimated from responses at selected set of spin speeds near, however, outside the half−power points, i.e. at ω_1= 99 rad/s, ω_2= 109 rad/s, ω_3= 121 rad/s and ω_4= 136 rad/s. From Figure 4.13, it could be analysed that most of the parameters show variation with assumed values for 1% measurement noise and it increases as the noise percentage increases. It could be seen from Table 4.2 that the improvement in condition number is of the order 10^{18}. From Table 4.3, it is comprehensible that after the column scaling 67% and 47% improvement in estimates of parameters takes place for the 1% and 5% noise cases, respectively. From this analysis one can conclude that this is the case in which deviation starts even at 1% noise condition and increases drastically as measurement noise increases.

***Case B*:** Parameters are identified from responses at selected set of spin speeds away from half−power points, i.e. ω_1= 54 rad/s, ω_2= 79 rad/s, ω_3= 159 rad/s and ω_4= 171 rad/s. From Figure 4.14, it could be analysed that most of the stiffness and unbalance parameters represent well agreement with assumed values at 1% measurement noise case, whereas some of the damping (mostly bearing damping) parameters show considerable variation even at 1% noise case and increases as noise percentage increases (i.e. up to 5%). From Table 4.2, it could be seen that after column scaling improvement in condition number is of the order 10^{18}. Another

important effect of column scaling could be seen From Table 4.3, that the percent increase in accuracy of estimated parameters is 83% and 78% for 1% and 5% noise cases, respectively. From this analysis it can be concluded that the aforementioned case is the better case of estimation as compared to *Case A* under *Method I* up to 5% noise case.

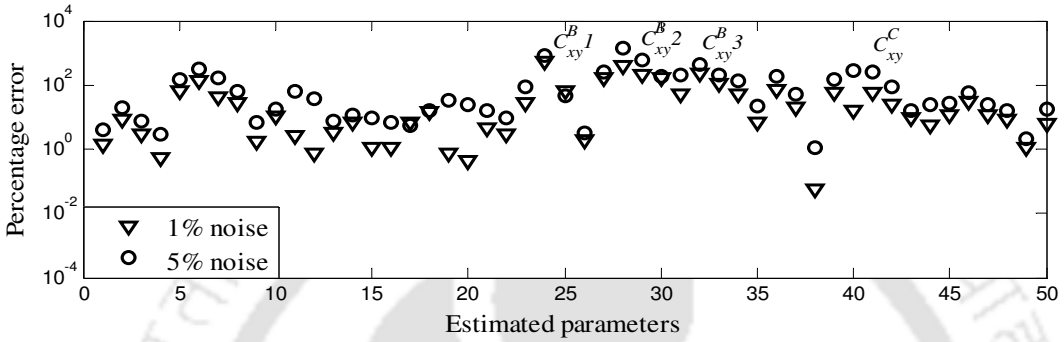

Figure 4.13 Comparison of errors of estimated parameters for different level of measurement noise (for *Case A* under *Method I*)

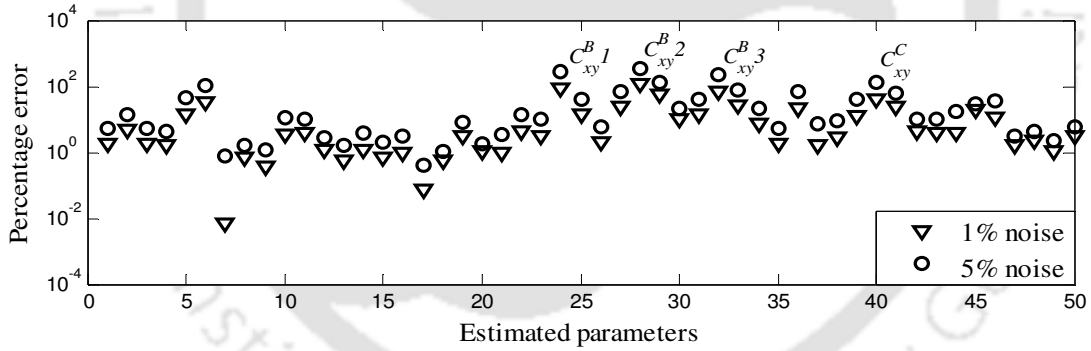

Figure 4.14 Comparison of errors of estimated parameters for different level of measurement noise (for *Case B* under *Method I*)

***Case C_{fb3}*:** Parameters are identified by increasing the number of measurement speeds up to 100. Vibration responses are calculated at different frequency bands i.e., ω = 150−175 rad/s and 275−300 rad/s, with a step size of 0.5 rad/s. From Figure 4.15, it could be examined that the most of parameters show well agreement with assumed values for 1% measurement noise and increases slightly (mostly bearing damping parameters) as the noise percentage increases.

It is evident from Figure 4.15 that the maximum error in the estimation of cross–coupled damping parameters is around 28% and 38% for 1% and 5% measurement noise, respectively. From Table 4.2, it can be seen that the improvement in the condition number is maximum for this case under *Method I* and of the order of 10^{21}. From Table 4.3, it is apprehensible that after column scaling estimation of the parameters are improved by 86% and 84% for 1% and 5% measurement noise, respectively. From Table 4.2 and Table 4.3, it can also be analysed that under *Method I*, *Case* C_{fb3} is the best case of estimation.

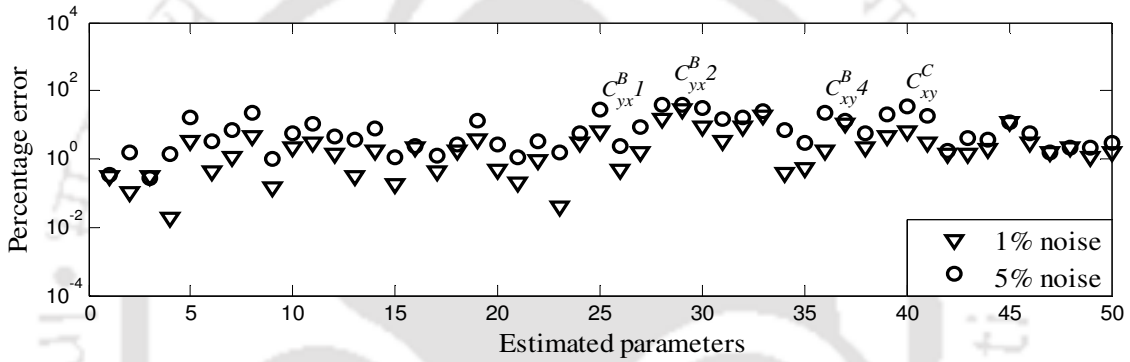

Figure 4.15 Comparison of errors of estimated parameters for different level of measurement noise (for *Case* C_{fb3} under *Method I*)

4.5.2 Method II: Rotating the Rotor Alternately in the CW or CCW Direction

From the previous section, it is evident that the estimation *Method I*, is effective to estimate the bearing and coupling dynamic parameters along with residual unbalances only up to 1% noise condition for different cases discussed. However, the estimation is poor as we increase the noise percentage level. So *Method II* is proposed to take measurements by rotating the rotor alternately in the CW and CWW directions, to improve the effectiveness of the estimation and to sort out the problem arises in *Method I*. By doing this effectively the measurement has both forward and backward whirl information (in fact now–a–days the trend is to use full–spectrum (Shravankumar and Tiwari, 2012) to get information of the rotor

forward and backward whirl amplitudes simultaneously). It should be noted that such excitation can also be generated by an independent excitation unit without rotating rotor in the CW and CCW, alternately (Tiwari, 2005) or auxiliary active devices could be used such as active magnetic bearings (Sawicki *et al*, 2011).

***Case A*:** Parameters are identified by operating the rotor system at selected set of speeds near, however, outside half–power points. Vibration responses are calculated at four speeds, i.e. for the CW and CCW directions: ω_1= 121 rad/s and ω_2= 136 rad/s. From Figure 4.16, it is evident that most of parameters show well agreement with assumed values for 1% measurement noise but some of the parameters (mostly bearing damping parameters) increases as the noise percentage increases; however most of the unbalance parameters show good agreement with the assumed values. From Table 4.2, it could be seen that the improvement in the condition number is of the order of 10^{18}. It could also be seen from Table 4.3, that the percentage improvement in the estimation is 97% and 94% for 1% and 5% noise, respectively after column scaling. From this analysis and discussion on Section 4.5.1, it can be concluded that although, in this case deviation of estimated parameters start even at 1% noise case but the estimation is better as compared to *Case A* under *Method I* up to 5% noise case (refer Table 4.3).

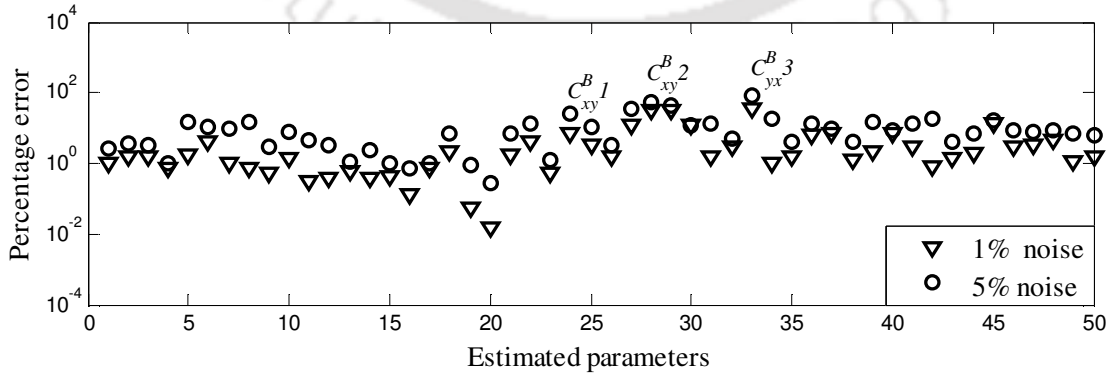

Figure 4.16 Comparison of errors of estimated parameters for different level of measurement noise (for *Case A* under *Method II*)

Case B: Parameters are identified at selected set of spin speeds away from half−power points. Vibration responses are calculated at four speeds i.e. for the CW and CCW directions: ω_1= 159 rad/s and ω_2= 171 rad/s. From Figure 4.17, it could be analysed that most of the stiffness, damping and unbalance parameters have well agreement with assumed values at 1% measurement noise case, whereas, some of the damping (mostly bearing damping) parameters represent considerable variation at 5% noise case. From Table 4.2 and Table 4.3, it could be analysed that after column scaling the condition number is improved by the order 10^{18} and percentage improvement in accuracy on estimates are around 93% and 92% for 1% and 5% noise cases, respectively, for the aforementioned case. It could also be concluded that the aforementioned case is better case of estimation as compared to *Case A* & *B*, under *Method I* and *Case A* under *Method II*.

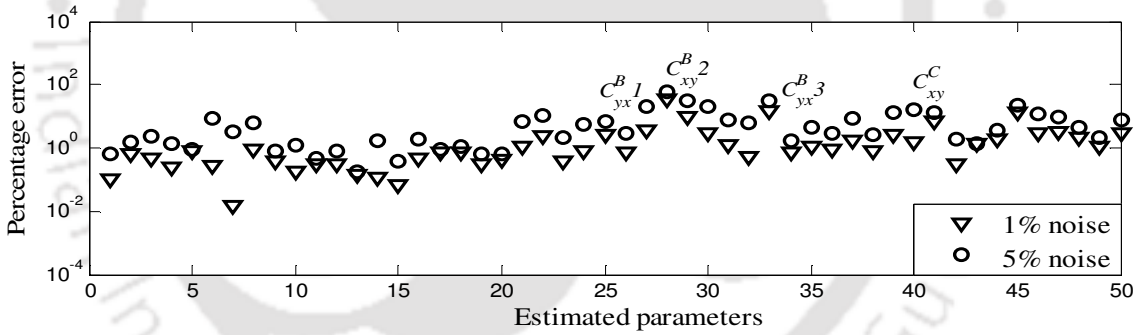

Figure 4.17 Comparison of errors of estimated parameters for different level of measurement noise (for *Case B* under *Method II*)

***Case C_{fb3}*:** Parameters are identified by increasing the number of measurement speeds up to 100. Vibration responses are calculated at different frequency bands, i.e. for the CW and CCW directions: ω = 150−175 rad/s and 275−300 rad/s, with a step size of 1 rad/s, (i.e. 50 numbers of different speeds for each frequency band). From Figure 4.18 and Figure 4.19, it could be analysed that most of the stiffness, damping and unbalance parameters represent well agreement with assumed ones at 1% noise case, and deviates negligibly at 5% noise case

except few cross–coupled damping parameters. After column scaling, the condition number is improved by the order 10^{23} and percentage improvement in accuracy on estimates of parameters are 97% and 95% for 1% and 5% noise cases, respectively, for the aforementioned case (refer Table 4.2 and Table 4.3). It could also be concluded that the aforementioned case is best case of estimation among all the *Cases* under *Method I* & *II*.

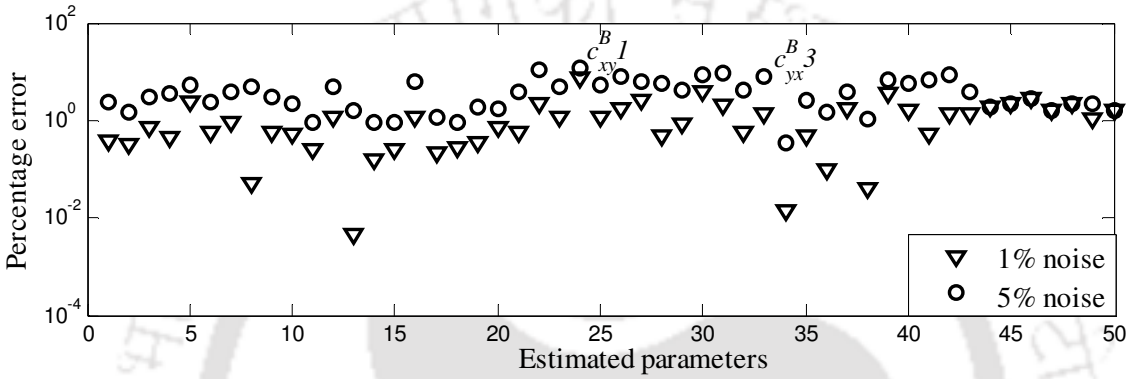

Figure 4.18 Comparison of errors of estimated parameters for different level of measurement noise (for *Case* C_{fb3} under *Method II*)

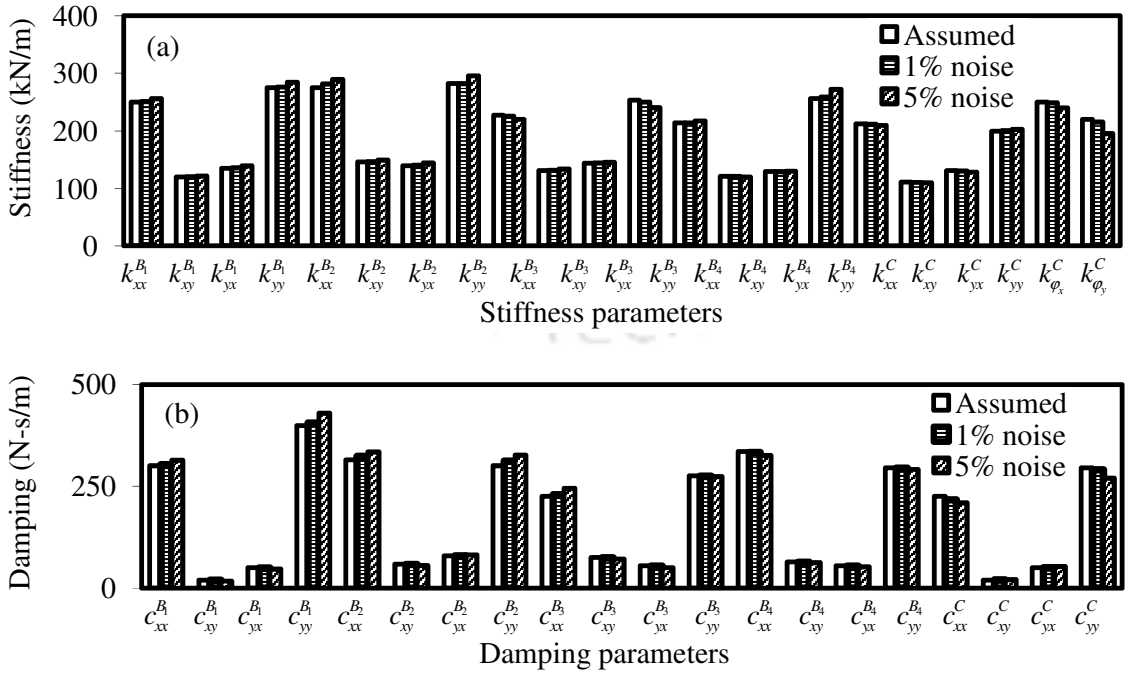

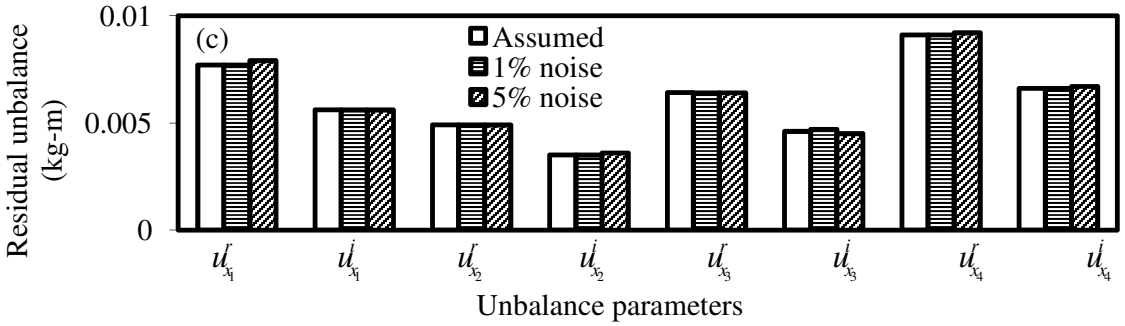

Figure 4.19 Comparison of estimated ((a) stiffness (b) damping (c) unbalance) parameters for different levels of measurement noise (*Case* C_{fb3} under *Method II*)

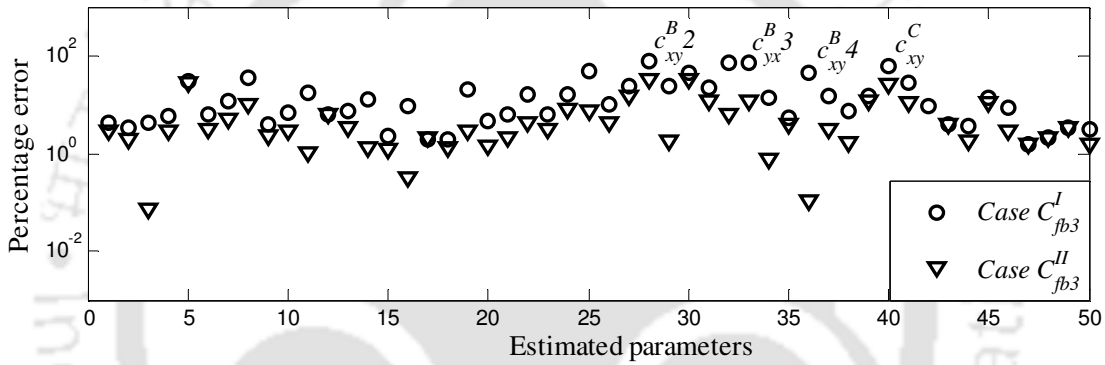

Figure 4.20 Comparison of errors of estimated parameters for *Case* C_{fb3}, under *Method I* and *Method II*, for 5% variation in E and ρ)

The effect of bias error in the model on estimated parameters has also been considered and shown in Figure 4.20, for *Case* C_{fb3} under *Method I* and *II* for 5% measurement noise. Here 5% variation in the modulus of elasticity (E) and the density (ρ) is considered and from Figure 4.20, it can be seen that the maximum error on estimates with bias error in error in the model are ($c^{B_2}_{xy}$, 78%) and ($c^{B_2}_{xy}$, 33%) for ***Case*** $\boldsymbol{C_{fb3}}$ under ***Method I & II***, respectively. It could also be analysed that the improvement in the estimation is around $(45\%, c^{B_2}_{xy})$ for ***Case*** $\boldsymbol{C_{fb3}}$ under ***Method II*** as compared to ***Case*** $\boldsymbol{C_{fb3}}$ under ***Method I***. Although the percentage error in estimation of some of the cross–coupled (mostly bearing damping) parameters is more but the

absolute deviation of these parameters as compared to direct parameters are less or comparable. It should also be noted that the absolute magnitude (assumed values) of the direct bearing damping parameters are (5 to 10) times more than these cross–coupled bearing damping parameters.

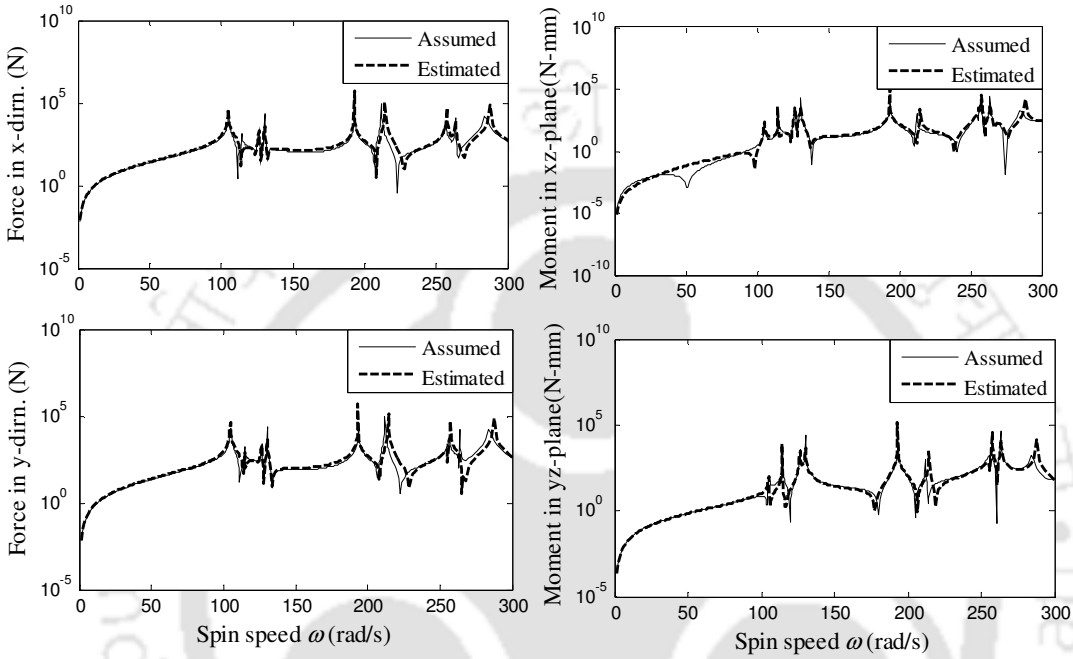

Figure 4.21 Misalignment forces and moments with spin speed for 5 % noise case (*Case* C_{fb3} under *Method II*)

After estimating coupling dynamic parameters and responses at coupling location these could be used to estimate the misalignment forces and moments (refer Eqn. (2.12), Chapter 2). The angular DOFs required for estimating the misalignment moments could be obtain through numerical simulation from updated numerical model of the system. For the best estimated case to estimate the bearing and coupling dynamic parameters (i.e., *Case* C_{fb3} under *Method II*) the variation of misalignment forces and moments are plotted with respect to the spin speed. From Figure 4.21, it is apprehensible that the misalignment forces and moments are very high at or near critical speeds of the system which reveals the misalignment forces and moments are dependent on the spin speed.

Table 4.2 Summary of the condition number for different cases

Methods	Cases	Condition number before column scaling		Condition number after column scaling		Order of improvement in condition number	
		For 1% noise	For 5% noise	For 1% noise	For 5% noise	For 1% noise	For 5% noise
Method *I*	Case A	6.64×10^{26}	7.46×10^{26}	3.27×10^{8}	4.84×10^{8}	2.03×10^{18}	1.66×10^{18}
	Case B	5.94×10^{26}	6.83×10^{26}	2.81×10^{8}	4.03×10^{8}	2.11×10^{18}	1.69×10^{18}
	Case C_{fb3}	3.72×10^{26}	5.01×10^{26}	1.40×10^{5}	3.03×10^{5}	2.65×10^{21}	1.89×10^{21}
Method *II*	Case A	4.79×10^{26}	5.07×10^{26}	2.07×10^{8}	3.15×10^{8}	2.31×10^{18}	1.60×10^{18}
	Case B	3.75×10^{26}	4.03×10^{26}	1.31×10^{8}	2.18×10^{8}	2.86×10^{18}	1.84×10^{18}
	Case C_{fb3}	1.10×10^{26}	2.71×10^{26}	0.71×10^{5}	1.41×10^{5}	1.54×10^{21}	1.92×10^{21}

Table 4.3 Summary of estimated parameters having maximum percentage error for different cases

Methods	Cases	Estimated parameters having max. % error before column scaling		Estimated parameters having max. % error after column scaling		% improvement in accuracy or % reduction in error on estimates after column scaling		Estimated parameters having max. % error with 5% bias error	
		For 1% noise	For 5% noise	For 1% noise	For 5% noise	For 1% noise	For 5% noise	For 1% noise	For 5% noise
Method *I*	Case A	$c_{xy}^{B_1}$ (1683.00)	$c_{xy}^{B_1}$ (2530.50)	$c_{xy}^{B_1}$ (545.69)	$c_{xy}^{B_1}$ (1342.2)	67.57	46.95	$c_{xy}^{B_2}$ (215.18)	$c_{xy}^{B_2}$ (500.35)
	Case B	$c_{xy}^{B_2}$ (678.67)	$c_{xy}^{B_2}$ (1570.31)	$c_{xy}^{B_2}$ (113.25)	$c_{xy}^{B_2}$ (343.06)	83.31	78.15	$c_{xy}^{B_4}$ (98.58)	$c_{xy}^{B_4}$ (362.18)
	Case C_{fb3}	$c_{yx}^{B_2}$ (217.60)	$c_{yx}^{B_2}$ (257.63)	$c_{yx}^{B_2}$ (28.94)	$c_{yx}^{B_2}$ (38.74)	86.70	84.96	$c_{xy}^{B_2}$ (31.23)	$c_{xy}^{B_2}$ (78.76)
Method *II*	Case A	$c_{yx}^{B_3}$ (1318.20)	$c_{yx}^{B_3}$ (1570.63)	$c_{yx}^{B_3}$ (34.96)	$c_{yx}^{B_3}$ (83.50)	97.34	94.68	$c_{yx}^{B_3}$ (107.17)	$c_{yx}^{B_2}$ (306.00)
	Case B	$c_{xy}^{B_2}$ (550.84)	$c_{xy}^{B_2}$ (853.87)	$c_{xy}^{B_2}$ (34.15)	$c_{xy}^{B_2}$ (62.03)	93.80	92.73	$c_{xy}^{B_2}$ (46.87)	$c_{xy}^{B_2}$ (96.01)
	Case C_{fb3}	$c_{xy}^{B_1}$ (169.85)	$c_{xy}^{B_1}$ (231.63)	$c_{xy}^{B_1}$ (7.00)	$c_{xy}^{B_1}$ (11.50)	97.64	95.03	$c_{xy}^{B_2}$ (11.06)	$c_{xy}^{B_2}$ (32.97)

4.5.3 Discussions on Various Numerical Studies Performed

The bearing and coupling dynamic parameters and residual unbalances are assumed to obtain simulated responses, which is shown in Figure 4.5. It could be seen that at all forward critical frequencies, the resonance condition prevails both in the amplitude and the phase. Thereafter, the assumed and estimated parameters are compared and percentage improvement in the estimation of parameters is discussed in Sections 4.5.1 and 4.5.2, for different cases mentioned in Section 4.5. These studies have been performed for various level of measurement noise. Following observations could be made from discussions of Sections 4.5.1 and 4.5.2.

- ***Case A*** is the worst case of estimation for both methods (i.e., *Method I* & *II*) in which deviation starts even at 1% noise case and increases drastically for 5% noise (refer Table 4.3).

- The effect of different frequency bands is shown in Figure 4.6, for *Method I* and it could be observed that ***Case*** C_{fb3} is the best estimation case among different frequency bands.

- For *Method I*, ***Case*** C_{fb3} is the best case of estimation. The maximum error occurred in this case is around (38%, $c_{yx}^{B_2}$) at 5% measurement noise. The order of improvement in condition number is the maximum for this case under *Method I*.

- ***Case*** C_{fb3} under *Method II* is the overall best case of estimation of parameters; the maximum error observed in this case is around (7%, $c_{xy}^{B_1}$) and (11%, $c_{xy}^{B_1}$) for 1% and 5% noise, respectively. Among all the three cases discussed above for both methods (i.e., *I* & *II*) the order of improvement in condition is maximum in this case (refer Table 4.2).

- From Table 4.3, it is accessible that only the cross–coupled damping terms show the maximum deviation in estimation for all the cases discussed above. It could also be noted that assumed values of the direct damping parameters are very high compared to these cross–coupled damping parameters. So, although the percentage error of these cross–coupled parameters is more but the absolute magnitude deviations of these estimates are appreciably less or comparable to other direct damping parameters.

- From Table 4.3, it is apparent that the cross–coupled damping parameters $c_{xy}^{B_1}, c_{xy}^{B_2}$, $c_{yx}^{B_2}$ and $c_{yx}^{B_3}$ are more sensitive due to noise because in most of the cases these parameters show the maximum percentage error.

Estimated parameters show the maximum percent error due to bias error in the model has been summarised in Table 4.3. To have an idea the effect of the bias error on estimated parameter is also compared for the best case of estimation under *Method I & II*. From Table 4.3, it is apprehensible that the cross–coupled damping parameters $c_{xy}^{B_2}$, $c_{yx}^{B_2}$ and $c_{yx}^{B_3}$ are most sensitive parameters corresponding to bias error in physical parameters of the model.

4.6 Summary

The present chapter aimed at the application of a novel condensation scheme to quantitatively estimate the MFPs by the use of incomplete rundown data. The proposed algorithm is illustrated through a simplified numerical example to estimate the speed independent bearing and coupling dynamic parameters and residual unbalances at predefined planes. The conditioning of the matrix is also analysed and is found that after the column scaling condition number of regression matrix improved that reflects in the estimates especially for data with more number of frequencies. Different frequency bands have also been considered

based on the possibility of obtaining information of different modes in responses. The advantage of the present identification algorithm is that it could also be used to quantitatively estimate the speed dependent bearing and coupling dynamic parameters along with residual unbalances. It also overcomes the difficulty arises due to conventional reduction schemes. The advantage of the present method in respect to existing methods of the estimation of misalignment is that it does not assume equivalent forces and moments of faults, which often suffers from erroneous estimation of fault parameters due to severe ill–conditioning of regression equations and the non–uniqueness of the estimation. Application of the proposed identification algorithm in a laboratory test rig would be a real challenge and that has been handled in the subsequent chapter.

CHAPTER 5

Experimental Validation of the Identification Algorithm

5.1 Introduction

The identification algorithm developed in Chapter 0 to estimate multiple fault parameters in rotor systems based on forced response measurements have been tested with actual experimental data in the present chapter. The experimental setup was designed and developed, and experimental observations through necessary instruments were performed at the Vibration and Acoustics Laboratory at IIT Guwahati. Unbalance responses from the rotor–bearing–coupling system were measured at bearing locations at several rotor speeds. Transducer signals were sampled and stored on a personal computer using a data acquisition system. Obtained responses were further processed to make it suitable for the testing of the identification algorithm. A study on the effect of different level of misalignments on estimated parameters was performed.

5.2 The Description of Rotor Model and Support Conditions

The test setup consisted of two shafts connected together with a flexible coupling (Coupling 2). Each shaft was mounted on two deep–grove ball bearings at ends as shown in Figure 5.1. A hollow hub made of the mild steel was prepared and press–fitted into the bearing inner race to accommodate the shaft. Threaded holes were made on the hub for easy mounting/dismounting and to adjust the axial length of the shaft (refer Figure 5.2). The rotor system via a flexible coupling (Coupling 1) was powered through a 0.55 kW (0.75HP) DC motor source (Marathon make) that could be operated at variable speeds by changing the frequency though its controller (i.e. Delta make variable frequency drive). The geometrical and physical parameters of the rotor system are shown in Table 5.1. Relatively heavy discs are symmetrically placed on shafts and due to this unbalance are expected to be concentrated at disc locations only. Bearings were

accommodated in specially fabricated split–type bearing housings (made from rectangular mild steel plates) as shown in Figure 5.2(a), which provided a firm support and simple means of mounting/dismounting of bearings. Rolling element bearings gave a very high transverse stiffness; however, it allowed rotation of the shaft. Layers of soft material were put between the outer race of bearing and the inner bore of bearing housing to increase its flexibility (refer Figure 5.2(b)). Bearing specifications are shown in Table 5.2. A flexible coupling with spiral cuts made of aluminium was used to connect two rotor shafts and a close view of the coupling is shown in Figure 5.3. The bearing housing was mounted over sets of rectangular plates made of the mild steel, which was fixed to heavy rectangular mild steel plate via C–channels. The rectangular plate was again fixed to the aluminium base by aluminium blocks and bolted joints (Figure 5.1).

The effect of Coupling 1 is ignored in the identification procedure. However, the care was taken to have a perfect alignment of the coupling. The motor shaft had relatively rigid bearings and the motor shaft diameter was relatively more than other shafts. Moreover, the overhang portion of the motor shaft was relatively smaller to have any appreciable comparative displacement of shafts at Coupling 1. Whereas at Coupling 2, shafts overhang lengths were longer and mounted on relatively flexible bearing arrangement at both ends and this caused relative displacement of shafts appreciably in comparison to shafts at Coupling 1. With these arrangements it was expected that effect of Coupling 1 would be negligibly small and effectively it would work as a pivot to the rotor train. The misalignment effect on Coupling 2 was studied by changing elevation of bearing housings which supported Rotor 2 (i.e. Shaft 2 and Disc 2). This ensured no consequence on Coupling 1 due to the misalignment at Coupling 2.

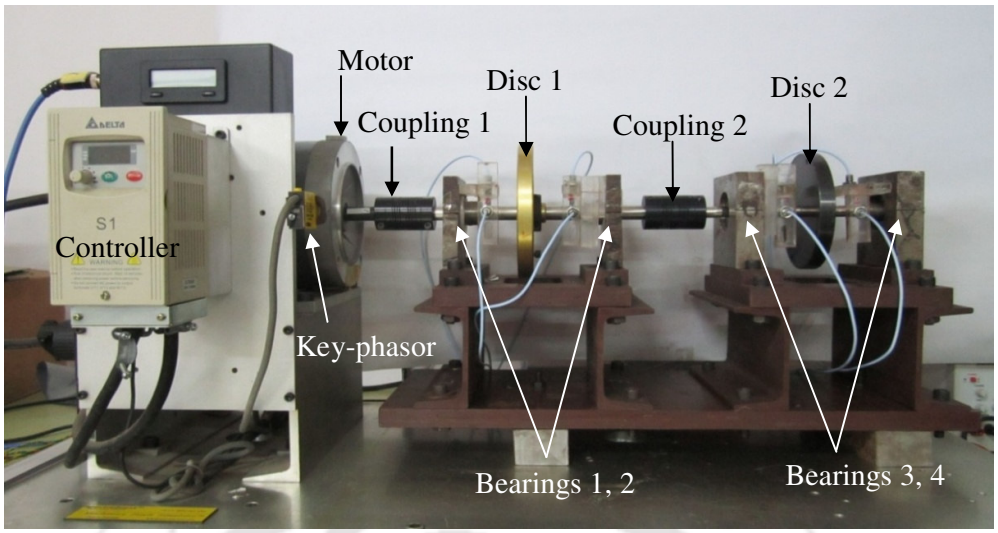

Figure 5.1 An experimental setup of rotor–bearing–coupling system

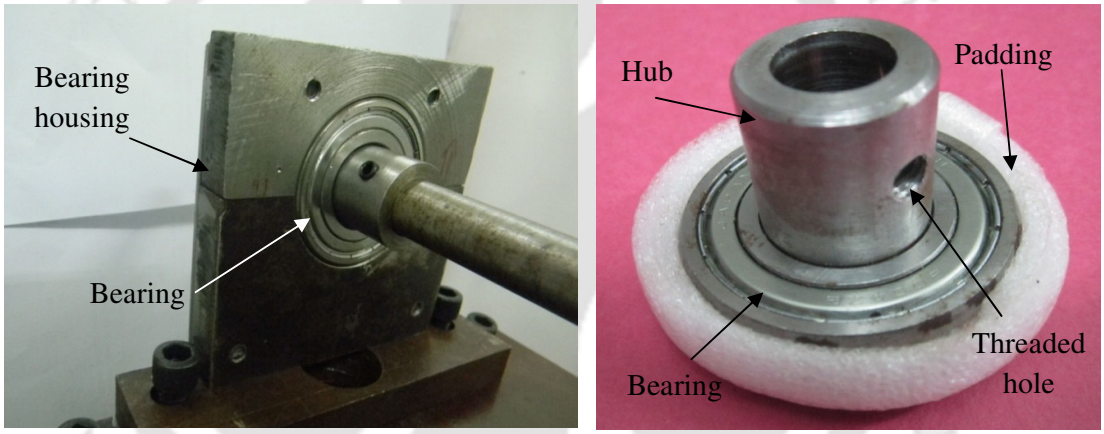

Figure 5.2 Close view of (left) bearing housing (right) rolling bearing with soft padding

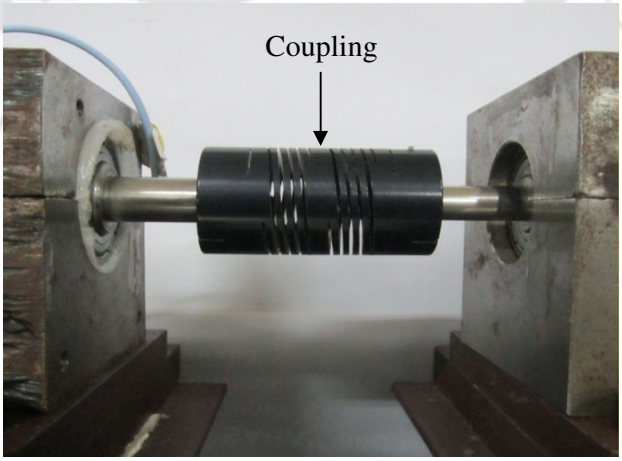

Figure 5.3 A close view of the coupling with a spiral cut

Table 5.1 Rotor geometrical and physical properties

S.N.	Object no.	Length/width (m)	Diameter (m)	Density (kg/m^3)	Mass (kg)	Diametral mass moment of inertia ($kg–m^2$)
1	Shaft 1	0.27	0.012	7740	0.39	2.39×10^{-3}
2	Shaft 2	0.27	0.016	7740	0.32	1.90×10^{-3}
3	Disc 1	0.01	0.010	2600	0.66	8.25×10^{-6}
4	Disc 2	0.01	0.012	7800	1.01	18.20×10^{-6}

Table 5.2 Bearing specifications

S.N.	Bearing location	Bearing no.	Bore diameter (mm)	Outer diameter (mm)	Width (mm)
1	1 and 2	6005 ZNR (SKF)	25	47	12
2	3 and 4	6004 ZNR (SKF)	20	42	12

Schematics of typical misalignments in rigid rotors are shown in Figure 5.4. These aspects have been checked by impact test in subsequent section. Here B_1 to B_4 are original bearing elevation, B_3' and B_4' are new bearing elevation after the introduction of misalignments. $\Delta\alpha$ and $\Delta\delta$ are the amount of angular and parallel misalignments. The misaligned rotor system with the help of thin sheets is shown in Figure 5.5(a) and a close view of sheets used for the introduction of misalignment is shown in Figure 5.5(b). While inserting these sheets between the bearing housing and the base at most care were taken to keep the tightening of bearing housing constant on the base with the help of a torque wrench. Moreover, the addition of soft padding, due to its higher flexibility, ensured negligible effects on the overall base flexibility due the level of tightening of housing bolts on the base since it was relatively rigid. Figure 5.6 shows the schematic of rotor system with the location of sheets inserted below the bearing housing to create different type of misalignment conditions.

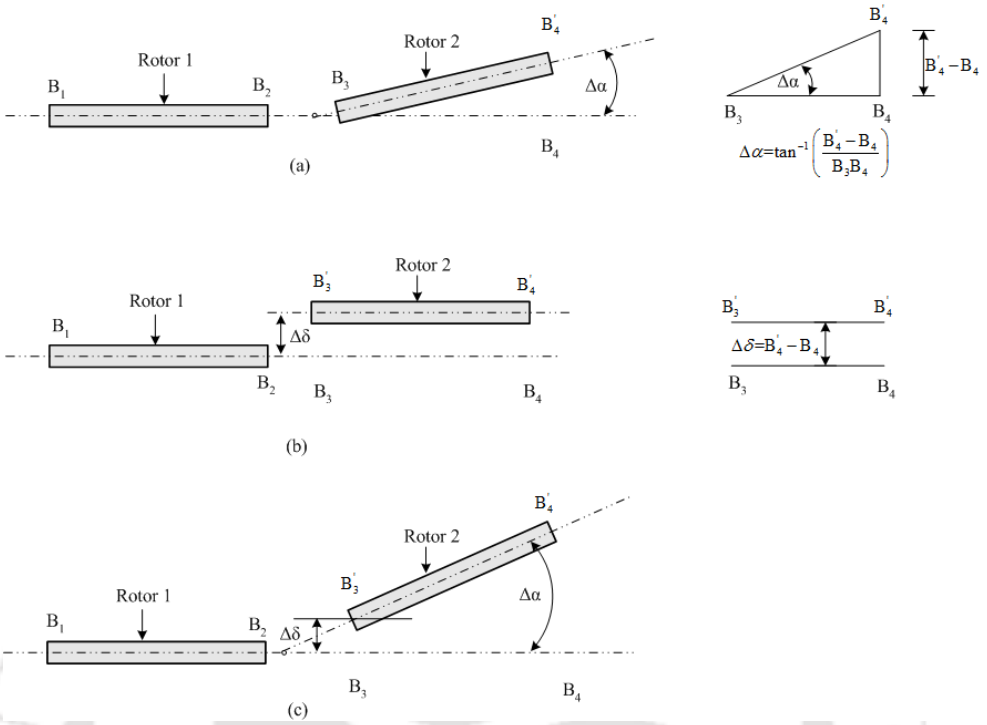

Figure 5.4 Types of misalignment between rigid shafts for (a) pure angular (b) pure parallel (c) combined angular and parallel

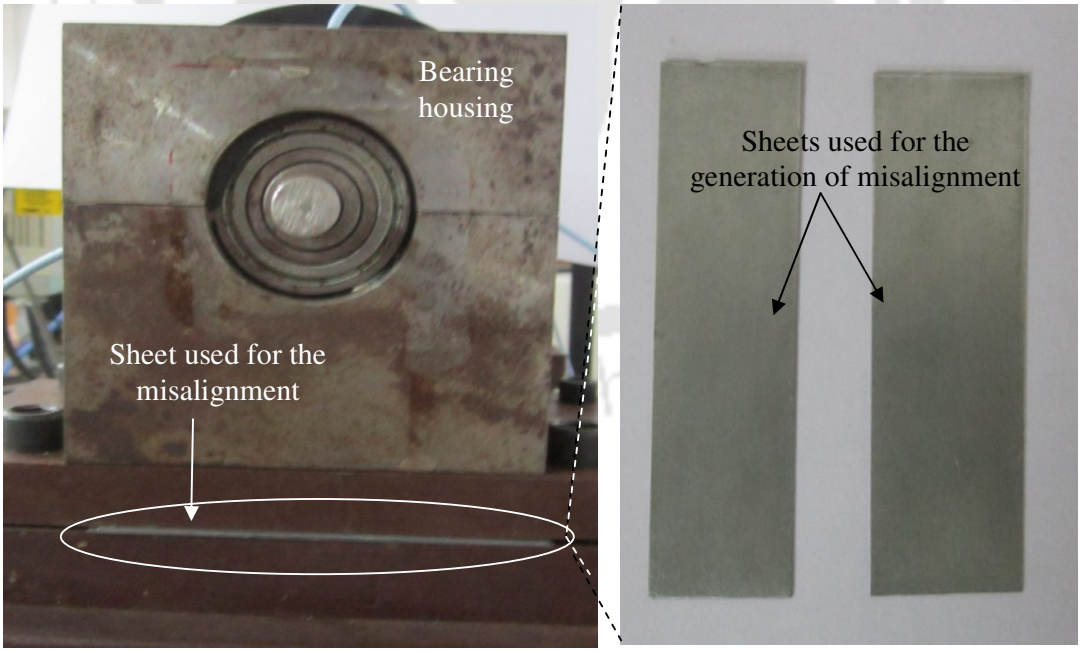

Figure 5.5(a) Misaligned rotor system (b) A close view of sheets used for the introduction of misalignment

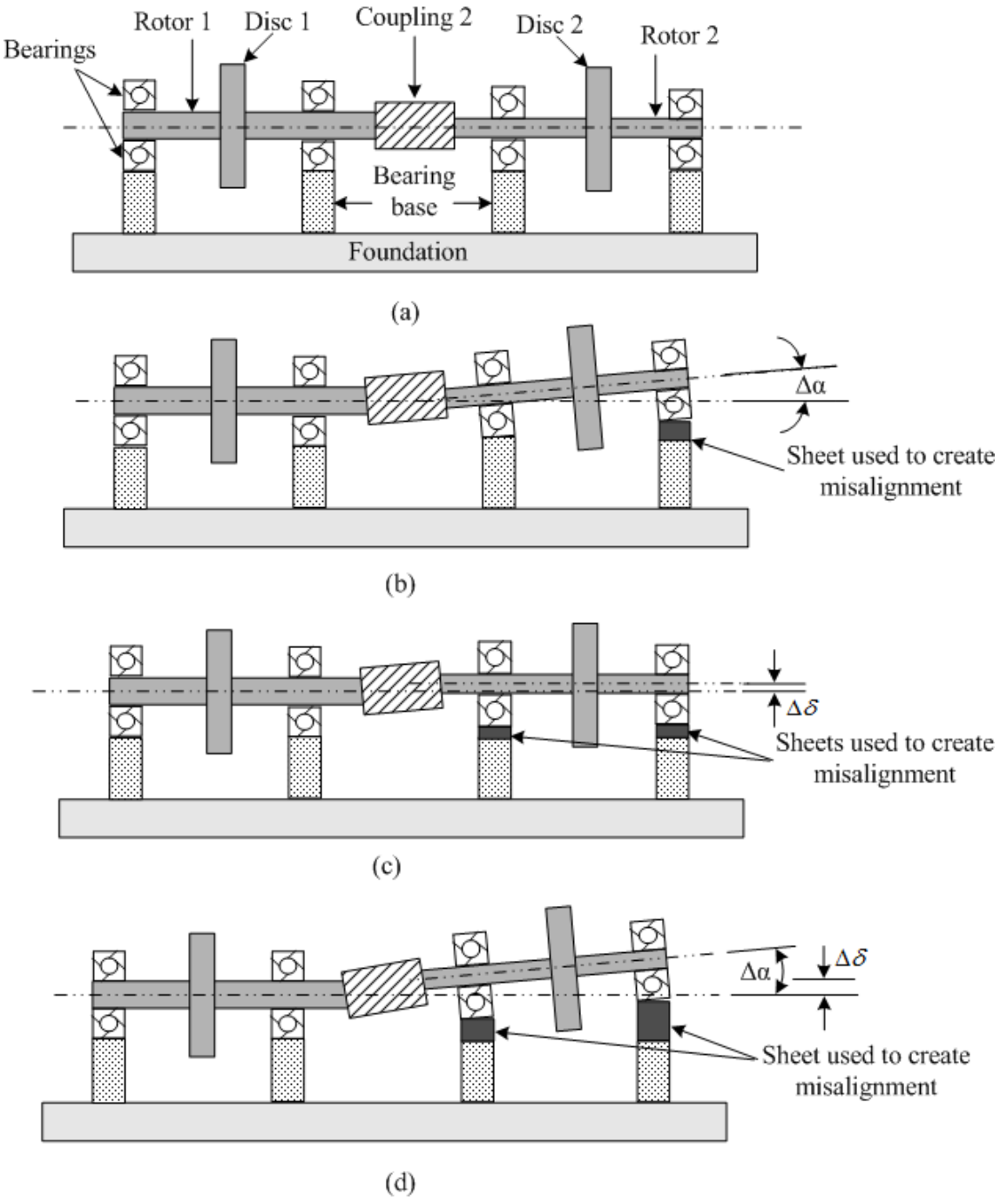

Figure 5.6 A schematic of the rotor system with aluminium sheets used to create the misalignment (a) perfect aligned (b) pure angular (c) pure parallel (d) combined misalignment

5.3 Experimental Setup and Instrumentations

The complete experimental setup with instrumentation is shown in Figure 5.7, and it consisted of following units

1. Experimental setup
2. Proximitor sensor and proximitor amplifier unit (Make Bently Nevada)
3. Constant DC power source unit (Make Scientific MES Technike PVT. LTD.)
4. Data acquisition system (Make National Instruments, USA)

These are described in detail in subsequent subsections.

5.3.1 Experimental Setup

Figure 5.8 shows a schematic diagram of the present experimental setup with instrumentations. A sensor stand was designed and fabricated in the laboratory to mount proximity sensors. Total eight proximity sensors were mounted in two transverse directions to capture responses at each bearing locations.

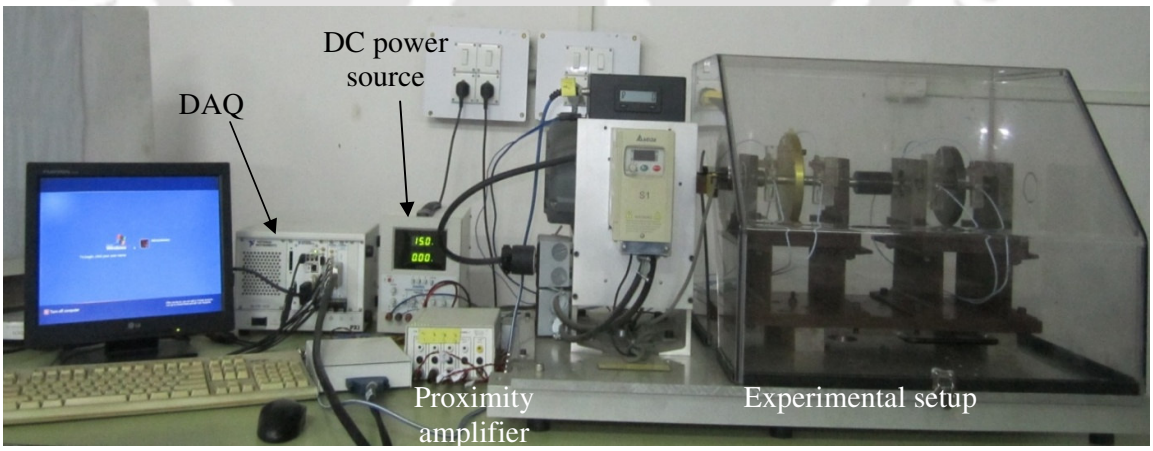

Figure 5.7 An experimental setup developed with instrumentations

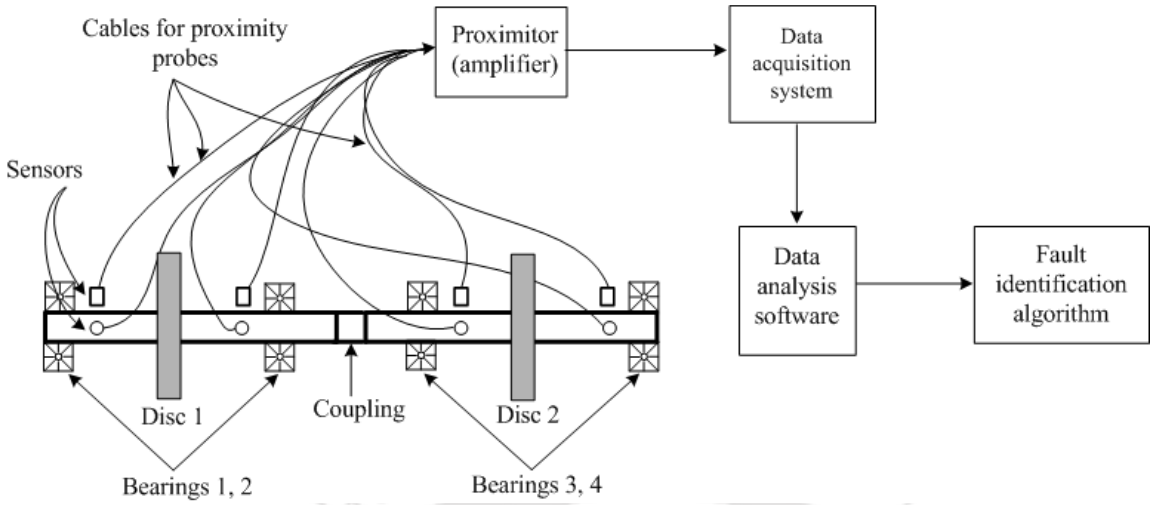

Figure 5.8 A schematic diagram of the experimental setup with instrumentations

5.3.2 Proximity Sensors and Amplifier Unit

The probe stand was specially fabricated by acrylic sheet, which had threaded holes. Proximity sensors were fitted in these holes in two transverse directions. Probe stands were rigidly fixed to the bearing housing to capture displacement signals of the shaft with respect to the bearing in two transverse directions. Non–contact type displacement transducers as shown in Figure 5.9(a), which operates on eddy current principles (i.e., it provides a voltage signal proportional to the gap between the probe tip and the shaft) were used. The gap between the probe and the shaft was adjusted such that the DC voltage was in the range of 5.24–6.24V approximately and it was measured via a DC voltmeter. A close view of proximity sensor and its stand is shown in Figure 5.9(b). It comprised of a probe, a length of extension cable and an oscillator demodulator. The proximity probe sensitivity was 7874V/m. Displacements of the rotor were sensed by proximity sensors, and signals were amplified to the required level by the proximitor amplifier. Figure 5.10 shows a photovoltaic sensor used to get the phase information or reference signal of the responses with respect to a physical mark on to the shaft. The photovoltaic sensor emits laser beam which strikes over the reflecting strip pasted on the motor shaft.

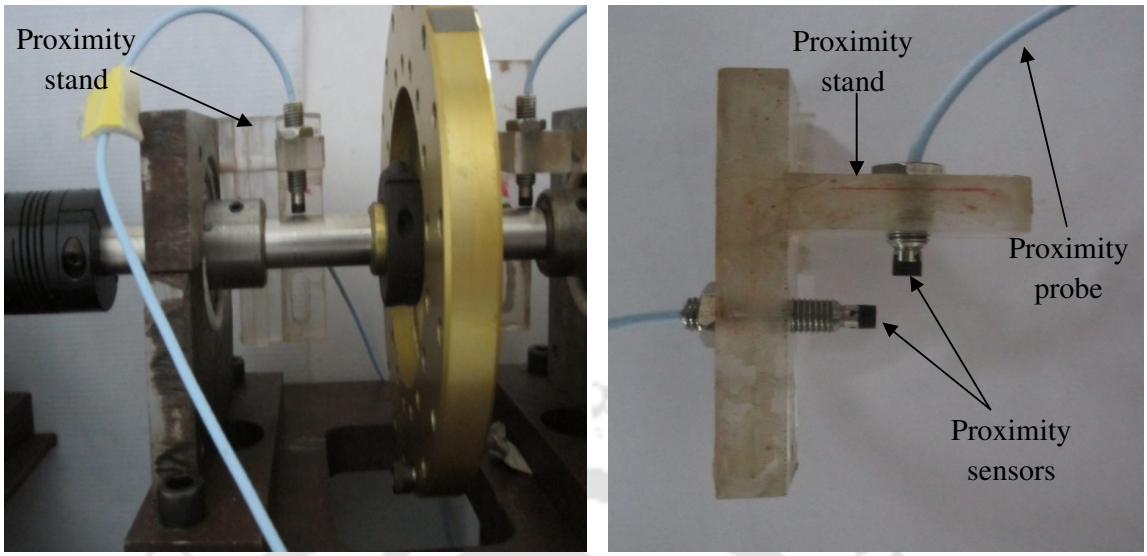

Figure 5.9 (a) Proximity sensors and its mounting (b) A close view of proximity sensor and its mounting (without shaft)

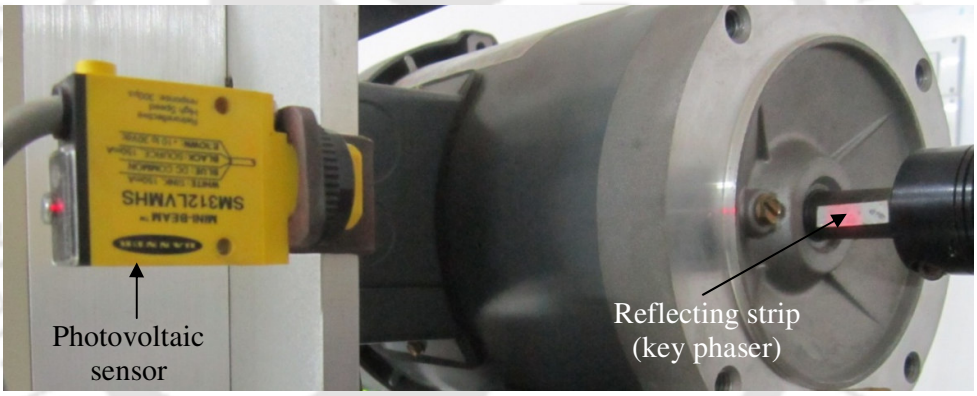

Figure 5.10 A photovoltaic sensor and a reflecting strip

Figure 5.11 A proximity amplifier with four channels

Figure 5.12 A constant DC power source

Figure 5.13 A data acquisition system

5.3.3 Constant DC Power Source Unit

The photovoltaic sensor (Figure 5.10) and the proximity amplifier (Figure 5.11) required DC power supply of the range ±30 V/2A and ±15 V/1A, respectively, to operate and it was

provided through a constant DC power supply. The programmable constant DC power supply source offered high–resolution, high–power voltage and current outputs for the present set up. The programmable DC power supply source, as shown in Figure 5.12, was consisted of:

- Three independent DC power supplies: 0 to 5V/5A, 0 to ±15 V/1A and 0 to 30V/2A.
- A channel corresponding to ±15 V is capable of delivering up to 1A; channel corresponding to 30V is capable of delivering up to 2A whereas channel corresponding to 5V is capable of delivering up to 5A.

5.3.4 Data Acquisition system

A data acquisition (DAQ) is the process of measuring an electrical or physical phenomenon such as voltage, current, temperature, pressure, or sound with the help of a computer. A DAQ system consists of sensors, DAQ measurement hardware, and a computer with programmable software as shown in Figure 5.13. Compared to traditional measurement systems, PC–based DAQ systems exploit the processing power, display and connectivity capabilities.

The basic objective of the data acquisition and processing mechanism is to measure signals developed by the sensing mechanism and to ascertain the magnitude and phase of responses. There are devices for this purpose called analyser, which incorporate many functions and even include the signal generation component. Among many analysers, time capture module (or analyser) was used to capture signals in time domain format. This feature enabled easier extraction of the magnitude of response signal and the phase information of response with respect to a key phaser signal (for the present case with a photovoltaic probe). Whereas the frequency capture module was another important analyser used to capture signals in frequency domain format. This feature enabled easier extraction of natural or excitation frequencies of the system.

After detailed description of the experimental setup, its components and the signal measuring and processing instruments now in the subsequent section the procedure of conducting experiment will be presented.

5.4 Test Procedure

Before conducting experiments best possible alignment was carried out at both coupling locations. To check initial alignment of shafts at coupling a dial indicator as shown in Figure 5.14 was used. The least count of dial indicator was 1 μm. Main steps of experimental procedure, measurement of response signals and signal processing are described as follows.

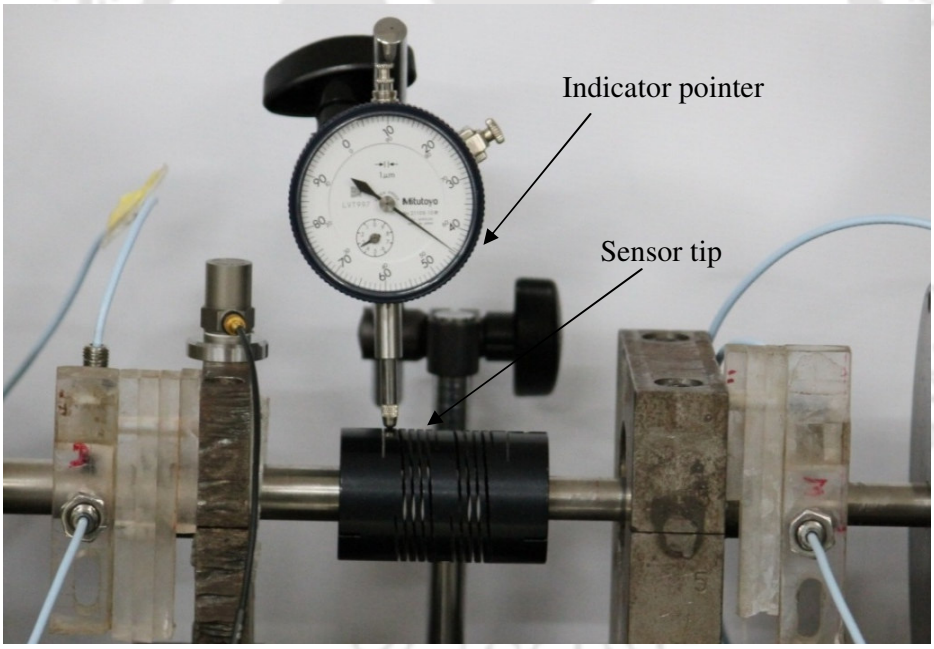

Figure 5.14 A dial indicator for checking alignment of shafts at the coupling

Forced vibration analysis

1. The LabView™ was configured to capture time domain signals in order to ensure working of all 9 input channels of the DAQ. The experimental setup was made ready to measure displacement signals at a particular speed of the rotor.

2. In the time capture module of LabView^{TM}, displacements in two orthogonal planes at four bearing locations were sensed by proximity sensors, amplified in the proximitor amplifier and sent to the DAQ for digitization. A sample time history data at 17 Hz of rotor speed is shown in Figure 5.15.

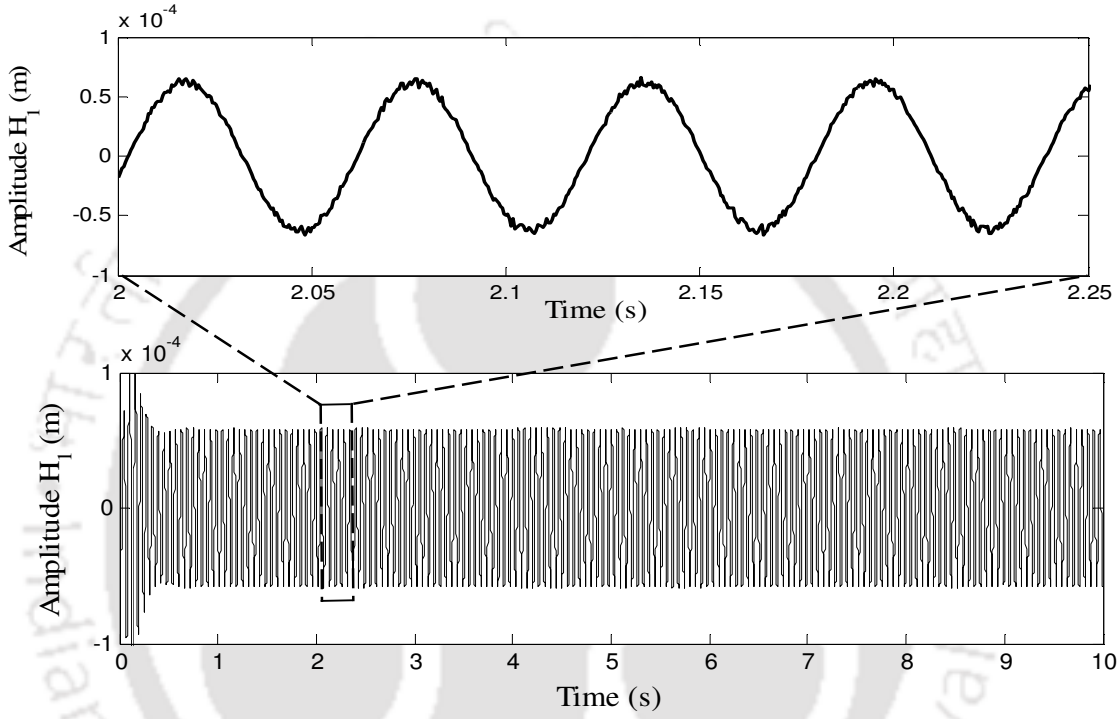

Figure 5.15 A sample time history data of the horizontal direction response at bearing location 1 at 17 Hz

3. The digitized measurement data, which was recorded at different rotor speeds (i.e. 17 Hz, 21Hz, 25Hz, 29Hz, 31Hz, 33Hz, 37Hz and 41Hz) with the sampling frequency of 1 kHz, were stored in a personal computer for post processing.
4. There are different sources of noise in electronic instruments. Response signals, e.g. Figure 5.15, contained noise. Hence, a digital filter was used to reduce the effect of noise in the measurement. It also eliminated any DC component contained in the signal.

5. Filter was designed by using the '*Filter design and analysis tool*' from MATLAB toolbox. A band–pass filter was designed using the Butterworth method. The sampling frequency was obtained from the measured signal 1 kHz and cut–off frequencies were selected based upon the excitation frequency (i.e. ± 2 Hz of excitation frequency). The sample unfiltered signals, i.e. Figure 5.15, is filtered and shown in Figure 5.16.

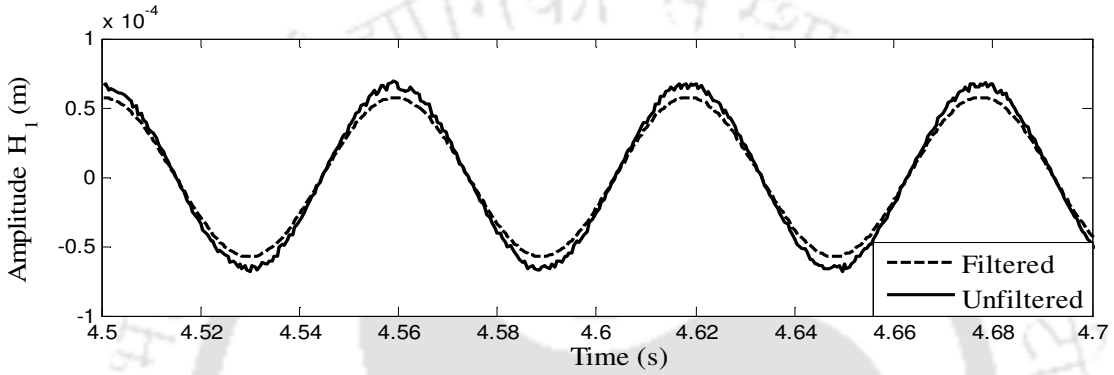

Figure 5.16 The filtered and unfiltered signal for the sample time history of Figure 5.15

6. A computer code was written in MATLAB to find out one pair of adjacent maxima and minima from the filtered data of time history. After choosing a particular maxima and minima, the response amplitude *X*, are found out, similarly after obtaining the time period of the response signal and the phaser signal, the phase angle (ϕ) are found out (refer Figure 5.17) as follows

$$X = \frac{\text{Maxima in response time history - Minima in response time history}}{2} \text{ (mm)} \qquad (5.1)$$

$$\phi = \frac{t}{T} \times 360 \text{ (degree)} \qquad (5.2)$$

The phase of the displacement was obtained with respect to a key phaser signal for all displacement data measured at various independent rotor spin speeds. After obtaining the

response amplitude and phase by using Eqns. (5.1) and (5.2), the real part ($X\cos\varphi$) and the imaginary part ($X\sin\varphi$) of the response could be obtained.

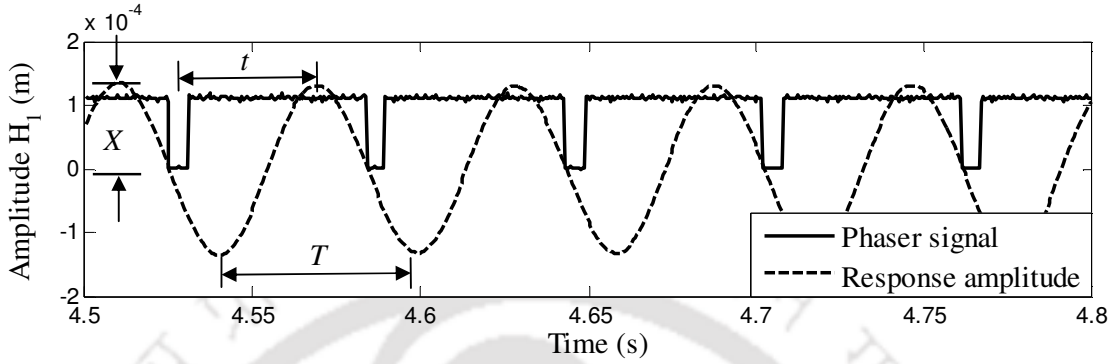

Figure 5.17 The time history of a response at bearing 1 at spin speed of 17 Hz with a phaser signal

7. Sample measured responses (in complex form with real and imaginary parts which contain both magnitude and phase of responses) are given in Table 5.3, for a horizontal response H_1, at all the eight independent operating speeds. Subscripts r and i represent real and imaginary parts of the response H_1.

Table 5.3 A sample stored response (in complex form with magnitude and phase information) at different operating speed

S. N.	Response components (m)	Response components (m) at operating speeds (Hz)							
		17	21	25	29	31	33	37	41
1	$H_{1r}=X\cos\varphi$	5.57 $\times10^{-5}$	-4.63 $\times10^{-5}$	1.17 $\times10^{-5}$	4.04 $\times10^{-5}$	4.11 $\times10^{-5}$	4.77 $\times10^{-5}$	8.91 $\times10^{-6}$	-5.82 $\times10^{-5}$
2	$H_{1i}=X\sin\varphi$	-3.57 $\times10^{-6}$	3.43 $\times10^{-5}$	5.29 $\times10^{-5}$	2.99 $\times10^{-5}$	-4.67 $\times10^{-5}$	-4.57 $\times10^{-5}$	6.45 $\times10^{-5}$	-3.77 $\times10^{-5}$

8. These response data in real and imaginary form (with magnitude) are required for the present identification algorithm (Eqn. (4.71) in Chapter 0).

The above procedure was repeated to check the repeatability of the identification algorithm. Overall time domain data were processed to get the frequency response and were used in the identification algorithm. The FFT from the impact test was used to obtain natural frequencies.

5.5 Parameter Estimations without Misalignment

The experimental complex response obtained in previous section is used into Eqn. (4.71) with some modifications regarding unbalances, to estimate the bearing and coupling dynamic parameters, and residual unbalances. It is given as

$$\left[A(\omega)\right]^{h}_{16\times 46}\left\{X\right\}^{h}_{46\times 1}=\left\{B(\omega)\right\}^{h}_{16\times 1} \tag{5.3}$$

with

$$\left\{X\right\}^{h}_{46\times 1}=\{k^{B_1}_{xx},k^{B_1}_{xy},k^{B_1}_{yx},k^{B_1}_{yy},k^{B_2}_{xx},k^{B_2}_{xy},k^{B_2}_{yx},k^{B_2}_{yy},k^{B_3}_{xx},k^{B_3}_{xy},k^{B_3}_{yx},k^{B_3}_{yy},k^{B_4}_{xx},k^{B_4}_{xy},k^{B_4}_{yx},k^{B_4}_{yy},k^{C}_{xx},k^{C}_{xy},k^{C}_{yx},k^{C}_{yy},k^{C}_{\varphi_x},k^{C}_{\varphi_y},$$
$$c^{B_1}_{xx},c^{B_1}_{xy},c^{B_1}_{yx},c^{B_1}_{yy},c^{B_2}_{xx},c^{B_2}_{xy},c^{B_2}_{yx},c^{B_2}_{yy},c^{B_3}_{xx},c^{B_3}_{xy},c^{B_3}_{yx},c^{B_3}_{yy},c^{B_4}_{xx},c^{B_4}_{xy},c^{B_4}_{yx},c^{B_4}_{yy},c^{C}_{xx},c^{C}_{xy},c^{C}_{yx},c^{C}_{yy},U^{r}_{x_1},U^{i}_{x_1},U^{r}_{x_2},U^{i}_{x_2}\}^{T}$$

The only difference between Eqn. (4.71) and Eqn. (5.3) is that for the present chapter it is derived for a single disc on each rotor. So the size of the unknown parameters vector $\{X\}_{46\times 1}$ has been reduced in Eqn. (5.3) instead of $\{X\}_{50\times 1}$ in Eqn. (4.71) and accordingly the size of regression matrix $[A(\omega)]_{16\times 46}$ has been reduced instead of $[A(\omega)]_{16\times 50}$. From above equation, it could be seen that this is the case of underdetermined system of linear simultaneous equations in which number of unknowns i.e. forty six are far more than the number of equations, i.e. sixteen. So, entire unknown can only be obtained with the help of sets of independent force–response measurements such that the number of equations is increased at least equal or more than the unknowns. For the present case, the minimum number of independent measurements required is three.

Here the estimation has been performed with measurements at eight independent spin speeds, i.e. ω_1= 17 Hz, ω_2= 21 Hz, ω_3= 25 Hz, ω_4= 29 Hz, ω_5= 31 Hz, ω_6= 33 Hz, ω_7= 37 Hz and ω_8= 41 Hz. The repeatability of the estimates has been checked with three different such sets of measured data. Figure 5.18 shows experimentally estimated the bearing and coupling dynamic parameters, and residual unbalances. It could be observed that most of the estimated stiffness, damping and unbalance parameters are consistent even with different sets of measurements.

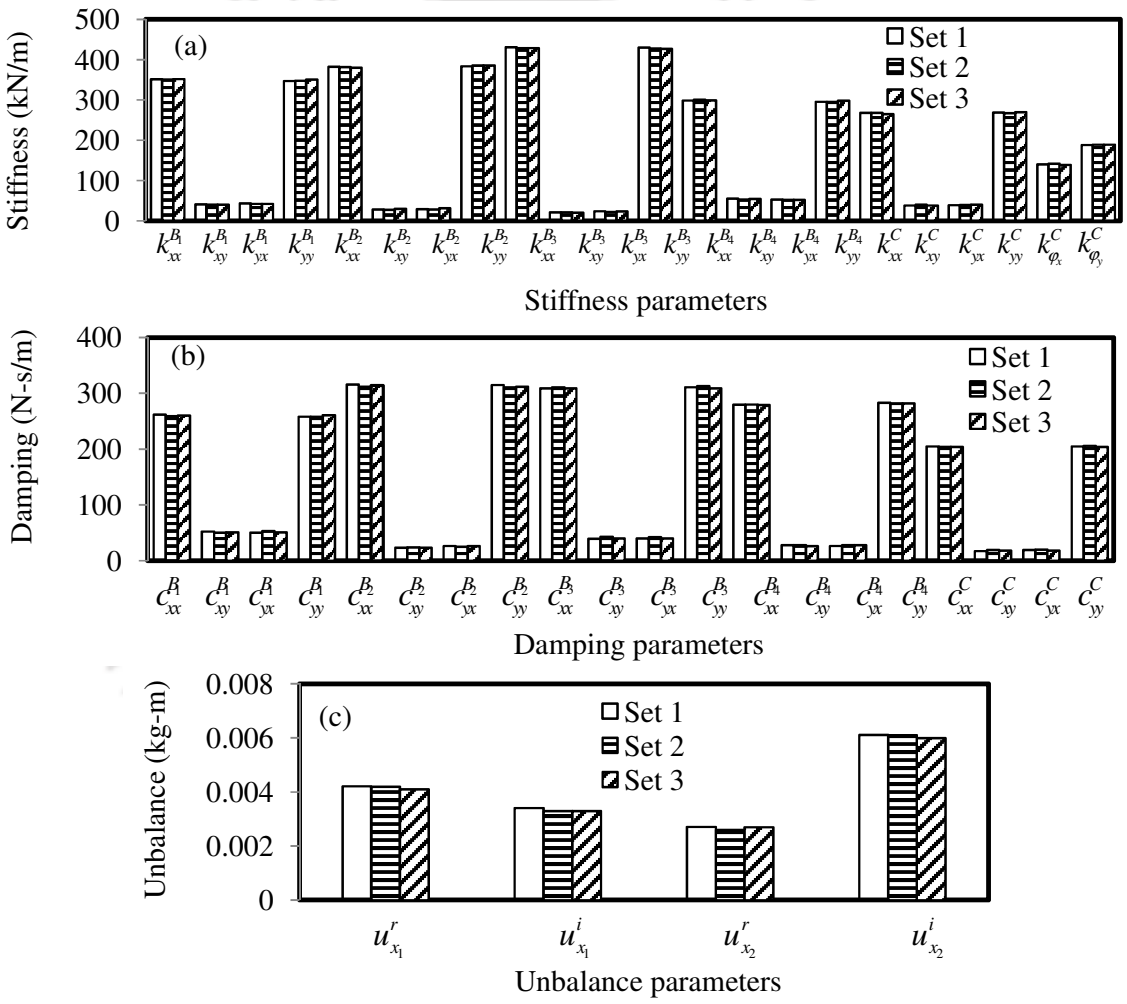

Figure 5.18 Experimentally estimated parameters (a) stiffness (b) damping (c) residual unbalance for three different sets of measured data

5.6 Validation of Estimated Parameters for without Misalignment

Free vibration analysis

1. The LabView™ was configured to capture frequency domain signals.
2. After ensuring the working of a channel properly, the frequency capture module of the DAQ started to perform the standard impact test to identify natural frequencies of the system. To capture this signal the accelerometer was mounted over the bearing housing near Coupling 2.
3. First both couplings (i.e. Couplings 1 and 2) were removed and an impact test was performed for individual rotor systems (i.e. Rotors 1 and 2). A typical frequency domain data is shown in Figure 5.19 from the impact test on *Rotor system* 1. In frequency domain data predominant peak was observed at 357 Hz corresponding to natural frequency of the system. The close form expression to obtain the natural frequency for the simply supported rotor (discrete case) is given in Appendix C and it gives the natural frequency for the present rotor configuration as 373 Hz. Since approximation of the simply support and the massless shaft is involved so some deviation is expected but it confirms that the identified peak from the impact test is the natural frequency of the rotor system.
4. Next the impact test was performed on *Rotor system* 2 alone and the FFT response plot is shown in Figure 5.20. It indicates the natural frequency equal to 144 Hz and from the closed form solution for simply supported conditions the natural frequency is obtained as 169 Hz. It confirms that the identified peak from the impact test is the natural frequency of the rotor system.
5. Subsequently, the impact test was performed when both rotor systems (Rotors 1 and 2) was joined by Coupling 2 alone. Figure 5.21 gives the FFT plot and it indicates that natural frequencies of the rotor system are 149Hz, 201 Hz and 362 Hz. On comparison with previous frequencies it could be observed that there is slight change in them from

145 Hz to 149 Hz and from 357 Hz to 362 Hz. Apart from these frequencies introduction of a new natural frequency at 201 Hz due to effect of the coupling.

6. A FE model with the Timoshenko beam theory and simply supported boundary conditions are developed to correlate results obtained experimentally. Modelling of Timoshenko beam is given in Appendix A. The coupling is modeled as flexible with eight linearized stiffness and damping coefficients. The input data for theoretical model are according to the experimental setup and provided in Table 5.1 and Table 5.2. From forced vibration responses that are given in Figure 5.25(a) forward critical speeds are 155 Hz, 239 Hz and 419 Hz. Because of simply supported conditions as well as gyroscopic effects these critical speeds are higher than corresponding natural frequencies (155 Hz instead of 149 Hz, 239 Hz instead of 201 Hz and 419 Hz instead of 362 Hz) in actual test rig due to the flexibility of bearings and couplings, and non−rotating condition of the impact test. On considering flexibility at bearings, it is expected that FE model natural frequencies would be close to experimental natural frequencies.
7. Finally, Coupling 1 was also connected along with Coupling 2 to see its effect on the rotor system natural frequencies. Figure 5.22 shows the FFT plot of the impact test for assembled rotor system and natural frequencies of the rotor system are 150 Hz, 203 Hz and 364 Hz. In comparison with previous case in which only Coupling 2 was connected there is a slight change in natural frequencies. The variation in natural frequencies for this two cases are 0.67%, 0.99% and 0.55% for the first, second and third natural frequencies, respectively.

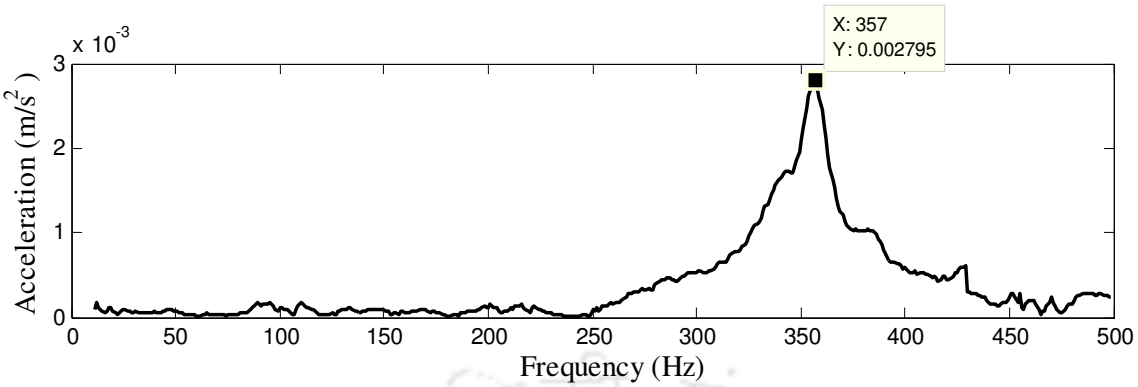

Figure 5.19 A FFT plot from an impact test on rotor system 1 (near motor end) without couplings

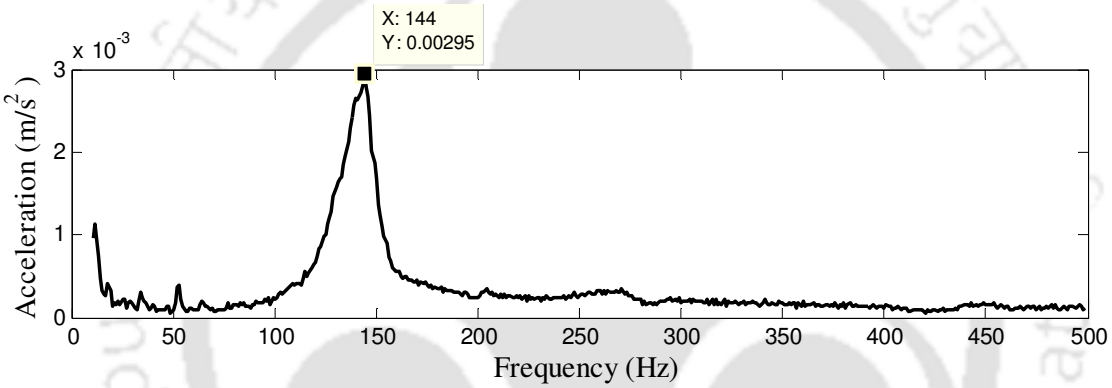

Figure 5.20 A FFT plot from an impact test on rotor system 2 (away from motor) without couplings

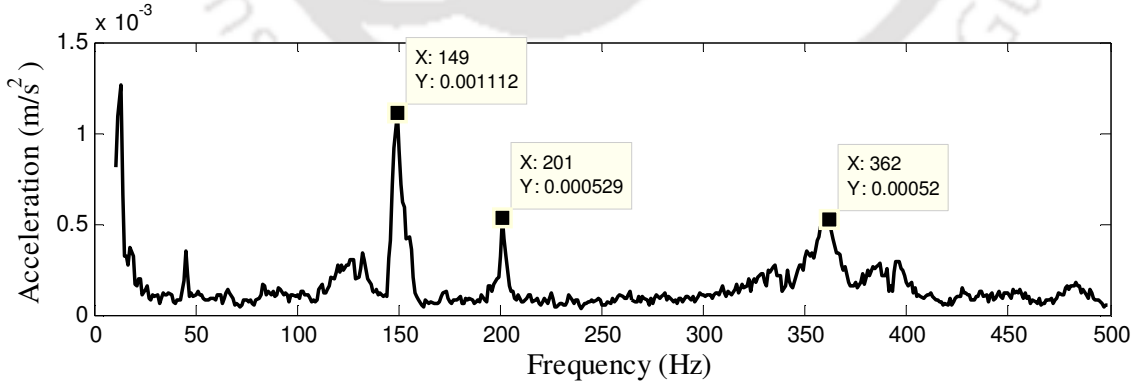

Figure 5.21 A FFT plot from an impact test on Rotor systems 1 and 2 with only Coupling 2

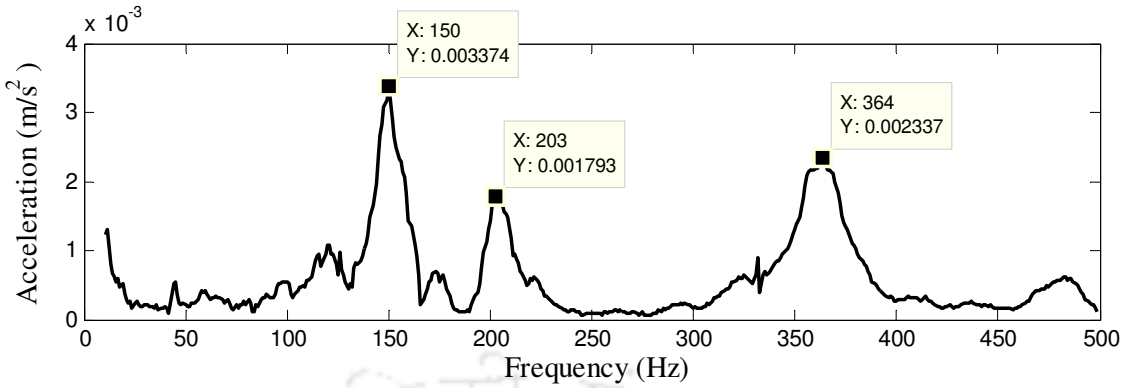

Figure 5.22 A FFT plot from an impact test on Rotor systems 1 and 2 with both Couplings 1 and 2

The impact test was repeated several times by changing the impact location and the sensor position for checking the consistency of appearance of predominant peaks. The consistency of peaks was also checked by exciting a particular mode at a time by hitting the rotor at more than one place simultaneously (up to the third mode). An eigen value problem was solved to obtain natural frequencies and mode shape of the system. The natural frequencies of the system are ω_{nf1}=155.7 Hz, ω_{nf2}=239.3 Hz and ω_{nf3}=419.9 Hz. Figure 5.23 shows the mode shape of the complete rotor system. From Figure 5.23, it could be analysed that Mode 1 has all displacements of the same sign (i.e. no node). It will happen if both rotors are impacted downward (or upward) direction. Mode 2 has one node at around coupling location (either side has opposite sign). It will happen if both the shafts are impacted in opposite direction. Mode 3 has two nodes one at each shaft. This will happen if both the shafts are impacted in the same direction but in opposite direction at the coupling. From this analysis we can obtain the approximate location of forcing to get different modes of vibration in actual system. Figure 5.24 shows the schematic diagram of experimental setup with forcing direction to get different modes of vibration. From Figure 5.25(b–d) it can be seen that while trying to excite a particular mode (e.g. according to Figure 5.24(a)) that particular natural frequency (e.g. Figure 5.25(b))

has a predominant peak as compared to other modes (e.g. Figure 5.25(c–d)). This is valid for all modes excited according to Figure 5.24.

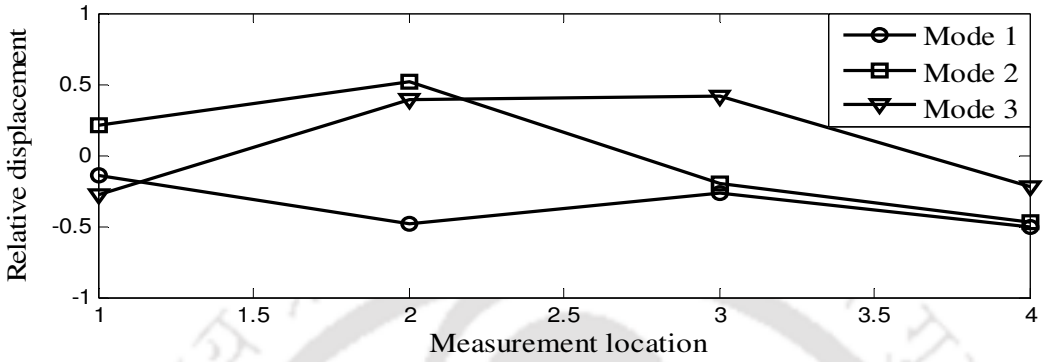

Figure 5.23 First three modes of the rotor system

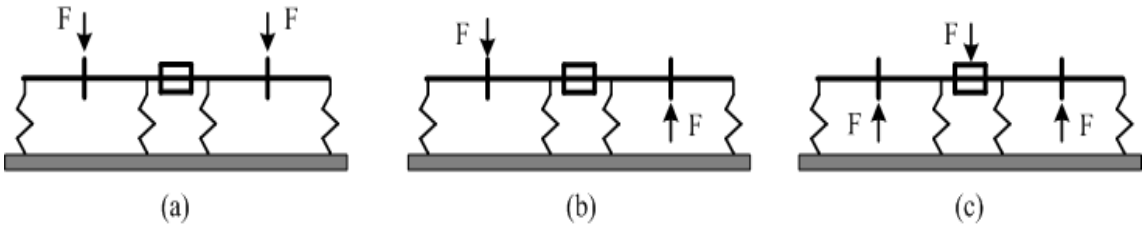

Figure 5.24 A schematic diagram of experimental setup with forcing directions to excite different modes of vibration (a) first mode (b) second mode (c) third mode

It is very difficult to mimic the same boundary condition experimentally. In practice the supports would provide some flexibility. For the rolling element bearing theoretical formulae are available to obtain the stiffness approximately (Goodwin, 1989), however, they are not reliable.

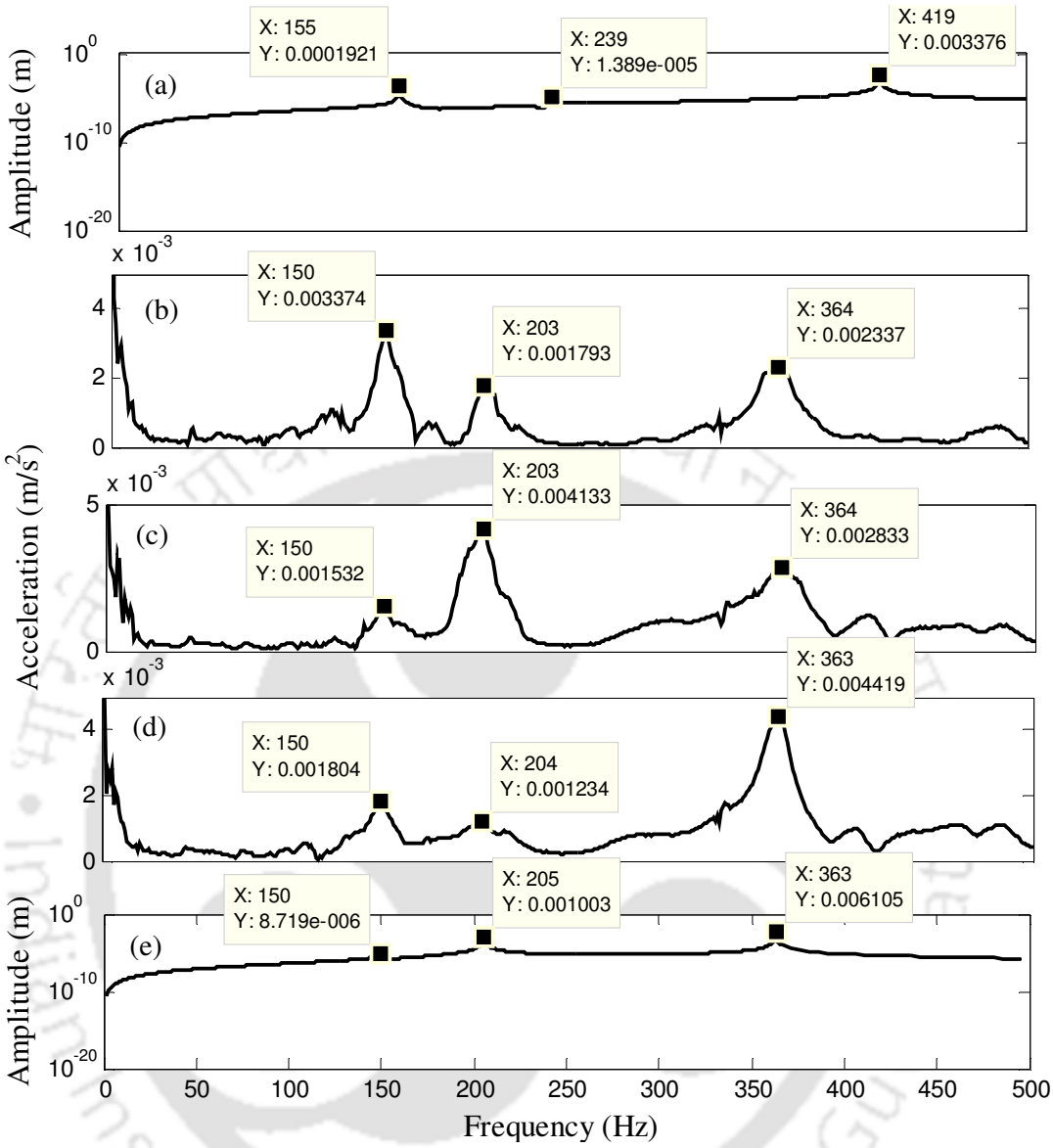

Figure 5.25 Comparison of natural frequencies (a) FE forced vibration solution with SSBC (critical speeds) (b) Impact test with 1st mode excitation (c) Impact test with 2nd mode excitation (d) Impact test with 3rd mode excitation (e) Updated FE model

After the estimation of the bearing and coupling dynamic parameters and residual unbalances these information were used to update the FE model. From Figure 5.25(e), it could be concluded that that critical speeds (more precisely the forward critical speed since the response is generated by unbalances) from the FE analysis are close to experimental natural frequencies,

i.e. Figure 5.25(b)−(d). Since the impact test was conducted while the rotor was stationary. The effect of gyroscopic couple is seen to be minimal in experimental setup since the discs were place at mid−spans of both the rotors.

After the estimation of bearing and coupling dynamic parameters, and residual unbalances, for without misalignment condition, the next step is estimation under misalignment conditions and it is discussed in the subsequent section.

5.7 Parameter Estimation with Different Misalignment Conditions

Here the bearing and coupling dynamic parameters and residual unbalances are estimated under different level of misalignment conditions (refer Table 5.4), where $\Delta\alpha$ and $\Delta\delta$ represent amount of the angular and parallel misalignment, respectively. Calculations of the angular and parallel misalignments are presented in Figure 5.4.

Table 5.4 Misalignment specifications

S. N.	Types of misalignment	Cases	Amount of misalignment (degree, mm)	
1	Pure angular	*Case* A_1	Δα=0.16,	Δδ= 0.0
		Case A_2	Δα=0.32,	Δδ= 0.0
2	Pure parallel	*Case* B_1	Δα=0.00,	Δδ= 0.5
		Case B_2	Δα=0.00,	Δδ= 1.0
3	Combination of both	*Case* C_1	Δα=0.16,	Δδ= 0.5
		Case C_2	Δα=0.32,	Δδ= 1.0

Forced Vibration Analysis

A sample time history data under different misalignment condition at 17 Hz is shown in Figure 5.26. With the help of Eqns. (5.1) and (5.2), one may calculate the amplitude and phase of the response signals due to misaligned conditions. This information was used to obtain the complex (i.e., the real and the imaginary) response of the signal. Now by using Eqn. (5.3), the bearing and coupling dynamic parameters and residual unbalances were estimated under different misalignment conditions (refer Table 5.4).

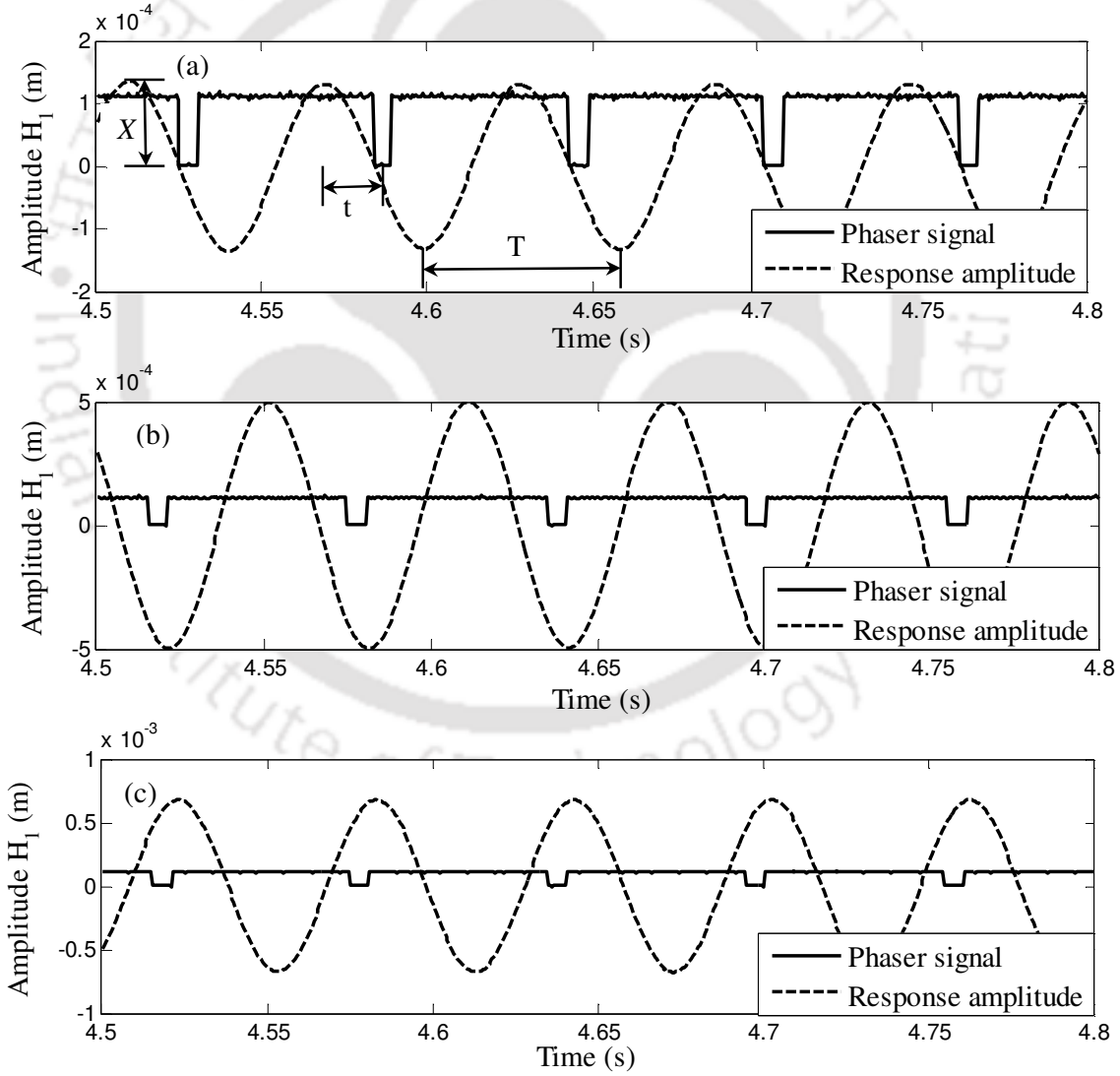

Figure 5.26 Time history at bearing 1 for (a) *Case A1* (b) *Case B1* (c) *Case C1* at the spin speed of 17 Hz along with the phaser signal

Pure angular misalignment

Under the pure angular misalignment two different misalignment condition, mentioned in Table 5.4, is carried out. Figure 5.27 represents the comparison of deviations of estimated parameters with the aligned case under the aforementioned case. From Figure 5.27, it could be observed that as the amount of misalignment increases the bearing and coupling dynamic parameters increases, especially the cross–coupled bearing damping parameters. The maximum variation occurred in this case is ($c_{yx}^{B_4}$, 12%) and ($c_{yx}^{B_4}$, 18%) for *Case A*$_1$ and *Case A*$_2$, respectively.

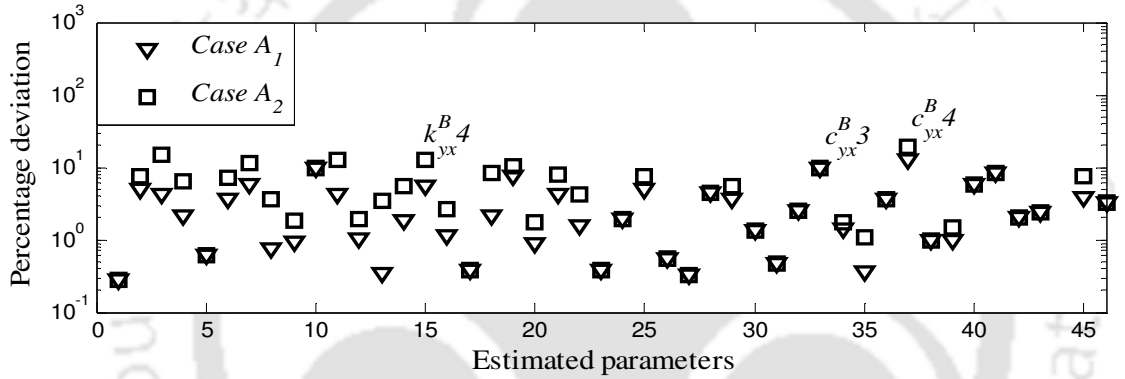

Figure 5.27 Comparison of deviations of estimated parameters with aligned case and for pure angular misalignment conditions *Case A*$_1$ ($\Delta\alpha$=0.16°, $\Delta\delta$= 0mm) and *Case A*$_2$ ($\Delta\alpha$=0.32°, $\Delta\delta$= 0 mm)

Pure Parallel misalignment

Thereafter experimentations were carried out under pure parallel misalignment condition as mentioned in Table 5.4. Figure 5.28 shows the comparison of errors of estimated parameters under two different parallel misalignment conditions. From Figure 5.28, it could be analysed that as the amount of misalignment increases the estimated bearing and coupling dynamic parameters also increases. The maximum variation occurred are ($c_{yx}^{B_4}$, 31%) and ($c_{yx}^{B_4}$, 56%) for *Case B*$_1$ and *Case B*$_2$, respectively. From Figure 5.27 and Figure 5.28, it could be concluded that under parallel misalignment condition variation in the estimated parameters were relatively

high this is because the coupling considered was having spiral cuts that allowed tilting motion relatively easy as compared to the translational motion and because of it the angular misalignment effect was less as compared to the parallel misalignment.

Combined misalignment

Next experimentations were also performed for two different combinations of the angular and parallel misalignments as mentioned in Table 5.4. Comparison of errors of estimated parameters under combined misalignment conditions is shown in Figure 5.29. It could be analysed that as the amount of misalignment increases some of the estimated cross–coupled bearing damping parameters increases. The maximum variation occurred are ($c_{yx}^{B_4}$, 60%) and ($c_{yx}^{B_4}$, 68%) for *Case* C_1 and *Case* C_2, respectively. From Figure 5.27, Figure 5.28 and Figure 5.29, it could be concluded that under the combined misalignment condition the variation in the estimated parameters is the maximum.

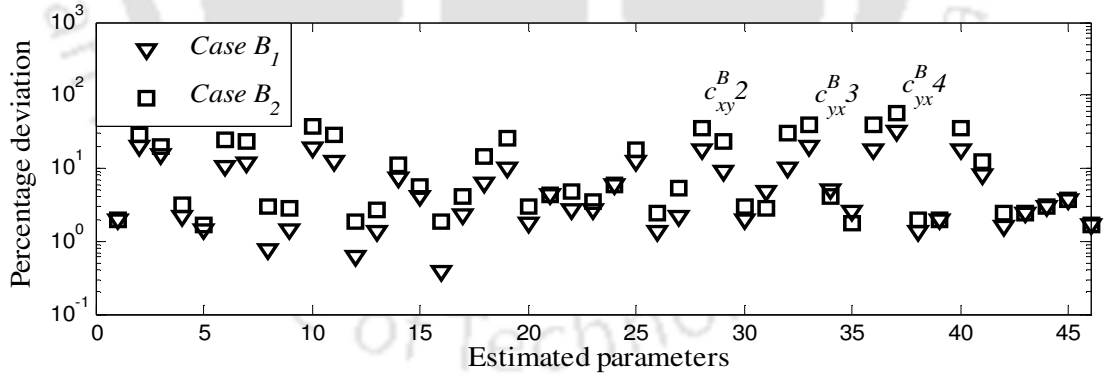

Figure 5.28 Comparison of deviations of estimated parameters with aligned case and for pure parallel misalignment conditions *Case* B_1 ($\Delta\alpha=0^{\circ}$, $\Delta\delta$= 0.5 mm) and *Case* B_2 ($\Delta\alpha=0^{\circ}$, $\Delta\delta$=1.0 mm)

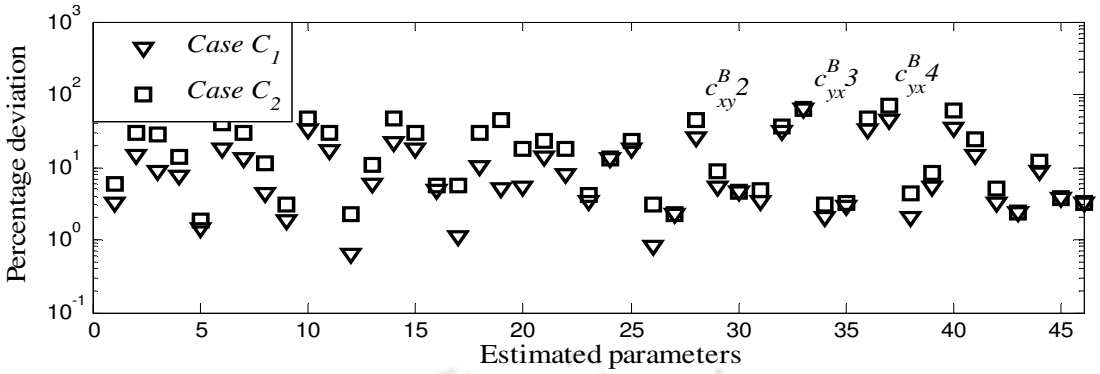

Figure 5.29 Comparison of deviations of estimated parameters with aligned case and for combined misalignment conditions *Case* C_1 ($\Delta\alpha$=0.16°, $\Delta\delta$= 0.5 mm) and *Case* C_2 ($\Delta\alpha$=0.32°, $\Delta\delta$= 1.0 mm)

5.8 Validation of Estimated Parameters with Misalignment Conditions

Free Vibration Analysis

The standard impact test was performed on the misaligned rotor system for different misalignment conditions mentioned in Table 5.4. On comparing the impact test FFT response plots under misalignment conditions, i.e. Figure 5.30, Figure 5.31 and Figure 5.32; and for without misalignment condition, i.e. Figure 5.22, it represented a slight variation (refer Table 5.5) in natural frequencies. From Table 5.5, it could be analysed that after misalignment natural frequencies of the system increases, this is due to the increase in the stiffness after the misalignment. On comparing Figure 5.30–Figure 5.32 with Figure 5.22, it should be noted that additional peak at 307 Hz appeared in between the previous second and third natural frequencies and this was appreciable for the combined misaligned condition. This might be due to the misalignment, which resulted in the anisotropic support flexibility and that led to an additional peak. This is a well known phenomenon that due to anisotropy of the bearings splitting of natural frequency takes place and is described in classical books by Tondl (1965) and Rao (1996).

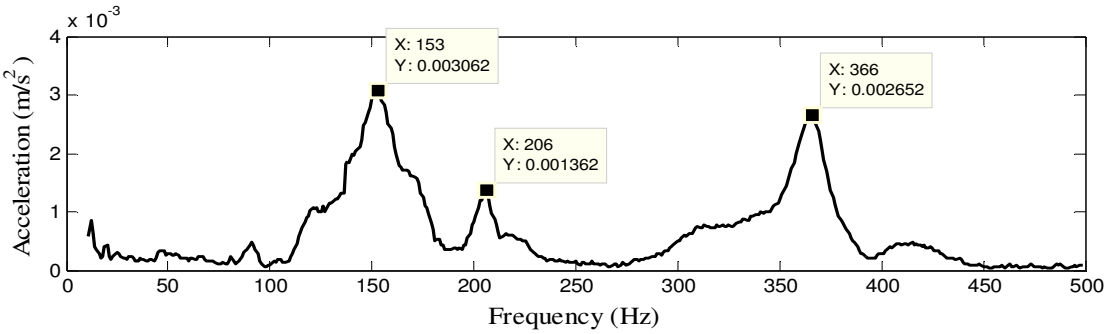

Figure 5.30 A FFT plot from an impact test for *Case A_1* (i.e. $\Delta\alpha=0.16^{\circ}$, $\Delta\delta=0$ mm)

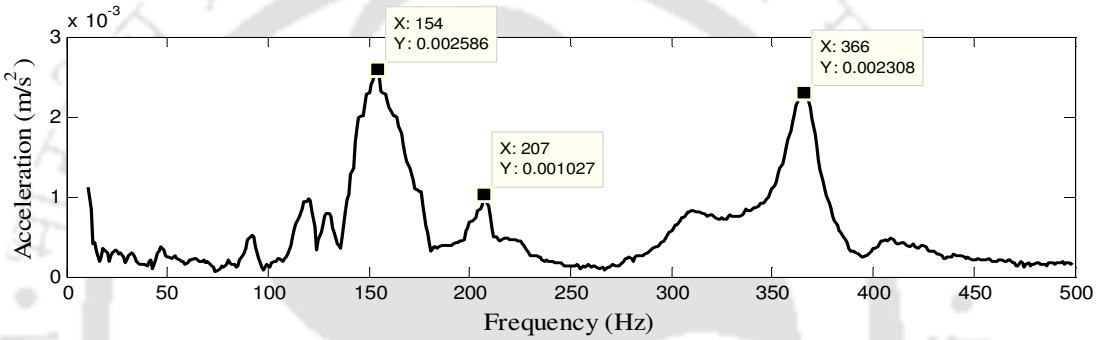

Figure 5.31 A FFT plot from an impact test for *Case B_1* (i.e. $\Delta\alpha=0^{\circ}$, $\Delta\delta=0.5$ mm)

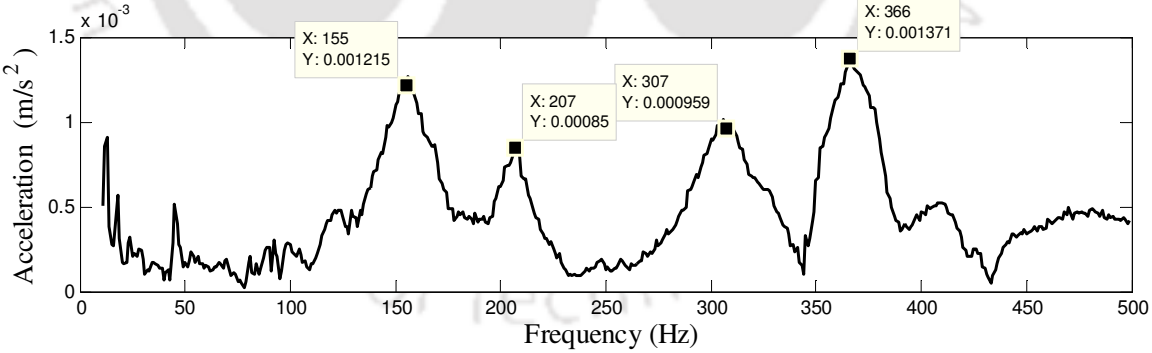

Figure 5.32 A FFT plot from an impact test for *Case C_1* (i.e. $\Delta\alpha=0.16^{\circ}$, $\Delta\delta=0.5$mm)

Table 5.5 Comparison of natural frequencies with and without misalignment conditions

S. N.	Natural frequencies (Hz)	Impact test result with 1st mode excitation			
		Without misalignment	With misalignment (percentage deviation)		
			Pure angular (*Case* A_1)	Pure parallel (*Case* B_1)	Combined (*Case* C_1)*
1	1st	150	153 (2.0)	154 (2.66)	156 (4.00)
2	2nd	203	206 (1.40)	207 (1.97)	207 (1.97)
3	3rd	364	366 (0.54)	366 (0.54)	366 (0.54)

* There was an additional peak at 307 Hz due to splitting of third natural frequency due to anisotropy of the support condition in case of the severe misalignment

After the estimation of bearing and coupling dynamic parameters and residual unbalances for various misaligned conditions, this information was used to update the FE model. From Figure 5.33(d), it could be concluded that forward critical speeds from updated the FE model are close to experimental natural frequencies, i.e. Figure 5.33(a)–(c). Due to the symmetry of disc location at the mid–span of shafts, gyroscopic effects are not predominant, and hence critical speeds and natural frequencies are close.

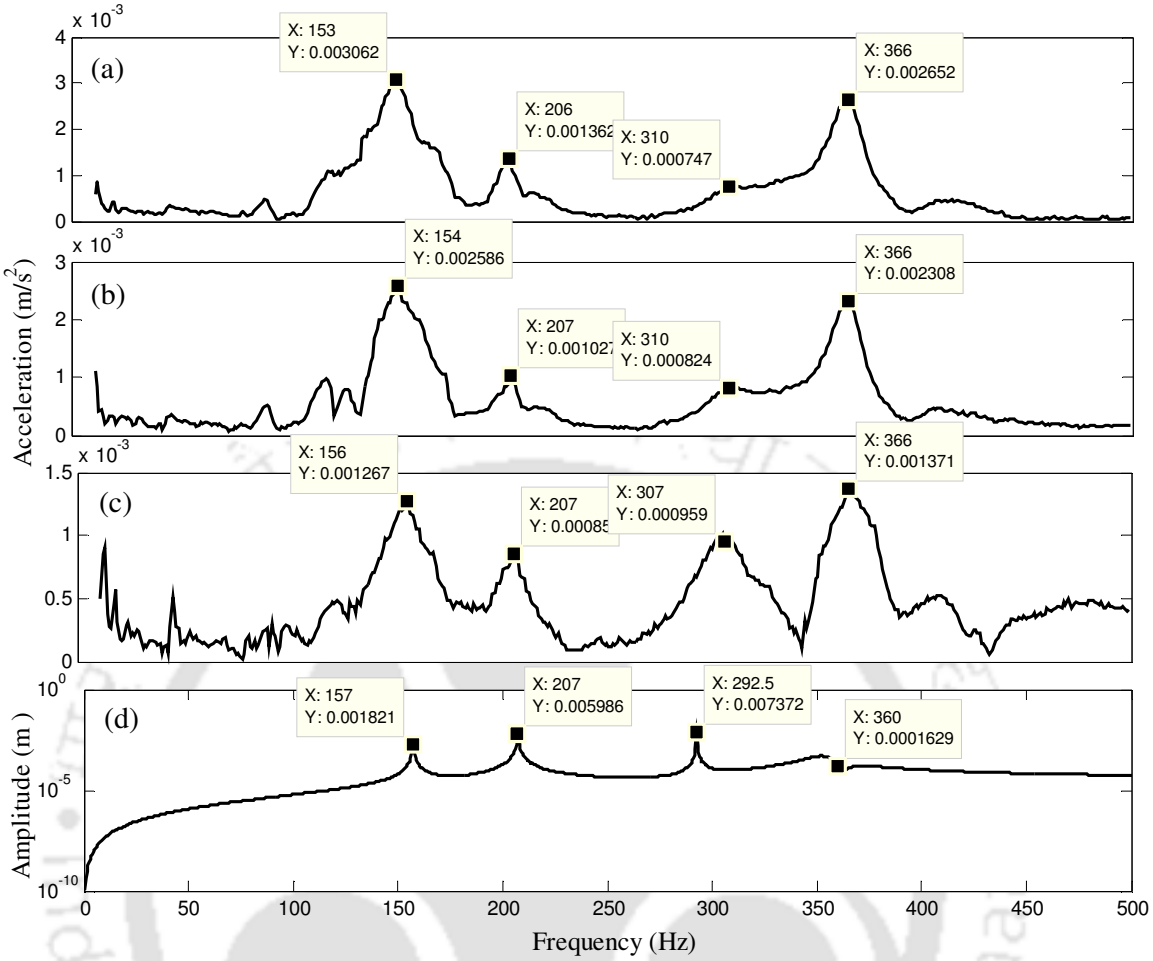

Figure 5.33 Comparison of natural frequencies (a) Impact test for *Case* A_1 (b) Impact test for *Case* B_1 (c) Impact test for *Case* C_1 (d) Updated FE model with misalignment condition (critical speeds)

From Table 5.6, it should be noted that effects on natural frequencies due to misalignments were appreciably small; however, effects on estimated the bearing and coupling dynamic parameters are appreciable. And this could be used to find the condition of misalignments better way. However, it has been observed that in the case of severe misalignments additional peaks appears in the impulse response that could be additional confirmation of the misalignment at the coupling and bearings.

Table 5.6 Summary of natural frequencies/critical speeds with and without misalignment conditions

S. N.	Mode of natural frequency (Hz)	FE modelling with SSBc* (critical speeds)	Without misalignment				With misalignment			
			Impact test result			Updated FE model (critical speeds)	Impact test result			Updated FE model (critical speeds)
			1st mode excitation	2nd mode excitation	3rd mode excitation		Pure angular (*Case* A_1)	Pure parallel (*Case* B_1)	Combined (*Case* C_1)	
1	1st	155	150	150	150	150	153	154	156	157
2	2nd	239	203	204	205	205	206	207	207	207
3	3rd	419	364	363	363	363	366	366	366	360

*SSBc: Simply supported boundary conditions.

5.9 Summary

An experimental investigation has been carried out in the present chapter to validate the algorithm proposed in Chapter 0, to estimate the bearing and coupling dynamic parameters along with residual unbalances. A laboratory rotor rig was designed and developed to perform experiments. The rotor shaft displacements were measured for with and without misalignment conditions, and the estimation of the bearing and coupling dynamic parameters along with residual unbalances was performed by using these measured forced response data. After the estimation the standard impact test was performed to check the accuracy of the estimated parameters by the measured and predicted frequency spectra. Theoretical predictions are in well agreement with the experimental results. Moreover, for a severe misalignment the splitting of the natural frequency of the rotor system took place, even at the non–rotating condition, which is an indication of misalignment. The updated FE model also mimics the similar behaviours to establish the robustness and the effectiveness of the identification algorithm.

CHAPTER 6

Conclusions and Scopes for Future Work

6.1 Summary of the Present Work

In the present study analytical and experimental work has been performed to identify the multiple fault parameters (MFPs) associates with turbine–generator systems rotor model. The study performed here is concerned with the development of the identification methodology to quantitatively estimate the bearing and coupling dynamic parameters along with residual unbalances of complete turbine–generator rotor systems. The present identification algorithm relies upon independent forced response measurements at several frequencies (i.e., the run–down or run–up data at several rotor operating speeds). The analytical and experimental results were examined in frequency domain.

Development of the identification algorithm has been carried out in such a way that it can be applied to real machineries. First, an identification algorithm has been developed to estimates MFPs in a rigid–rotor and flexible bearing–coupling system (refer Figure 2.1) by using the analytical approach, which gave more insight during overall development of the identification algorithm. Since this model is not a realistic one and the modelling approach is not practical, hence in the next work, a more realistic model, i.e. the flexible rotor–bearing–coupling system (refer Figure 3.1) has been considered and a more practical modelling approach i.e., the FEM has been used to develop system EOMs.

The identification algorithm developed in previous work has the main practical limitation in that it requires the measurement of several translational as well as rotational displacements. Because of it, not only the number of sensors for translational displacements would be more and associated accessibility of them, but major constraint would be to accurately measure all rotational displacements in practice. These limitations have been relaxed innovatively in the

next work by developing the identification algorithm with integration of two condensation techniques. In this work along with the estimation of MFPs, i.e. the bearing and coupling dynamic parameters and residual unbalances at predefined planes with incomplete rundown data have been performed. Moreover, the bias error in shaft material physical properties (5% variation in E (modulus of elasticity) and ρ (density)) in the model has also been analysed.

Finally, the algorithm developed was tested with a real experimental setup developed (refer Figure 5.1) in the Vibration and Acoustic Laboratory at IIT Guwahati. In the experimental section, the estimation of the bearing and coupling dynamic parameters along with residual unbalances was performed for the case of with and without misalignment conditions. The accuracy of the estimated the bearing and coupling dynamic parameters and residual unbalances were checked by matching natural frequencies (i.e., up to the third mode). Major conclusions from the present study are summarized below.

6.2 General Conclusions from the Present Work

Some of the important observations obtained from the present study are as follows:

- An identification algorithm has been proposed to quantitatively estimate the MFPs (i.e., the bearing and coupling dynamic parameters along with residual unbalances) based on forced response measurements.
- After estimating the coupling dynamic parameters, misalignment forces and moments has also been calculated and it is found that misalignment forces and moments are speed dependent and having maximum forces and moments at or near critical frequencies.
- The present algorithm uses minimum the number of test runs required to estimate the unbalance correctly with the magnitude and the phase.

- Estimation of residual unbalances is also checked with different sets of disc masses and with different unbalances (i.e., the magnitude and the phase).
- The identification algorithm is also checked for different level of measurement noise and found robust up to 5% measurement noise.
- Different methods have been proposed to improve the condition of regression matrix. And it is observed that the improvement in the condition number improves the accuracy of the estimated parameters.
- Present identification algorithm has the flexibility to incorporate any number of bearings, couplings and balancing planes.
- Generalised identification algorithm for the speed–dependent bearing and coupling dynamic parameters has also been developed.
- Estimation of the bearing and coupling dynamic parameters and residual unbalances has been carried out for different frequency bands and best estimation case is obtained.
- The bias error in shaft material physical properties (5% variation in E (modulus of elasticity) and ρ (density)) in the model has also been analysed.
- An experimental investigation has been carried out on a test rig to estimate the bearing and coupling dynamic parameters along with residual unbalances for with and without misalignment conditions.
- The consistency of the estimated parameters was checked for different sets of measured data and found well agreement between each other.
- After estimation the standard impact test was performed to check the accuracy of the estimated parameters by the measured and predicted frequency spectra. Theoretical predictions are in well agreement with the experimental results, for both with and without misalignment conditions.

- For a severe misalignment condition the splitting of the natural frequency of the rotor system has been observed, even at the non–rotating condition, which is an indication of the misalignment.

6.3 Major Conclusions from the Present work

Major contributions from the present research work are as follows:

- Modelling of the coupling model is new. Damping parameters for the coupling has also been added in the model.
- The identification algorithm developed for the estimation of the speed–dependent bearing and coupling dynamic parameters for the rotor–bearing–coupling model.
- The study of misalignment at couplings and bearings must be performed together since these effects are interrelated.
- The splitting of natural frequencies was observed from test rig for the severe misalignment.

6.4 Applicability

The algorithm developed in the present work can be applied in real machineries like turbine–generator systems, gas–turbine systems, propulsion systems, etc. where rotor trains are connected together with some kind of coupling (either rigid or flexible) and mounted over bearings. Limited data measured at bearing locations only would be sufficient for the present identification algorithm.

6.5 Scopes for the Future Work

- Coupling model could be improved with the inclusion of cross–coupled torsional dynamic parameters.

- Cross coupling between the linear and torsional dynamic parameters could be added in the bearing and coupling models.
- The proposed identification algorithm is sensitive to the measurement noise. It would be appropriate to improve the signal measurement and analysis techniques. Moreover, regularization techniques (Tikhonov and Arsenin, 1977) during identification could also be applied so as to reduce the noise affect on the estimation.
- In the present work the identification algorithm has been developed for the speed–dependent bearing and coupling dynamic parameters, however, in numerical simulations and experimental works the bearing and coupling dynamic parameters has been treated as constant coefficients. However, couplings have speed–dependency due to stiffening effects at high–speed conditions. The proposed identification algorithm could be tested for the quantification of the speed–dependent bearing and coupling dynamic parameters along with residual unbalances.
- Coupling parameters have been reported in literature as a time–varying, identification of such model would be a great challenge; however, responses in the full–spectrum form (Shravankumar and Tiwari, 2012) would definitely help in the identification for such cases.
- Various other types of coupling in use could be modelled and characterise based on forced measurement in line with the present work.
- In modelling along with bearings, seals could also be included in the rotor model; and apart from the estimation of bearing dynamic parameters, the dynamic parameters of seals also could be estimated.
- The real challenge would be to apply the proposed algorithm to real machinery.
- Proposed identification algorithm could be improved by inclusion of some more faults like bow/bent, cracks, etc.

- Internal damping could also be incorporated in the present identification algorithm.

Appendix A: Timoshenko Beam Model (Nelson, 1980)

A.1. Translational mass matrix

$$[M_t] = [M_t]_0 + \phi[M_t]_1 + \phi^2[M_t]_2 \tag{A.1}$$

$$[M_t]_0 = \frac{\rho Al}{420(1+\phi)^2}\begin{bmatrix} 156 & 0 & 0 & 22l & 54 & 0 & 0 & -13l \\ & 156 & -22l & 0 & 0 & 54 & 13l & 0 \\ & & 4l^2 & 0 & 0 & -13l & -3l^2 & 0 \\ & & & 4l^2 & 13l & 0 & 0 & -3l^2 \\ & & & & 156 & 0 & 0 & -22l \\ & & & & & 156 & 22l & 0 \\ & \text{Sym} & & & & & 4l^2 & 0 \\ & & & & & & & 4l^2 \end{bmatrix} \tag{A.2}$$

$$[M_t]_1 = \frac{\rho Al}{420(1+\phi)^2}\begin{bmatrix} 294 & 0 & 0 & 38.5l & 126 & 0 & 0 & -31.5l \\ & 294 & -38.5l & 0 & 0 & 126 & 31.5l & 0 \\ & & 7l^2 & 0 & 0 & -31.5l & -7l^2 & 0 \\ & & & 7l^2 & 31.5l & 0 & 0 & -7l^2 \\ & & & & 294 & 0 & 0 & -38.5l \\ & & & & & 294 & 38.5l & 0 \\ & \text{Sym} & & & & & 7l^2 & 0 \\ & & & & & & & 7l^2 \end{bmatrix} \tag{A.3}$$

$$[M_t]_2 = \frac{\rho Al}{420(1+\phi)^2}\begin{bmatrix} 140 & 0 & 0 & 17.5l & 70 & 0 & 0 & -17.5l \\ & 140 & -17.5l & 0 & 0 & 70 & 17.5l & 0 \\ & & 3.5l^2 & 0 & 0 & -17.5l & -3.5l^2 & 0 \\ & & & 3.5l^2 & 17.5l & 0 & 0 & -3.5l^2 \\ & & & & 140 & 0 & 0 & -17.5l \\ & & & & & 140 & 17.5l & 0 \\ & \text{Sym} & & & & & 3.5l^2 & 0 \\ & & & & & & & 3.5l^2 \end{bmatrix} \tag{A.4}$$

with

$$\phi = \frac{12EI}{k_{sc}GAl^2}, \qquad k_{sc} = \frac{6(1+\upsilon)}{(7+6\upsilon)}$$

Displacement vector $\{\eta\}^s = \{x_i, y_i, \varphi_{x_i}, \varphi_{y_i}, x_{i+1}, y_{i+1}, \varphi_{x_{i+1}}, \varphi_{y_{i+1}}\}^T$, where sub–script i is element number

A.2. Rotational mass matrix

$$[M_r] = [M_r]_0 + \phi[M_r]_1 + \phi^2[M_r]_2 \tag{A.5}$$

$$[M_r]_0 = \frac{\rho Al}{(1+\phi)^2}\begin{bmatrix} 6/5l & 0 & 0 & 1/10 & -6/5l & 0 & 0 & 1/10 \\ & 6/5l & -1/10 & 0 & 0 & -6/5l & -1/10 & 0 \\ & & 2l/15 & 0 & 0 & 1/10 & -l/30 & 0 \\ & & & 2l/15 & -1/10 & 0 & 0 & -l/30 \\ & & & & 6/5l & 0 & 0 & -1/10 \\ & & & & & 6/5l & 1/10 & 0 \\ & \text{Sym} & & & & & 2l/15 & 0 \\ & & & & & & & 2l/15 \end{bmatrix} \tag{A.6}$$

$$[M_r]_1 = \frac{\rho Al}{(1+\phi)^2}\begin{bmatrix} 0 & 0 & 0 & -1/2 & 0 & 0 & 0 & -1/2 \\ & 0 & 1/2 & 0 & 0 & 0 & 1/2 & 0 \\ & & l/6 & 0 & 0 & -1/2 & -l/6 & 0 \\ & & & l/6 & 1/2 & 0 & 0 & -l/6 \\ & & & & 0 & 0 & 0 & 1/2 \\ & & & & & 0 & -1/2 & 0 \\ & \text{Sym} & & & & & l/6 & 0 \\ & & & & & & & l/6 \end{bmatrix} \tag{A.7}$$

$$[M_r]_2 = \frac{\rho Al}{(1+\phi)^2}\begin{bmatrix} 0 & 0 & 0 & 0 & 0 & 0 & 0 & 0 \\ & 0 & 0 & 0 & 0 & 0 & 0 & 0 \\ & & l/3 & 0 & 0 & 0 & l/6 & 0 \\ & & & l/3 & 0 & 0 & 0 & l/6 \\ & & & & 0 & 0 & 0 & 0 \\ & & & & & 0 & 0 & 0 \\ & \text{Sym} & & & & & l/3 & 0 \\ & & & & & & & l/3 \end{bmatrix} \tag{A.8}$$

A.3. Stiffness matrix

$$[K]=[K]_0+\phi[K]_1 \tag{A.9}$$

$$[K]_0=\frac{EI}{(1+\phi)l^3}\begin{bmatrix} 12 & 0 & 0 & 6l & -12 & 0 & 0 & 6l \\ & 12 & -6l & 0 & 0 & -12 & 6l & 0 \\ & & 4l^2 & 0 & 0 & 6l & 2l^2 & 0 \\ & & & 4l^2 & -6l & 0 & 0 & 2l^2 \\ & & & & 12 & 0 & 0 & -6l \\ & & & & & 12 & 6l & 0 \\ & \text{Sym} & & & & & 4l^2 & 0 \\ & & & & & & & 4l^2 \end{bmatrix} \tag{A.10}$$

$$[K]_1=\frac{EI}{(1+\phi)l^3}\begin{bmatrix} 0 & 0 & 0 & 0 & 0 & 0 & 0 & 0 \\ & 0 & 0 & 0 & 0 & 0 & 0 & 0 \\ & & l^2 & 0 & 0 & 0 & -l^2 & 0 \\ & & & l^2 & 0 & 0 & 0 & -l^2 \\ & & & & 0 & 0 & 0 & 0 \\ & & & & & 0 & 0 & 0 \\ & \text{Sym} & & & & & l^2 & 0 \\ & & & & & & & l^2 \end{bmatrix} \tag{A.11}$$

A.4. Gyroscopic matrix

$$[G]=[G]_0+\phi[G]_1+\phi^2[G]_2 \tag{A.12}$$

$$[G]_0=\frac{\rho Ar^2}{60(1+\phi)^2 l}\begin{bmatrix} 0 & 36 & -3l & 0 & 0 & -36 & -3l & 0 \\ & 0 & 0 & -3l & 36 & 0 & 0 & -3l \\ & & 0 & 4l^2 & -3l & 0 & 0 & -l^2 \\ & & & 0 & 0 & -3l & l^2 & 0 \\ & & & & 0 & 36 & 3l & 0 \\ & & & & & 0 & 0 & 3l \\ & \text{Skew} & \text{Sym} & & & & 0 & 4l^2 \\ & & & & & & & 0 \end{bmatrix} \tag{A.13}$$

$$[G]_1 = \frac{\rho A r^2}{60(1+\phi)^2 l}\begin{bmatrix} 0 & 0 & 15l & 0 & 0 & 0 & 15l & 0 \\ & 0 & 0 & 15l & 0 & 0 & 0 & 15l \\ & & 0 & 5l^2 & 15l & 0 & 0 & -5l^2 \\ & & & 0 & 0 & 15l & 5l^2 & 0 \\ & & & & 0 & 0 & 0 & -15l \\ & & & & & 0 & 0 & 5l^2 \\ & \text{Skew} & \text{Sym} & & & & 0 & 5l^2 \\ & & & & & & & 0 \end{bmatrix} \quad \text{(A.14)}$$

$$[G]_2 = \frac{\rho A r^2}{60(1+\phi)^2 l}\begin{bmatrix} 0 & 0 & 0 & 0 & 0 & 0 & 0 & 0 \\ & 0 & 0 & 0 & 0 & 0 & 0 & 0 \\ & & 10l^2 & 0 & 0 & 0 & 0 & 5l^2 \\ & & & 0 & 0 & 0 & 5l^2 & 0 \\ & & & & 0 & 0 & 0 & 0 \\ & & & & & 0 & 0 & 0 \\ & \text{Skew} & \text{Sym} & & & & 0 & 10l^2 \\ & & & & & & & 0 \end{bmatrix} \quad \text{(A.15)}$$

A.5. Rigid disc model

Mass matrix

$$[M]^d = \begin{bmatrix} m_d & 0 & 0 & 0 \\ 0 & m_d & 0 & 0 \\ 0 & 0 & I_d & 0 \\ 0 & 0 & 0 & I_d \end{bmatrix} \quad \text{(A.16)}$$

Gyroscopic matrix

$$[G]^d = \begin{bmatrix} 0 & 0 & 0 & 0 \\ 0 & 0 & 0 & 0 \\ 0 & 0 & 0 & I_p \\ 0 & 0 & -I_p & 0 \end{bmatrix} \quad \text{(A.17)}$$

Displacement vector

$$\{\eta\}^d = \{x, y, \varphi_x, \varphi_y\}^T \quad \text{(A.18)}$$

Appendix B: Rayleigh Damping (Clough and Penzien, 1993)

The relation between damping ratio, ζ, and natural frequency. ω_n, is expressed as

$$\zeta = \frac{a_0}{2\omega_n} + \frac{a_1\omega_n}{2} \tag{B.1}$$

Where a_0 and a_1 are Rayleigh damping factors and this can be evaluated by the solution of a pair of simultaneous equations, if the damping ratios ζ_m and ζ_n associated with two specific known frequencies ω_m and ω_n respectively, writing equation (B.1) for each of these two cases and expressing them in the matrix form leads to

$$\begin{Bmatrix} \xi_m \\ \xi_n \end{Bmatrix} = \frac{1}{2}\begin{bmatrix} 1/\omega_m & \omega_m \\ 1/\omega_n & \omega_n \end{bmatrix}\begin{Bmatrix} a_0 \\ a_1 \end{Bmatrix} \tag{B.2}$$

From equation (B.2), a_0 and a_1 can be obtained as,

$$\begin{Bmatrix} a_0 \\ a_1 \end{Bmatrix} = \frac{2\omega_m\omega_n}{\omega_n^2 - \omega_m^2}\begin{bmatrix} \omega_n & -\omega_m \\ -1/\omega_n & 1/\omega_m \end{bmatrix}\begin{Bmatrix} \xi_m \\ \xi_n \end{Bmatrix} \tag{B.3}$$

Where ω_m and ω_n are the system fundamental and highest natural frequencies of interest

$$[C]^s = a_0[M]^s + a_1[K]^s \tag{B.3}$$

Appendix C: Natural Frequencies for Simply Supported Rotor Systems

Closed form solution is provided to obtain natural frequencies of a simply supported rotor system (see Fig. C.1) and is given as

$$\omega_{nf} = \frac{1}{2\pi}\sqrt{\frac{k}{m}}\ \text{Hz} \tag{C.1}$$

where $k = \frac{48EI}{L^3}$ (C.2)

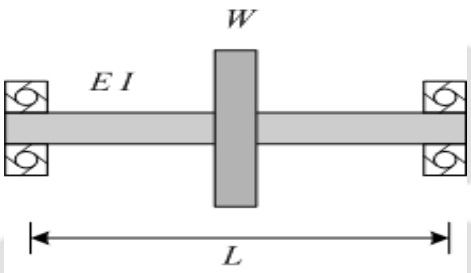

Figure C.1 Rigid rotor with a disc at the mid span

Material properties and rotor dimensions are taken from Table 5.1 and natural frequencies are summarised in Table C.1.

Table C.1 Natural frequencies with simply supported boundary conditions

S. N.	System	Natural frequencies (Hz)
1	Rotor 1	373
2	Rotor 2	169

Appendix D: Conditioning of Ill–Conditioned Regression Matrix

The condition number of a matrix (with respect to inversion) measures the sensitivity of the solution of a system of linear equations to errors in the data. It gives an indication of the accuracy of the results from matrix inversion and the linear equation solution. Values of condition number near 1 indicate a well–conditioned matrix. The 2–norm condition number, which is used in the present case, is defined as the ratio of the largest singular value of regression matrix to the smallest (Kreyszig, 2006).

The linear least–squares problem of Eqn. (2.14)

$$[A_2]\{X_2\} = \{B_2\} \tag{D.1}$$

to determine the bearing and coupling dynamic parameters along with the residual unbalances is said to be ill–conditioned if the singular values of $[A_2]$ decay gradually to zero and the ratio between the largest and smallest non–zero singular values of $[A_2]$ is large. Ill–conditioning of matrix $[A_2]$ implies that the solution is sensitive to perturbations and regularization is imperative for a stabilized solution.

Appendix E: Relationship between Signals–to–Noise Ratio (SNR) in dB and Noise in Percentage

The signal–to–noise ratio in dB is defined as

$$(\mathrm{SNR})_{\mathrm{dB}} = 10\log_{10}\left(\frac{A_{Signal}}{A_{Noise}}\right)^2 \tag{E.1}$$

where A is the amplitude of the signal or noise. Table E.1 lists the comparison of noise in percentage and dB.

Table E.1 Noise in percentage and SNR in dB

S. N.	Noise (%)	Signal to Noise Ratio (SNR) (db)
1	1 %	40.00
2	2 %	33.98
3	5 %	26.02
4	100%	0

References

Al–Hussain, K. M., (2003), Dynamic stability of two rigid rotors connected by a flexible coupling with angular misalignment, Journal of Sound and Vibration 266, 217–234.

Al–Hussain, K. M. and Redmond, I., (2002), Dynamic response of two rotors connected by rigid mechanical coupling with parallel misalignment, Journal of Sound and Vibration 249, 483–498.

Attiahili, M., Fakhfakh, T., Hammami, L. and Haddar, M., (2005), Shaft misalignment effect on bearings dynamical behavious, International Journal of Advanced Manufacturing Technology 26 (5).

Bachschmid, N. and Pennacchi, P., (2003), Accuracy of fault detection in real rotating machinery using model based diagnostic techniques, JSME International Journal Series C 46 (3).

Bachschmid, N., Pennacchi, P. and Vania, A., (2002), Identification of multiple faults in rotor systems, Journal of Sound and Vibration 254, 327–366.

Black, P. H. and Adams, O. E., Machine Design, McGraw Hill, Third Edition, 1981.

Bouaziz, S., Hilli, M. A., Mataar, M., Fakhfakh, T. and Haddar, M., (2009), Dynamic behaviour of hydrodynamic journal bearings in presence of rotor spatial angular misalignment, Mechanism and Machine Theory 44, 1548–1559.

Changlin, Z. Q. W. D. F. and Yiqun, D., (2010), The dynamical behaviors of a misalignment rotor–bearing system, Proc. of IEEE (978) 4518–4521.

Cho, H. W. and Jeong, M. K., (2008), Enhanced prediction of misalignment conditions from spectral data using feature selection and filtering, Expert Systems with Applications 35, 451–458.

Clough, R. W. and Penzien, J., (1993), Dynamics of Structures, 2nd edition, (McGraw–Hill, NewYork).

DeSmidt, H. A., Wang, K. W. and Smith, E. C., (2004), Stability of a segmented supercritical driveline with non constant velocity couplings subjected to misalignment and torque, Journal of Sound and Vibration 277, 895–918.

Dewell D. L. and Mitchell, L. D., (1984), Detection of misaligned disk coupling using spectrum analysis, Journal of Vibration, Acoustics, Stress and Reliability in Design 106, 9–16.

Dharmaraju, N., Tiwari, R. and Talukdar, S., (2004), Identification of an open crack model in a beam based on forced–response measurements, Computers and Structures 82, 167–179.

Dharmaraju, N., Tiwari, R. and Talukdar, S., (2005), Development of a novel hybrid reduction scheme for identification of an open crack model in a beam, Mechanical System and Signal Processing 19, 633–657.

Didier, J., Sinou, J. J. and Faverjon, B., (2012), Study of the non–linear dynamic response of a rotor system with faults and uncertainties, Journal of Sound and Vibration 331, 671–703.

Dimarogonas, A. D., (1996), Vibration of cracked structures: A state of the art review, Engineering Fracture Mechanics 55 (5) 831–857.

Doubling, S.W., Farrar, C. R. and Prime, M. B., (1998), A summary review of vibration based damage identification methods, Shock and Vibration Digest 30 (2) 91–105.

Drechsler, J., (1980), Processing surplus information in computer aided balancing of large flexible rotors, IMechE Conference on Vibrations in Rotating Machinery, Cambridge, UK 65–70.

Edwards, S., Lees, A. W. and Friswell, M. I., (1998), Fault diagnosis of rotating machinery, Shock Vibration Digest 30, 4–13.

Edwards, S., Lees, A. W. and Friswell, M. I., (2000), Experimental identification of excitation and support parameters of a flexible rotor bearing foundation system from a single run down, Journal of Sound and Vibration 232, 963–992.

Ewins, D. J., (1984), Modal Testing, Theory and Practice, (John Wiley, New York).

Friswell, M. I., Garvey, S. D. and Penny, J. E. T., (1994), Model reduction using an iterated improved reduced system technique, Fifth International Conference on Recent Advances in Structural Dynamics, UK July 879–889.

Friswell, M. I. and Mottershead, J. E., (1995), Finite element model updating in structural dynamics, (Kluwer Academic Publishers, London).

Ganesan, S. and Padmanabhan, C., (2011), Modelling of parametric excitation of a flexible coupling–rotor system due to misalignment, Proceedings IMechE, Part–C: Journal of Mechanical Engineering Science.

Gasch, R., (1993), A survey of the dynamic behaviour of a simple rotating shaft with a transverse crack, Journal of Sound and Vibration 160 (2) 313–332.

Gibbons, C. B., (1976), Coupling misalignment forces, 5th turbo machinery symposium 111–116.

Gnielka, P., (1983), Modal balancing of flexible rotors without test runs: an experimental investigation, Journal of Vibration 90, 157–172.

Goodwin, M. J., (1989), Dynamics of rotor bearing systems, Unwin Hyman Publishers, London.

Goodwin, M. J., (1991), Experimental techniques for bearing impedance measurement, ASME Journal of Engineering for Industry 113 (3) 335–342.

Guo, H. Y., and Li, Z. L., (2009), A two stage method to identify structural damage sites and experiments by using evidence theory and micro search genetic algorithm, Mechanical Systems and Signal Processing 23 (3) 769–782.

Guyan, R. J., (1965), Reduction of stiffness and mass matrices, AIAA Journal 3, 280.

Hamrock, B.J., (1994), Fundamentals of Fluid Film Lubrication, (McGraw–Hill).

Hariharan, V. and Srinivasan, P. S. S., (2009), Vibration analysis of misaligned shaft ball bearing system, Indian Journal of Science and Technology 2 (9) 45−50.

Hart, A. J., Slocum, A. and Willoughby, P., (2004), Kinematic coupling interchange ability, Precision Engineering 28, 1−15.

Heng, A., Zhang, S., Tan, A. C. C. and Mathew, J., (2009), Rotating machinery prognostics: state of the art, challenges and opportunities, Mechanical Systems and Signal Processing 23, 724−739.

Hou, Z. and Chen, S., (1995), Iterated dynamic condensation technique and its applications in modal testing, Shock and Vibration 4, 143–151.

Hori, Y. and Uematsu, R., (1980), Influence of misalignment of support journal bearings on stability of a multi−rotor system, Tribology International 249−252.

Hu, W., Miah, H., Feng, N. S. and Hahn, E. J., (2000), A rig for testing lateral misalignment effects in a flexible rotor supported on three or more hydrodynamic journal bearings, Tribology International 33, 197−204.

Huer, S. and Zhaojian, Y., (2010), Study on lateral vibration response of misalignment rotor−bearing systems based on linear torsion excitation, Proc. of IEEE (978) 1−4.

Isermann, R., (1997), Supervision, fault detection and fault diagnosis methods− An introduction, Control Engineering Practice 5 (5) 639−652.

Isermann, R. and Balle, P., (1997), Trends in the application of model based fault detection and diagnosis of technical process, Control Engineering Practice 5 (5) 709−719.

Jain, J. R. and Kundra, T. K., (2004), Model based online diagnosis of unbalance and transverse fatigue crack in rotor systems, Mechanics Research Communications 31, 557−568.

Jalan, A. K. and Mohanty, A. R., (2009), Model based fault diagnosis of a rotor bearing system for misalignment and unbalance under steady state condition, Journal of Sound and Vibration 327, 604–622.

Jardine, A. K. S., Lin, D. and Banjevic, D., (2006), A review on machinery diagnostics and prognostics implementing condition–based maintenance, Mechanical Systems and Signal Processing 20, 1483–1510.

Jayaswal, P., Wadhwani, A. K. and Mulchandani, K. B., (2008), Machine fault signature analysis–Review article, International Journal of Rotating Machinery 1–10.

Jordan, M. A., (1993), What are orbit plots, anyway? Orbit, December 8–15.

Kane, K. and Torby, B. J., (1991), The extended modal reduction method applied to rotor dynamic problems, ASME Journal of Vibration and Acoustics 113, 79–84.

Kim, D. and Lee, S., (2010), Structural damage identification of a cantilever beam using excitation force level control, Mechanical Systems and Signal Processing 24 (6) 1814–1830.

Kim, K. O. and Choi, Y. J., (2000), Energy method for selection of degrees of freedom in condensation, AIAA Journal 38 (7) 1253–1259.

Kreyszig, E., (2006), Advance Engineering Mathematics, 8th Edition, (John Wiley: NewYork).

Krodkiewski, J. M. and Ding, J., (1993), Theory and experiment on a method for on site identification of configurations of multi bearing rotor systems, Journal of Sound and Vibration 164 (2) 281–293.

Krodkiewski, J. M., Ding, J. and Zhang, N., (1994), Identification of unbalance change using a non–linear mathematical model for rotor bearing systems, Journal of Vibration 169, 685–698.

Lee, Y. S. and Lee, C. W., (1999), Modelling and vibration analysis of misaligned rotor ball bearing systems, Journal of Sound and Vibration 224, 1–12.

Lees, A. W., (2007), Misalignment in rigidly coupled rotor, Journal of Sound and Vibration 305, 261–271.

Lees, A. W. and Friswell, M. I., (1997), The evaluation of rotor unbalance in flexibly mounted machines, Journal of Sound and Vibration 208 (5) 671–683.

Lees, A. W., Sinha, J. K. and Friswell, M. I., (2009), Model–based identification of rotating machines, Mechanical Systems and Signal Processing, Special Issue: Inverse Problems, 23, 1884–1893.

Lei, Y., Lin, J., He, Z. and Zuo, M. J., (2013), A review on empirical mode decomposition in fault diagnosis of rotating machinery, Mechanical Systems and Signal Processing 35, 108–126.

Li, M. and Yu, L., (2001), Analysis of the coupled lateral torsional vibration of a rotor bearing system with a misaligned gear coupling, Journal of Sound and Vibration 243, 283–300.

Lorenzen, H., Niedermann, E. A. and Waittinger, W., (1989), Solid couplings with flexible intermediate shafts for high speed turbo compressor trains, proc of the 18th Turbomachinery Symposium, Texas 101–110.

Lund, J. W. and Thomson, K. K., (1978), A calculation method and data for the dynamic coefficients of oil–lubricated journal bearings, Topics in fluid bearing and rotor bearing system, ASME 1–28.

Maleev, V. L. and Hartman, J. B., (1999), Machine Design, C.B.S. Publishers & Distributors, Fifth Indian Edition.

McCloskey, T. H. and Adams, M. L., (1992), Trouble shooting power plant rotating machinery vibration using computational techniques: case histories. IMechE Conference on Vibrations in Rotating Machinery, Bath, UK, Paper C432/137, 239–250.

Mills, J. K. and Ing, J. G. L., (1996), Dynamic modelling and control of a multi–robot system for assembly of flexible payloads with applications to automotive body assembly, Journal of Robotic Systems 13, 817–836.

Morton P.G., (1975), The derivation of bearing characteristics by means of transient excitation applied directly to a rotating shaft, Dynamics of Rotors, IUTAM Symposium, Lyngby, Denmark, 350–379. Springer–Verlag, Berlin, Heidelberg, New York.

Morton P.G., (1985), Modal balancing of flexible shafts without trial weights, Proc IMechE Part C Mechanical Engineering Science 199 (1) 71–78.

Muszynska, A., (2005), Rotordynamics, New York: Marcell Dekker.

Naucler, P. and Soderstrom, T., (2010), Unbalance estimation using linear and nonlinear regression, Automatica 46, 1752–1761.

Nelson, H. D., (1980), A finite rotating shaft element using Timoshenko beam theory, ASME Journal of Mechanical Design 102, 793–803.

Nelson, H. D. and Crandall, S. H., (1992), Analytic prediction of rotor dynamic response, In Handbook of Rotor dynamics (Ed. F.E. Ehrich), (McGraw–Hill: New York).

Nelson, H.D. and McVaugh, J. M., (1976), The dynamics of rotor–bearing system using finite elements, ASME Journal of Engineering for Industry 593–600.

Nordmann, R. and Scholhorn K., (1980), Identification of stiffness and damping coefficients of journal bearings by impact method, Proceedings of IMechE, 2nd International Conference on Vibration in rotating machinery, C285/80 231–238.

Parkinson, A. G., (1991), Balancing of rotating machinery. Proceedings of the IMechE Part C–Journal of Mechanical Engineering Science, 205, 53–66.

Patel, T. H. and Darpe, A. K., (2009a), Vibration response of misaligned rotors, Journal of Sound and Vibration 325, 609–628.

Patel, T. H. and Darpe, A. K., (2009b), Experimental investigation on vibration response of misaligned rotors, Mechanical Systems and Signal Processing 23, 2236–2252.

Paz. M., (1984), Dynamic condensation, AIAA Journal 22, 724–727.

Pennacchi, P., and Vania, A., (2005), Diagnosis and model based identification of a coupling misalignment, Shock and Vibration 12, 293–308.

Pennacchi, P., Vania, A. and Chatterton, S., (2012), Nonlinear effects caused by coupling misalignment in rotors equipped with journal bearings, Mechanical systems and Signal Processing 30, 306–322.

Pennacchi, P., Bachschmid, N., Vania, A., Zanetta, G.A. and Gregori, L., (2006a), Use of modal representation for the supporting structure in model based fault identification of large rotating machinery: part 1 theoretical remarks, Mechanical Systems Signal Processing 20, 662–681.

Pennacchi, P., Bachschmid, N., Vania, A., Zanetta, G.A. and Gregori, L., (2006b), Use of modal representation for the supporting structure in model based fault identification of large rotating machinery: part 2– Application to a real machine, Mechanical Systems Signal Processing 20, 682701.

Ping, J. J. and Guang, M. A., (2009), Novel method for multi fault diagnosis of rotor system, Mechanism and Machine Theory 44, 697–709.

Piotrowski, J., (1986), Shaft alignment handbook, New York: Marcel Dekker.

Prabhakar, S., Sekhar, A. S., Mohanty, A. R., (2002), Crack versus coupling misalignment in a transient rotor system, Journal of Sound and Vibration 256, 773–786.

Rao, J. S., (1996), Rotor dynamics, Third Edition, New Age Publications, New Delhi.

Saavedra, P. N. and Ramirez, D. E., (2004a), Vibration analysis of rotors for the identification of shaft misalignment Part I: Theoretical analysis, IMechE Part C, 218, 971–985.

Saavedra, P. N. and Ramirez, D. E., (2004b), Vibration analysis of rotors for the identification of shaft misalignment Part II: Experimental validation, IMechE Journal of Mechanical Engineering Science 218, 987–999.

Sabnavis, G., Kirk, R. G., Kasarda, M. and Quinn, D., (2004), Cracked shaft detection and diagnostics: A literature review, Shock and Vibration Digest 36 (4) 287–296.

Sarkar, S., Nandi, A., Neogy, S., Dutt, J. K. and Kundra, T. K., (2010), Finite element analysis of misaligned rotors on oil–film bearings, Sadhana Indian Academy of Science 35, 45–61.

Sawicki, J. T., Friswell, M. I., Kulesza, Z., Wroblewski, A, Lekki, J. D., (2011), Detecting cracked rotors using auxiliary harmonic excitation, Journal of Sound and Vibration 330, 1365–1381.

Sekhar, A. S. and Prabhu, B. S., (1995), Effect of coupling misalignment on vibration of rotating machines, Journal of Sound and Vibration 185, 655–671.

Sekhar, A. S. and SrinivasaRao, A. S., (1996), Crack versus misalignment in rotor–coupling bearing system, Journal of Machine Vibration 5, 179–188.

Shih, Y. P. and Lee, A. C., (1997), Identification of the unbalance distribution in flexible rotors, International Journal of Mechanical Science 39, 841–857.

Shravankumar, C. and Tiwari, R., (2012), Identification of Stiffness and Periodic Breathing Forces of A Transverse Switching Crack in a Laval Rotor, Fatigue and Fracture of Engineering Materials and Structures (In press).

Sinha, J. K., Friswell, M. I. and Lees, A. W., (2002), The identification of the unbalance and the foundation model of a flexible rotating machine from a single run down, Mechanical Systems and Signal Processing 16 (2) 255–271.

Sinha, J. K., Lees, A. W. and Friswell, M. I., (2004a), Estimating unbalance and misalignment of a flexible rotating machine from a single run down, Journal of Sound and Vibration 272, 967–989.

Sinha, J. K., Lees, A. W. and Friswell, M. I., (2004b), Estimating the static load on the fluid bearings of a flexible machine from run down data, Mechanical Systems and Signal Processing 18, 1349–1368.

Singh, M. P. and Suarez, L. E., (1992), Dynamic condensation with synthesis of substructure eigen properties, Journal of Sound and Vibration 159, 139–155.

Singh, S. K. and Tiwari, R., (2010), Identification of a multi crack in a shaft system using transverse frequency response functions, Mechanism and Machine Theory 45, 1813–1827.

Smith, D. M., (1969), Journal Bearings in Turbomachinery, (Chapman and Hall).

Someya, T., (1976), An investigation into the spring and damping coefficients of the oil film in journal bearing. Transactions of the Japan Society of Mechanical Engineers 42 (360) 2599–2606.

Song, J. H. and Chung, Y. I., (2010), A review of crack closure measurement by compliance technique and the normalized–extended ASTM method as a currently most refined, practical and simple one, Procedia Engineering 2, 777–786.

Sudhakar, G. N. D. S. and Sekhar, A. S., (2011), Identification of unbalance in a rotor bearing system, Journal of sound and Vibration 330 (10) 229–2313.

Stodola, A., (1925), Critical shaft perturbation as a result of the elasticity of the oil cushion in the bearing, Schweizersche Bauzeitung 85 (25).

Swanson, E. E. and Kirk, R. G., (1997), Survey of experimental data for fixed geometry hydrodynamic journal bearings, ASME Journal of Tribology 119 (4) 704–710.

Tadeo, A. T., Cavalca, K. L. and Padmanabhan, C., (2011), Dynamic characterization of a mechanical coupling for a rotating shaft, Proc. IMechE, Part–C: Journal of Mechanical Engineering Science.

Tasi, C. Y. and Huang, S. C., (2009), Transfer matrix for rotor coupler with parallel misalignment, Journal of Mechanical Science and Technology 23, 1383–1395.

Tieu, A. K. and Qiu, Z. L., (1994), Identification of sixteen dynamic coefficients of two journal bearings from experimental unbalance responses, Wear 177, 63–69.

Tikhonov, A. N. and Arsenin, V. Y., (1977), *Solutions of Ill–Posed Problems*, Winston & Sons, Washington, D.C.

Tiwari, R., (2005), Conditioning of regression matrices for simultaneous estimation of the residual unbalance and bearing dynamics parameters, Mechanical Systems and Signal Processing 19, 1085–1095.

Tiwari, R. and Chakravarthy, V., (2006), Simultaneous identification of residual unbalances and bearing dynamic parameters from impulse responses of rotor–bearing systems, Mechanical Systems and Signal Processing 20, 1590–1614.

Tiwari, R. and Chakravarthy, V., (2009), Simultaneous estimation of the residual unbalance and bearing dynamic parameters from the experimental data in a rotor–bearing system, Mechanism and Machine Theory 44, 792–812.

Tiwari, R. and Dharmaraju, N., (2006), Development of a condensation scheme for the transverse rotational DOFs elimination in identification of beam crack parameters, Mechanical Systems and Signal Processing 20, 2148–2170.

Tiwari, R., Lees, A. W. and Friswell, M. I., (2002), Identification of speed dependent bearing parameters, Journal of Sound and Vibration 254 (5) 967–986.

Tiwari, R., Lees, A. W. and Friswell, M. I., (2004), Identification of dynamic bearing parameters: A review, The Shock and Vibration Digest 36**,** 99–124.

Tiwari, R., Manikandan, S. and Dwivedy, S. K., (2005), A review on experimental estimation of the rotor dynamic parameters of seals, The Shock and Vibration Digest 37, 261–284.

Tiwari, R. and Vyas, N. S., (1995), Estimation of nonlinear stiffness parameters of rolling element bearings from random response of rotor–bearing systems, Journal of Sound and Vibration 187 (2) 229–239.

Tondl A., (1965), Some Problems of Rotor Dynamics, Chapman & Hall, London.

Wowk, V., (2000), Machinery vibration alignment, McGraw–Hill.

Xu, M. and Marangoni, R., (1994a), Vibration analysis of a motor flexible coupling rotor system subjected to misalignment and unbalance – Part 1: Theoretical model and analysis, Journal of Sound and Vibration 176, 663–679.

Xu, M. and Marangoni, R., (1994b), Vibration analysis of a motor flexible coupling rotor system subjected to misalignment and unbalance – Part 2: Experimental validation, Journal of Sound and Vibration 176, 681–691.

Yang, Q. W., (2011), A new damage identification method based on structural flexibility disassembly, Journal of Vibration and Control 17 (7) 1000–1008.

Zeng, S. and Wang, X. X., (1999), Unbalance identification and field balancing of dual rotors system with slightly different rotating speeds, Journal of Sound and Vibration 220 (2) 343–351.

Zhang, Z. X., Zhang, Q., Li, X. L. and Qian, T. L., (2011), The whole–beat correlation method for the identification of an unbalance response of a dual–rotor system with a slight rotating speed difference, Mechanical Systems and Signal Processing 25, 1667–1673.

Zhao, G., Liu, Z. and Chen, F., (2008), Meshing force of misaligned spline coupling and the influence on rotor system, International Journal of Rotating Machinery 1–8.

Zhou, S and Shi, J., (2001), Active balancing and vibration control of rotating machinery: A survey, The Shock and Vibration Digest 33 (4) 361–371.

Publications from the Present Work

Journals:

1. **M. Lal** and R. Tiwari, Multi–Fault Identification in Simple Rotor–Bearing–Coupling Systems Based on Forced response Measurements**,** Mechanism and Machine Theory, 51(2012) 87–109.

2. **M. Lal** and R. Tiwari, Quantification *of* Multiple Fault Parameters in Flexible Turbo–Generator Systems with Incomplete Rundown Data, Mechanical System and Signal Processing, (http://dx.doi.org/10.1016/j.ymssp.2013.06.025).

3. **M. Lal** and R. Tiwari, Estimation of Multiple Machine–Element Parameters Based on Rundown Data, International Journal of Acoustics and Vibration (Under review).

4. **M. Lal** and R. Tiwari, Estimation of Multiple Fault Parameters in a Turbo Generator System–An Experimental Investigation, Measurement (Under review).

Conferences:

1. **M. Lal** and R. Tiwari, Identification of Multiple Faults in Rotor–Bearing–Coupling Systems, Proc. of Sixth International Conference on Vibration Engineering and Technology of Machinery (VETOMAC–VI), December 13–15, IIT Delhi, India (2010).

2. **M. Lal** and R. Tiwari, Identification of Multiple Fault Parameters in a Flexible Rotor–Bearing–Coupling System Based on Forced Response Measurements, Proc. of Tenth International Conference on Vibrations in Rotating Machinery, IMechE, September 11–13, one Birdcage Walk, London (2012).

3. **M. Lal** and R. Tiwari, Identification of Multiple Faults with Incomplete Response Measurements on Rotor–Bearing–Coupling Systems, ASME Gas Turbine India Conference, December 1, Bombay, India (2012).

4. **M. Lal** and R. Tiwari, Identification of Multiple Faults Parameters in a Rigid–Rotor and Flexible Bearing–Coupling System – An Experimental Investigation, ASME Gas Turbine India Conference, December 5–6, Bangalore, India (2013) (Accepted for presentation).